The Geochemistry of Albitisation in the Nechalacho Layered Alkaline Suite, Northwest Territories, Canada

By

Kent MacWilliam

Earth and Planetary Sciences, McGill University
3450 University Street, Montreal, QC
Canada H3A 0E8

December 2014

A thesis submitted to McGill University in partial fulfillment of the requirements of the degree of Master of Science

Abstract

The Nechalacho Layered Alkaline Suite (NLAS), which hosts the Nechalacho REE deposit containing a measured and indicated resource of 121.26 Mt grading 1.50% REE_2O_3 (0.25% $HREE_2O_3$, including Y_2O_3), 2.56% ZrO_2, 0.34% Nb_2O_5 and 0.03% Ta_2O_5, and located in the Slave Craton, NWT, is pervasively altered by secondary albite. Albitisation was most severe along the southern and western margins of the NLAS, overprinting all rock types and mineralised zones, and forming a porous, pink rock (>50% pink, bladed albite, <10% ferromagnesian minerals), i.e., albitite, which contains hydrothermal REE and HFSE minerals e.g.: Bastnäsite-(Ce), monazite-(Ce), columbite and zircon. The albitite underwent brittle deformation; the matrices of the resulting breccias as well as pore space between secondary albite crystals contain an intergrowth of quartz and fluorite and host the REE and HFSE mineralization. Secondary albite also contains REE-, Nb-, Y-, Zr-, Ti- and U-bearing solid micro-inclusions. Conditions of albitisation were constrained from phase relationships assuming 4.0k bar (Mumford 2013) and 367°C (Feng 2014) where fO_2 is at the H-M buffer = -29.3, aNa^+ = 2.80 and aK^+ = 0.14, pH is between 5.6 and 6.0 and log$aSi0_2$ is between -2.2 and -1.4. The $\delta^{18}O$ values calculated at 367°C for the hydrothermal fluid in equilibrium with quartz (NLAS) range from 8.8 to 11.4‰, 8.8 to 16.1‰ in secondary albite and 6.7 to 12.2‰ in secondary microcline. Along with the presence of Ca-bearing minerals in the albitised rocks, not present in the magmatic rocks, the isotopic values suggest an external fluid source.

The NLAS is the youngest and only silica-undersaturated intrusion of the Blachford Lake Complex. Discrete hydrothermal satellite deposits are hosted within the Grace Lake Granite (GLG) and Thor Lake Syenite units peripheral to the NLAS, the largest of these deposits being the T-Zone (1.1 million tons grading 0.71 wt. % REE_2O_3, 0.48 wt. % BeO and 0.53 wt. % Nb_2O_5). Fenitisation of the GLG and TLS is evident in hand samples within 2 km of the NLAS manifested by the replacement of K-feldspar and riebeckite by albite and magnetite, and, within 100m of the NLAS, in discontinuous veinlets composed of fluorite, calcite and hematite (Type B veins) surrounded by haloes of albite, aegirine and fluorite. Another vein type (Type C) affects the TLS close to the NLAS, and is calcite-dominant, up to several cm wide, with alteration

haloes greater than a metre thick, in which all ferromagnesian minerals and quartz have been removed or replaced by calcite, and primary K-feldspar has been albitised. It is proposed that formation waters in equilibrium with the GLG were drawn into the younger NLAS intrusion by convection, thereby shifting the two-feldspar phase boundary to be consistent with fluid compositions in the field of stability of albite. This promoted albitisation. Another effect of drawing fluids through the GLG and warming them was to dissolve quartz due to its increased solubility with increasing temperature, resulting in episyenitisation and veining (Type C). This also created pore spaces that were filled by albite. Exsolved magmatic fluids from the cooling NLAS were saturated in REE, preferentially mobilising the LREE over the HREE, which were later precipitated in pore space within the albitite.

Sommaire

La suite alkaline litée de Nechalacho (SALN), située dans le craton des Esclaves, T. N.-O., est l'hôte du gîte d'éléments de terres rares (ETR) de Nechalacho. Celui-ci contient une ressource mesurée et indiquée de 121,26 Mt à 1,50 % oxydes de terres rares (ETR_2O_3) (0,25 % ETR_2O_3 lourds, incluant Y_2O_3), 2,56 % ZrO_2, 0,34 % Nb_2O_5 et 0,03 % Ta_2O_5. La SALN a été altérée en albite secondaire de façon généralisée. L'albitisation a été la plus prononcée le long des marges sud et ouest de la SALN où elle a affecté tous les lithofaciès et toutes les zones minéralisées. L'albitisation a produit une roche rose et poreuse (>50 % albite rose lamellaire et <10 % minéraux ferromagnésiens), soit une albitite. Cette roche contient des minéraux hydrothermaux d'ETR et d'éléments à potentiel ionique élevé, par exemple, la bastnäsite-(Ce), la monazite-(Ce), la columbite et le zircon. L'albitite a subi une déformation cassante, produisant des brèches; la matrice de ces brèches ainsi que les pores entre les cristaux d'albite secondaire contiennent une intercroissance de quartz et de fluorite et sont l'hôte de la minéralisation en ETR et en éléments à potentiel ionique élevé. L'albite secondaire contient également des micro-inclusions solides porteuses d'ETR et de Nb, Y, Zr, Ti et U. Nous avons déterminé les conditions d'albitisation à partir des relations de phases, assumant une pression de 4,0 kbar (Mumford 2013) et une température de 367 °C (Feng 2014), où fO_2 se situe au tampon hematite-magnétite soit –29,3, $a\mathrm{Na}^+ = 2{,}80$, $a\mathrm{K}^+ = 0{,}14$, le pH est entre 5,6 et 6,0 et $\log a\mathrm{SiO}_2$ est entre –2,2 et –1,4. Les valeurs de $\delta^{18}O$ calculées à 367 °C pour le fluide hydrothermal en équilibre avec le quartz (SALN) s'étendent de 8,8 à 11,4 ‰, de 8,8 à 16,1 ‰ dans l'albite secondaire et de 6,7 à 12,2 ‰ dans le microcline secondaire. Comme le suggère la présence de minéraux calciques dans les roches albitisées, lesquels ne sont pas présents dans les roches magmatiques, les valeurs isotopiques indiquent une source externe pour les fluides.

Le SALN est l'intrusion la plus jeune et la seule intrusion dans le Complexe de Blachford Lake qui est sous-saturée en silice. Des gîtes satellites hydrothermaux ponctuels se trouvent dans les unités du Granite de Grace Lake (GGL) et de la Syénite de Thor Lake (STL) qui sont périphériques à la SALN; le plus gros de ces gîtes est la T-Zone (1,1 million de tonnes à 0,71 % poids ETR_2O_3, 0,48 % poids BeO et 0,53 % poids Nb_2O_5). La fénitisation du GGL et de la STL est évidente en échantillons choisis prélevés à l'intérieur de 2 km de la SALN. Cette altération se

manifeste par le remplacement du feldspath-K et de la riébeckite par l'albite et de la magnétite et, à moins de 100 m de la SALN, par des veinules discontinues de fluorite, de calcite et d'hématite (veines de type B) entourées d'auréoles d'albite, d'aegirine et de fluorite. On observe un autre type de veines (type C) dans la STL près de la SALN. Ces veines ont jusqu'à plusieurs centimètres de largeur et consistent majoritairement en calcite; elles possèdent des auréoles d'altération de plus de 1 m d'épaisseur dans lesquelles tous les minéraux ferromagnésiens et le quartz ont été enlevés ou remplacés par de la calcite et le feldspath-K primaire a été albitisé.

Nous proposons que les eaux de formation en équilibre avec le GGL soient entrées dans la SALN, plus jeune, par convection. Ainsi, la limite de phase à deux feldspaths a été déplacée pour demeurer cohérente avec les compositions des fluides dans le champ de stabilité de l'albite. Ces effets ont promu l'albitisation. Une autre conséquence du passage des fluides à travers le GGL et du réchauffement de ces fluides a été la dissolution du quartz à cause de l'augmentation de sa solubilité avec la température, ce qui a résulté en l'épisyénitisation et la mise en place des veines (type C). Ce processus a également créé des pores qui ont été remplis d'albite. Les fluides magmatiques produits par l'exsolution et provenant de la SALN pendant son refroidissement étaient saturés en ETR; ils ont mobilisé préférentiellement les ETR légers par rapport aux ETR lourds, et ces derniers ont été précipités dans les pores de l'albitite.

Contributions of the Authors

This thesis has been written in manuscript format and in accordance with the regulations set forth by the Faculty of Graduate Studies, McGill University. The manuscript entitled "Geochemistry of Albitisation in the Evolution of the Nechalacho Rare Earth Element Deposit, Northwest Territories, Canada" has been co-authored by Kent MacWilliam and Anthony E. Williams-Jones. The research was carried out by Kent MacWilliam in collaboration with Anthony E. Williams-Jones. Samples were collected by MacWilliam over the course of field work in 2009, 2010 and 2011. Sample preparation, analyses, and interpretation of results were conducted by Kent MacWilliam under the guidance and with the help of Anthony Williams-Jones.

Acknowledgements

I'd like to thank the technicians, laboratory staff, graduate students and research assistants of the McGill Earth and Planetary Sciences department. Lang Shi was invaluable for assistance on microprobe analyses and imaging. Thank you to Jim Clark for facilitating non-technical aspects of the project. Artas Migdisov was critical in providing assistance with phase diagrams and thermodynamic modeling throughout my research. I am appreciative of Vincent van Hinsberg, Alex Gysi and Nicole Hurtig for insightful discussions on mineralogy, mineral chemistry and metal solubility. This project was a product of the "Hydrothermal Geochemistry Group", better known as the "Willy Group" at McGill University, whose member's (2009-2011) input, particularly during "Beer Seminars", was greatly appreciated. Michel Preda at UQAM and Simon Jackson at the GSC are recognised for their assistance in using the XRD and LA-ICPMS machines, respectively. Dr. Clark is thanked for assisting in French translation.

Funding for this project was provided by grants from Avalon Rare Metals Inc. and the National Science and Engineering Research Council, Canada to A.E. Williams-Jones. I'd like to thank all those working at the Nechalacho deposit (Thor Lake), notably Chris Pederson and Martin Heiligmann, for providing a geological foundation for the project. Bill Mercer, VP Exploration and Don Bubar, CEO of Avalon Rare Metals Inc. are recognised for their continued commitment in advancing our scientific understanding of the Nechalacho deposit. I'd particularly like to thank the students working on the Nechalacho deposit through McGill University, notably Emma Sheard, Volker Möller and Alex Timofeev, as well as Yonggang Feng and Thomas Mumford working at The University of Windsor and Carleton University respectively.

Thank you to my friends and family who were so encouraging during the thesis writing process. And thank you to the earth's crust for supporting me.

Above all, I'd like to thank "Willy" A.E. Williams-Jones for years of supervision and assistance. He once told me that there were numerous theses and dissertations tucked away in the fold of the Thor Lake deposit, I guess he was right.

Table of Contents

The Geochemistry of Albitisation in the Nechalacho Layered Alkaline Suite, Northwest Territories, Canada

Abstract i

Sommaire iii

Contributions of the Authors v

Acknowledgements vi

Table of Contents vii

List of Figures ix

List of Tables xi

Chapter 1: Introduction 1

Motivation 3

Background 3

Previous Work on Thor Lake 11

Objectives and Methodology 17

Organisation of Thesis 19

Chapter 2: Journal Manuscript 21

Abstract 25

Introduction 26

Geological Setting 28

Methodology 32

Alteration of the Grace Lake Granite 34

Alteration of the Nechalacho layered alkaline suite 39

The albitite 46

Isotopic Analyses 57

Discussion 59

Pressure and Temperature 59

fO_2 60

The activities of Na^+ and K^+ 61
pH 61
The activity of SiO_2 62
The activity of Ca^{2+} 64
Mobilisation of the REE and HFSE 65
Fluid Source 69
The Mechanisms of Albititisation 71
Fluid Pathway 72
The Source of the REE and HFSE 74
Fenitisation 76
Albitisation and REE Mineralisation 76
Conclusion 76
Acknowledgements 77
References 77

Chapter 3: Conclusions and Contributions to Knowledge 85
Conclusions 87
Contributions to Knowledge 88
References 91

Appendices 103
Appendix I: Microprobe analyses (wt%) 105
Appendix II: Trace element data (ppm) 142
Appendix III: Fluid inclusion data 164
Appendix IV: Granite sample whole rock analyses 169
Appendix V: Activities calculated 173
Appendix VI: Isotope analyses 174
Appendix VII: Reactions and thermodynamic constants 175

List of Figures

Figure 1: Map showing the location and geology of the Blachford Lake Complex 29
Figure 2: Geological map of the Nechalacho Layered Syenite 31
Figure 3: Mineralogical changes within the TLS and GLG 34
Figure 4: Common vein types within the GLG in hand samples 35
Figure 5: Whole rock compositions of samples of the GLG and TLS versus distance from the NLAS. 37
Figure 6: Isocon plots for Type B vein halo and Type C vein halo 38
Figure 7: Mass changes in percent (%) relative to the unaltered Grace Lake Granite 39
Figure 8: Images showing textural relationships among primary and secondary minerals within the NLAS. 41
Figure 9: Diagrams showing the composition of biotite within distinct units of the upper 300m of the NLAS 43
Figure 10: Alteration textures within the albitite and Upper Ore Zone 45
Figure 11: Late-stage alteration textures within the albitite 46
Figure 12: Geological map showing the surface expression of the NLAS 47
Figure 13: Section A-A' through the NLAS 48
Figure 14: Feldspar textures in the albitite 50
Figure 15: LA-ICPMS counts versus ablation time for a location in a secondary albite crystal ..51
Figure 16: Textures in albitite 52
Figure 17: Replacement textures within the albitite 53
Figure 18: Spider diagram showing the average trace element concentration 55
Figure 19: Measured isotopic compositions of alteration minerals in the NLAS 59
Figure 20: The stability of albite, K-feldspar, muscovite, paragonite and daphnite (chlorite) as a function of log (aNa^+/aH^+) and log (aK^+/aH^+) at a temperature of 367°C 62
Figure 21: A paragenetic chart for the upper, hydrothermally altered part of the Nechalacho Layered Suite 63
Figure 22: Stability relationships for minerals in the system Fe-O-Al-Si-Na-K system as a function of temperature and log$a$$SiO_2$ 64
Figure 23: The concentration of Y versus the Y/Ho ratio of fluorite from the NLAS 68

Figure 24: A plot of δD vs $\delta^{18}O$ of fluids interpreted to have been responsible for albitisation...70
Figure 25: The stability of albite, K-feldspar and muscovite as a function of log (aNa^+/aH^+) and log (aK^+/aH^+) at temperatures from 150 to 400°C.....72
Figure 26: Model of alteration and late stage enrichment of the albitite unit within the NLAS...75

List of Tables

Table 1: Major and minor element concentration the NLAS (wt.%) 56
Table 2: Mean trace element concentration of minerals in the NLAS (ppm) 57
Table 3: $\delta 18O_{(VSMOW)}$ and $\delta D_{(VSMOW)}$ for albite, K-feldspar and quartz from the albitite.. 58
Table 4: Mean values for T-zone fluid inclusion compositions and homogenization temperatures 65

Chapter 1: Introduction

Motivation

The rare earth elements (REE), defined as the lanthanoid elements (lanthanum through to lutetium plus yttrium and scandium), are of growing economic importance. They are in high demand due to numerous applications in high technology industries. Examples of these applications are their use: 1) as permanent magnets (e.g., in synchronous electric motors in hybrid cars), which contain Nd, Pr, Sm, Tb and Dy; 2) as LaNiMH batteries (e.g., rechargeable batteries including those used in hybrid cars), which contain the light rare earth elements (LREE); 3) as phosphors for lighting and electronic displays which use Eu, Y, Tb, La and Ce; and 4) as signal amplifiers in fibre optics, which use Er, Y, Tb, Eu. The world's supply of the REE comes dominantly from the Bayan Obo, a carbonatite-related, deposit in China. As demand for the REE has risen considerably in recent years, and China is restricting its export of the REE, there is an urgent need to find new REE resources, particularly outside China.

Hydrothermal alteration is commonly an important manifestation of the processes that lead to the genesis of metallic mineral deposits. Consequently, the alteration that accompanies the formation of many types of hydrothermal ore deposits, notably porphyry and epithermal deposits, has been documented and interpreted in considerable detail. An important exception, however, is the alkali-metasomatism and fenitisation associated with alkaline igneous systems hosting rare earth element (REE) deposits. This alteration has been poorly documented and, as a result, the sources, pathways and physicochemical conditions of the late to post-magmatic fluids of alkaline igneous systems hosting REE deposits are poorly understood.

Background

Alkaline intrusives are exceptionally enriched in REE and other rare elements, such as Nb, Ta, and Zr. Highly evolved alkaline melts, with high concentrations of the halogens, Cl and F, have a great capacity to dissolve the REE and other rare elements (Sørrensen 1992). Agpaitic alkaline intrusive complexes such as Lovozero, Russia; Ilímaussaq, Greenland; Thor Lake, Northwest Territories; and Strange lake, Quebec; have been subject to extensive REE-mineral exploration due to their high potential to host economic deposits.

Alteration of the rocks is an important manifestation of the hydrothermal processes that lead to the genesis of metallic mineral deposits. It also provides an important vector for exploration designed to discover deposits. Consequently, the alteration that accompanies formation of many types of ore deposits, for example porphyry and epithermal deposits, has been documented in considerable detail (e.g., White and Hedenquist 1990). An important exception, however, is the alteration of alkaline igneous systems hosting rare metal deposits, which has received comparatively little documentation. As a result, the significance of hydrothermal processes for the concentration of ore metals in these systems is not well understood.

Alkaline magmatism

Continental alkaline magmatism, manifested as large complex intrusions, isolated intrusions and peripheral pegmatites, is developed in tectonic regimes of spreading and transtension (Martin 2006). Continental "A-type" alkaline intrusives have a chemical composition ranging from peraluminous to peralkaline, silica saturated to undersaturated and carbonatitic. Martin (2006) highlighted several features of these intrusives: 1) the occurrence of granites of variable composition in large igneous complexes; 2) a lack of xenoliths; 3) highly variable Sr, Nd and O isotopic signatures, ranging from those of the mantle to the crust; and 4) open system behavior, with metasomatic reactions affecting the intrusions, and local fenitisation of the country rocks.

The aforementioned features of A-type magmas are attributed to high temperature, high alkalinity, and high volatile concentration. High temperature and the concentration of network modifiers (volatiles, halogens, alkalies and Al^{VI}) promote melt depolymerisation, resulting in a low-viscosity (e.g., Martin and De Vito 2005). This, in turn, ensures that dense xenoliths are not suspended, explaining why they are rarely observed in crystalline intrusions (Martin 2006). In plan view, many such complexes are subcircular (e.g., the Blachford Lake intrusives, Davidson 1982; and the Bokan mountain ring dyke complex, Thompson et al. 1982), and frequently form cylindrical plugs (e.g., the Monteregian intrusions, Eby 1985). The viscous magma is able to assimilate crustal rocks easily, explaining the variability of the isotopic values and chemical composition. Increased solubility of the REE and HFSE elements is also related to the depolymerisation potential of A-type magmas, increasing with the activity of F and Cl (Keppler 1993).

Alkaline igneous rocks are classified using the ratio of Na_2O+K_2O to Al_2O_3, as well as their mineralogy. Chemically, metaluminous melts have $Na_2O+K_2O<Al_2O_3$ and peralkaline melts $Na_2O+K_2O>Al_2O_3$ both with $Na_2O+K_2O+CaO<Al_2O_3$ (Shand 1947). Peralkaline and metaluminous rocks may be either silica-oversaturated granite or undersaturated syenite. Silica undersaturated rocks of both groups may contain assemblages of zircon and titanite, in which case they are termed miaskitic. In contrast, agpaitic rocks, defined as having $Na_2O+K_2O/Al_2O_3 \geq 1.2$ (Ussing 1912) are an highly alkaline subset of peralkaline silica undersaturated syenites. Mineralogically, agpaitic rocks contain a complex array of Na, K and Ca silicate minerals with high Zr and Ti minerals, such as eudialyte (Sörensen 1997).

The petrology of alkaline intrusions and the relationships of phases within alkaline complexes are highly diverse. Commonly, there are several chemically distinct generations of crosscutting magmatic bodies, including dykes. Silica-oversaturated and -undersaturated rocks are frequently juxtaposed. The apparently cogenetic relationship of such magmas provides a paradox. Magma evolution by fractionation of alkali feldspar produces melt compositions that evolve away from the albite-orthoclase join (a thermal divide). The melt should evolve towards either more quartz rich or more nepheline rich compositions of the quartz-nepheline-kalsilite "petrogeny's residua" system (Bowen 1937). A single magmatic body would be expected to evolve by fractionation to either a phonolitic thermal minimum if silica-undersaturated, or a granitic thermal minimum if silica- saturated. The frequent association of silica-saturated and -undersaturated rocks must then be due to a process other than fractionation. According to many, this process is crustal assimilation (Foland et al. 1993; Harris 1995; Schmitt et al. 2000; Anderson et al. 2003). Both a decrease of $a SiO_2$ due to fractionation as well as localised shifts to silica saturation due to xenolith assimilation have been observed in silica-undersaturated intrusions (Marks and Markl 2001).

The origin of alkaline intrusions, such as those discussed above, is highly debated. Possible sources of the magmas are: partial melting of the continental crust (Whalen et al. 1987; Trønnes and Brandon 1992); fractionation of mantle derived basalt or trachyte (Turner et al. 1992; Boily and Williams-Jones 1994; Kramm and Kogarko 1994; Schmitt et al. 2000; Anderson et al. 2003); a combination of the two processes (Davies and Macdonald 1987; Eby 1992); and a

metasomatised lower crust (Martin 2006). A basaltic source, which is supported by the bimodal nature of many anorogenic suites, requires a very high degree of fractionation (Turner et al. 1992; Kramm and Kogarko 1994). A-type melts are highly enriched in incompatible elements, and their trace element patterns will overwhelm those from assimilated rocks. Based on REE and HFSE discriminants, A-type igneous rocks are either similar to ocean-island or to island and continental arc rocks (Eby 1992). A-type magmas cannot be highly fractionated I-type magmas because there would then be a correlation of trace element abundance with a negative Eu anomaly (caused by plagioclase fractionation), which is not seen (Eby 1992). A residual source may explain the major element behavior, but cannot also satisfy the extreme trace element and volatile element enrichment (Eby 1992; Martin 2006). A low degree of partial melting of crust, causing HFSE and REE phases to melt, may account for the high concentration of these elements. The high halogen content of these melts may be due to scavenging of halogens from the surrounding crustal rocks (Davies and Macdonald 1987). Mantle degassing is an alternative source of halogens (Bailey 1980). Open system reactions that fertilise the lower crust may provide volatiles and halogens, alkalis, heat and trace elements. The resulting bulk composition of the fertilised crust could then be subject to any degree of partial melting to produce A-type magmas. Evidence for this is scarce, though signs of processes such as nephelinisation of gneiss from the lower crust are observed (Martin 2006).

The best studied agpaitic intrusions are Ilímaussaq, Greenland (Ussing 1912; Marks et al. 2004; Sörensen et al. 2006) and Lovozero, Russia (Gerasimovsky et al. 1966; Féménias et al. 2005). These intrusions exhibit repetitive magmatic layering (Sörensen 1969; Mitchell and Chakhmouradian 1996; Markl et al. 2001; Féménias et al. 2005), a feature also observed in the agpaitic Nechalacho intrusion, N.W.T (Sheard et al. 2012). Within the Ilímaussaq intrusion, sodalite-rich floatation cumulates (naujaites) were emplaced before the crystallisation of the central units (Sörensen et al. 2006). Within the central units, some layers of lujavrite (residual liquid) and kakortakite (cumulate) track cyclical crystal fractionation trends (Rataschabacher et al. 2011). Similar to the kakortakites of Ilímaussaq, the cyclical units at-Lovozero comprise a lower nepheline rich unit (urtite) grading vertically into a K-feldspar- rich trachyte (foyaite) and finally into a pyroxene rich unit (lujavrite). Layered units of the Lovozero complex disappear in contact with the country rock, where a massive, coarse-grained foyaite is found (Féménias et al.

2005). The Ilímaussaq, Lovozero and the Nechalacho intrusions are rare element exploration targets. In these agpaitic intrusions, complex Zr and Ti silicate phases, rich in the REE, Nb and Ta are cumulate minerals within primary igneous layers as well as within related pegmatites and veins (Sørrensen 1992; Mitchell and Chakhmouradian 1996; Kogarko et al. 2002; Sheard et al. 2012). The Strange lake intrusion, Quebec, containing an agpaitic assemblage hosted by granite (Salvi and Williams-Jones 1990), is also currently undergoing rare element exploration.

Autometasomatic reactions due to late-magmatic fluids play a critical role in alkaline complexes. Originally considered to be dry melts, based on the results of experimental investigations (e.g., Turner et al. 1992), A-type magmas are not completely anhydrous. They show evidence of having evolved from hyper-solvus to subsolvus alkali feldspars, suggesting that pH_2O increased with evolution. At the evolved, hyper-agpaitic end of the spectrum, the presence of highly soluble sodic carbonate minerals such as trona and thermonatrite indicates that the late fluid-rich magmas are very basic. At Ilímaussaq, nepheline-absent ussingite vein assemblages are also indicative of high pH. The pH of late magmatic fluids is made increasingly basic by the isovolumetric replacement of nepheline by analcime, increasing Na/Cl (Markl and Baumgartner 2002). Agpaitic mineral assemblages are stable at low aH_2O and high aNaCl. Under less alkaline conditions, miaskitic hydrothermal assemblages are more stable (Marks et al. 2011). Orthomagmatic fluids may recrystalise, remobilise and precipitate REE- and HFSE-bearing minerals such as eudialyte and rinkite (Olivo and Williams-Jones 1999; Salvi et al. 2000). The REE and HFSE become soluble due to the high Cl^- content of the exsolved fluids (Williams-Jones et al. 2012; Migdisov et al. 2014). Fluid inclusions in alkaline rocks may have appreciable Cl- and F^- concentrations (Banks et al. 1994) and some inclusions even contain REE and HFSE mineral daughter crystals such as parisite-(Ce) and zircon (Salvi et al. 2000). Exsolved alkaline-magmatic fluids trapped as inclusions have been observed to have moderate and even high salinity (Graser et al. 2008).

Fenitisation

Fenitisation, defined as metasomatism of host rock adjacent to alkaline magmatic rocks, was first described by (Brögger 1921) at the type locality Fen, in Norway. Examples of localities where fenitised rocks have been studied in detail are Fen, Norway (Brögger 1921; Kresten and Morogan 1986; Kresten 1988), Seiland, Norway (Robins 1984), Alnö, Sweden (Morogan and

Woolley 1988), Monchique, Portugal (Rock 1976), Gifford Creek and Mudtank, Australia (Currie et al. 1992; Pearson et al. 1996), Borralan and the Great Glen fault, Scotland (Martin et al. 1978; Garson et al. 1984), Kisingiri, Kenya (Rubie 1982), Oldoinyo Lengai, Tanzania (Morogan and Martin 1985), and the Ottawa-Bonnechere graben, Ontario (Currie and Ferguson 1971; Siemiatkowska and Martin 1975) and Amba Dongar, India (Williams-Jones and Palmer 2002). Fenitisation is commonplace adjacent to carbonatites and silica-undersaturated (including agpaitic) rocks. The fluids exsolved by silica-under-saturated melts are strong fenitising agents. With decreasing content of Si in the fluid, Al and Na are more soluble and the fluid and melt eventually becomes miscible (Preston et al. 2003).

Fenitisation varies in style and intensity depending on the fluid-rock ratio, the type of host rock, and the physicochemical conditions. No element has been clearly demonstrated to be immobile during fenitisation. With increasing intensity of fenitisation, Al, Na, Mg, K and Fe, (and H_2O and CO_2) are generally added, together with the REE and other HFSE. This is accompanied by a marked decrease in the concentration of Si. Aluminium has been shown to be mobile in basic fluids by Beitter et al. (2008) and such mobility has been documented for fenitising fluids (Currie and Ferguson 1971; Siemiatkowska and Martin 1975; Williams-Jones and Palmer 2002). Standard cell studies (Appleyard and Woolley 1979; Kresten 1988; Rubie 1982) do not rigorously quantify fenitisation, as oxygen is not immobile. Minerals commonly associated with fenitisation are alkali-amphibole, aegirine-augite, biotite, albite and K-feldspar. Minor quantities of titanite, apatite, pyrite and magnetite are also observed (Martin et al. 1978; Veksler and Keppler 2000). Host rocks display variable susceptibility to fenitisation. For example, granodiorite is more readily fenitised than granite or diorite in the Kisingiri complex of Kenya (Rubie 1982). The variability of LREE/HREE within fenitised rocks demonstrates that these elements are mobile in such alkaline solutions (Martin et al. 1978). The solubility of the REE in hydrothermal fluids has been demonstrated to increase with increasing temperature and decreasing atomic number because of the formation of chloride complexes (Migdisov et al. 2009; Williams-Jones et al. 2012), and therefore the LREE should be more mobile than the HREE at lower temperatures, i.e., further from the source.

Albitisation and Albitites

Albitites, rocks composed largely of albite, form largely due to hydrothermal albitisation but also crystallise from melts. Albitisation is a common alteration type, and is associated with several deposit types, e.g., IOCG deposits (Hitzman et al. 1992) and granite-hosted uranium deposits (Thompson 1988). It is a type of fenitisation (Garson et al. 1984), occurring locally as halos around crustal scale fluid conduits (Boulvais et al. 2007), and regionally as reddened calcite-vein selvedges (Engvik et al. 2008). Magmatic corundum-bearing albitites may form as a result of small degrees of partial melting of the mantle (Pin et al. 2006). Minor albitisation, as both replacement and vein filling, is found adjacent to eudialyte in the Tamazeght complex (Schilling et al. 2009).

Albite crystals resulting from fenitisation are commonly intergrown with quartz and aegirine. They are saccroidal in texture, and display "checkerboard" twinning (Rock 1976; Siemiatkowska and Martin 1975; Kresten and Morogan 1986). On a larger scale, albite within fenites can occur as discontinous veins (Currie and Ferguson 1972) and breccias (Garson et al. 1984) with several generations of albite overprinting each other. Crosscutting veins, brecciation and hydrothermal flow textures are observed. Such textures result from overpressuring of exolved fluids in the adjacent alkaline melt (Siemiatkowska and Martin 1975). Albitites have not been described as replacement products of the silica-undersaturated source rocks.

Albitisation has been recognised as a regional metasomatic effect, with mineral replacement occurring on the microscale. Recently, a number of researchers have identified likely mechanisms for the precipitation of secondary albite (Engvik et al. 2008; Plümper and Putnis 2009). Reactions of both orthoclase to albite and oligoclase to albite result in significant volume decreases, 8% and 14%, respectively, and create porosity. On the micro-scale, hematite rosettes within pores of secondary K-feldspar adjacent to primary plagioclase, occupy this pore space (Putnis et al. 2007). Pore space creation is evidence of a replacement mechanism involving a reaction front moving through the crystal in which a thin veneer of hydrothermal fluid lies between the dissolution and growth surfaces of the primary and secondary feldspar crystals, respectively (Putnis et al. 2007). Along the reaction front, tetrahedral bonds involving Si and Al are broken and rebuilt. This replacement is evidenced by deuteric $\delta^{18}O$ values for albitised

granites (Hoefs and Emmermann 1983). The pores are transient, and textural re-equilibration occurs (surface area decreases) resulting in pore closure and the isolation of pores (Putnis et al. 2005). Pore closure is responsible for trapping crystal and fluid inclusions (Putnis et al. 2007). Muscovite, calcite, chlorite, epidote and rutile are observed accompanying albite within large pores (Plümper and Putnis 2009; Engvik et al. 2008). Other trace element oxides occurring as inclusions within secondary albite have not been as well documented.

The red colour of secondary feldspars is due to the presence of Fe^{3+} in the form of a fine dusting of hematite. The source of the iron and the trigger for its deposition are poorly understood. Possible Fe sources include the breakdown of associated amphibole or other mafic Fe-bearing phases, Fe in solid-solution within primary feldspars (Fe^{3+} within tetrahedral sites in primary alkali-feldspar), or an external environment (Putnis et al. 2007). It is evident that, in cases where primary feldspars have been replaced completely by iron oxides (e.g., Olympic Dam, Oreskes and Einaudi 1990), an external Fe source is needed.

The formation of secondary albite by hydrothermal fluids can be attributed to rising regional geothermal gradients. Albite becomes the stable feldspar, if a fluid initially in equilibrium with two feldspars undergoes an increase in temperature without a change in composition (Boulvais et al. 2007). Fluid source and temperature gradient along fluid pathways become the important controls. Surface-derived waters have been identified as the source for albitising fluids in a metamorphic terrain (McLelland et al. 2002). In many cases, a large alteration footprint is too extensive to be the result of magmatism; fluid source must be sought elsewhere.

A magmatic origin for albitites has been proposed to explain the isotopic signature and the textures. Corundum-bearing albitite dykes of the western Pyrenees underwent high T - low P metamorphism (Pin et al. 2006). The εNd and $^{87}Sr/^{86}Sr$ signatures of the dykes indicate a mantle source that underwent a very low (>1%) degree of partial melting. The coarsely crystalline nature of the dykes contrasts with the finer-grained, red and commonly brecciated nature of the hydrothermal albitites (Monchoux et al. 2006).

Concluding statement

Albitite is an enigmatic rock type, with no single genetic origin. Thor Lake provides an ideal setting in which to study processes of albitisation, especially in association with peralkaline rocks. Alkaline intrusives are chemically varied, but show remarkable potential to concentrate REE and HFSE minerals through magmatic and hydrothermal processes. Alteration associated with alkaline intrusions is normally manifested by fenitisation of the surrounding country rocks. Albitisation of silica-undersaturated intrusions has not yet been described. Albitisation at Thor Lake represents a snapshot of the upper level alteration processes operating during alkaline magmatism, evidence of which is normally eroded away.

Previous Work on Thor Lake

Exploration

Interest in the mining potential of the Thor Lake area was first shown in 1970 when K.D. Hannington laid claims over several geophysical anomalies (Bakker et al. 2011). However, it was not until 1976, with the discovery of Nb and Ta mineralisation by Highwood Resources Inc., that there was systematic exploration of the area (Trueman et al. 1988). Early exploration lead to the discovery of five separate rare-metal prospects, the T-zone, R-zone, S-zone, Fluorite zone and the Lake zone (now referred to as the Nechalacho deposit). Over the next decade, the T-zone was delineated as a wineglass-shaped Be, Nb, Ta, REE, Y and Zr deposit with an estimated resource of 1.6Mt grading 0.85Be + 435kt grading 1.4 wt/%Be and 0.26 wt.% Y_2O_3 (Pederson and Le Couteur 1991). However, owing to the complex mineralogy and low metal prices, a mine was not put into production. Avalon Rare Metals Inc. acquired the Thor Lake property in 2005 and initiated a program of exploration designed to identify a mineable REE resource in the Lake zone. Since then, Avalon has drilled >350 holes and recovered >60,000 m of NQ, HQ and PQ diameter core, drilled 10s of geotechnical holes, and carried out a comprehensive sampling program. Definition drilling has delineated the Nechalacho deposit with a measured and indicated resource of 121.26 Mt grading 1.50% REE_2O_3 (0.25% $HREE_2O_3$, including Y_2O_3), 2.56% ZrO_2, 0.34% Nb_2O_5 and 0.03% Ta_2O_5 (Ciuculescu et al. 2013).

Research: regional

Regional studies included mapping and geochemical characterisation of the Blachford Lake complex (Davidson 1972; Davidson 1978; Davidson 1981; Davidson 1982). Dating of the Athapuscow aulacogen, host to the blachford Lake complex was conducted by (Bowring et al. 1984). Large-scale stratigraphic correlations of the Slave Craton are summarised by Bleeker and Hall (2007). Radiometric, magnetic, electromagnetic (Charbonneau and Legault 1994) and gravity (Birkett et al. 1994) surveys of the Blachford Lake complex have been carried out.

The Blachford lake intrusive complex was first mapped by Davidson (1972). It is located in the Slave craton, on the margin of the Hearne-Channel of the Great Slave lake. The complex is one of ten known alkali complexes including the Squalus lake and Big Spruce alkaline complexes, marking the breakup of the Sclavia supercraton (Bleeker and Hall 2007). The complex was recognised as a multi-phase alkaline system. Davidson (Davidson 1972; Davidson 1978; Davidson 1982) subdivided the 1500 km^3 alkaline complex into six units: the Caribou Lake gabbro, the Whitman Lake quartz syenite, the Hearne Channel and Mad Lake granite (western lobe), and the Grace Lake granite and Thor Lake syenite (eastern lobe), which generally share steep contacts. Their geometry resembles a series of circular intrusions crosscutting and younging eastward. A gravity survey and subsequent modeling of the data suggest that the complex is a tabular body with a maximum thickness of 1 km thickness (Birkett et al. 1994). Hole L10-194 drilled by Avalon Rare Metals Inc., shows that the Nechalacho nepheline syenite is at least 1.1 km thick as this hole failed to intersect the base of the intrusion.

The contact between the Thor Lake syenite and the surrounding Grace Lake granite is marked by a decrease in the quartz content. Normally, the decrease is gradational, although it has been observed to be razor-sharp in places. The Thor Lake syenite has been subdivided into five generally concentric units based on textural and mineral differences. The most distinctive of the units is the fayalite-bearing rim-syenite, which passes outwards into the Grace Lake granite. This unit is fine-grained and crescent-shaped. Feldspar crystal alignment suggests an inward plunging contact with the Grace Lake granite. Davidson (1982) interpreted the Thor Lake syenite and Grace Lake granite, which are texturally and mineralogically similar and share an inwardly dipping contact, to represent a single, bowl-shaped intrusion. He proposed a fractionation trend

in which quartz content increased outward According to this proposal, a feldspar cumulate roof-pendant, supported by magmatic convection, formed the Thor Lake syenite within the Grace Lake granite magma chamber. Major element, trace element and Sr isotope data support a fractionation model for the entire Blachford Lake intrusive complex (Davidson 1982). Calcium content decreases and alkalinity increases with increasing silica and younging of the intrusive phases. The REE distribution varies regularly and the total REE concentration increases inwards consistent with fractionation.

Rare-element exploration uncovered nepheline syenites within the centre of the Thor Lake syenite (Sinclair et al. 1994; Birkett et al. 1994; Charbonneau and Legault 1994; Pinkston and Smith 1995). The silica-undersaturated intrusion does not outcrop. Although not mapped explicitly by Davidson (1978), it corresponds to an alteration and veining unit on his map. This unit was later classified as a subsolvus nepheline monzosyenite to feldspathic ijolite (Pinkston and Smith 1995), and recognised to be agpaitic and layered (Sheard et al. 2012). The silica-undersaturated unit has recently been named the Nechalacho Layered Alkaline Suite (NLAS) (Sheard et al. 2012).

Regional age dating established that the East arm of the Great Slave lake represented a Paleoproterozoic failed rift. This rift, called the Athapuscow aulacogen (Bowring et al. 1984), is located along the southern margin of the slave craton. Ages of 2175±5Ma (Hearne Channel granite) and 2094±10Ma (Thor Lake syenite) were determined using U-Pb isotopes in zircon. The description of the zircon analysed by Bowring et al. (1984) and attributed by them to the Thor Lake syenite matches that of the mineralised zone in the NLAS. More recent dating of the Grace Lake granite, determined an age of 2176.2±1.3 Ma (Birkett et al. 1994), indistinguishable within error from that for the Hearne Channel granite. Sinclair (1994) used this argument to interpret the age of 2094±10 Ma determined by Bowring et al. (1984) to represent the "age of rare-metal mineralisation, rather than that of the emplacement of the host Thor Lake syenite". Some consequences of the re-interpretation of the age data are: 1) uncertainty of the relationship of the silica-saturated Thor Lake syenite to the silica-undersaturated NLAS units; 2) an implied age difference of at least 70Ma between mineralisation of the NLAS and the emplacement of the rest of the Blachford Lake complex and; 3) a disputable age date for the NLAS. Plateau

$^{40}Ag/^{39}Ag$ ages of 2125±31Ma, 2118±16Ma and 2087±25Ma were measured for late polylithionite collected within the T-zone (Taylor and Pollard 1996). Recent U-Pb dating has yielded ages of 2176.8 ± 1.6Ma for the TLS and 2164 ± 11Ma (Mumford 2013) and 2175.6 ± 3.1Ma (Möller and Williams-Jones 2013) for the NLAS, which would appear to resolve the timing issues referred to above. Hence, the GLG, TLS and NLAS are dated within error of each other suggesting emplacement in quick succession.

Research: local

The T-zone is a prospect-turned-deposit at Thor Lake. It is an eliptical body trending NNE which straddles the margins of the Grace Lake granite and the Thor Lake syenite. The T-zone is pervasively metasomatised and brecciated (Černý and Trueman 1985). It can be subdivided into four, roughly concentric bowls based on the distribution of alteration and ore mineral assemblages. The lowest unit is an assemblage of pink, massive albite, K-feldspar and quartz. Above it is the lower intermediate zone characterized by higher contents of magnetite, riebeckite, chlorite, various micas, fluorite and HFSE minerals including REE-bearing varieties. The third unit is the upper intermediate zone, which is composed of quartz, polylithionite, lepidolite, biotite, muscovite, albite and aegirine, as well as Fe-oxides and carbonates, and HFSE minerals. The final unit is the quartz core, which consists dominantly of quartz and locally contains minor albite, muscovite, polylithionite, carbonates, fluorite, hematite and sulphide minerals (Černý and Trueman 1985). Fluid inclusions in the T-Zone contain up to 20 wt.% NaCl equivalent, variable proportions of CO_2 and homogenize at an average temperature of 350˚C (Taylor and Pollard 1996). Feng (2014) reported detailed fluid inclusion analyses and distinguished six main assemblages petrographically. Fluid inclusion compositions were measured by microthermometry or laser ablation. Of the six assemblages, two main groups exist, a high entrapment temperature moderate salinity group, and a low temperature high salinity group. The feldspars in the T-zone and Lake zone (now Nechalacho deposit) were reported by de St. Jorre and Smith (1988) to contain elevated concentrations of Ga interpreted to reflect a metasomatic overprint.

Several other prospects occur adjacent to the T-zone (Černý and Trueman 1985). The R-zone, S-zone and Fluorite zone are all rare-metal prospects peripheral to the NLAS and hosted within the Thor Lake syenite. These peripheral prospects display similar mineral assemblages to the T-

zone. The "Lake zone", now called the Nechalacho deposit is hosted by the NLAS (Pinkston and Smith 1995; Sheard et al. 2012). Pinckston and Smith (1995) recognised 41 silicates, 23 oxides, 9 sulphides, 10 carbonates, 3 phosphates, and several minerals that remain unidentified. Most of these minerals are REE/HFSE-bearing. Sheard et al. (2012) sub-divided the zircon of the Nechalacho deposit into four separate types. They also added eudialyte to the list of minerals that occur within the NLAS

Zircon occurs in three distinct morphologies within the two main ore zones. Upper zone REE/HFSE mineral assemblages include fergusonite-(Y), ferrocolumbite, allanite-(Ce), monazite-(Ce) and bastnäsite-(Ce). Type I zircon is the dominant zircon type in the upper zone. This variety occurs as 30µ to 60µm diameter euhedral bipyramidal crystals. Their cores are preferentially altered, displaying an atoll texture. They are commonly metamict and the REE are concentrated along fractures that extend from the altered core to the rim. This has been interpreted to indicate that hydrothermal fluids allowed migration of the REE from the core to the rim and beyond, where REE minerals such as fergusonite-(Y) and allanite-(Ce) are found (Sheard et al. 2012). In hand specimen, this zircon is observed in isolated layers or in ribbon-like laminations interpreted to be primary igneous cumulates. Type II zircon dominates within the lower of the two ore zones. Type II zircon, which occurs generally as anhedral grains, is present within completely replaced pseudomorphs after eudialyte and rarely elpidite (Sheard et al. 2012). It is richer in the HREE than Type I zircon. Type III zircon occurs mainly in association with albitisation, and is commonly replaced by albite. This zircon type forms large anhedral masses, and displays distinct yellowish green cathodoluminescence, due likely to Sm^{3+} or Dy^{3+} activation (Sheard et al. 2012).

The Nechalacho nepheline syenite has been divided into four primary units: an aegirine-nepheline syenite; a trachytic nepheline syenite (lujavrite); zirconosilicate cumulates; and the sodalite cumulate (Sheard et al. 2012). These four units form repetitive layers of tens to several tens of cms in thickness, sharing sharp contacts with each other. The layers are commonly graded internally by grain size. Nepheline forms the main phenocryst phase in the lujavrite, and is accompanied by small aegirine and feldspar crystals, which are aligned and wrap around the larger nepheline crystals. Aegirine is the dominant phenocryst phase in the aegirine-nepheline

syenite, and occurs with secondary feldspar and nepheline (commonly altered). The sodalite syenite, normally 10s of ms in thickness, is composed of closely packed sodalite and aegirine crystals with interstitial albite. It occurs mainly as the uppermost and outermost marginal unit of the NLAS in contact with the Grace Lake granite where it is intensely altered to muscovite. The sodalite syenite is also found at depth, forming lenses which display diffuse contacts with the other units. The zirconosilicate clumulates make up two distinct ore horizons. The ore mineralogy between the two horizons is similar: zirconium is hosted mainly by zircon, niobium by ferrocolumbite and fergusonite-(Y), yttrium and the other HREE by fergusonite-(Y) and zircon and the LREE by monazite-(Ce), allanite-(Ce), bastnäsite-(Ce) and parisite-(Ce)/synchysite-(Ce). The zircon making up the upper ore horizon is the type 1 variety and is interpreted to represent a primary cumulate. The lower ore horizon (Basal Zone) is richer in HREE. It comprises pseudomorphs after cumulate eudialyte, and is dominated by type II zircon.

Alteration of the NLAS was pervasive within the upper 300m, commonly leaving only relicts of primary minerals (Sheard et al. 2012). Magnetite and biotite are the main alteration minerals within the upper ore horizon. Spatially, magnetite and biotite occur with fergusonite-(Y), ferrocolumbite, allanite-(Ce), monazite-(Ce) and bastnäsite-(Ce). Within the Basal zone, magnetite is dominant with minor hematite alteration and less important biotite. Hematite is a late alteration product, having replaced aegirine and magnetite. Hematisation is also associated with the removal of magnetite, biotite, quartz and zircon within pseudomorphs after eudialyte. Albitisation overprints other alteration styles, and is commonly manifested by bladed albite (cleavlandite), which replaced primary K-feldspar crystals. Within heavily albitised intervals, quartz, carbonate minerals (siderite, ankerite, calcite), illite and muscovite are late stage alteration minerals of local importance.

The layers of the NLAS are analogous to the primary igneous layers observed in the Ilímaussaq intrusion, Greenland (Sörensen 1969; Sörensen et al. 2006). At Ilímaussaq, naujaite, a sodalite floatation cumulate unit, occurs as the upper most unit, and also occurs as rafts or large inclusions within the lower units of the intrusion. The same is true in the NLAS. The thicknesses of individual layers within the NLAS are variable. For example, the ore horizon, interpreted to be a primary igneous cumulate unit, varies in thickness from 10m to >70m over lateral intervals of

100s of metres. The complexity of the layering, in contrast to Ilímaussaq, which displays consistent layers that can be easily correlated, is likely due to slumping of distinct layered magmatic units. Slumping of primary units is analogous to soft-sediment deformation (e.g., the Merensky Reef of the Bushveld Igneous Complex, Vermaak 1976). Lithological units show variably sharp contacts with each other and commonly grade in and out from one unit to the next.

Objectives and Methodology

Albitisation strongly affected the Nechalacho deposit, but the nature of the alteration and the conditions under which it occurred have been poorly described and poorly constrained, respectively. Magnetite, biotite and quartz are the dominant alteration minerals within the ore horizons. Hematitisation is widespread throughout the NLAS replacing primary and secondary minerals. Albitisation is a final overprint, which is conspicuous in the upper 300m of the complex. Exsolved magmatic fluids, external hydrothermal fluids or both have been interpreted to have altered other peralkaline complexes, such as the Strange Lake pluton (Salvi and Williams-Jones 1990). It is therefore important to evaluate possible fluid conditions and sources within the NLAS, both in their role in albitisation and their relationship with mineralisation.

The purpose of this study is to develop a model to explain the genesis of the albitite and its genetic relationships to the different types of alteration in the NLAS. This study focuses on the effects that alteration fluids had on the bulk rock chemistry, mineralogy and late REE remobilisation. The study also considers the fenitisation and albitisation of the rocks adjacent to the NLAS. In order create a model for albitisation and to evaluate the physicochemical conditions of the alteration fluid, it is necessary to: 1) evaluate mineral paragenesis and discriminate generations of the same minerals; 2) determine the extent of alteration of the country rock and establish protoliths for the altered rocks where possible; 3) identify fluid pathways; 4) determine the likely source of the alteration fluids; and 5) evaluate phase relationships to constrain alteration conditions.

The above objectives were met using the following:

- Detailed field work, including drill core logging and extensive sampling for petrographic and geochemical analyses

- Detailed petrographic analyses using optical microscopy, cathodoluminescense, backscatter electron microscopy and X-ray diffraction to identify minerals, determine textural relationships among them and develop a paragenetic sequence
- In situ major and minor element analysis by electron microprobe (JEOL JXA-8900L electron microprobe equipped with 5 WDS spectrometers and a Si(Li) EDS detector at McGill University). Concentrations of Na_2O, K_2O, SiO_2, Al_2O_3, Fe_2O_3, MgO, MnO, CaO, Rb_2O, SrO and Ga_2O_3 were measured in quartz, albite, microcline and aegirine. Biotite grains were probed for concentrations of these oxides together with F and Cl. A 10μm beam diameter, a 15keV excitation voltage and a $3x10^{-8}$ A beam current were used to analyse albite, microcline, nepheline and sodalite, whereas biotite and aegirine were analysed using a 10μm beam, a 20keV excitation voltage and a $3x10^{-8}$ A beam current. Detection limits ranged from 120 to 220 ppm except for Sr, for which the detection limit was 500 to 550 ppm (Sr). All minerals were analysed with a 5 minute dwell time to accommodate low detection limits for Ga_2O_3
- Trace element analysis by Laser-ablation inductively-coupled-plasma mass-spectrometry (Photon-Machines Analyte193 excimer laser ablation system, $\lambda = 193$ nm, and an Agilent 7700 quadrupole ICP-MS at the Geological Survey of Canada) of albite, microcline, sodalite fluorite and aegirine. A beam with a diameter of 138 μm or 172 μm for albite and K-feldspar, and 52 μm to 69 μm for the other minerals, at 10Hz was used, and the mass spectrometric data were reduced using *GLITTER!* Software
- Evaluation of whole rock analyses and lithological logs to establish the spatial distribution of units using ArcGIS (ESRI) and Target (Geosoft) software
- X-ray fluorescence analysis to determine the whole rock composition and inductively couple plasma mass-spectrometry to determine trace element composition of samples in traverses through zones of increasing intensity of alteration (ALS labs). Iron oxide (FeO) concentration was determined using sulphuric and hydrofluoric acid digestion with titration finish
- X-ray Diffraction analysis (Bruker D5000 cobalt tube sol-x detector at UQAM/GEOTOP) to identify the mineral composition of mineral separates
- Oxygen and deuterium isotope analyses preformed on albite, microcline and quartz at the Queen's University isotope laboratory. All mineral separates were hand-picked and

prepared using a dilute HCl solution. Primary and secondary minerals to determine the source of the alteration fluids; the oxygen isotope values represent analyses of the minerals, whereas δD values were obtained by decrepitation and measurement of the isotopic composition of the included fluids.

Organisation of Thesis

The thesis is divided into three chapters: an introduction; an original scientific manuscript; and conclusions. The introduction is a literature review divided into topics relevant to the subject of the thesis, alkaline magmatism, fenitisation, albitites and regional studies. In addition, the methods and objectives are described. The scientific manuscript describes observations, hypotheses, methods, analytical findings and the model encompassing this study. The conclusion is a summary of results from the thesis, as well as a statement regarding contributions to science.

Chapter 2: Journal Manuscript

The Geochemistry of Albitisation associated with Rare Earth Element Mineralisation in the Nechalacho Layered Alkaline Suite, Northwest Territories, Canada

Kent MacWilliam[†] and Anthony E. Williams-Jones

Earth and Planetary Sciences, McGill University
3450 University Street, Montreal, QC
Canada H3A 0E8

[†]Corresponding author: email, kent.macwilliam@mail.mcgill.ca

For submission to Economic Geology

Abstract

The Nechalacho Layered Alkaline Suite (NLAS), which hosts the Nechalacho REE deposit containing a measured and indicated resource of 121.26 Mt grading 1.50% REE_2O_3 (0.25% $HREE_2O_3$, including Y_2O_3), 2.56% ZrO_2, 0.34% Nb_2O_5 and 0.03% Ta_2O_5, and located in the Slave Craton, NWT, is pervasively altered by secondary albite. Albitisation was most severe along the southern and western margins of the NLAS, overprinting all rock types and mineralised zones, and forming a porous, pink rock (>50% pink, bladed albite, <10% ferromagnesian minerals), i.e., albitite, which contains hydrothermal REE and HFSE minerals e.g.: Bastnäsite-(Ce), monazite-(Ce), columbite and zircon. The albitite underwent brittle deformation; the matrices of the resulting breccias as well as pore space between secondary albite crystals contain an intergrowth of quartz and fluorite and host the REE and HFSE mineralization. Secondary albite also contains REE-, Nb-, Y-, Zr-, Ti- and U-bearing solid micro-inclusions. Conditions of albitisation were constrained from phase relationships assuming 4.0k bar (Mumford 2013) and 367°C (Feng 2014) where $\boldsymbol{f}O_2$ is at the H-M buffer = -29.3, $a\mathrm{Na}^+$ = 2.80 and $a\mathrm{K}^+$ = 0.14, pH is between 5.6 and 6.0 and $\log a\mathrm{Si}0_2$ is between -2.2 and -1.4. The $\delta^{18}O$ values calculated at 367°C for the hydrothermal fluid in equilibrium with quartz (NLAS) range from 8.8 to 11.4‰, 8.8 to 16.1‰ in secondary albite and 6.7 to 12.2‰ in secondary microcline. Along with the presence of Ca-bearing minerals in the albitised rocks, not present in the magmatic rocks, the isotopic values suggest an external fluid source.

The NLAS is the youngest and only silica-undersaturated intrusion of the Blachford Lake Complex. Discrete hydrothermal satellite deposits are hosted within the Grace Lake Granite (GLG) and Thor Lake Syenite units peripheral to the NLAS, the largest of these deposits being the T-Zone (1.1 million tons grading 0.71 wt. % REE_2O_3, 0.48 wt. % BeO and 0.53 wt. % Nb_2O_5). Fenitisation of the GLG and TLS is evident in hand samples within 2 km of the NLAS manifested by the replacement of K-feldspar and riebeckite by albite and magnetite, and, within 100m of the NLAS, in discontinuous veinlets composed of fluorite, calcite and hematite (Type B veins) surrounded by haloes of albite, aegirine and fluorite. Another vein type (Type C) affects the TLS close to the NLAS, and is calcite-dominant, up to several cm wide, with alteration haloes greater than a metre thick, in which all ferromagnesian minerals and quartz have been

removed or replaced by calcite, and primary K-feldspar has been albitised. It is proposed that formation waters in equilibrium with the GLG were drawn into the younger NLAS intrusion by convection, thereby shifting the two-feldspar phase boundary to be consistent with fluid compositions in the field of stability of albite. This promoted albitisation. Another effect of drawing fluids through the GLG and warming them was to dissolve quartz due to its increased solubility with increasing temperature, resulting in episyenitisation and veining (Type C). This also created pore spaces that were filled by albite. Exsolved magmatic fluids from the cooling NLAS were saturated in REE, preferentially mobilising the LREE over the HREE, which were later precipitated in pore space within the albitite.

Introduction

Hydrothermal alteration is commonly an important manifestation of the processes that lead to the genesis of metallic mineral deposits. Consequently, the alteration that accompanies the formation of many types of hydrothermal ore deposits, notably porphyry and epithermal deposits, has been documented and interpreted in considerable detail. An important exception, however, is the alkali-metasomatism and fenitisation associated with alkaline igneous systems hosting rare earth element (REE) deposits. This alteration has been poorly documented and, as a result, the sources, pathways and physicochemical conditions of late to post-magmatic fluids of the alkaline igneous systems hosting REE deposits are poorly understood.

The transition from magmatic to hydrothermal conditions within miaskitic-agpaitic intrusions has received limited study. As a result, the effects of hydrothermal activity within such intrusions are not well understood. Of particular interest, from an economic perspective, are examples of natural systems in which the hydrothermal fluids are able to concentrate REE and high field strength elements (HFSE) to potentially exploitable levels (Kogarko 1990; Sørrensen 1992; Gysi and Williams-Jones 2013). Magmas in these systems are marked by unusually high concentrations of Na^+, and F^- and Cl^-, which are thought to form stable complexes with ions of the rare-earth elements and thereby enrich them in these elements (Larsen 1979; Collins et al. 1982; Kogarko 1990; Salvi and Williams-Jones 1990; Sørrensen 1992; Boily and Williams-Jones 1994; Olivo and Williams-Jones 1999; Salvi et al. 2000; Schmitt et al. 2002; Sheard et al. 2012). The REE and other HFSE are highly soluble in these highly alkaline, halogen-rich melts (Watson

1979; Linnen and Keppler 1997). This can lead to the formation of "agpaitic" syenites and the crystallization of mineral assemblages that include complex Na-Ca, Zr- and Ti-silicates such as aenigmatite, eudialyte and narsarsukite (Sörensen 1997; Kogarko et al. 2002; Marks et al. 2011). Deuteric fluids of highly alkaline intrusions are capable of altering "miaskitic" syenites, which contain zircon and titanite, to more agpaitic assemblages that contain complex Zr and Ti minerals such as catapleiite and lamprophyllite, respectively (Mitchell and Liferovich 2006). During the transition to hydrothermal conditions, the Na, Si and Al concentrations of the exsolved fluids vary inversely with the silica activity of the parent magma; in the extreme, either phase may be the solvent (Preston et al. 2003). The exsolved fluids from alkaline intrusions have been shown to both fenitise (alkali-metasomatise) adjacent country rocks (eg: Morogan and Woolley 1988; Sörensen and Laren 2001), and auto-metasomatise the parent pluton (Boily and Williams-Jones 1994; Mitchell and Liferovich 2006; Schönenberger et al. 2006). External fluids have also been invoked to explain the alteration of highly alkaline intrusions. For example, the alteration of primary and secondary sodic minerals at Strange Lake, Québec, to calcic minerals has been explained by the circulation of formation waters (Salvi and Williams-Jones 1996; Gysi and Williams-Jones 2013).

Albitisation is a common alteration type that is associated with several deposit types, e.g., IOCG deposits (Hitzman et al. 1992) and granite-hosted uranium deposits (Porto da Silveira et al. 1991), including deposits enriched in REE (Thompson 1988; Oreskes and Einaudi 1990), and commonly occurs as halos around crustal scale fluid conduits, as well as regionally (Boulvais et al. 2007). In many cases, it is genetically associated with anorogenic magmatism (Abdel-Rahman and El-kibbi 2001), including REE-bearing agpaitic rocks (Schilling et al. 2009). Albitised rocks therefore make promising exploration targets for REE deposits.

The highly altered and REE/HFSE-enriched upper parts of the Nechalacho Layered Alkaline Suite (NLAS), Northwest Territories, Canada, provide an excellent setting in which to investigate the origin and effects of alkali metasomatism in alkaline igneous systems hosting potentially economic REE mineralisation. The NLAS experienced three main alteration events, biotite-magnetite alteration, albitisation and hematitisation. These strongly affected its upper 300m. Albitisation, the focus of this study, records fluid pathways and late REE mobilisation.

Secondary albite supplants most earlier-occurring minerals; only relicts or pseudomorphs of primary minerals, such as microcline, remain. Primary feldspathoids and mafic phases, such as aegirine, were almost entirely replaced by very fine-grained minerals including biotite, chlorite, muscovite, fluorite, quartz and carbonate minerals; dissolution and brecciation textures are ubiquitous. The albitite surrounds and locally replaced the high-grade ore horizons within the Nechalacho. It also hosts REE minerals and the albite is highly enriched in gallium (Timofeev and Williams-Jones 2014). The Zr- and REE- bearing minerals present in the albitite are similar to assemblages found in miaskitic rocks, consisting dominantly of zircon, bastnäsite-(Ce), and monazite-(Ce). This study aims to determine the source of the albitising fluids, the conditions of albitisation and the effect of this process on the Nechalacho REE deposit.

Geological Setting

The Nechalacho Layered Alkaline Suite (NLAS) is the youngest and only silica-undersaturated intrusion of the Aphebian Blachford Lake Complex (BLC, Figure 1). The BLC lies 100km east of Yellowknife and 5km north of the north shore of the Great Slave Lake, and covers an area of 1500 km^2. Regionally, the Blachford Lake intrusive complex is one of approximately ten alkaline complexes that were associated with the breakup of the Sclavia supercraton (Bleeker and Hall 2007). The BLC was emplaced in the southwest of the Slave Craton within metapelites of the Yellowknife supergroup (Davidson 1978). It is a multi-phase alkaline system younging eastward, the units of which generally share steep contacts. Davidson (1972; 1978; 1982) subdivided the complex into the Caribou Lake Gabbro, the Whitman Lake Quartz Syenite, the Hearne Channel and the Mad Lake Granite, which make up the western lobe, and the Grace Lake Granite (GLG) and the Thor Lake Syenite (TLS), which make up the eastern lobe. The TLS is the only intrusion that deviates from the fractionation trend of the Blachford Lake intrusive suite, and was considered by Davidson (1982) to represent a roof pendant cumulate. In the early 1980s, exploration for rare-elements lead to the discovery of nepheline syenite (formerly referred to as the Lake Zone and now as the Nechalacho Layered Suite, NLAS) at the centre of the TLS (Trueman et al. 1988). This unit was described as a subsolvus, nepheline monzosyenite to feldspathic ijolite by Pinkston and Smith (1995) and subsequently as a layered alkaline complex by Sheard et al. (2012). Sinclair et al. (1994) reported a U-Pb isotopic zircon age for the GLG of

2176.2 ± 1.3 Ma. Recent U-Pb dating yielded ages of 2176.8 ± 1.6Ma for the TLS and 2164 ± 11Ma (Mumford 2013) and 2175.6 ± 3.1Ma (Möller and Williams-Jones 2013) for the NLAS.

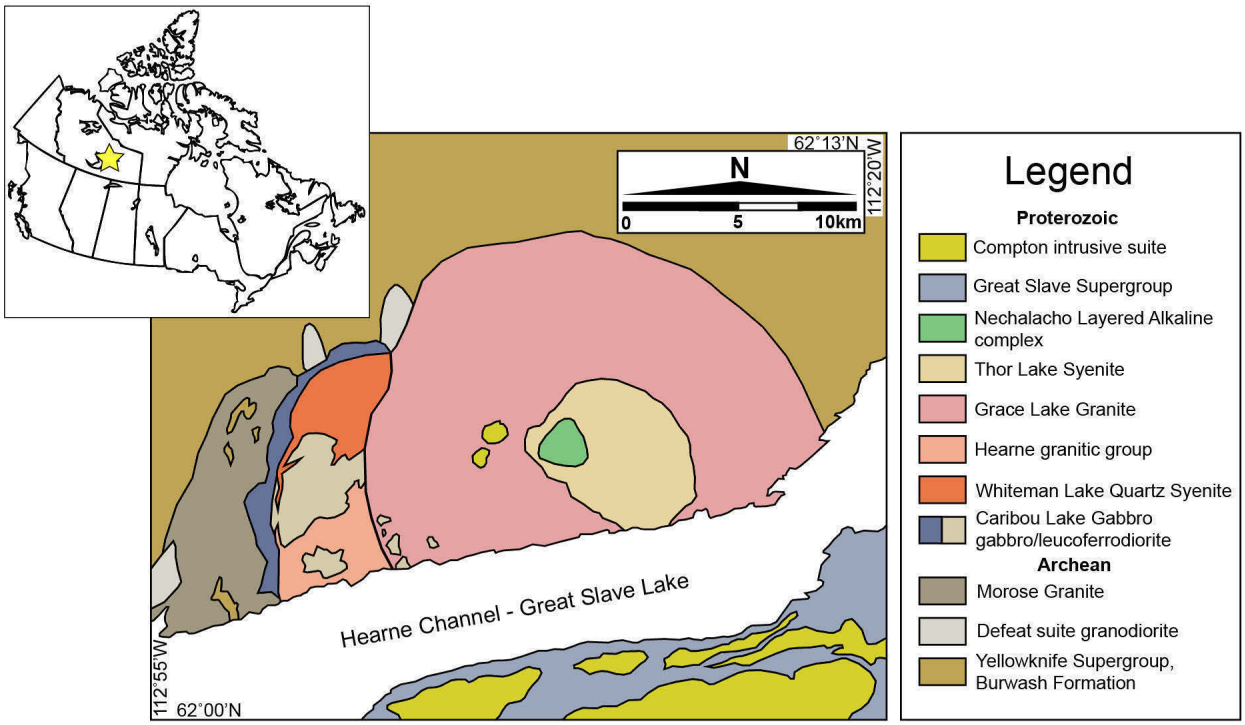

Figure 1: Map showing the location and geology of the Blachford Lake Complex, after Davidson (1972) and Mumford (2013).

The NLAS is roughly 2km (Figure 2) in diameter at surface, and is hosted by the TLS with which it shares a sharp, outwardly dipping contact. Five primary units make up the NLAS stratigraphy: a sodalite cumulate, a strongly altered aegirine-nepheline syenite, a trachytic microcline-phyric nepheline syenite (foyaite), a REE- and HFSE mineral-bearing zirconosilicate cumulate unit (upper and basal mineralised zones), and relatively unaltered aegirine, nepheline and sodalite syenites (Sheard et al. 2012). These five units form repetitive layers of tens of centimetres to tens of metres in thickness, sharing either sharp or gradational contacts with each other. In the thinner layers, internal grading of grain-size is evident. Overall, the grain-size ranges from fine to coarse to megacrystic, with microcline crystals, for example, ranging in length from 0.5 cm in the finest-grained layers to >10cm in the coarsest-grained, pegmatitic layers.

The sodalite syenite forms the uppermost and outermost marginal unit of the NLAS, but also occurs as lenses lower in the NLAS, sharing gradational contacts with other units. A K-feldspar

pegmatite developed at the contact between the upper NLAS and the GLG, with nepheline syenite infilling open space in the pegmatite. The sodalite syenite is made up of closely packed cumulate sodalite and aegirine crystals with interstitial albite. This unit dips steeply at the margin of the NLAS, and is up to 78m thick. Below the sodalite syenite is the aegirine syenite, which also contains significant proportions of microcline and albite and pseudomorphs after sodalite and nepheline, and is the dominant rock type within the upper 300m of the complex. In the uppermost 100m, microcline crystals in this unit decrease in size erratically downwards from >10cm to <1cm in diameter. The foyaite is a fine- to coarse-grained trachytic, microcline- or nepheline-phyric unit. Within the upper 300m of the complex, the foyaite has a highly altered groundmass of biotite, hematite or rarely magnetite, and albite. The foyaite hosts the zirconosilicate cumulates of the lower ore zone. This is evident from the alignment of microcline phenocrysts in both the foyaite and the underlying zirconosilicate ore zone. Nepheline-phyric foyaite, lujavrite, ijolite and biotite-nepheline syenite comprise the bulk of the NLAS below the lower ore zone. The lujavrite is composed of fine-grained albite and microcline laths and aegirine needles, aligned and wrapped around idiomorphic nepheline crystals. Ijolite is a coarse-grained rock composed of anhedral sodalite, nepheline and aegirine. Mono-mineralic aggregates of fine translucent to white albite laths occur at 2 to 5 cm vertical intervals within the aegirine-nepheline syenite and lujavrite.

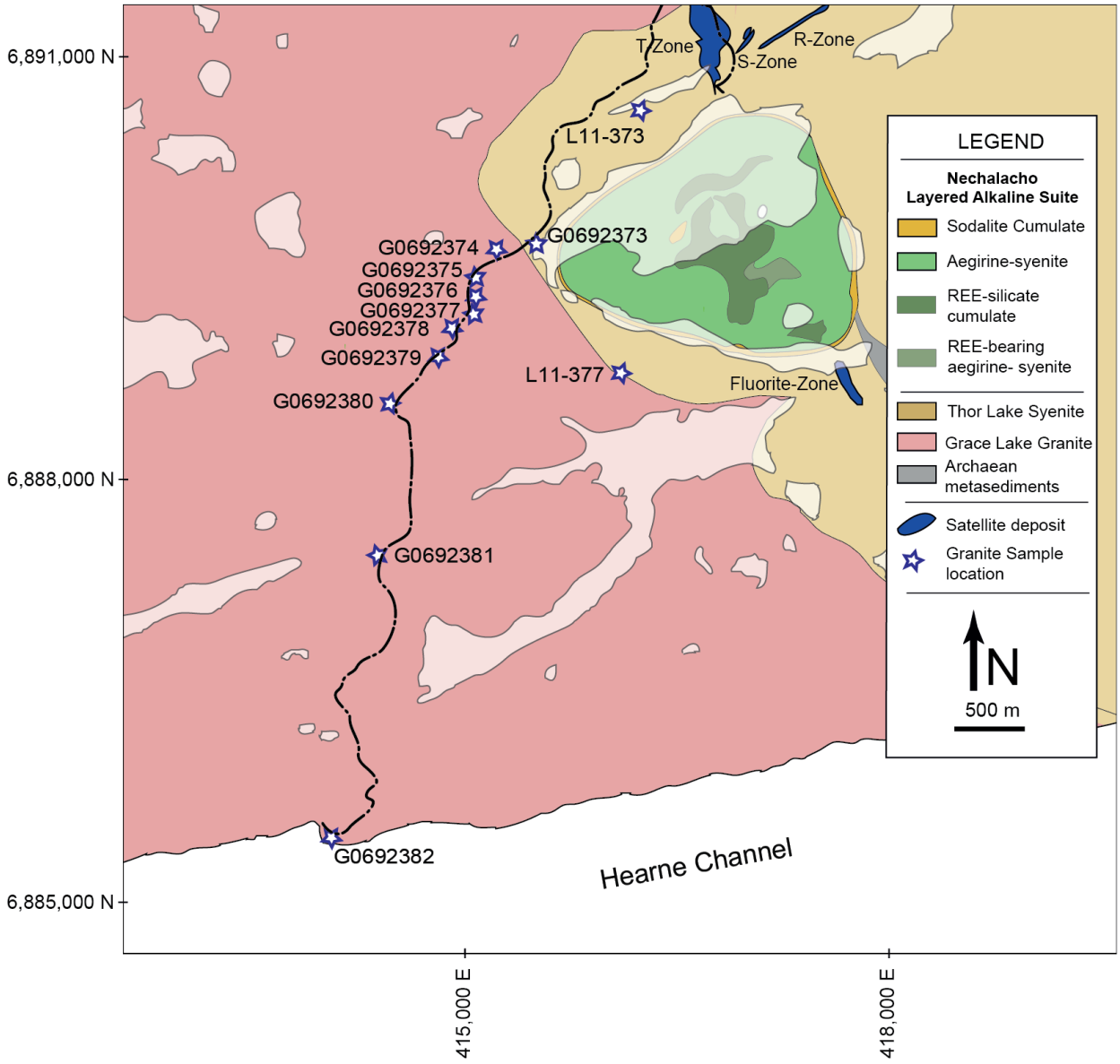

Figure 2: Geological map of the Nechalacho Layered Alkaline Suite and surrounding Thor Lake syenite and Grace Lake granite, after Davidson (1972) and Mumford (2013). Outcrops that were sampled are indicated by sample numbers. Locations of drill holes that were sampled for fenitised granite are also shown

The Nechalacho deposit, hosted within the NLAS, is one of the more important rare element deposits in the world, with a measured and indicated resource of 121.26 Mt grading 1.50% REE_2O_3 (0.25% $HREE_2O_3$, including Y_2O_3), 2.56% ZrO_2, 0.34% Nb_2O_5 and 0.03% Ta_2O_5 (Ciuculescu et al. 2013). The ore horizons form two distinct types of zircon-bearing cumulates. These are referred to as the "Upper Ore Zone" and "Basal Ore Zone" based on their stratigraphic arrangement, and are distinguished by textures and mineralogy. The Upper Ore Zone contains small euhedral zircon crystals, which form thin (mm scale) discontinuous layers that wrap

around phenocrysts of other minerals, such as aegirine and microcline (now pseudomorphs containing microcrystalline albite and hematite; Sheard et al. 2012). The Basal Zone comprises pseudomorphs of a cumulate phase interpreted to be eudialyte; the secondary phases contained therein are zircon, fergusonite-(Y), bastnäsite-(Ce), parisite-(Ce)/synchysite-(Ce), allanite-(Ce), albite, quartz, biotite, fluorite, kutnahorite ± minor hematite. The ore mineralogy of the two ore zones is similar: zirconium is hosted mainly by zircon, niobium by ferrocolumbite and fergusonite-(Y); yttrium and the HREE by fergusonite-(Y) and zircon, and the LREE by monazite-(Ce), allanite-(Ce), bastnäsite-(Ce) and parisite-(Ce)/synchysite-(Ce). The two ore horizons are geochemically different; the Basal Zone is richer in HREE, has higher Fe^{2+} relative to Fe^{3+} and is more alkaline in character (Sheard et al. 2012).

Discrete hydrothermal satellite deposits of albite ± polylithionite, bastnäsite-(Ce), monazite-(Ce), zircon and ilmenite (Černý and Trueman 1985) are hosted within the GLG and TLS peripheral to the NLAS. The largest of these deposits, the T-Zone, has received considerable attention. It contains 1.1 million tons grading 0.71 wt. % REE_2O_3, 0.48 wt. % BeO and 0.53 wt. % Nb_2O_5 (Paul and Stubens 2009). Rocks hosting this deposit have been subdivided into four main lithological units (Černý and Trueman 1985). The outermost of these units is a pink shell of albite and microcline megacrysts (Wall Zone), which is in sharp contact with the host GLG. Nested within the Wall Zone are the Lower and Upper Intermediate Zones, composed of albite and quartz with significant proportions of polylithionite, $K(Li_2Al)Si_40_{10}(F,OH)$, magnetite, riebeckite, aegirine and ankerite. The Upper Intermediate Zone is distinguished by less albite and abundant polylithionite, and is interfingered with the Lower Intermediate Zone. The central unit is composed almost entirely of quartz. The other satellite deposits adjacent to the T-Zone, namely the R-Zone, S-Zone and Fluorite Zone, display similar mineral assemblages to the T-Zone. The relatively close proximity of these deposits to the NLAS suggests a genetic association with the latter, and alludes to its presence at depth within the granite (Pinkston and Smith 1995; Sheard et al. 2012).

Methodology

Sampling was carried out on site at the Nechalacho deposit. Access to drill core, which was provided by Avalon Rare Metals Inc., was essential as outcrops of the NLAS are poor and few.

Rock samples for whole rock analysis and thin sections were selected so as to represent the full range of textures observed, and also were selected at predetermined intervals from a large number of drill holes covering most of the layered complex and some of the adjacent GLG. Whole rock analyses were undertaken at ALS labs. X-ray Fluorescence and Inductively Coupled Plasma Mass Spectrometry were used for major and trace element analysis, respectively. Iron oxide (FeO) was determined using sulphuric and hydrofluoric acid digestion with titration finish. Mineral separates for isotopic analysis were hand-picked, cleaned using a dilute HCl solution and analysed for purity using a Bruker D5000 cobalt tube sol-x detector X-ray diffraction analyser at UQAM/GEOTOP. Oxygen and Hydrogen isotope analyses of microcline, albite and quartz were performed by the isotope laboratory in the Department of Geological Sciences at Queen's University, Kingston. The oxygen isotope values represent analyses of the minerals, whereas δD values were obtained by decrepitation and measurement of the isotopic composition of the included fluids. *In situ* chemical analyses of minerals were conducted on thin sections at McGill University using a JEOL JXA-8900L electron microprobe equipped with five wavelength dispersive spectrometers (WDS) and a Si(Li) EDS detector. Concentrations of Na_2O, K_2O, SiO_2, Al_2O_3, Fe_2O_3, MgO, MnO, CaO, Rb_2O, SrO and Ga_2O_3 were measured in quartz, albite, microcline and aegirine; concentrations of these oxides together with those of F and Cl were measured in biotite. Albite, microcline, nepheline and sodalite were analysed using a 10μm beam diameter, a 15keV excitation voltage and a $3x10^{-8}$ A beam current, whereas biotite and aegirine were analysed using a 10μm beam, a 20keV excitation voltage and a $3x10^{-8}$ A beam current. Detection limits ranged from 120 to 220 ppm, except for Sr, for which the detection limit was 500 to 550 ppm (Sr). Dwell times ranged from 20s for most major and minor elements to 150s for Ga. Trace element concentrations in albite, microcline, sodalite, fluorite and aegirine were analysed by laser-ablation inductively-coupled plasma mass-spectrometry (ICP-MS), using a Photon-Machines Analyte193 excimer laser ablation system and an Agilent 7700 quadrupole ICP-MS at the Geological Survey of Canada in Ottawa. A beam with a diameter of 138 μm or 172 μm for albite and K-feldspar, and 52 μm to 69 μm for the other minerals, at 10Hz was used. The mass spectrometric data were reduced using *GLITTER!* software. Trace element detection limits for individual analyses varied by 0.4 ppm to 0.5 ppb. The absolute detection limit was <10 ppb.

Alteration of the Grace Lake Granite

Hydrothermal alteration affected all samples of the GLG, TLS and NLAS that were studied. Fenitisation of the GLG is evident in hand samples within 2km of the NLAS, and increases in intensity towards the NLAS. It is manifested by the replacement of K-feldspar by albite, and riebeckite with magnetite (Figure 3a). These replacements were complete in the first two hundred metres adjacent to the NLAS and partial at greater distance. The TLS is texturally identical to the GLG and differs mineralogically from it only in the absence of quartz (Figure 3b). The contact may either be sharp as in Figure 3b, or gradational with the quartz content of the GLG decreasing to zero over a distance of up to 12 m.

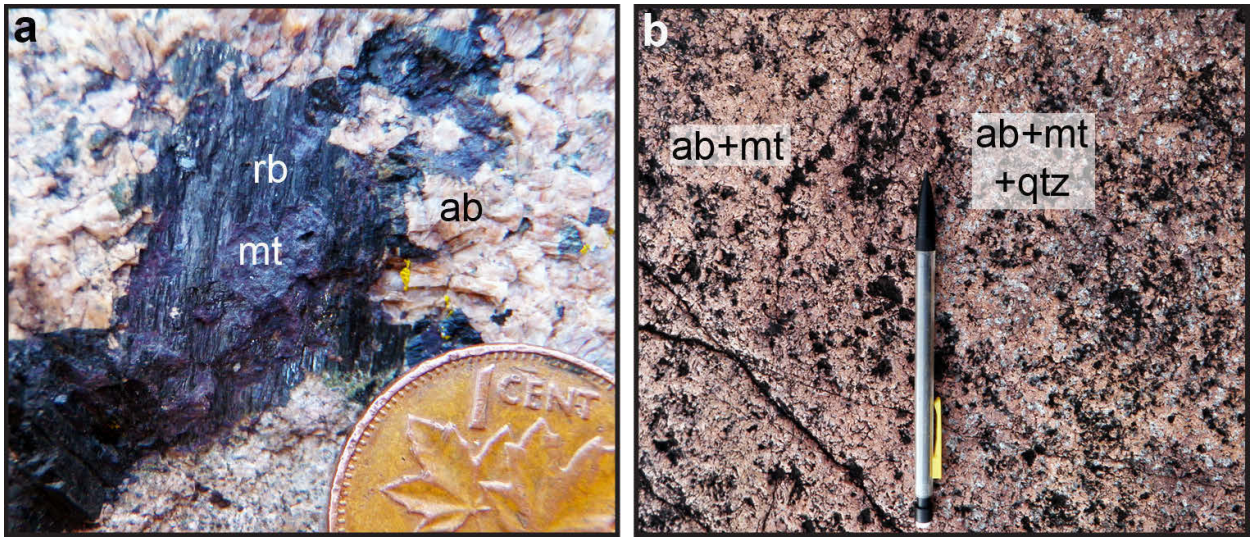

Figure 3: Mineralogical changes within the TLS and GLG adjacent to the NLAS in outcrop. a) riebeckite replaced by magnetite interstitial to albitised K-feldspar (penny for scale) and b) contact between texturally identical TLS (left) and GLG (right) (pencil for scale); ab = albite, mt = magnetite, qtz = quartz, rb = riebeckite.

Veins are common in the fenitised GLG and TLS, within 2 km of the NLAS. Chlorite forms veins and veinlets (Type A veins), and occurs as well in the matrix of breccias (Figure 4a). Feldspar and mafic minerals in the host rocks were replaced by chlorite, particularly in proximity to chlorite veins. Within 300 m of the NLAS, two other vein-types are observed, which crosscut the Type A veins. The first of these comprises mm-thick discontinuous veinlets composed of fluorite, calcite and hematite (Type B veins), which are surrounded by haloes of albite, aegirine and fluorite up to 3cm wide (Figure 4b). Calcite-dominant veins (Type C) containing significant pyrite and chalcopyrite comprise the second of these vein-types, and are thicker, up to several cm wide, with alteration haloes greater than a metre thick (Figure 4c). In these haloes, all

ferromagnesian minerals and quartz have been removed or replaced by calcite, and primary K-feldspar has been albitised. Crosscutting relationships between Type B and Type C veins were not observed.

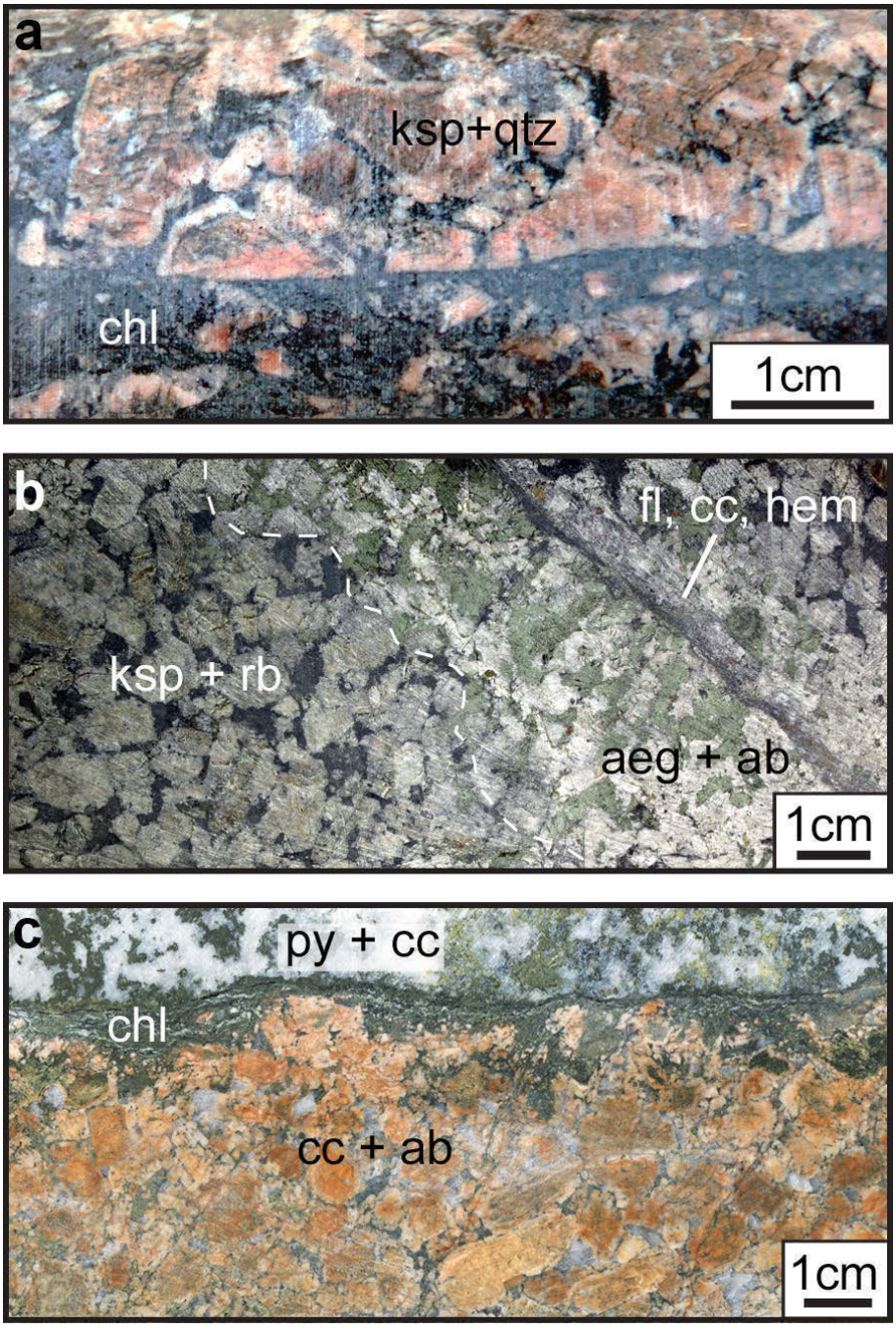

Figure 4: Common vein types within the GLG in hand samples: a) a chlorite vein cutting partially sericitised and chloritised K-feldspar megacrysts; b) a fluorite,-calcite-hematite vein with an albite and aegirine alteration halo; and c) a calcite-pyrite vein (white, above) and chlorite dominant vein margin (green) with an albite-calcite altered vein halo (orange, below). ab = albite, aeg = aegirine, cc = calcite, chl = chlorite, fl = fluorite, hem = hematite, ksp = K-feldspar, rb = riebeckite.

Mass Changes during fenitisation of the GLG

In order to evaluate the potential size and nature of the pervasive fenite aureole around the NLAS, samples were collected and analysed at exponentially increasing distance from the NLAS. This permitted mass changes to be evaluated as a function of distance from the presumed source of the fluids (the NLAS). As the GLG and TLS do not display any evidence of textural change on approaching the NLAS, e.g., porosity development, it is reasonable to assume that volume was roughly conserved and that any differences in element contents per unit volume of rock analysed approximate absolute changes in these contents. Mass changes of trace elements, including the REE, are poorly correlated with distance from the NLAS. The most striking change with increasing distance from the NLAS is the decrease in the mass of Na_2O and to a lesser extent the sum of the masses of CaO, $Fe_2O_{3(t)}$, MgO and Al_2O_3, and the corresponding increase in SiO_2 content. (Figure 5). There is no apparent change in the concentration of K_2O with SiO_2 content. However, there is a weak positive correlation between K_2O and Na_2O contents. The REE content does not appear to vary with distance from the NLAS (Figure 5b). The onset of these changes occurs approximately 1 km from the NLAS.

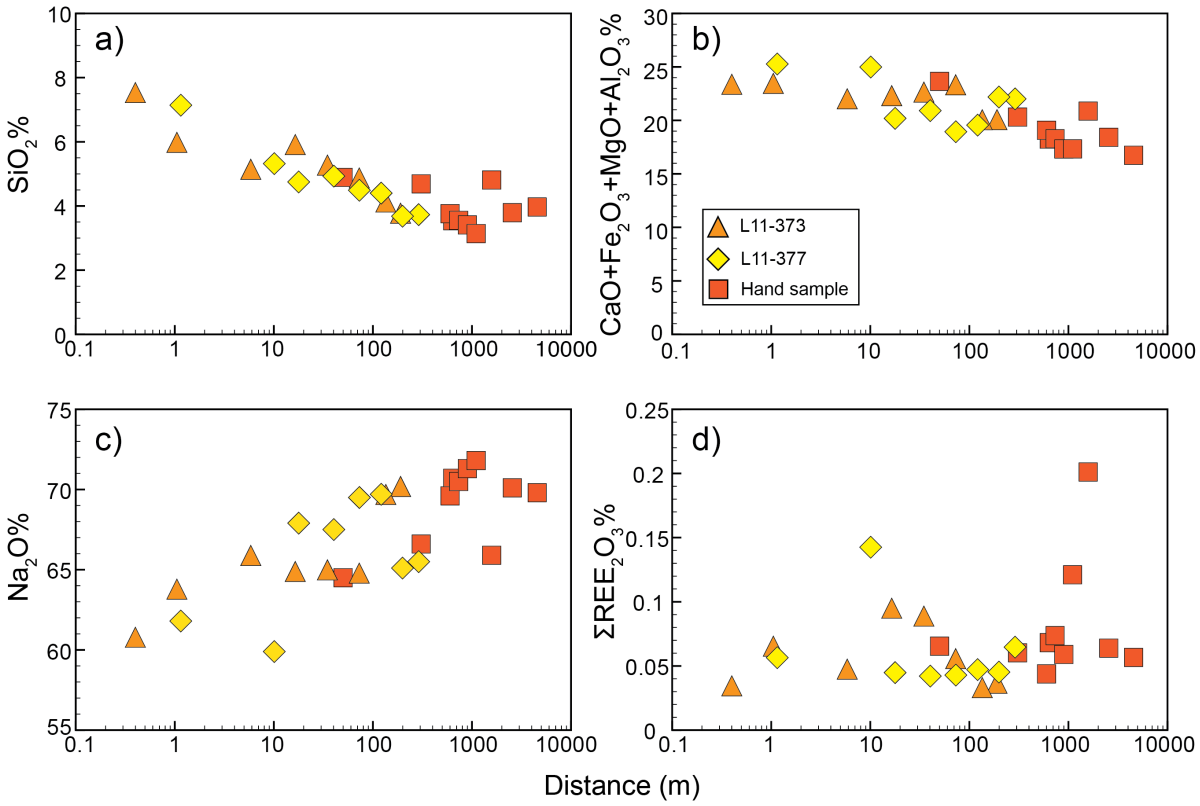

Figure 5: Whole rock compositions of samples of the GLG and TLS versus distance from the NLAS.

Mass changes accompanying the alteration associated with Type B and C veins (vein-related fenitisation B and C) were evaluated by comparing the composition of samples in the alteration haloes to samples of GLG/TLS immediately adjacent to the haloes. This was done using the isocon method of Grant (1985), which involves identifying a set of immobile elements and normalising the compositions to one of these elements. Immobile elements were identified from linear distributions of elements in isocon plots relating their contents in altered rocks to those in rocks that were not subject to vein-associated alteration (Figure 6). As the primary textures of the protolith, notably those involving feldspar, are perfectly preserved in the altered rocks, the isocon was predicted to be close to the line representing constant volume. This, indeed, is the case for the halo around both the Type B and Type C veins depicted in Figure 6. The apparent small loss of Al_2O_3 (an oxide that is commonly immobile) in the halo of the Type B vein likely reflects heterogeneity in the sampling due to the relatively large grain-size of the feldspars and mafic minerals, whereas the apparently large addition of TiO_2 is probably an artifact due to a nugget effect (Figure 6a). The apparent losses of Zr, Hf and TiO_2 in the halo of the Type C vein are also interpreted to be nugget effects (Figure 6b). The equation of Grant (1985) was used to calculate

the relative gain/loss of mobile components, assuming constant volume ($\Delta C_i/C^O$) = $(M^A/M^O)(C^A{}_i/C^O{}_i) - 1$.

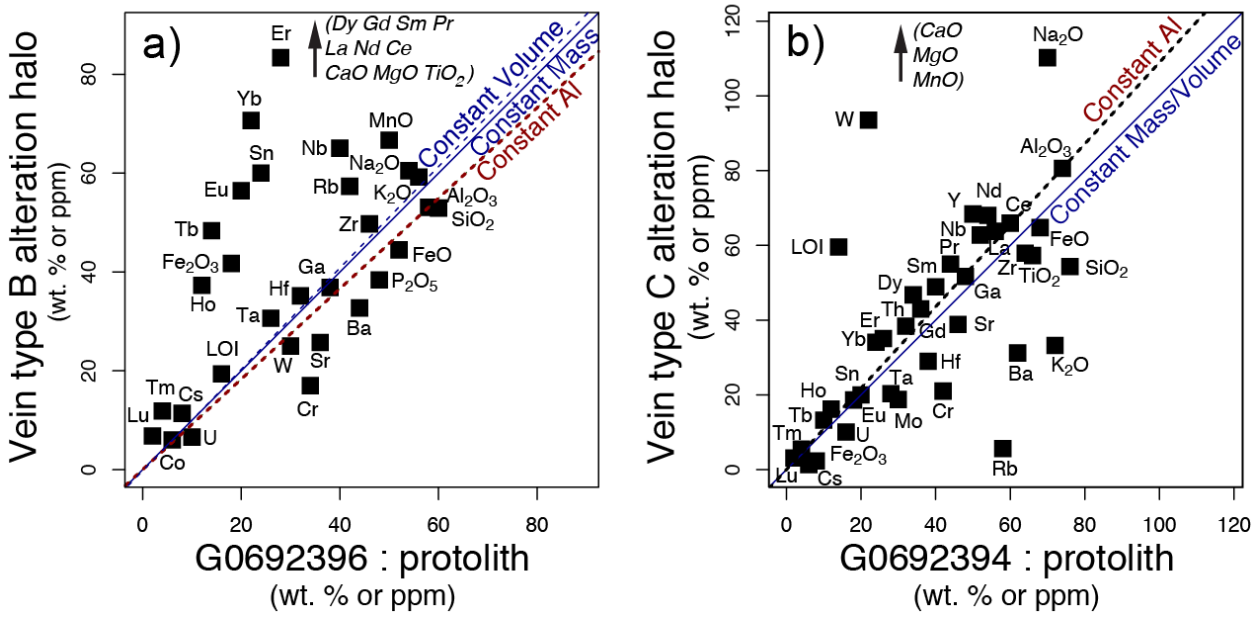

Figure 6: Isocon plots for a) a Type B vein halo versus adjacent unaltered rock and b) a Type C vein halo versus the corresponding unaltered rock.

The fenite haloes around Type B and C veins underwent contrasting mass changes (Figure 7). The former haloes were enriched relative to the unaltered protolith in Mg, Ca, Fe^{3+}, Mn, Na and K (261%, 131%, 125%, 29.9%, 9.11% and 2.30%, respectively) and depleted in Si and Fe^{2+} (14.1% and 16.6% respectively) (Figure 6a, Figure 7a). Trace element concentrations in the fenite adjacent to Type B veins underwent variable mass changes. Base metals, like Mo and Zn, posted gains (221% and 27.5 respectively) as did the REE (average 213% gain). Among the LIL elements, Cs and Rb, experienced mass gains (38.6% and 33.0% respectively) and Ba experienced a mass loss of 27.6% (Figure 7a). Fenite C underwent extreme gains in Mg, Ca, Mn, and Na (829%, 706%, 267% and 57.7% respectively), and losses in Fe^{2+}, Si, K and Fe^{3+} (4.60%, 28.4%, 53.8% and 71.1% respectively). The LIL elements Ba, Cs and Rb experienced mass losses (49.6%, 77.4% and 90.3% respectively). The REE experienced mass gains (between 14.0% for La and 55.6% for Lu). Uranium posted mass losses in both vein haloes (36% and 37% for Vein type B and C, respectively, Figure 7b).

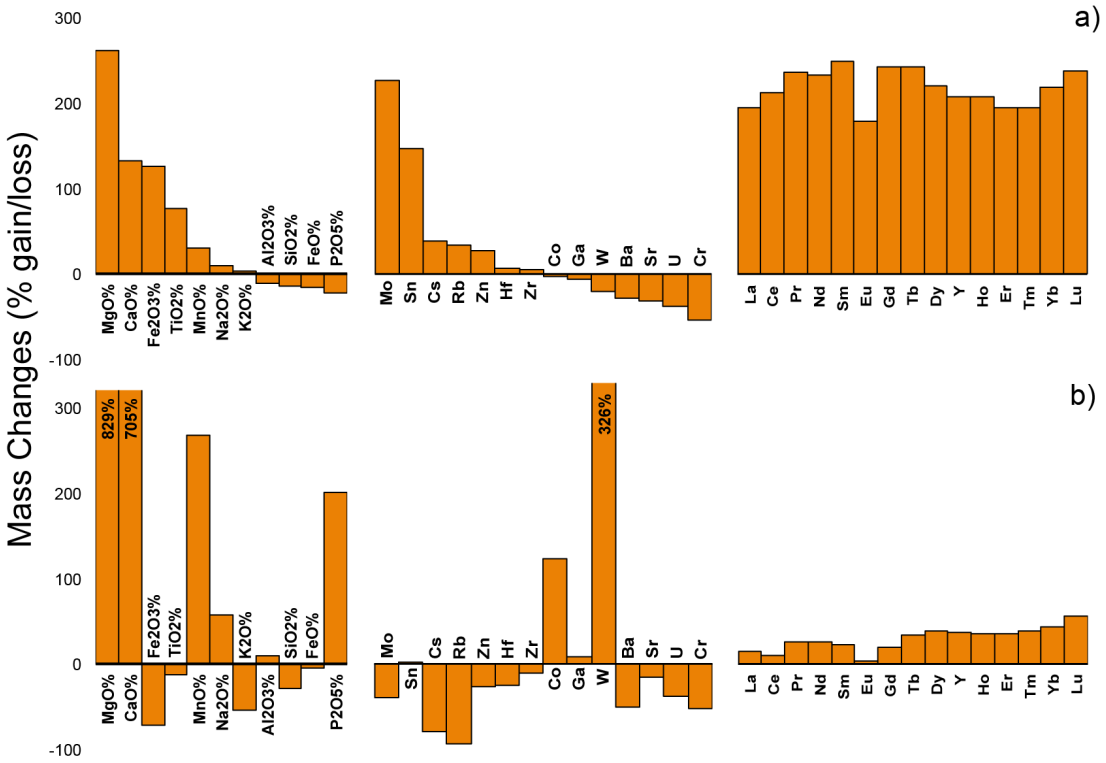

Figure 7: Mass changes in percent (%) relative to the unaltered Grace Lake Granite in alteration haloes around the Type B and C veins depicted in Figure 6: a) alteration halo around the Type B vein and b) alteration halo around the Type C vein. The mass changes were calculated assuming that volume was conserved. See text for further detail.

Alteration of the Nechalacho layered alkaline suite

Alteration of the NLAS was pervasive within its upper 300 m, and generally left only textural relicts of the primary minerals. Magnetite and biotite are the main secondary minerals in the Upper Ore Zone. Spatially, magnetite and biotite are associated with zircon, fergusonite-(Y), ferrocolumbite, allanite-(Ce), monazite-(Ce) and bastnäsite-(Ce) (Figure 8a). Within the Basal Ore Zone, magnetite is the dominant alteration mineral, biotite is subordinate and hematite is locally important. Magnetite forms granular masses of euhedral crystals in the Upper Ore Zone (Figure 8a). These crystals commonly display an atoll texture, in which the cores were preferentially altered to biotite, muscovite, quartz, aegirine and/or allanite (Figure 8b). Locally, magnetite forms pseudomorphs after aegirine. Biotite occurs as aggregates of crystals ranging from 10 to 100μm in diameter that are commonly altered to chlorite (Figure 8c). Morphologically similar biotite is also observed throughout the upper aegirine syenite unit within large patches of dark groundmass surrounding microcline and iron-oxide pseudomorphs after

aegirine (Figure 8d); nepheline and sodalite are absent from the upper portion of the NLAS below the sodalite roof-cumulate. Biotite veinlets commonly cut microcline crystals, and the latter are commonly embayed by biotite crystals (Figure 8e). Hematite partially or completely replaced most minerals, including aegirine, K-feldspar and magnetite, and also occurs in pseudomorphs after inferred eudialyte (Sheard et al. 2012), together with biotite, quartz and zircon. Specular hematite, or finer-grained hematite, embayed or entirely pseudomorphed aegirine (Figure 8) and is accompanied in the pseudomorphs by quartz and minor albite.

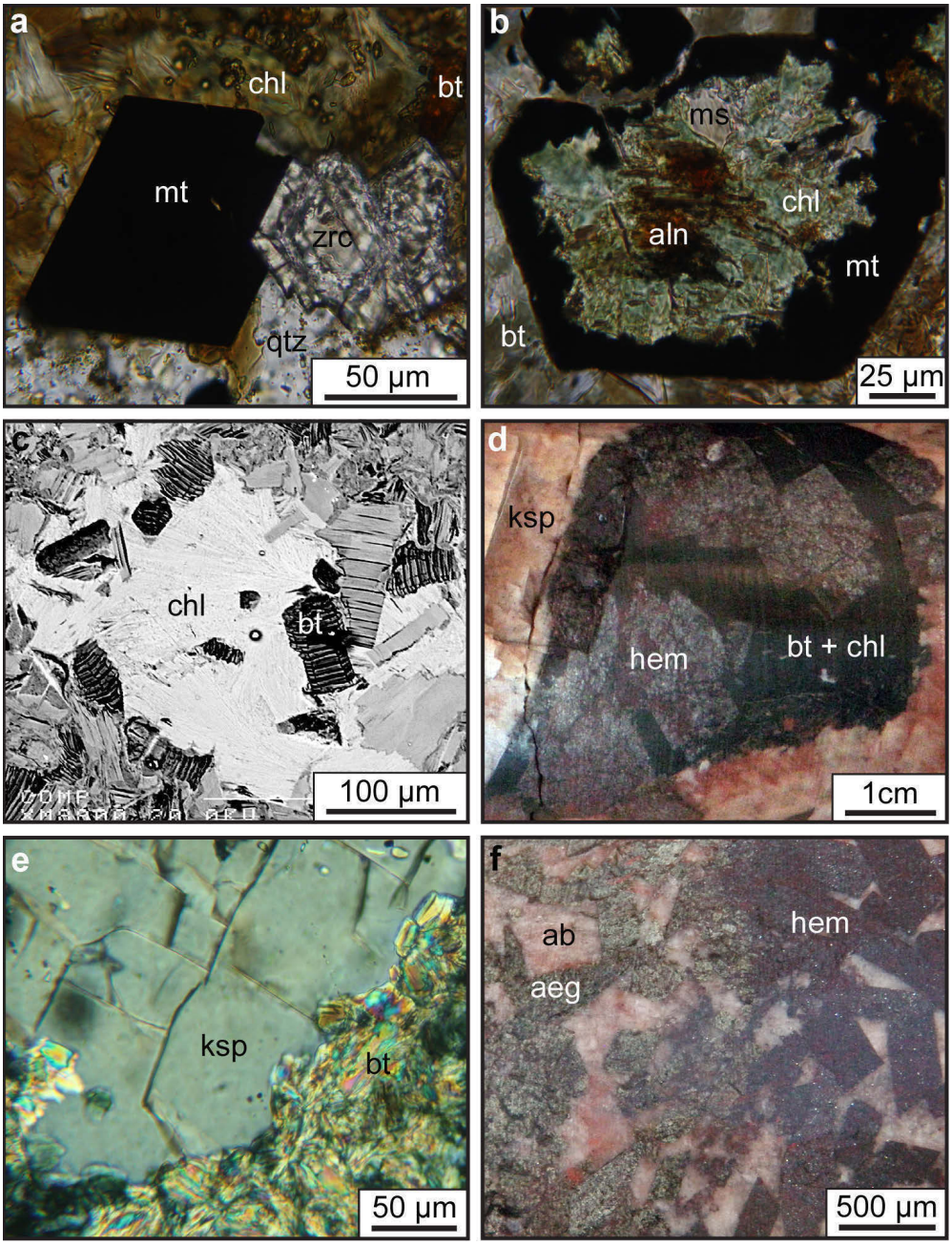

Figure 8: Images showing textural relationships among primary and secondary minerals within the NLAS. a) euhedral magnetite and zircon grains within the Upper Ore Zone (transmitted light); b) relicts of biotite including embayed crystals in chlorite (backscatter electron X-ray image); c) fine-grained biotite and chlorite interstitial to K-feldspar and pseudomorphs containing hematite after aegirine; d) embayments in K-feldspar filled by biotite (transmitted light, cross-polars; e) magnetite grain displaying core replacement by muscovite, chlorite and allanite (transmitted light, cross-polars); and f) alteration front showing aegirine (left) progressively altered to hematite (right); ab = albite, aeg = aegirine, aln = allanite, bt = biotite, chl = chlorite, fl = fluorite, hem = hematite, ksp = K-feldspar, ms = muscovite, mt = magnetite, qtz = quartz, zrn = zircon.

Biotite in the NLAS is dominantly a solid solution between phlogopite and annite end-members with only small proportions of the Al end-members, eastonite and siderophyllite. Variations in

composition, which are considerable, therefore mainly reflect changes in XFe. Nonetheless, there is a small but systematic increase in the proportion of Al(IV) with increasing XFe (Figure 9a). Biotite in the Basal Ore Zone ranges in composition from close to end-member phlogopite to biotite with a XFe of 0.41, whereas in the Upper Ore Zone, the biotite is richer in the annite component, with XFe ranging from 0.58 to 0.27. The composition of biotite in the altered nepheline syenite mirrors that of the Upper Ore Zone biotite with XFe between 0.56 and 0.25. In the foyaite and albitite, the biotite has XFe between 0.60 and 0.45, and between 0.63 and 0.50, respectively. Biotite from the different units in the NLAS can also be distinguished on the basis of its halogen content (F, Cl). In the Basal Ore Zone, the content of F ranges from 0.97 to 0.40 apfu and the Cl content from 0.068 to 0.0012 apfu (Figure 9b). Similar ranges are observed in biotite from the Upper Ore Zone, 1.0 to 0.13 and 0.077 to 0.0020 apfu, respectively. The halogen contents of biotite in the aegirine syenite are also similar, from 0.91 to 0.059 apfu F and 0.077 to 0.0052 apfu Cl. By contrast, biotite in the albitite has significantly lower concentrations of F and Cl, from 0.76 to 0.33 and from 0.056 to 0.012 apfu, respectively. Even lower concentrations of F and Cl were observed in biotite from the foyaite, i.e., from 0.51 to 0.32 and from 0.056 to 0.0071 apfu, respectively. Values of XFe versus XF for individual biotite crystals lie below the line representing XF_{max} of the F-Fe avoidance rule, where XF_{max}=1-XFe (Figure 9c). Furthermore, most biotite compositions lie in the region of "short-range order", where preferential association of Mg with F and Fe with OH is predicted from the F-Fe avoidance rule (Mason 1992). Most of the biotite in the Basal Ore Zone, as well as an appreciable proportion of the biotite of the aegirine syenite and Upper Ore Zone has a composition that lies in the "disorder permitted" region where composition is not constrained by the F-Fe avoidance rule.

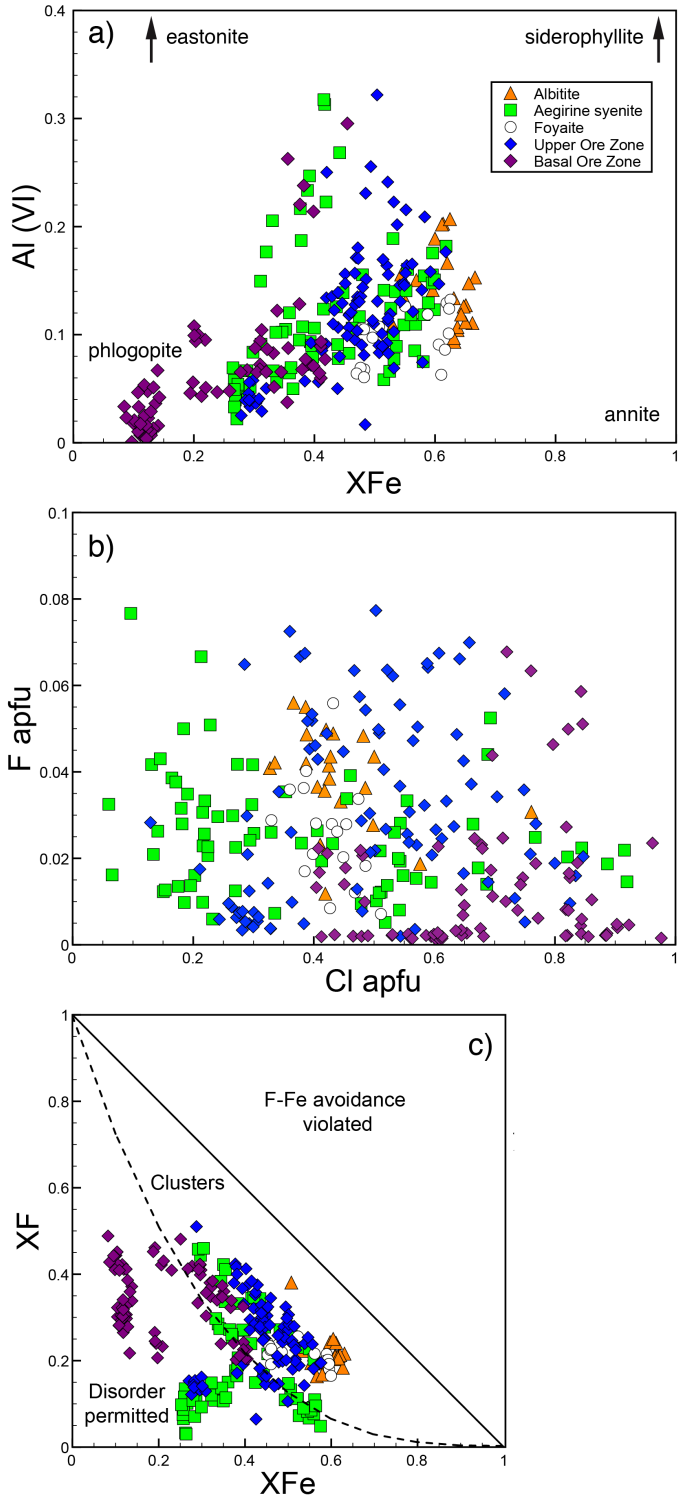

Figure 9: Diagrams showing the composition of biotite within distinct units of the upper 300m of the NLAS: a) The mole proportion of Al(VI) in biotite from the albitite, altered syenite, foyaite, Basal Ore Zone and Upper Ore Zone of the NLAS, versus the mole fraction Fe (XFe), b) the proportion of F versus that of Cl per formula unit in biotite from the albitite, altered syenite, foyaite, and Basal and Upper ore zones of the NLAS, c) the mole fraction of F (XF) versus that of Fe (XFe) in biotite from the albitite, altered syenite, foyaite, and the Basal and Upper ore zones of the NLAS; the bounding lines for the ordering of biotite are from Mason 1992.

Albitisation overprinted magnetite-biotite alteration but is most evident as the replacement of microcline by albite (Figure 10a). Secondary albite is ubiquitous within the upper 300m of the NLAS and also is present in the surrounding GLG. Carbonate minerals (ankerite, calcite) and muscovite are locally abundant and represent a late stage alteration that overprinted the other alteration types, including albitisation (Figure 10b). Where altered, biotite was replaced mainly by chlorite (Figure 8e), and to a lesser extent by fluorite, quartz and muscovite. Quartz and fluorite occur together (Figure 10c,d), the latter commonly in association with REE- and HFSE-bearing minerals such as bastnäsite-(Ce) and monazite-(Ce) (Figure 10e), rutile, zircon, and ferro-columbite (Figure 10f), and sulphides such as pyrite, pyrrhotite, sphalerite and galena (Figure 11a). Chlorite replaced fluorite (Figure 11b); chlorite commonly occurs with syntactic intergrowths of Ca-bearing REE-fluorocarbonate (either parisite-(Ce) or röntgenite-(Ce)) (Figure 11c). Muscovite is dominant within the sodalite cumulate unit, and occurs mainly with chlorite in pseudomorphs after sodalite (Figure 11d). Muscovite also occurs throughout the GLG and TLS as a replacement of biotite and K-feldspar.

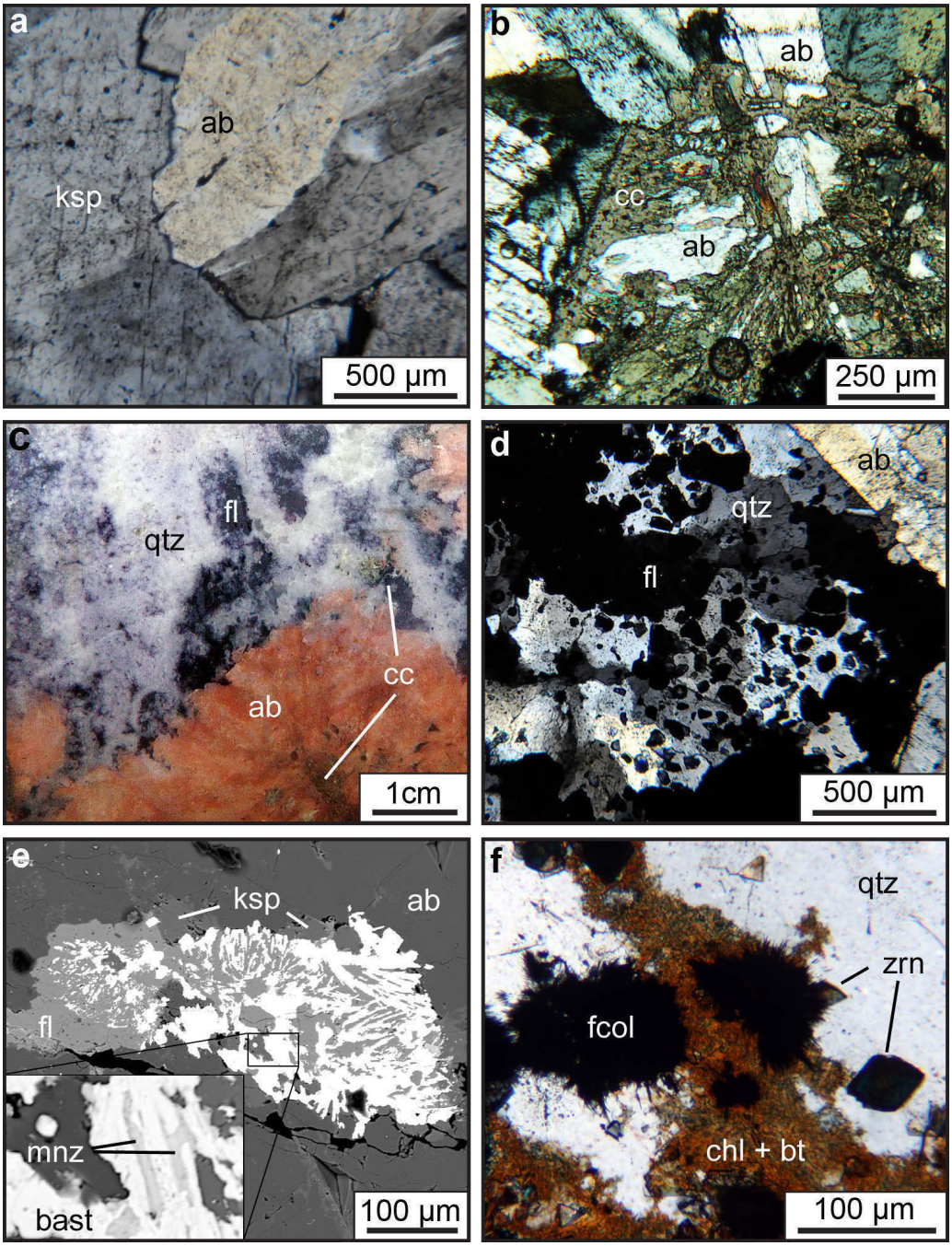

Figure 10: Alteration textures within the albitite and Upper Ore Zone. a) secondary albite embaying K-feldspar (transmitted light, cross-polars; b) Relict albite in late-stage calcite (transmitted light, cross-polars); c) intergrown fluorite and quartz with minor calcite interstitial to secondary albite (hand sample photograph); d) fluorite and quartz interstitial to secondary albite (transmitted light, cross-polars); e) acicular bastnäsite-(Ce) and monazite-(Ce) intergrown with fluorite in a vug interstitial to secondary albite (X-ray backscatter image); f) zircon and ferro-columbite in contact with quartz and chlorite from the Upper Ore Zone (transmitted light, cross-polars); ab = albite, bast = bastnäsite-(Ce), bt = biotite, cc = calcite, chl = chlorite, fcol = ferrocolumbite, fl = fluorite, hem = hematite, ksp = K-feldspar, ms = muscovite, mnz = monazite-(Ce), qtz = quartz, zrn = zircon.

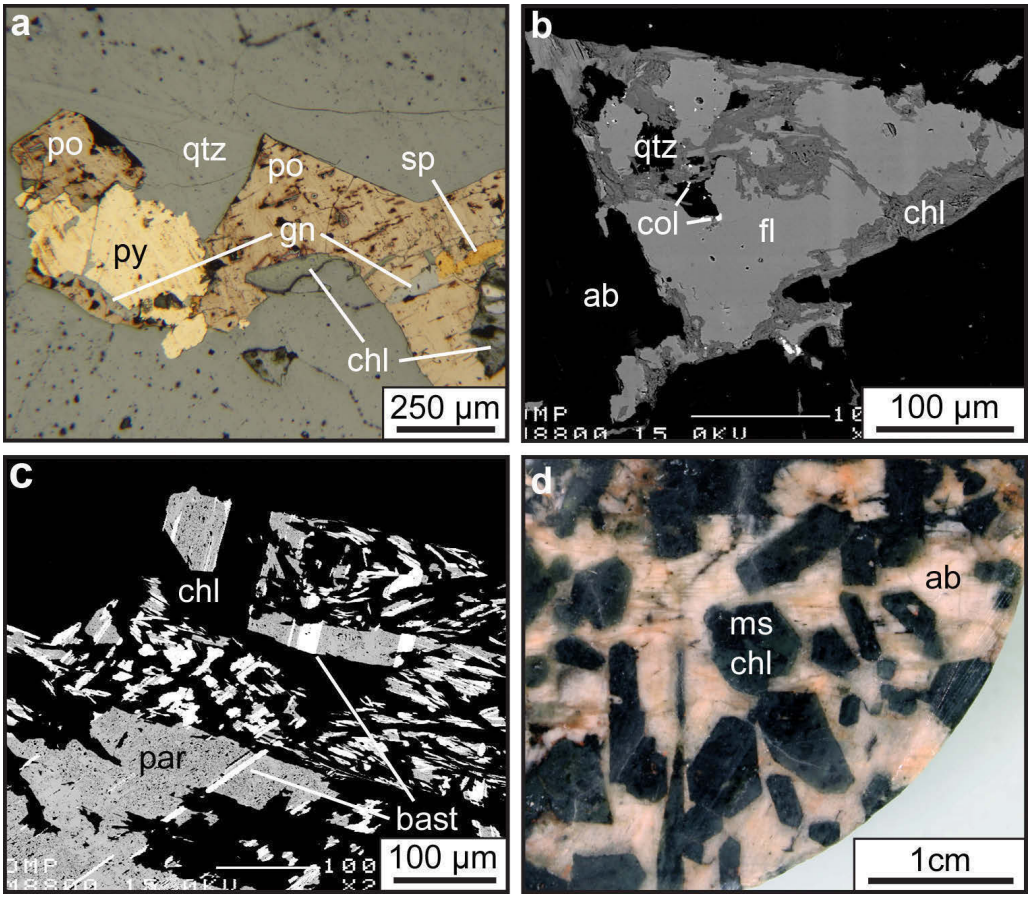

Figure 11: Late-stage alteration textures within the albitite. a) pyrite, pyrrhotite, galena and sphalerite interstitial to quartz (reflected light); b) chlorite embaying fluorite in a vug interstitial to albite (transmitted light); c) syntactic intergrowth of Ca-bearing fluorocarbonate embayed by chlorite (X-ray backscatter image); d) fine-grained muscovite-chlorite assemblage forming pseudomorphs after sodalite and aegirine, accompanied by interstitial secondary albite; ab = albite, bast = bastnäsite-(Ce), chl = chlorite, col = columbite, fl = fluorite, gn = galena, ms = muscovite, par = parisite-(Ce), po = pyrrhotite, qtz = quartz, sp = sphalerite.

The albitite

The albitite is a porous, pink rock (>50% pink, bladed albite, <10% ferromagnesian minerals), which occurs where albitisation was most intense, and is found mainly along the southern and south-eastern margins of the NLAS (Figure 12). It has a maximum vertical thickness of 140m; some drill holes intersect it as multiple zones interspersed among non-albitised rocks. Four satellite rare-element (Be, Nb, Y) deposits hosted within the GLG, namely the T-Zone, R-Zone S-Zone and Fluorite-Zone, are also highly albitised and share textures similar to those of albitite within the NLAS. These deposits and the albitite of the NLAS form a broad halo of albitite along the margin of the NLAS. The albitite is spatially separate from, albeit adjacent to the high-grade ore horizons within the Nechalacho, but does host uneconomic REE mineralization. Moreover,

the thickest albitite intervals are in close proximity to the thickest mineralised horizons of the NLAS (Figure 13).

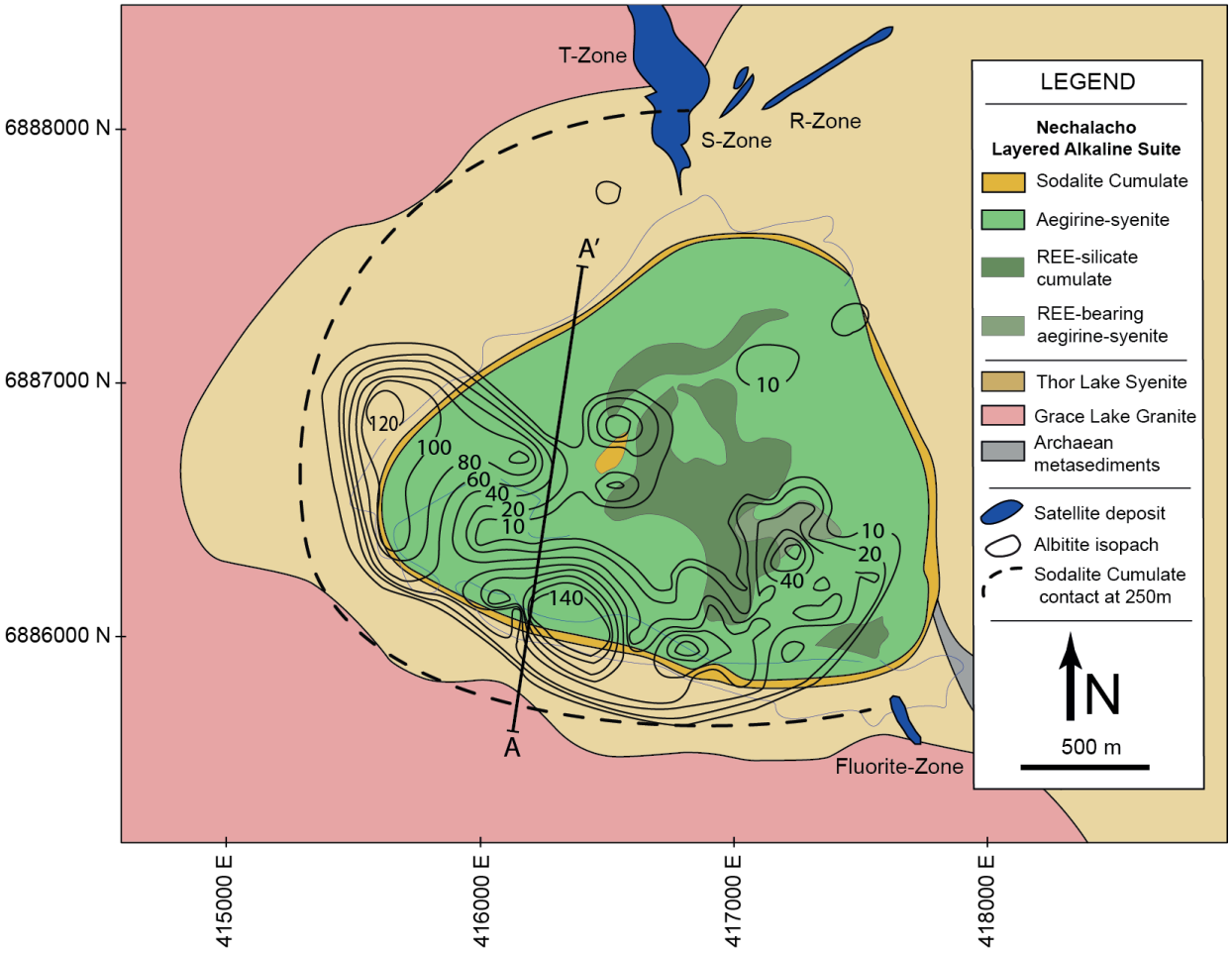

Figure 12: Geological map showing the surface expression of the NLAS and the surrounding TLS and GLG, together with the satellite REE deposits (S-Zone, R-Zone, T-Zone and Fluorite Zone). Overlain on the map are isopach contours indicating the thickness of the albitite hosted by the NLAS, and the NLAS-GLG contact at 250m. The line labeled A-A' shows the location of the cross-section illustrated in Figure 13.

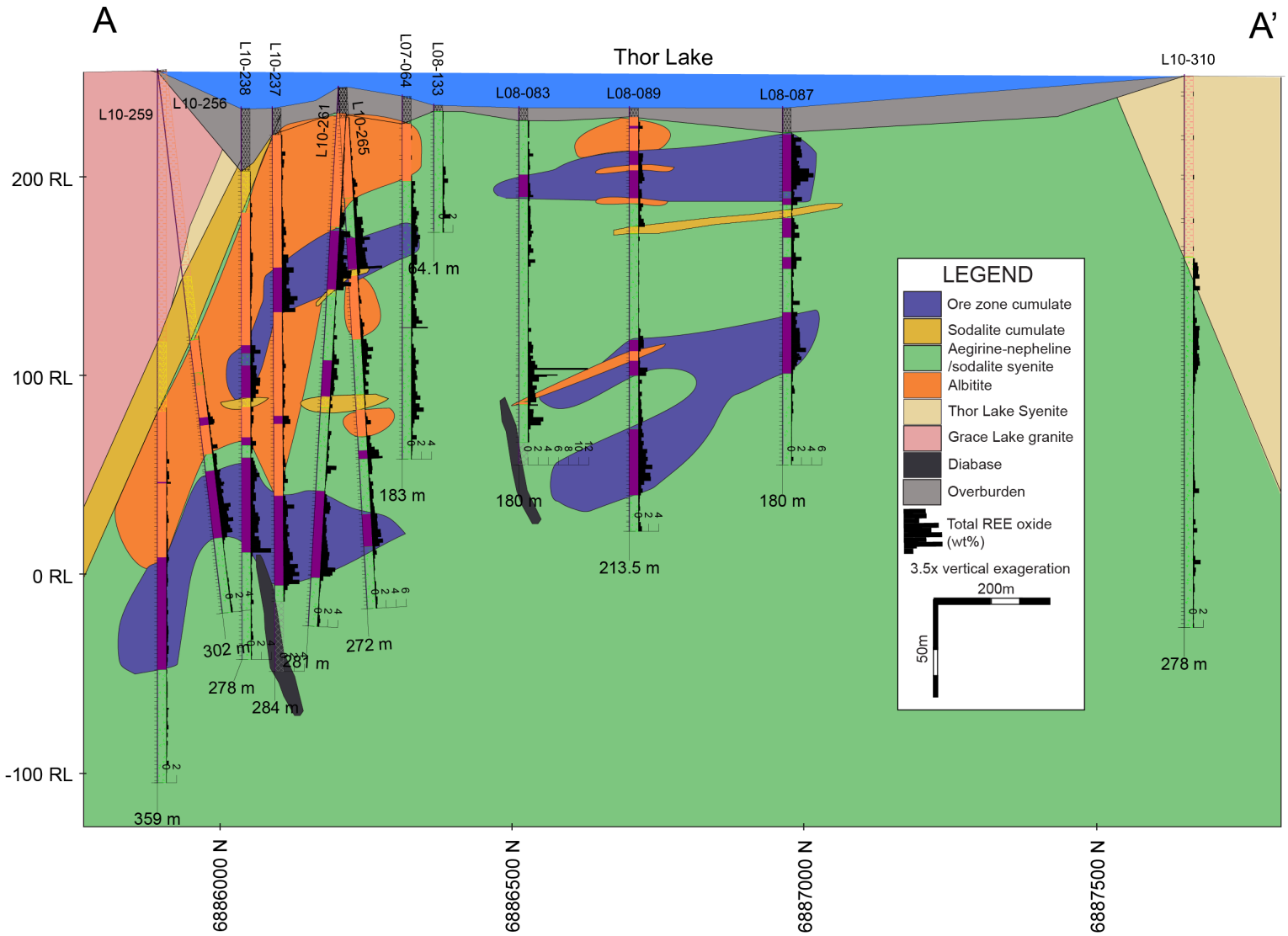

Figure 13: Section A-A' through the NLAS (refer to Figure 12 for the location of A-A'). The primary lithological units are the Thor Lake Syenite, the sodalite cumulate and aegirine-nepheline/sodalite syenite (this includes the altered and unaltered aegirine-nepheline syenite, trachytic microsyenite and foyaite). The albitite and ore zones are outlined in orange and navy-blue, respectively.

Primary igneous textures are rarely observed in the albitite. Alteration to albitite involved replacement of microcline phenocrysts and megacrysts, which are commonly embayed or brecciated leaving both rounded and highly angular relicts (Figure 14a). Albitisation is most commonly manifested in the replacement of pink, secondary microcline by bladed albite (Figure 14b) and coarser massive albite, and infilling of void space by bladed albite (Figure 14c). The bladed albite contains abundant liquid-vapour-solid fluid inclusions <2μm in diameter as well as REE-, Nb-, Y-, Zr-, Ti- and U-bearing solid micro-inclusions (Figure 15). Distinct, primary albite is ubiquitous in deeper, less altered rocks. The primary albite occurs as aggregates of white to translucent microcrystals. In contrast to secondary pink bladed albite, primary translucent albite is inclusion-free. Microcline occurs as both white (I) and pink (II) varieties, with the latter being most common in the albitite and absent from less altered rocks.

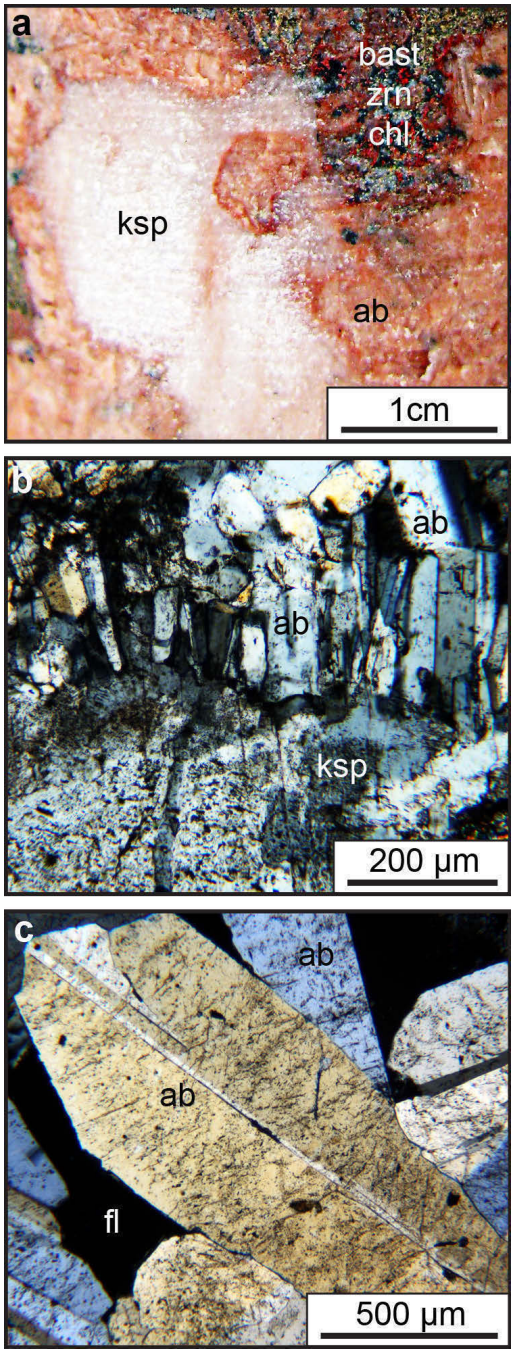

Figure 14: Feldspar textures in the albitite: a) relict K-feldspar embayed by secondary albite (hand specimen photograph); b) acicular albite nucleated on the corroded surface of a K-feldspar crystal (transmitted light, cross-polars); c) a euhedral bladed albite crystal displaying characteristic carlsbad twinning, and interstitial fluorite (transmitted light, cross-polars); ab = albite, bast = bastnäsite-(Ce), chl = chlorite, fl = fluorite, ksp = K-feldspar, zrn = zircon.

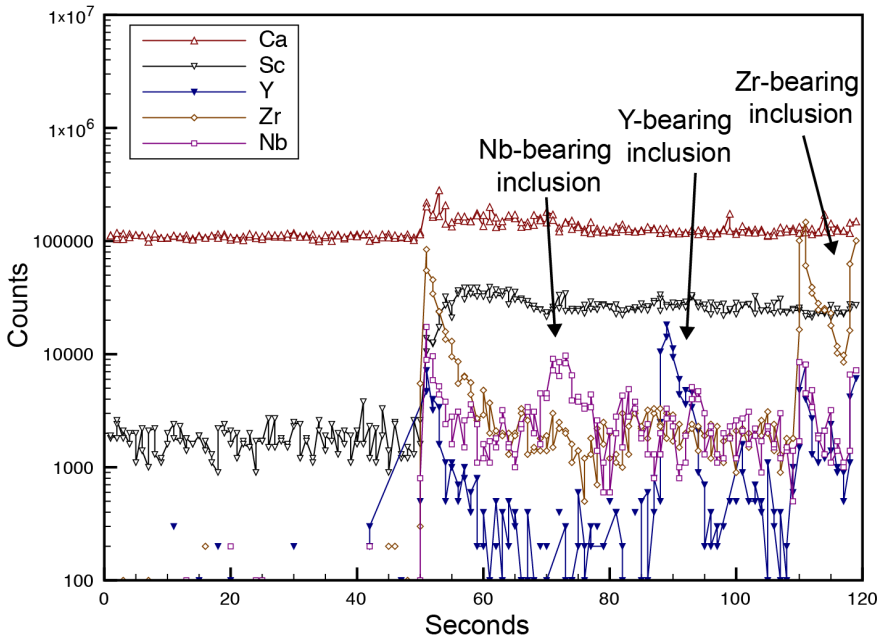

Figure 15: LA-ICPMS counts versus ablation time for a location in a secondary albite crystal. The sharp peaks represent solid inclusions encountered by the laser.

The albitite underwent brittle deformation (Figure 16a) due possibly to hydrofracturing, and albite and microcline were brecciated at all scales. Both feldspars are locally cross-cut by micro-breccias containing angular and rounded feldspar grains. The matrices of the micro-breccias consist mainly of an intergrowth of quartz and fluorite (Figure 16b). Vugs interstitial to albite and microcline are filled by fluorite and quartz, and commonly also by sulphides (pyrite, pyrrhotite, sphalerite and galena; Figure 11a), REE-fluorocarbonates and zircon. Bastnäsite-(Ce), monazite-(Ce), columbite and sphalerite occur as inclusions within fluorite (Figure 11b). Euhedral, zoned zircon, typical of the Upper Ore Zone, is commonly found whole or as fragments within fluorite and quartz (Figure 16c). Minor secondary microcline locally rims albite, where it is in contact with fluorite, quartz, calcite or chlorite (Figure 16d). The resulting albitite has a porosity of up to 20%.

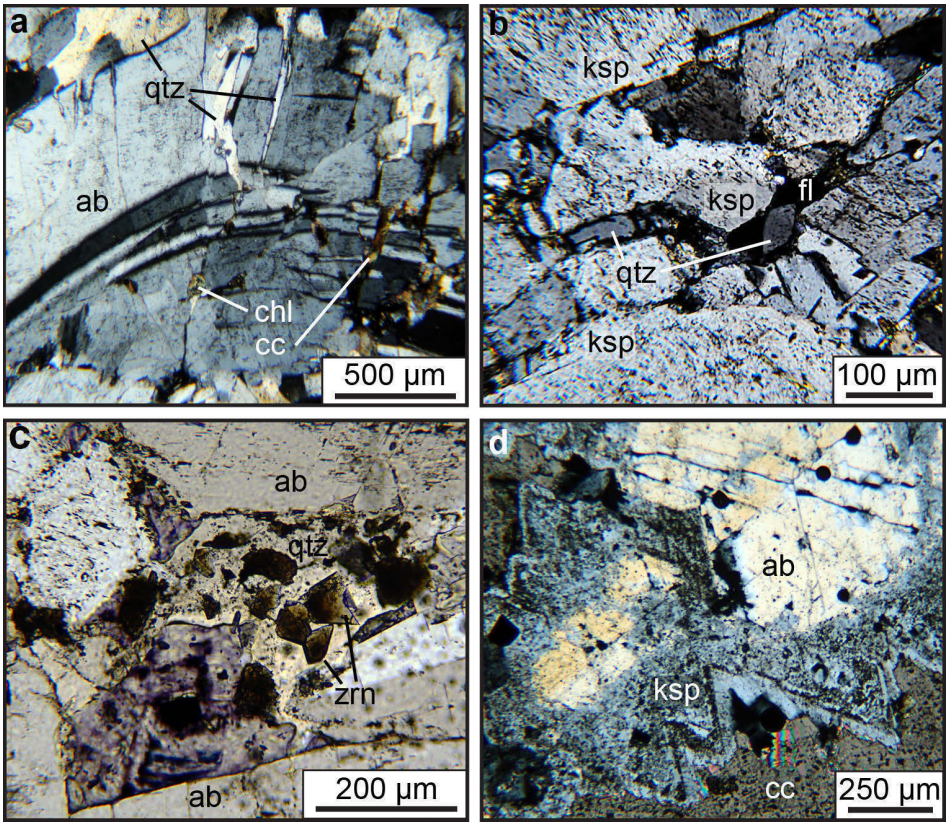

Figure 16: Textures in albitite: a) brittle-ductile deformation of a bladed albite crystal, in which fractures are filled by quartz, chlorite and calcite (transmitted light, cross-polars); b) clasts composed of quartz and K-feldspar in micro-breccia containing a matrix of quartz and fluorite (transmitted light, cross-polars); c) zircon crystals included in quartz and fluorite (transmitted light); and d) secondary K-feldspar that overgrew and overprinted a bladed albite crystal in a calcite matrix (transmitted light, cross-polars); ab = albite, cc = calcite, chl = chlorite, fl = fluorite, ksp = K-feldspar, qtz = quartz, zrn = zircon.

Megacrystic hexagonal pseudomorphs after biotite (Figure 17a) and tabular prismatic pseudomorphs after aegirine (Figure 17b) are filled by an assemblage that includes albite, fluorite and quartz. They are enclosed by microcline megacrysts or occur within the pink albite matrix. Interstitial white to silver zircon crystals, 5mm or greater in diameter, were resorbed (Type 3 zircon; Sheard et al. 2012). Embayments within this zircon are filled by albite or quartz, and cross-cut zones in this mineral (Figure 17c). These zircon crystals are also present as elongate slivers among albite crystals.

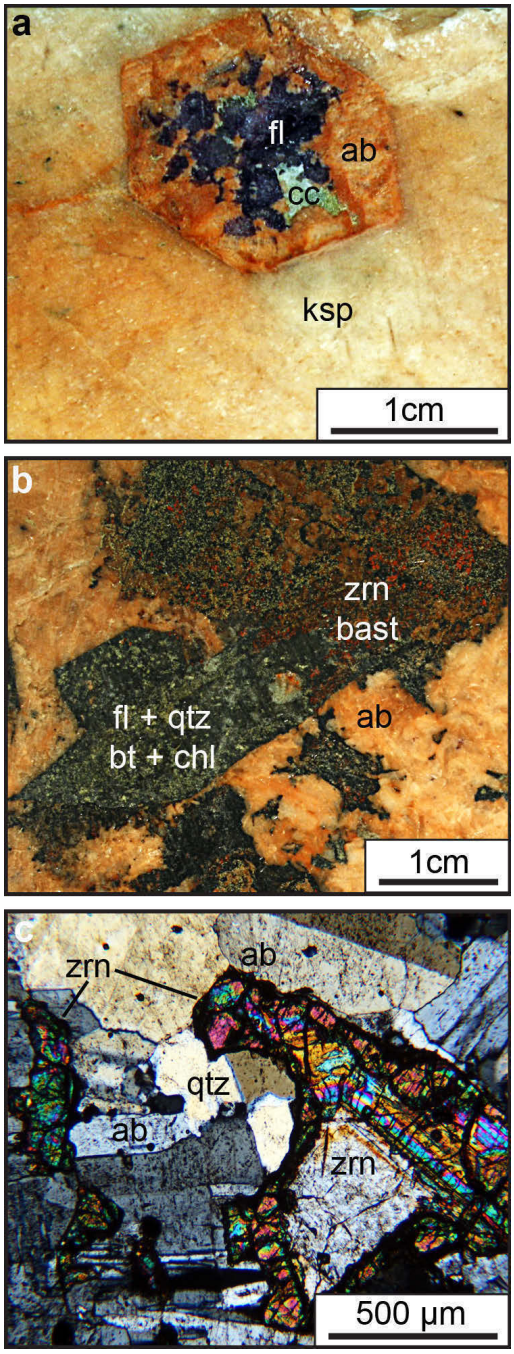

Figure 17: Replacement textures within the albitite: a) an unidentified hexagonal pseudomorph enclosed in K-feldspar that was replaced by bladed albite and an interstitial assemblage of chlorite and calcite; b) a prismatic pseudomorph of former eudialyte, sodalite or biotite enclosed by secondary albite and filled by fluorite, quartz, biotite, chlorite, zircon and bastnäsite-(Ce); and c) quartz and albite that embayed zircon (transmitted light, cross-polars); ab = albite, bast = bastnäsite-(Ce), bt = biotite, cc = calcite, chl = chlorite, fl = fluorite, ksp = K-feldspar, zrn = zircon.

Albitite mineral chemistry

All albite encountered in the NLAS has a composition of An0; the Ca content is < 200ppm in all samples analysed (Table 1). Relative to primary albite I, secondary bladed, pink albite II is

enriched in large ion lithophile elements such as Li (169 times); Ba (114 times); Cs (12 times) and the HFSE such as Nb (21 times); Ta (19 times); and Zr (4.7 times, Figure 18). Albite II has high REE concentrations compared to albite I, particularly La (5.8 times), Gd (3.7 times) and Tb (3.3 times). The two albite varieties have opposite europium anomalies in most samples; primary albite has Eu/Eu* values generally above 1, and up to 2.9, whereas the secondary pink albite has an average of Eu/Eu* of 0.61. Primary albite contains an average of 960 ppm Fe, whereas secondary albite only contains 300 ppm Fe on average.

Albite II is more similar to microcline II than primary albite in its concentrations of most trace elements. Both minerals are ubiquitous in the albitite and coexist intimately. Albite II is enriched in Li (22 times), Co (4.8 times), Sn (3.2 times), Hf (2.5 times) and Sr (1.5 times), and depleted in Pb (0.86 times), Ti (0.43 times), U (0.39 times) and Rb (0.0017 times) relative to microcline II. The HREE are higher in concentration in albite II, La (6.4 times higher), Ce (3.9 times higher), Eu (1.6 times), Gd (1.9 times), Yb (3.6 times) and Lu (5.7 times). However the two varieties of microcline are quite similar. Microcline I contains more Ba (8.8 times), Nb (3.8 times), Rb (2.6 times) and U (2.4 times) and less Sr (0.17 times), Cs (0.11 times), Pb (0.10 times) and Li (0.018 times) than microcline II (Figure 18).

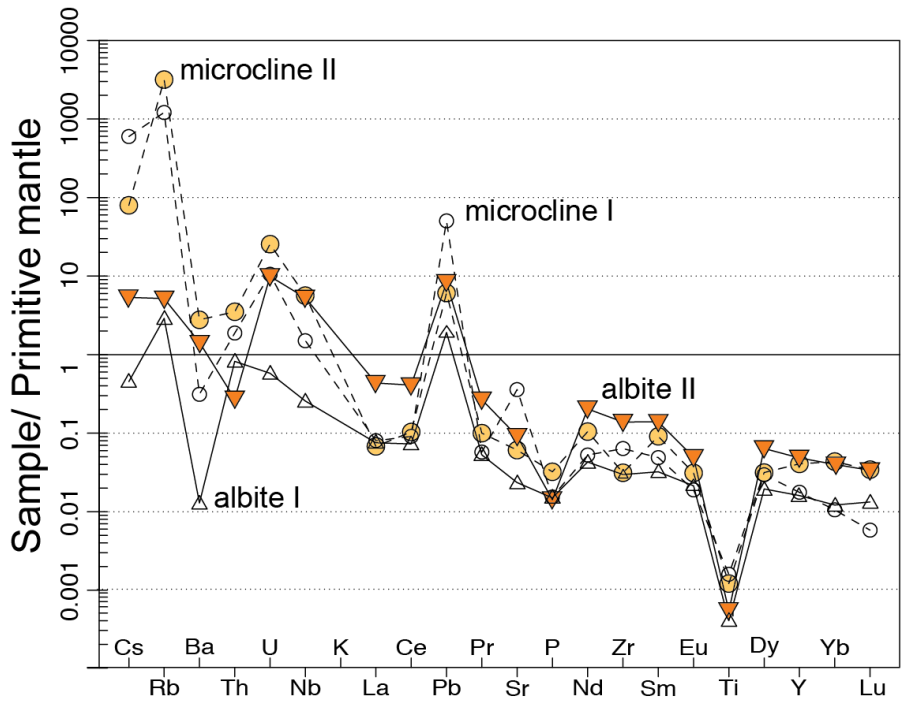

Figure 18: Spider diagram showing the average trace element concentration normalized to primitive mantle (Sun and McDonough 1989) of primary and secondary albite from the NLAS, together with pink microcline in the albitite and white microcline in unaltered rocks of the NLAS.

Fluorite has significant REE concentration, notably of the MREE and Y. The measured average concentrations were 3.3 ppm Ce, 7.7 ppm Gd, 0.75 ppm Ho, 0.34 ppm Yb and 153 ppm Y. The Y/Ho ratio varies from 119 to 672 and averages 280 (Table 2).

Table 1: Major and minor element concentration in the NLAS (wt.%), I and II refer to primary and secondary respectively

Mineral	# of analyses	Na_2O	SiO_2	K_2O	Al_2O_3	Ga_2O_3	MgO	Rb_2O	CaO	SrO
Albite (I)	34	11.76	68.72	0.14	19.16	0.004	0.044	0.00	0.018	-
Albite (II)	182	11.76	68.42	0.10	19.54	0.012	0.002	0.00	0.010	0.017
K-feldspar(II)	72	0.51	64.82	16.77	18.41	0.013	0.005	0.10	0.012	0.073
Nepheline	2	16.16	43.70	6.62	33.21	-	0.000	-	0.053	-
Sodalite	8	25.58	38.31	0.009	31.47	-	0.004	-	0.006	-
Aegirine	11	13.23	52.35	0.008	3.35	-	0.002	-	1.15	-
Biotite	57	0.14	37.50	9.26	12.80	0.013	10.57	-	0.12	-
Mineral	**# of analyses**	**FeO**	**TiO2**	**MnO**	**Cr_2O_3**	**BaO**	**Cl**	**F**	**H_2O**	**Total**
Albite (I)	34	0.19	-	-	-	0.012	0.014	-		100.04
Albite (II)	182	0.044	-	-	-	0.035	0.020	-		99.90
K-feldspar(II)	72	0.059	-	-	-	0.012	0.024	-		100.72
Nepheline	2	0.44	-	-	-	0.021	0.016	-		100.21
Sodalite	8	0.047	-	-	-	0.014	6.65	-		100.59
Aegirine	11	29.28	0.07	0.15	0.00	-	-	-		99.60
Biotite	57	24.14	0.12	0.32	0.01	-	0.24	1.63	2.99	99.80

Table 2: Mean trace element concentration of minerals in the NLAS (ppm), I and II refer to primary and secondary respectively

Mineral	# of analyses	Li	Be	B	Na	Mg	P	K	Ca(42)
Aegirine	9	13.8	0.412	1.05	-	115	0.847	-	8360
Albite (II)	76	4.46	0.528	1.01	-	123	1.32	-	81.8
Albite (I)	26	0.0273	0.466	0.605	-	4.65	1.4	-	22
Fluorite	18	0.181	0.0734	0.511	147	4.8	6.44	15.6	470000
Microcline (II)	29	0.203	0.386	2.93	-	20.9	3.06	-	13.6
Microcline (I)	30	10.9	1.85	1.87	-	21.5	1.46	-	500
Sodalite	8	45.1	6.16	0.99	-	0.372	0.894	-	263
Mineral	**Ca(44)**	**Sc**	**Ti**	**Co**	**Ga**	**Ge(72)**	**Ge(73)**	**Rb**	**Sr**
Aegirine	8400	2.29	367	0.0634	40.6	4.54	4.28	0.246	0.604
Albite (II)	112	1.07	0.684	0.00712	139	0.433	0.53	3.32	1.92
Albite (I)	68.7	0.726	0.515	0.00706	103	0.633	0.633	1.85	0.488
Fluorite	460000	0.0201	0.0708	29.1	0.0296	0.0406	0.0951	0.248	67.1
Microcline (II)	73.2	1.23	1.58	0.00148	125	0.535	0.543	2010	1.29
Microcline (I)	575	0.715	2.08	0.00504	64.4	0.495	0.484	769	7.57
Sodalite	301	0.337	6.72	0.0133	71.3	0.332	0.32	120	18.3
Mineral	**Y**	**Zr**	**Nb**	**Sn**	**Cs**	**Ba**	**La**	**Ce**	**Pr**
Aegirine	2.54	2710	24	113	0.0954	0.243	1.73	6.23	1.13
Albite (II)	0.218	1.54	3.82	0.482	0.0428	10.1	0.299	0.726	0.0736
Albite (I)	0.0718	0.328	0.182	0.0421	0.00358	0.0885	0.0513	0.128	0.0144
Fluorite	153	0.0501	0.266	0.267	0.0397	0.477	0.826	3.33	0.64
Microcline (II)	0.0803	0.351	4.02	0.152	0.629	19.4	0.0466	0.184	0.0276
Microcline (I)	0.185	0.712	1.07	0.108	4.72	2.19	0.055	0.161	0.0158
Sodalite	0.00658	0.0305	0.0151	0.0792	0.685	0.0809	0.0338	0.0599	0.00493
Mineral	**Nd**	**Sm**	**Eu**	**Gd**	**Tb**	**Dy**	**Ho**	**Er**	**Tm**
Aegirine	5.85	1.41	0.157	0.883	0.116	0.662	0.134	0.579	0.168
Albite (II)	0.274	0.0615	0.00824	0.0526	0.00772	0.0465	0.00784	0.0201	0.00281
Albite (I)	0.0574	0.0141	0.00354	0.0142	0.00231	0.0141	0.00259	0.00711	0.000718
Fluorite	3.82	2.79	0.647	7.74	1.33	5.85	0.747	1.19	0.0803
Microcline (II)	0.142	0.0404	0.00521	0.0274	0.00381	0.0218	0.00284	0.00614	0.000688
Microcline (I)	0.0713	0.0217	0.00318	0.0202	0.00317	0.0232	0.00475	0.0152	0.00275
Sodalite	0.0153	0.00287	0.000586	0.00154	0.000176	0.000881	0.000075	0.00071	0.000134
Mineral	**Yb**	**Lu**	**Hf**	**Ta**	**Pb(206)**	**Pb(207)**	**Pb(208)**	**Th**	**U**
Aegirine	2.21	0.578	103	8.86	1.79	1.41	1.44	0.0842	2.57
Albite (II)	0.0195	0.00246	0.0338	0.226	0.595	0.315	0.295	0.0231	0.212
Albite (I)	0.00589	0.000967	0.012	0.0118	0.137	0.104	0.122	0.07	0.0122
Fluorite	0.338	0.0312	0.0039	0.0165	0.048	0.0231	0.0231	0.0454	0.0475
Microcline (II)	0.00519	0.000431	0.0133	0.0686	0.433	0.299	0.341	0.299	0.536
Microcline (I)	0.0214	0.00254	0.0252	0.156	3.57	3.04	3.3	0.16	0.221
Sodalite	0.00152	0.000116	0.000399	0.000431	0.591	0.6	0.616	0.00338	0.00522

Isotopic Analyses

The oxygen and hydrogen isotopic compositions of albite, microcline and quartz from the albitite and unaltered rocks in the NLAS, as well as unaltered GLG were analysed in 15 samples (Table , Figure 19). The $\delta^{18}O$ values represent those of the silicate minerals, whereas δD_{VSMOW} represents that of the included fluid (both primary and secondary inclusions) within those minerals (see

methodology). A single sample of albite I has a $\delta^{18}O_{VSMOW}$ value of 14.4‰ and the trapped fluids a δD_{VSMOW} value of -109‰. Albite II samples from the albitite have $\delta^{18}O_{VSMOW}$ values ranging from 12.5 to 19.9‰ and an average $\delta^{18}O_{VSMOW}$ value of 14.9‰. The δD_{VSMOW} values of trapped fluids in secondary albite range from -78 to -123‰ and average -103‰. Microcline I has an average $\delta^{18}O_{VSMOW}$ value of 13.3‰ and the trapped fluids an average δD_{VSMOW} value of -113.6‰. Microcline II has $\delta^{18}O_{VSMOW}$ values ranging from 10.6 to 14.4‰ and the trapped fluids δD_{VSMOW} values ranging from -153 to -104‰. Secondary quartz obtained from the quartz-fluorite assemblage within albitite has $\delta^{18}O_{VSMOW}$ values of 13.7 to16.4‰ and the fluids trapped in this quartz have δD_{VSMOW} values of -35 to -61‰. One primary quartz sample obtained from the GLG close to the NLAS has a $\delta^{18}O_{VSMOW}$ value of 9.0‰.

Table 3: $\delta 18O_{(VSMOW)}$ and $\delta D_{(VSMOW)}$ for albite, K-feldspar and quartz from the albitite. The data for δD aare for H_2O trapped as fluid inclusions in these minerals. The suffixes I and II refer to primary and secondary varieties of these minerals, respectively.

Sample	**Mineral**	**Origin**	**$\delta^{18}O_{(VSMOW)}$**	**$\delta D_{(VSMOW)}$**
L11-380 28	albite II	Albitite	19.9	-96
L10-232a 94.7	albite II	Albitite	15.8	-106
L10-232A 75.2	albite II	Albitite	13.6	-123
L10-232A 65.25	albite II	Albitite	12.6	-78
L09-203 6.5	albite II	Albitite	12.5	-113
L10-232A 75.2 B	microcline II	Albitite	13.8	-104
L10-232A 75.2	microcline II	Albitite	10.6	-125
L10-232a 94.7	microcline II	Albitite	14.4	-153
L09-203 6.5	microcline II	Albitite	16.4	-115
L11-380 28	quartz	Albitite	16.4	-35
L10-232a 78.25	quartz	Albitite	13.7	-61
L09-192 154.2	albite I	Unaltered	14.4	-109
L10-253 349.1	microcline I	Unaltered	11.6	-112
L10-253 349.1	microcline I	Unaltered	15.0	-115
L10-253164	quartz	GLG	9.0	NA

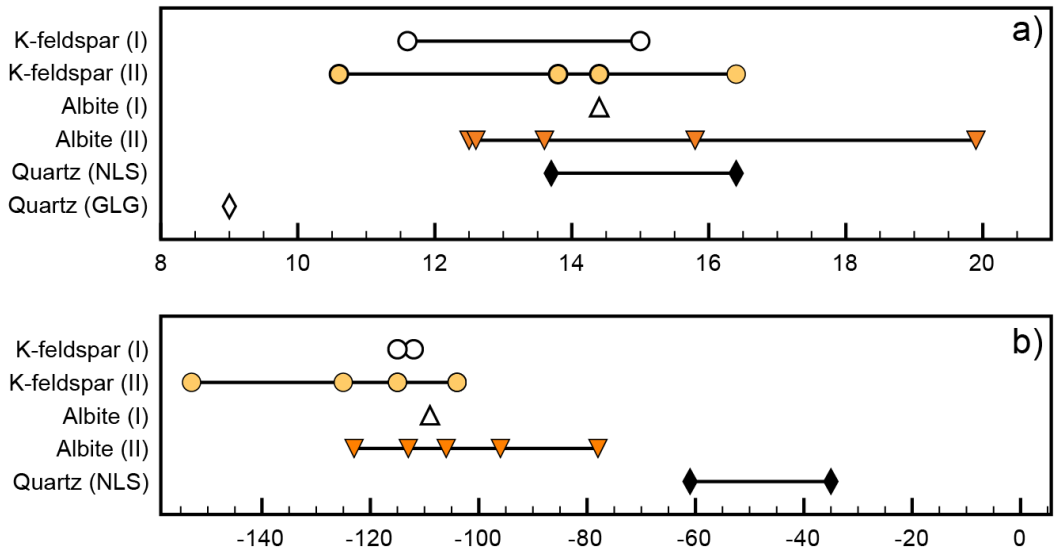

Figure 19: Measured isotopic compositions of alteration minerals in the NLAS: a) values of δD; and b) values of $\delta^{18}O$.

Discussion

Physicochemical conditions of albitisation

Albitisation locally overprinted a variety of rock types within the upper 300m of the NLAS, including the Upper Ore Zone. Textures within the resulting albitite record wholesale dissolution and replacement of primary magmatic minerals and magnetite-biotite alteration by albite and subsequent fine-grained assemblages including quartz, fluorite, chlorite, and calcite. They also show that there was a net loss of volume, which created significant porosity in the form of vugs. The latter were partly infilled by REE-fluorocarbonates and other minerals containing elements normally considered immobile. The alteration is similar to that found in satellite deposits adjacent to the NLAS but hosted by the TLS and GLG. The near-monomineralic nature of the albitite indicates that it was the product of a system open to a large number of components.

Pressure and Temperature

The general absence of minerals other than albite in the albitite alteration assemblage precluded geobarometric and geothermometric estimates that depend on the fractionation of elements or isotopes between minerals. However, based on U-Pb dating of zircon (Sinclair et al. 1994; Möller and Williams-Jones 2013; Mumford 2013), the NLAS, TLS and GLG (eastern lobe) were coeval with the intrusive units of the western lobe, which are estimated to have been emplaced at

depths corresponding to a lithostatic pressure of between 4.0 and 4.5 kbar using the Al-in-hornblende geobarometer (Mumford 2013). It therefore seems reasonable to conclude that albitisation of the NLAS and its satellites occurred at a similar pressure, perhaps near the lower end of the range, i.e., 4.0 kbar, because the pressure would have been partly hydrostatic.

Although it has not been possible to estimate the temperature of albitisation of the NLAS for the reasons given above and because the fluid inclusions are too small to analyse microthermometrically, fluid inclusion microthermometric data are available for the T-Zone. Homogenisation temperatures of fluid inclusions in hydrothermal quartz in the T-Zone reported by (Feng 2014) fall into a moderate salinity group (4.4m) and a high salinity group (9.0m). The average entrapment temperatures, determined by correcting the homogenization temperatures for a pressure of 4.0kbar (Steele-MacInnis et al. 2012), were 592 and 367°C for the moderate and high salinity groups, respectively. The high and low temperature groups have Ca/Na ratios of 0 and 0.004 respectively, i.e., effectively zero in both cases, consistent with their derivation from an environment dominated by peralkaline rocks, either the NLAS or the surrounding TLS and GLG. Inasmuch as magnetite-biotite alteration preceded albitisation and pervasively altered the NLAS from the bottom of the Basal Ore Zone upwards, whereas albitisation was restricted to the uppermost and outermost parts of the intrusion, it seems reasonable to infer that the high temperature fluid was responsible for the magnetite-biotite alteration and the low temperature fluid the albitisation. It also seems reasonable to infer that the high temperature fluid exsolved from the magma forming the NLAS, whereas the albitising fluid also had an external component, e.g., meteoric water that circulated in the GLG and TLS. The latter is consistent with the observation that the $\delta^{18}O$ of the fluid in equilibrium with secondary albite exceeded magmatic values.

$\boldsymbol{f}O_2$

Hematite is ubiquitous within the albitite, both as fine- to medium-grained crystals and disseminated within albite. The pink colour of the feldspar crystals in the albitite has elsewhere been shown to be the result of precipitation of hematite in micropores during crystallisation (Boone 1969; Putnis et al. 2007). Thus $\boldsymbol{f}O_2$ conditions surpassed the hematite-magnetite buffer, i.e. >-29.3 at a temperature of 367°C.

The activities of Na^+ and K^+

The activities of Na^+ and K^+ were calculated from the compositions of the low temperature fluid inclusions in the T-Zone analysed by Feng (2014), i.e., FIA 1, 2a, 3, 4 and 5, where the term FIA refers to fluid inclusion assemblage. Element concentrations of the various FIAs were determined from LA-ICP MS analyses of individual fluid inclusions. The value of $a\mathrm{Na}^+$ was calculated using the extended Debye-Huckel equation (Helgeson et al. 1981) assuming a temperature of 367 °C (see above) and is 2.80. Owing to the large variability in K^+ concentration, the median cation concentration was considered the most representative. The value calculated for $a\mathrm{K}^+$ is 0.14 (Table 4).

pH

In order to constrain the pH of the albitising fluids, stability relationships were evaluated for minerals in the Fe-O-Al-Si-Na-K system as a function of $a\mathrm{Na}^+/\ a\mathrm{H}^+$ and $a\mathrm{K}^+/\ a\mathrm{H}^+$ at a fixed pressure of 4kb (Figure 20). The calculations were made using the values of $a\mathrm{Na}^+$ and $a\mathrm{K}^+$ estimated for 367°C. The magnetite-hematite buffer represents the lower limit of $\log f\mathrm{O}_2$ of albitising fluids and was used for calculations. The $\log a\mathrm{Si0}_2$ was estimated to be -2, as discussed in the next section.

The stability field of the assemblage albite-hematite is bracketed by the equilibrium boundaries for the reactions:

$$\text{Paragonite} + 6\ \mathrm{SiO}_{2(aq)} + 2\ \mathrm{Na}^+ \rightarrow 3\ \text{Albite} + 2\ \mathrm{H}^+ \qquad (1)$$

and

$$2\ \text{Aegirine} + 2\ \mathrm{H}^+ \rightarrow 3\ \text{Hematite} + 4\ \mathrm{SiO}_{2(aq)} + 2\ \mathrm{Na}^+ + \mathrm{H}_2\mathrm{O} \qquad (2)$$

and governed by the parameter, $\log (a\mathrm{Na}^+/a\mathrm{H}^+)$. At values of this parameter below 6.1, albite breaks down to form paragonite (at slightly higher values it breaks down to muscovite) and at values above 6.4, hematite gives way to aegirine (Figure 20). Using the value for $a\mathrm{Na}^+$ estimated above, it therefore follows that albite and hematite coexisted stably at pH conditions between 5.6 and 6.

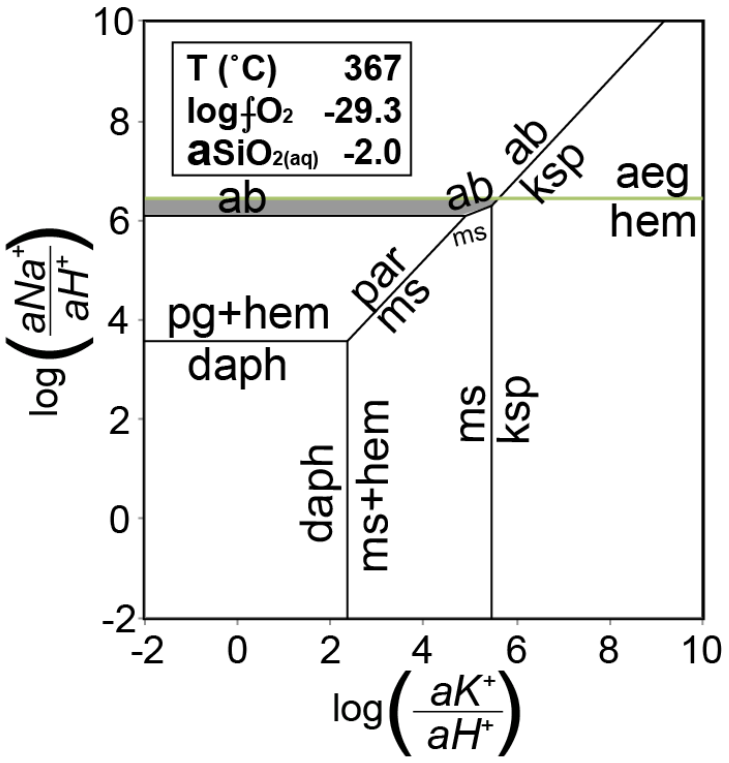

Figure 20: The stability of albite, K-feldspar, muscovite, paragonite and daphnite (chlorite) as a function of log (aNa^+/aH^+) and log (aK^+/aH^+) at a temperature of 367°C. Conditions during albitisation are indictated by the shaded field. Thermodynamic data from Shock and Helgeson (1988); Holland and Powell (1998)

The activity of SiO_2

During albitisation, silica-undersaturated magmatic minerals such as sodalite, nepheline and analcime were replaced by silica-saturated alteration assemblages, i.e., involving albite, chlorite and quartz, which precipitated in pore space created by dissolution (Figure 21). Quartz saturation occurred mainly after albitisation, with quartz filling fractures in albite and K-feldspar. The maximum $aSi0_2$ prior to albitisation was limited by Reaction (1) or

$$\text{Muscovite} + 3\ Na^+ + 6\ SiO_{2(aq)} \rightarrow 3\ \text{Albite} + K^+ + 2\ H^+ \qquad (3)$$

and that controlling quartz saturation (Figure 22). At a pH of 5.8, the minimum $log a Si0_2$ ranged from between -2.4 and -2.0 for temperatures of 250 to 400°C. The maximum $log a Si0_2$ set by the quartz saturation condition was from -2.2 to -1.4 for the same temperature range. For the purpose of estimating pH it was therefore assumed to be -2 (see above).

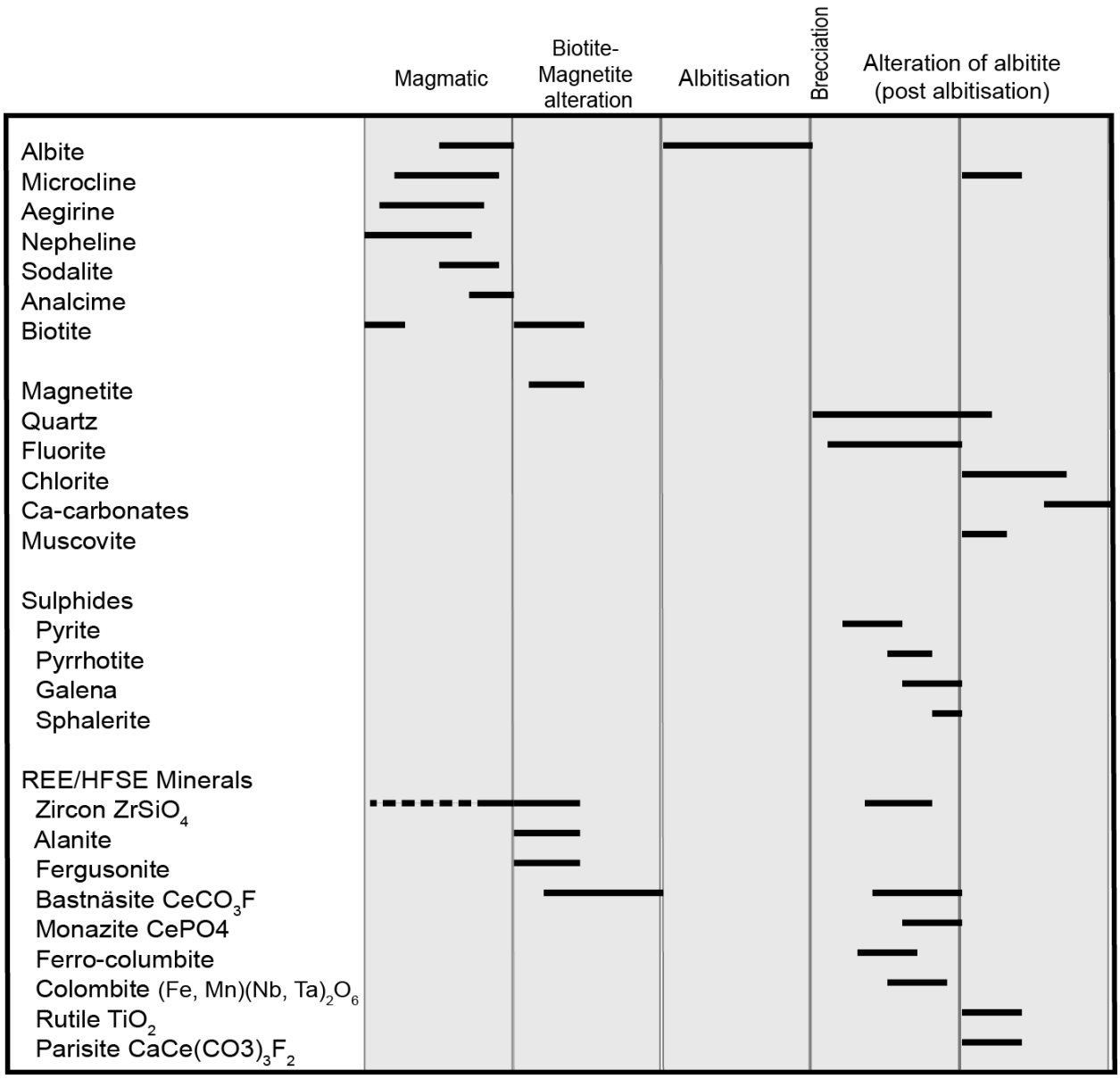

Figure 21: A paragenetic chart for the upper, hydrothermally altered part of the Nechalacho Layered Suite.

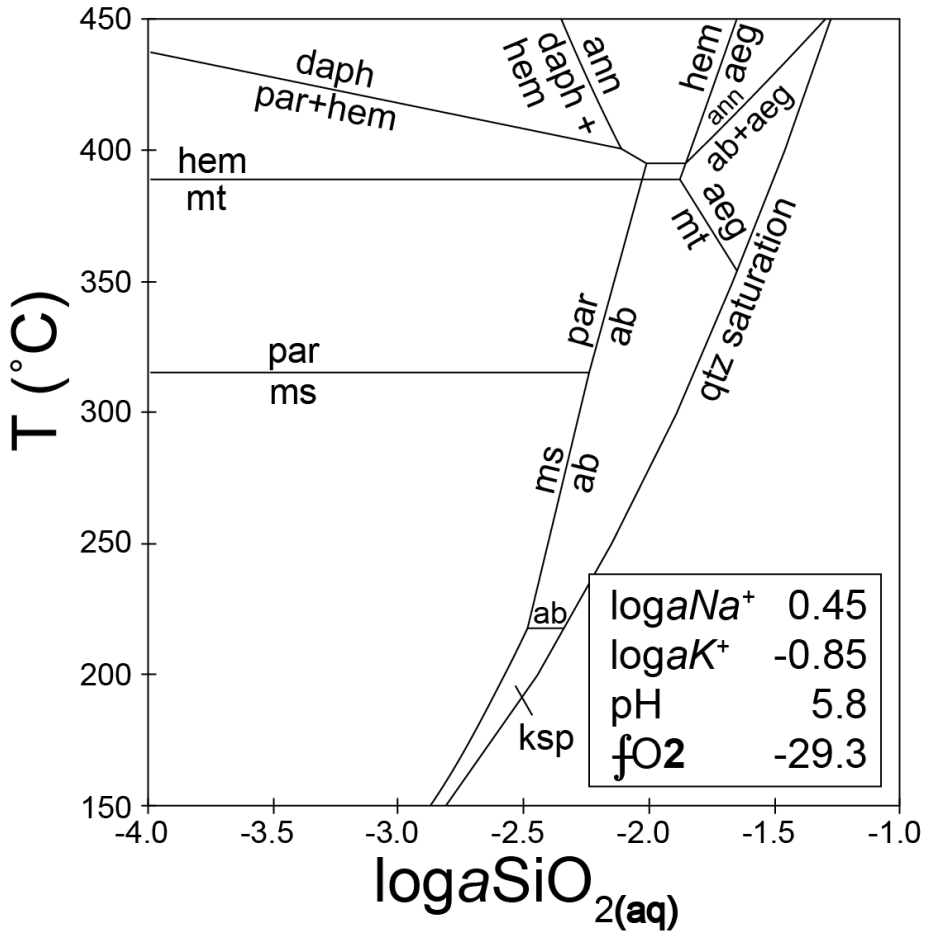

Figure 22: Stability relationships for minerals in the system Fe-O-Al-Si-Na-K system as a function of temperature and log$a$$SiO_2$.aeg = aegirine, ab = albite, anl = analcime, ann = annite, hem= hematite, ksp = K-feldspar, ms = muscovite, ne = nepheline, qtz = quartz. Thermodynamic data from Shock and Helgeson (1988); Holland and Powell (1998).

The activity of Ca^{2+}

The albitite is enriched in Ca compared to magnetite-biotite-altered aegirine syenite and the unaltered nepheline syenite because of the fluorite that was introduced into the albitite after its brecciation. As magmatic villiaumite is present at depth in the NLAS (in unaltered nepheline syenite) and the reaction:

$$2\ \text{Villiaumite} + Ca^{2+} \rightarrow \text{Fluorite} + 2\ Na^{+} \qquad (4)$$

has a log K value of ~10 for a temperature of 600 °C (the temperature assumed above for the exsolution of a magmatic hydrothermal phase; villiaumite occurs in miarolitic cavities in the lower unaltered part of the intrusion), we conclude that $a$$Ca^{+}$ was initially very low. This

interpretation is supported by the observation that all the primary magmatic minerals, i.e., aegirine, nepheline and albite contain almost no Ca. Low magmatic $a\mathrm{Ca}^{2+}$ is also typical of agpaitic intrusions (Sörensen 1997). Considering that secondary albite has a composition very close to that of its end-member, $a\mathrm{Ca}^{+}$ continued to be low during albitisation. However, $a\mathrm{Ca}^{+}$ started to increase with the post-albitisation precipitation of fluorite (accompanied by bastnäsite-(Ce)) in the upper 300 m of the NLAS and continued to increase with the replacement of bastnäsite-(Ce) by Ca-REE fluorocarbonates (parisite-(Ce) and synchisite-(Ce), Figure 11c). Some fluid inclusions in the T-Zone analysed by Feng (2014) contain detectable Ca, though in most cases the reported concentrations were below the detection limit. The median Ca concentrations in the lower temperature fluid yielded an aCa^{2+} value of 0.001 (Table 4). An external source of Ca has been invoked to explain the presence of calcium-bearing alteration minerals in other highly alkaline intrusions (e.g., Ilímaussaq, Salvi et al. 2000; Graser and Markl 2008), and is proposed for the NLAS.

Table 4: Mean values for T-zone fluid inclusion compositions and homogenization temperatures recalculated from Feng (2014)

Group	FIA	T (˚C)	P (bar)	Ionic Strength	Molality	aNa+	aK+	aNa+/aK+	aCa+ (median)
High Sal	1a,1b,1c, 2b,3a,3c	367	4000	4.5	9.0	2.80	0.14	20	0.0010
Mod Sal	2a and 6	592	4000	2.2	4.3	0.66	0.0091	73	0

Mobilisation of the REE and HFSE

Textural relationships and the distribution of albitite within the NLAS indicate that albitisation overprinted REE and HFSE mineralisation, including that within the Upper Ore Zone. The bladed albite contains abundant liquid-vapour-solid fluid inclusions (<2μm in diameter) as well as REE-, Nb-, Y-, Zr-, Ti- and U-bearing solid micro-inclusions (Figure 15), suggesting that these minerals were trapped during albitisation. This and the presence of secondary REE and HFSE minerals interstitial to secondary albite indicate that there was post-albitisation hydrothermal transport of REE and HFSE. The LREE are strongly enriched with respect to HREE in the albitite compared to the Basal Zone (the HREE/LREE ratio is 0.1 in the albitite versus 0.24 in the Basal Ore Zone; Ciuculescu et al. 2013). However, the HREE/LREE ratio of

the albitite is very similar to that of the Upper Ore Zone), which supports the notion that the albitite partly replaced the Upper Ore Zone This interpretation is consistent with the observation that in much of the NLAS, the albitite is located above and in contact with the Upper Ore Zone (Figure 13).

As the REE are dominantly present as REE fluorocarbonate minerals, e.g. bastnäsite-(Ce), it is attractive to speculate that they were transported as REE-fluoride complexes. However, REE phosphate minerals such as monazite-(Ce) are also found, commonly as inclusions in fluorite or intergrown with REE fluorocabonate minerals (Figure 10e). Moreover, recent modelling by Williams-Jones et al. (2012) has shown that the REE cannot be transported in significant concentrations as fluoride complexes because fluoride ion activity is very low at low pH due to dominance of HF, and at higher pH, the low solubility of REE-fluoride solid (fluocerite) buffers F^- activity to very low values. Although REE-chloride complexes are much less stable than REE-fluoride complexes, the relatively high chlorinity of the albitising fluids (9.0m; see earlier discussion of salinity) makes REE-chloride complexes a plausible alternative; these species are not subject to the same limitations as REE-fluoride species because HCl is a strong acid and REE-chloride solids are very soluble. Nonetheless, the modelling referred to above (Williams-Jones et al. 2012) requires that the pH of the mineralising fluid was relatively low, if the REE were transported as chloride complexes, i.e., considerably lower than that estimated for albitisation. Thus, either the REE were transported by a fluid different from the albitising fluid, the water/rock ratio was high enough to mobilise the REE at very low concentrations of these elements in the albitising fluid, or another ligand was involved in REE transport. We prefer the first of these explanations, because as discussed below, we consider it likely that the albitising fluid was a mixture of magmatic and external components and the external component likely drove pH to higher values. According to this explanation, the REE would have been transported by the magmatic hydrothermal fluid. Significantly, for the present discussion, chloride complexes mobilise the LREE preferentially to the HREE (Migdisov et al. 2009), which could explain the predominance in vugs within the albitite of REE minerals like bastnäsite-(Ce) and monazite-(Ce) that prefer the LREE.

Late fluorite within the albitite and aegirine syenite has exceptionally high Y/Ho ratios in comparison to fluorite reported from other localities (Figure 23). The identical charge and very similar radii of Y and Ho predict that the coefficients for the partitioning of these elements between hydrothermal fluids and fluorite should be similar. However, recent experimental studies have shown that in the system HF-H_2O, Y is transported predominantly as YF^{2+} (Loges et al. 2013), whereas Ho and the other REE are transported predominantly as $REEF_2^+$ (Migdisov et al. 2009). As the partitioning of the REE into fluorite is controlled dominantly by fluoride species, the concentration of Y in the fluid should be much higher than that of Ho for the same HF activity, assuming equal availability in the fluid of Y and Ho. As a result, uptake of Y in fluorite tends to be preferred over Ho (van Hinsberg et al. 2010) in cases where aF^- is high. The magmatic Y/Ho ratio of the NLAS from 25 to 27 is within the typical range of chondritic charge- and radius-controlled (CHARAC) values (24<Y/Ho<36). By contrast the Y/Ho ratio of the albitite-hosted fluorite ranges from 119 to 671. This is consistent with the experimental data of Loges et al. (2013) showing that Y is preferentially enriched relative to Ho by hydrothermal transport and observations that hydrothermal fluorite is typically characterized by high Y/Ho ratio (e.g., Bau et al. 2003; see Figure 23).

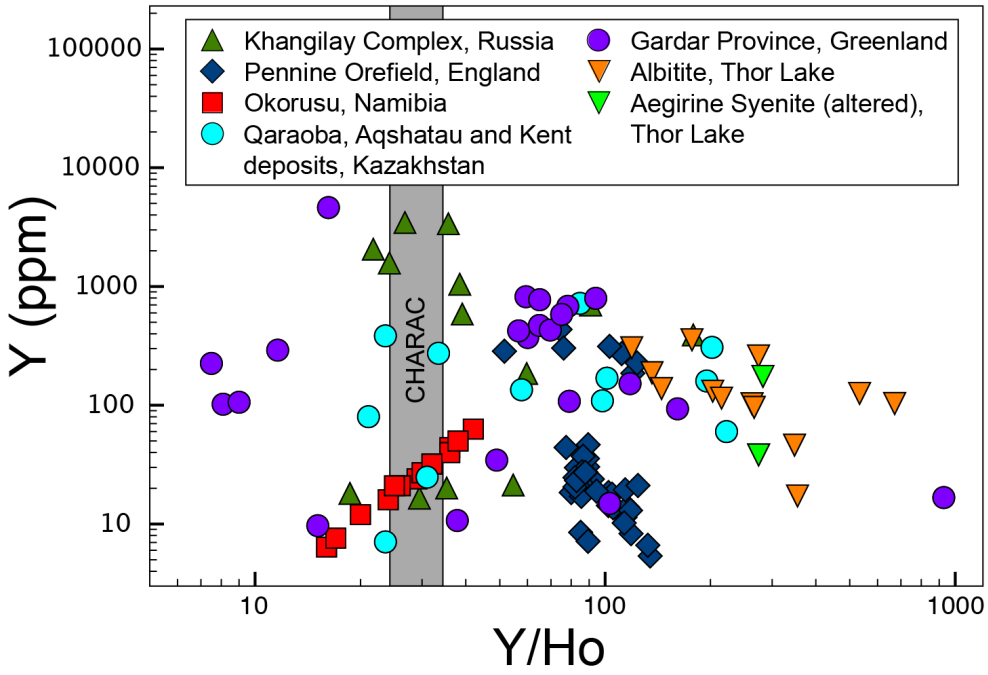

Figure 23: The concentration of Y versus the Y/Ho ratio of fluorite from the NLAS. Also shown are corresponding data for fluorite from other localities (Monecke et al. 2002, Bau 2003, Badanina et al. 2006, Buhn 2006, Schonenberger 2007). CHARAC is an abbreviation for charge- and radius-controlled. Elements of similar charge and radius should exhibit coherent behavior (Bau,1995).

Minerals rich in the HFSE, particularly those containing Y, Nb, Zr and the REE are commonly present as micron-scale inclusions within secondary albite in the albitite (Figure 15). Secondary Nb minerals, such as columbite-(Fe) and uranpyrochlore, are observed in altered rocks within and peripheral to the Upper Ore Zone and Basal Ore Zone, and are found in close proximity to primary niobium-zircon grains. It is believed that Nb was leached from zircon and primary Nb minerals and remobilised during alteration (Timofeev and Williams-Jones, in review). This suggests that, in addition to the REE, these HFSE were also soluble in the albitising fluids, and precipitated during and after albitisation. The elements, Zr and Nb, are readily transported as hydroxyl-fluoride complexes and their solubility, which increases with decreasing temperature, is unaffected by pH (Migdisov et al. 2011, Timofeev and Williams-Jones, in review).

As discussed above, we consider it likely that the REE were transported as chloride complexes in the magmatic hydrothermal fluid under acidic conditions. The exsolution of these fluids from the NLAS is interpreted to have been accompanied by circulation of formation waters derived from outside the NLAS. Mixing of these fluids resulted in cooling and increased pH, which triggered

the precipitation of REE minerals. Furthermore, this mixing increased $a\mathrm{Ca}^{2+}$, forcing the precipitation of fluorite, which has very low solubility. Decreased $a\mathrm{F}^{-}$ due to the precipitation of fluorite resulted in precipitation of Nb and Zr minerals, and the increase in pH, the precipitation of REE minerals as inclusions.

Fluid Source

As discussed earlier, the $\delta^{18}O$ values measured for secondary quartz from the NLAS were 13.7 to 16.4‰, secondary albite were 12.5 to 19.9‰, and secondary microcline were 10.6 to 14.4‰. Assuming a temperature of 367°C, these represent corresponding $\delta^{18}O$ values for the hydrothermal fluid in equilibrium with quartz (NLAS) ranging from 8.8 to 11.4‰, in albite II from 8.8 to 16.1‰ and in microcline II from 6.7 to 12.2‰ (Figure 24). Except for the lower end of the range, these values are heavier than those of magmatic waters (Taylor 1974; Sheppard 1986). The $\delta^{18}O$ values for primary albite were 14.4‰ and primary microcline were 11.6 and 15.0‰. These values are heavier than those of typical magmatic waters and indicate that these minerals likely re-equilibrated with an external fluid source.

Hydrogen isotopic values for decrepitated fluid inclusions in K-feldspar and albite range from δD_{VSMOW} -78‰ to -153‰ (Figure 24). Except for one measurement, these are lighter than magmatic values (Taylor 1974; Sheppard 1986). Owing to extensive alteration and fracturing of the feldspars, the measured waters are a composite of multiple generations of pore fluids. Hence hydrogen isotopic values record a large spectrum of hydrothermal activity. Another possible source for low deuterium values is the interaction of rocks with meteoric water at high latitudes.

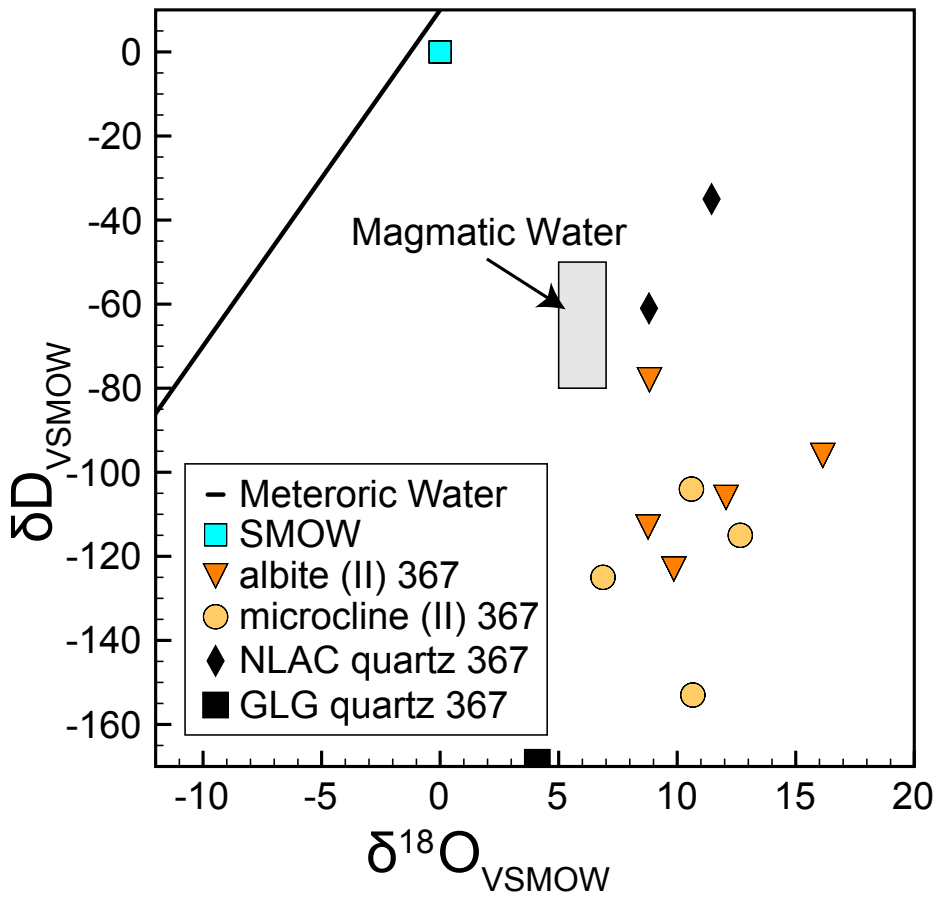

Figure 24: A plot of δD vs $\delta^{18}O$ of fluids interpreted to have been responsible for albitisation. The δD values are those of fluid inclusions extracted from the minerals indicated in the Figure and the $\delta^{18}O$ values those calculated to be in equilibrium with these minerals at 392 °C. The corresponding data are reported in Table 1 The data for the T-zone minerals were taken from Taylor and Pollard 1996.

Calcium is present in the albitite where it is mainly hosted by late alteration phases, fluorite and carbonate minerals. This represents an enrichment of Ca as there is a dearth of this element in primary magmatic mineral assemblages of the NLAS. Rocks external to the NLAS, i.e., the GLG and TLS, although relatively impoverished in Ca, contain more Ca than the NLAS (Davidson 1982) and could have supplied the Ca present in post-albitising fluorite and carbonate minerals.

In summary, the isotopic data and presence of Ca minerals in the albitite, point to an external fluid component. We propose that this fluid mixed with residual magmatic fluids near the outer and upper margins of the NLAS and that albitisation and post albitisation REE and HFSE mineralization were products of this mixing.

The Mechanisms of Albititisation

As discussed earlier, albitisation largely involved the replacement of primary K-feldspar by albite, and therefore was mainly the result of the cation-exchange reaction:

$$(Na^{+})_{aq} + \text{K-Feldspar} \rightarrow (K^{+})_{aq} + \text{Albite} \qquad (7).$$

Fluids in equilibrium with granite, and hence two alkali feldspars, become albitising when there is an increase in temperature, because of a displacement of the K-feldspar-albite stability boundary to higher $a K^{+}/a H^{+}$, which has the effect of placing the fluid composition in the field of stability of albite (Figure 25). Warming fluids in equilibrium with the GLG or TLS would be an obvious way of promoting the replacement of K-feldspar by albite in the NLAS. Indeed, using the values of $a Na^{+}$, $a K^{+}$ and pH estimated above, the values of log ($a Na^{+}/a H^{+}$) and log ($a K^{+}/a H^{+}$) would be 6.25 and 4.95, respectively. This would be consistent with equilibrium of the fluid with two feldspars at a temperature of 150 °C and its subsequent heating to the temperature of albitisation ~400 °C.

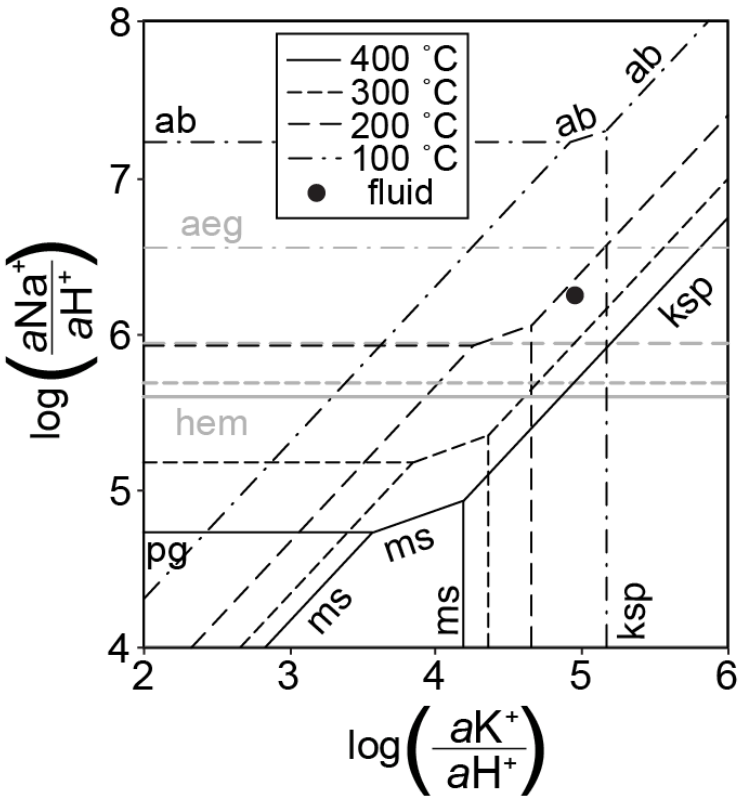

Figure 25: The stability of albite, K-feldspar and muscovite as a function of log (aNa$^+$/aH$^+$) and log (aK$^+$/aH$^+$) at temperatures from 150 to 400 °C. The SiO2 activity is that of quartz saturation, and the pressure, 4kbar. A black dot indicates the composition of the albitising fluid. The solid line shows the stability boundaries for 150 °C, the dashed lines indicate the stability boundaries at increasing 100 °C increments. Thermodynamic data from Shock and Helgeson (1988); Holland and Powell (1998)

Albitisation could also have been achieved by increasing aNa$^+$ at constant aK$^+$. Alteration of primary, end-member sodalite, aegirine and nepheline during cooling of the agpaitic NLAS, would have contributed sodium to the cooling magmatic fluids (which are inferred to have caused earlier biotite-magnetite alteration) or invading meteoric fluids. This explanation, however, is not consistent with the observation that within the albitite, secondary albite is commonly altered to K-feldspar along its rims (Fig 16d). Hence the former model is preferred, in which fluids external to the NLAS and in equilibrium with the GLG or TLS are drawn in and heated.

Fluid Pathway

Type C veins within the GLG are strongly albitised and are depleted in quartz and mafic minerals. Furthermore, Type C veins are filled with chlorite and calcite, which are also late alteration products within the NLAS. These veins may therefore represent conduits for fluids

within the granite that moved towards the NLAS. The TLS is adjacent to the NLAS and is texturally indistinguishable from the adjacent GLG, differing only in its lack of quartz. Although the boundary between the two units appears sharp in places, a gradual decrease in quartz content towards the NLAS is more common (e.g., Mumford et al. 2010, this study). The effect of drawing fluids through the TLS and warming them would be to dissolve quartz due to the increased solubility of the latter with increasing temperature. Hence, the TLS may simply be GLG that has furnished silica to the albitising fluids, and therefore represent a second, more diffuse, pathway for these fluids that acted in tandem with the narrow conduits represented by the Type C veins. An increase in temperature was needed to drive circulation of the altering fluids. This would have been provided by the intrusion of the NLAS into the GLG, which would have resulted in a temperature gradient that would have caused cool waters from the latter units to be drawn into the NLAS (Figure 26a).

Interaction of the NLAS with fluids initially in equilibrium with the two-feldspar-bearing GLG provides an attractive explanation for the albitisation. As noted above, these fluids would have been heated as they were drawn into the younger NLAS intrusion by convection, thereby, shifting the two-feldspar phase boundary resulting in fluid compositions in the field of stability of albite (Figure 25). This would have caused wholesale replacement of K-feldspar by albite within the upper NLAS. This interpretation is consistent with the observation that the albitite is dominant along the margin of NLAS as well as in satellite deposits such as the T-Zone. Warming fluids would also have promoted dissolution of the primary mineral assemblage, creating the observed porosity to allow open space filling by albite. Reaction of K-feldspar to albite results in a 9% molar volume decreases (Plümper and Putnis 2009), which creates porosity, promoting further replacement. Replacement of secondary albite by K-feldspar is consistent with decreasing fluid temperature, because of the expansion of the K-feldspar field with decreasing temperature, which causes a fluid initially in equilibrium with two feldspars to be in the K-feldspar field.

Fluid pressures caused by convecting formation waters derived from the GLG locally surpassed lithostatic pressures resulting in brecciation of the albitite. This lead to a decrease in temperature due to adiabatic expansion of the fluids, and triggered precipitation of quartz and fluorite in the breccia matrix.

The Source of the REE and HFSE

The late REE and HFSE mineralisation in the albitite was due to a preexisting endowment of these elements in the protolith and their hydrothermal mobilisation from the potential ore zones, particularly, the Upper Ore Zone, which it has been noted has a similar LREE/HREE ratio to that of the albitite. Magmatic endowment of the HFSE and REE prior to albitisation was possible as the albitites are generally stratigraphically superior to the Basal Ore Zone and overprinted the Upper Ore Zone (Figure 13). Rocks crystallising from magmas in the upper part of the complex are also interpreted to have undergone enrichment in the HFSE and REE due to magmatic fractionation of incompatible elements (Sheard et al. 2012).

Ascending exsolved magmatic fluids may have been responsible for transportation of the REE after albitisation. A decreasing vertical temperature gradient of alteration fluids precipitating biotite is supported by the observation of an increasing order of secondary biotite structure stratigraphically from the Basal Ore Zone through to the albitite (Figure 9c). This was the result of the ascent of hydrothermal fluids on a cooling path (Figure 26b). Exsolved magmatic fluids from the cooling NLAS were saturated in REE, preferentially mobilising the LREE over the HREE, which were later precipitated in pore space within the albitite.

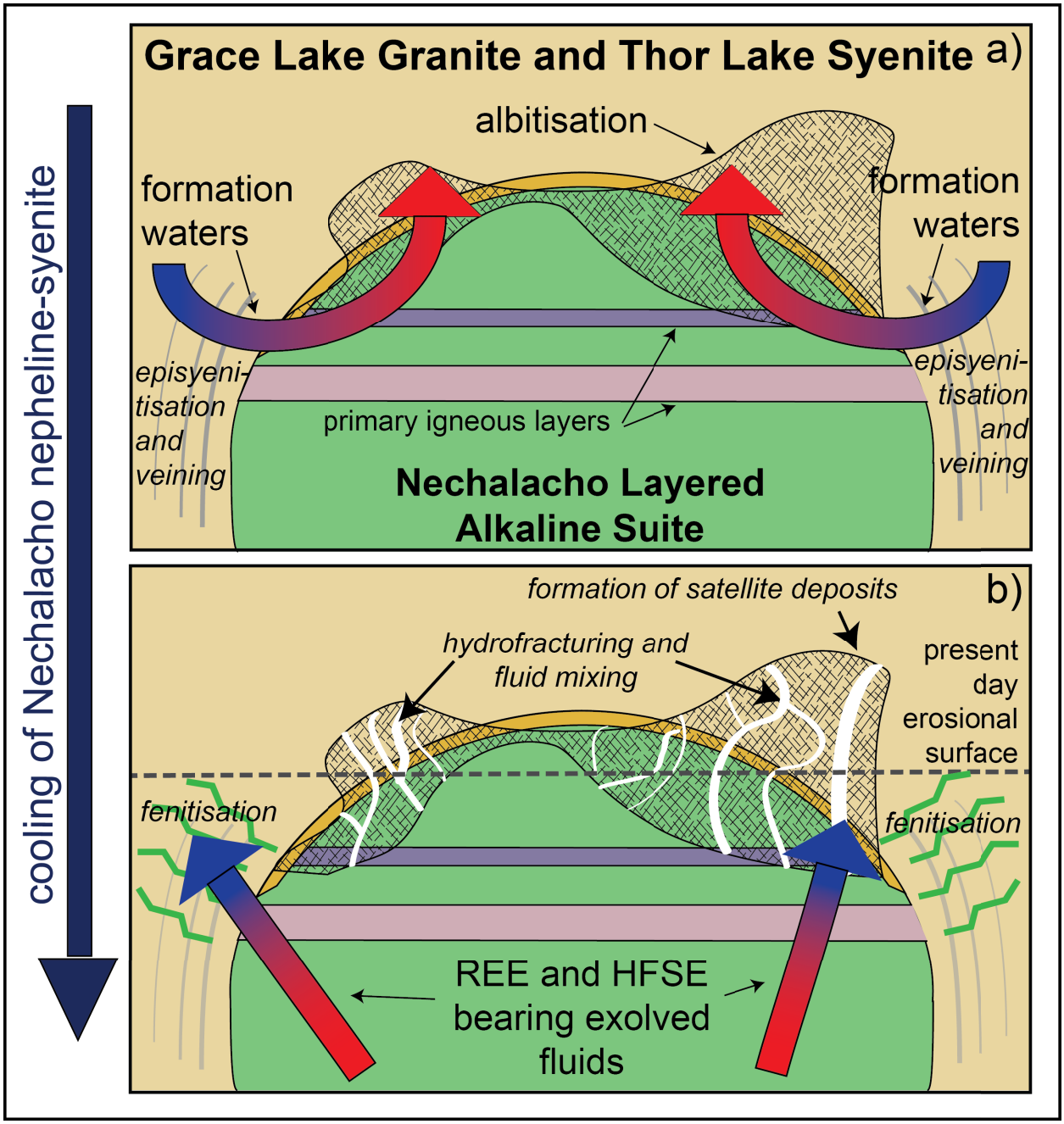

Figure 26: Model of alteration and late stage enrichment of the albitite unit within the Nechalacho Layered Alkaline Suite (NLAS). After emplacement and during cooling of the NLAS, convection occurred forcing formation waters to be drawn towards the hot intrusion from the Grace Lake Granite (GLG). The albitite was produced by the heating of formation waters initially in equilibrium with the GLG, and involved wholesale replacement of K-feldspar by albite and dissolution of mafic and undersaturated mineral phases. The convective hydrothermal regime was gradually replaced by exsolved magmatic fluids from within the NLAS. Hydrofracturing resulted from overpressuring within the altered cap. This caused a sudden drop in pressure and a corresponding drop in temperature due to adiabatic expansion of the fluid. The temperature decrease caused saturation of the fluid in quartz and fluorite. The REE were transported as chloride complexes in the magmatic hydrothermal fluid and were deposited in response to the decrease of temperature and an increase in pH (temperature also dropped and pH increased due to mixing with the formational waters) as(Ce)-bastnäsite-(Ce) and monazite-(Ce).

Fenitisation

The exsolved fluids were also responsible for alteration of the TLS and GLG. Type B veins within the GLG have aegirine and albite alteration halos similar to other fenites (e.g., Mississagi Quartzite, Siemiatkowska and Martin 1975; Oldoinyo Lengai, Morogan and Martin 1985; Alno, Morogan and Woolley 1988). In the GLG, the Type B veins were associated with mass additions of Ca, Mg, Fe^{3+}, Mn, Na and K, and large relative mass additions in REE. These localised mass changes were accompanied by losses in Si and Al. Mass changes such as these are similar to those observed in other fenites (e.g., Martin et al. 1978; Morogan 1989). Fenitisation does not increase in intensity with decreasing distance, but there is an increase in the number of veins with fenite haloes towards the NLAS.

Albitisation and REE Mineralisation

The albitite was porous, and provided an ideal environment for fluid mixing. Igneous rocks hosting REE deposits commonly show evidence of intense albitisation (e.g., IOCG deposits, Hitzman et al. 1992). In some cases, the fluids responsible for this alteration have also mobilised primary REE mineralisation and re-deposited it as secondary REE minerals (e.g., bastnäsite-(Ce) and monazite; Hitzman et al. 1992). In the NLAS, fluorite is commonly intergrown with acicular bastnäsite-(Ce) and monazite-(Ce), and minor sphalerite, suggesting that these minerals are genetically associated. A genetic link between bastnäsite-(Ce) and fluorite is also inferred for the Gallinas Mountains (Williams-Jones et al. 2000). We envisage a model in which the REE were transported as chloride complexes in the magmatic hydrothermal fluid, which subsequently mixed with the albitising formation waters, thereby cooling them and increasing pH, leading to the precipitation of REE minerals.

Conclusion

The results of this study show that the albitite is a hydrothermal overprint caused by the influx of external fluids into the NLAS. Formation waters in equilibrium with the surrounding GLG were heated due to the emplacement of the NLAS. Fluids in equilibrium with granite, i.e., with two feldspars, became albitising due to the increasing temperature, which expanded the stability field of albite to include conditions represented by the $a\mathrm{Na}^{+}/a\mathrm{K}^{+}$ ratio of the fluid. In addition, the

increase in temperature caused dissolution of quartz. Thus the heated fluids albitised and desilicified the granite along vein conduits within the GLG and also pervasively to produce the TLS. Interaction of these fluids with the NLAS had a profound effect resulting in large scale dissolution and replacement of the host rocks with secondary albite. External fluids were the source of Si and Ca added to the NLAS. The effects of exsolved fluids from the NLAS on the GLG are typical of those reported in country rocks adjacent to other silica-undersaturated alkaline intrusives. The HFSE, and in particular the REE were remobilized from the upper part of the NLAS, especially the Upper Ore Zone by magmatic hydrothermal fluids, and deposited as a result of mixing with external fluids enriching both the albitite and the granitic country rocks.

Acknowledgements

Financial support for this research was provided by a grant from Avalon Rare Metals Inc. and a matching grant from the NSERC Collaborative Research and Development Program, both to A.E. Williams-Jones. Avalon Rare Metals Inc. provided access to the field area, drill core and proprietary data. Geologists Chris Pederson and Martin Heiligmann are thanked for ground work on the deposit, as well as all those involved in exploration and research at Thor Lake.

References

Abdel-Rahman, M.A.-F. and El-kibbi, M.M., 2001. Anorogenic magmatism: chemical evolution of the Mount El-Sibai A-type complex (Egypt), and implications for the origin of within-plate felsic magmas. *Geological Magazine*, 138(1), pp.67–85.

Bau, M. et al., 2003. Tracing element sources of hydrothermal mineral deposits: REE and Y distribution and Sr-Nd-Pb isotopes in fluorite from MVT deposits in the Pennine Orefield, England. *Mineralium Deposita*, 38, pp.992–1008.

Bleeker, W. and Hall, B., 2007. The Slave Craton: Geology and metallogenic evolution. In W. D. Goodfellow, ed. *Mineral Deposits of Canada : a Synthesis of Major Deposit-types, District Metallogeny, the Evolution of Geological Provinces, and Exploration Methods*. St. John's, NL: Geological Association of Canada, Mineral Deposits Division, pp. 849–879.

Boily, M. and Williams-Jones, A.E., 1994. The role of magmatic and hydrothermal processes in the chemical evolution of the Strange Lake plutonic complex, Québec-Labrador. *Contributions to Mineralogy and Petrology*, 118, pp.33–47.

Boone, G.M., 1969. Origin of Clouded Red Feldspars; Petrologic Contrasts in a Granitic Porphyry Intrusion. *American Journal of Science*, 267(6), pp.633–668.

Boulvais, P. et al., 2007. Cretaceous albitization and dequartzification of Hercynian peraluminous granite in the Salvezines Massif (French Pyrénées). *Lithos*, 93, pp.89–106.

Černý, P. and Trueman, D.L., 1985. Polylithionite from the rare-metal deposits of the Blachford Lake alkaline complex, N.W.T., Canada. *American Mineralogist*, 70, pp.1127–1134.

Ciuculescu, T. et al., 2013. *Technical report disclosing the results of the feasibility study on the Nechalacho Rare Earth Elements project*,

Collins, W.J. et al., 1982. Nature and origin of A-type granites with particular reference to southeastern Australia. *Contributions to Mineralogy and Petrology*, 80, pp.189–200.

Davidson, A., 1972. Granite Studies in the Slave Province (parts of 85 I). *Report of Activities, Part A, Geological Survey of Canada*, Paper 72-1, pp.109–112.

Davidson, A., 1982. Petrochemistry of the Blachford Lake complex near Yellowknife, Northwest Territories. In Y. T. Maurice, ed. *Uranium in Granites*. Ottawa, Ontario: Canadian Government Publishing Centre, pp. 71–79.

Davidson, A., 1978. The Blachford Lake intrusive suite: an aphebian alkaline plutonic complex in the Slave Province, Northwest Territories. *Current Research, Part A, Geol. Surv, Can.*, Paper 78-1, pp.119–127.

Feng, Y., 2014. *Hydrothermal Geochemistry and Mineralizing Proessess in the T Zone, Thor Lake Rare-element Deposit, Northwest Territories*. University of Windsor.

Graser, G. and Markl, G., 2008. Ca-rich Ilvaite-Eepidote-hydrogarnet endoskarns: a record of late-magmatic fluid influx into the persodic Ilimaussaq Complex, South Greenland. *Journal of Petrology*, 49(2), pp.239–265.

Gysi, A.P. and Williams-Jones, A.E., 2013. Hydrothermal mobilization of pegmatite-hosted REE and Zr at Strange Lake, Canada: A reaction path model. *Geochimica et Cosmochimica Acta*, 122, pp.324–352.

Helgeson, H.C., Kirkham, D.H. and Flowers, G.C., 1981. Theoretical prediction of the thermodynamic behavior of aqueous electrolytes by high pressure and temperatures; IV, Calculation of activity coefficients, osmotic coefficients, and apparent molal and standard and relative partial molal properties to 600 de. *American Journal of Science*, 281, pp.1249–1516.

Van Hinsberg, V.J., Migdisov, A.A. and Williams-Jones, A.E., 2010. Reading the mineral record of fluid composition from element partitioning. *Geology*, 38(9), pp.847–850.

Hitzman, M.W., Oreskes, N. and Einaudi, M.T., 1992. Geological characteristics and tectonic setting of Proterozoic iron oxide (Cu-U-Au-REE) deposits. *Precambrian Research*, 58, pp.241–287.

Holland, T. and Powell, R., 1998. An internally consistent thermodynamic data set for phases of petrological interest. *Journal of metamorphic Geology*, 16, pp.309–343.

Kogarko, L.N., Williams, C.T. and Woolley, A.R., 2002. Chemical evolution and petrogenetic implications of loparite in the layered, agpaitic Lovozero complex, Kola Peninsula, Russia. *Mineralogy and Petrology*, 74, pp.1–24.

Kogarko, L.N.N., 1990. Ore-forming potential of alkaline magmas A. R. Woolley and M. Ross, eds. *Lithos*, 26, pp.167–175.

Larsen, L.M., 1979. Distribution of REE and other trace elements between phynocrysts and peralkaline undersaturated magmas, explified by rocks from the Gardar igneous province, South Greenland. *Lithos*, 12, pp.303–315.

Linnen, R.L. and Keppler, H., 1997. Columbite solubility in granitic melts: consequences for the enrichment and fractionation of Nb and Ta in the Earth's crust. *Contributions to Mineralogy and Petrology*, 128, pp.213–227.

Loges, A. et al., 2013. An Experimental Study of the Aqueous Solubility and Speciation of Y(III) Fluoride at Temperatures up to 250°C. *Geochimica et Cosmochimica Acta*, 123, pp.403–415.

Marks, M.A.W. et al., 2011. The Mineralogical Diversity of Alkaline Igneous Rocks: Critical Factors for the Transition from Miaskitic to Agpaitic Phase Assemblages. *Journal of Petrology*, 52(3), pp.439–455.

Martin, R.F., Whitley, J.E. and Woolley, A.R., 1978. An Investigation of Rare-Earth Mobility: Fenitized Quartzites, Borralan Complex, N.W. Scotland. *Contributions to Mineralogy and Petrology*, 66, pp.69–73.

Mason, R.A., 1992. Models of order and iron-fluorine avoidance in biotite. *The Canadian Mineralogist*, 30, pp.343–354.

Migdisov, A.A. et al., 2011. An experimental study of the solubility of baddeleyite (ZrO2) in fluoride-bearing solutions at elevated temperature. *Geochimica et Cosmochimica Acta*, 75, pp.7426–7434.

Migdisov, A.A., Williams-Jones, A.E. and Wagner, T., 2009. An experimental study of the solubility and speciation of the Rare Earth Elements (III) in fluorite- and chloride-bearing aqueous solutions at temperatures up to 300˚C. *Geochimica et Cosmochimica Acta*, 73, pp.7087–7109.

Mitchell, R.H. and Liferovich, R.P., 2006. Subsolidus deuteric/hydrothermal alteration of eudialyte in lujavrite from the Pilansberg alkaline complex, South Africa. *Lithos*, 91, pp.352–372.

Möller, V. and Williams-Jones, A.E., 2013. Magmatic Controls on the Formation of the Nechalacho Rare Metal Deposit (Thor Lake, NWT, Canada). In *Geoscience for Discovery (SEG 2013)*.

Morogan, V., 1989. Mass transfer and REE mobility during fenitization at Alnö, Sweden. *Contributions to Mineralogy and Petrology*, 103, pp.25–34.

Morogan, V. and Woolley, A.R., 1988. Fenitization at the Alnö carbonatite complex, Sweden; distribution, mineralogy and genesis. *Contributions to Mineralogy and Petrology*, 100, pp.169–182.

Mumford, T.R., 2013. *Petrology of the Blatchford Lake Intrusive Suite, Northwest Territories, Canada*. Carleton University.

Mumford, T.R., Martins, T. and Falck, H., 2010. Geochemical Results from the Blachford Lake Intrusive Suite Mapping Project (2009 field season). *Northwest Territories Geoscience Office*, NWT Open R, p.25.

Olivo, G.R. and Williams-Jones, A.E., 1999. Hydrothermal REE-rich eudialyte from the Pilanesberg Complex, South Africa. *Canadian Mineralogist*, 37, pp.653–663.

Oreskes, N. and Einaudi, M.T., 1990. Origin of rare earth element-enriched hematite breccias at the Olympic Dam Cu-U-Au-Ag deposit, Roxby Downs, South Australia. *Economic Geology*, 85(1), pp.1–28.

Paul, J. and Stubens, T.C., 2009. *Thor Lake - Lake Zone mineral resource update* G. Arseneau, ed., Toronto: Wordrop.

Pinkston, D.R. and Smith, D.G.W., 1995. Mineralogy of the Lake zone, Thor Lake rare-metals deposit, N.W.T., Canada. *Canadian Journal of Earth Sciences*, 32, pp.516–532.

Plümper, O. and Putnis, A., 2009. The complex hydrothermal history of granitic rocks: Multiple feldspar replacement reactions under subsolidus conditions. *Journal of Petrology*, 50(5), pp.967–987.

Porto da Silveira, C.L., Schorscher, H.D. and Miekeley, N., 1991. The geochemistry of albitization and related uranium mineralization, Espinharas, Paraiba (PB), Brazil. *Journal of Geochemical Exploration*, 40, pp.329–347.

Preston, R.F., Stevens, G. and McCarthy, T.S., 2003. Fluid compositions in equilibrium with silica-undersaturated magmas in the system Na2O–Al2O3–SiO2–H2O: clues to the

composition of fenitizing fluids. *Contributions to Mineralogy and Petrology*, 144, pp.559–569.

Putnis, A. et al., 2007. Hematite in porous red-clouded feldspars: Evidence of large-scale crustal fluid-rock interaction. *Lithos*, 95, pp.10–18.

Salvi, S. et al., 2000. Hydrothermal Mobilization of High Field Strength Elements in Alkaline Igneous Systems: Evidence from the Tamazeght Complex (Morocco). *Economic Geology*, 95, pp.559–576.

Salvi, S. and Williams-Jones, A.E., 1996. The role of hydrothermal processes in concentrating high-field strength elements in the Strange Lake peralkaline complex, northeastern Canada. *Geochimica et Cosmochimica Acta*, 60(11), pp.1917–1932.

Salvi, S. and Williams-Jones, A.E., 1990. The role of hydrothermal processes in the granite-hosted Zr, Y, REE deposit at Strange Lake, Quebec/Labrador: Evidence from fluid inclusions. *Geochimica et Cosmochimica Acta*, 54, pp.2403–2418.

Schilling, J. et al., 2009. Reconstruction of magmatic to subsolidus processes in an agpaitic system using eudialyte textures and composition: a case study from tamazeght, morocco. *The Canadian Mineralogist*, 47, pp.351–365.

Schmitt, A.K. et al., 2002. Zr-Nb-REE Mineralization in Peralkaline Granites from the Amis Complex, Brandberg (Namibia): Evidence for Magmatic Pre-enrichment from Melt Inclusions. *Economic Geology*, 97, pp.399–413.

Schönenberger, J. et al., 2006. Fluid-rock interaction in autoliths of agpaitic nepheline syenites in the Ilímaussaq intrusion, South Greenland. *Lithos*, 91, pp.331–351.

Sheard, E.R. et al., 2012. Controls on the concentration of zirconium, niobium, and the rare earth elements in the Thor Lake rare metal deposit, Northwest Territories, Canada. *Economic Geology*, 107, pp.81–104.

Shock, E.L. and Helgeson, H.C., 1988. Calculation of the thermodynamic and transport properties of aqueous species at high pressures and temperatures: Correlation algorithms for ionic species and equation of state predictions to 5 kb and 1000°C. *Geochimica et Cosmochimica Acta*, 52, pp.2009–2036.

Sinclair, W.D., P.A., H. and Birkett, T.C., 1994. U-Pb zircon and monazite ages of the Grace Lake Granite, Blatchford Lake Intrusive Suite, Slave Province, Northwest Territories. In *Radiogenic Age and Isotopic Studies*. Current Research. Geological Survey of Canada, pp. 15–20.

Sörensen, H., 1997. The agpaitic rocks; an overview. *Mineral Mag*, 61, pp.485–498.

Sörensen, H. and Laren, L.M., 2001. The hyper-agpaitic stage in the evolution of the Ilimaussaq alkaline complex, South Greenland. *Geology of Greenland survey bulletin*, 301, p.83.

Sørrensen, H., 1992. Agpaitic nepheline syenites: A potential source of rare elements. *Applied Geochemistry*, 7, pp.417–427.

Steele-MacInnis, M., Lecumberri-Sanchez, P. and Bodnar, R.J., 2012. HokieFlincs_H2O-NaCl A Microsoft Excel spreadsheet for interpreting microthermometric data from fluid inclusions based on the PVTX properties of H2O-NaCl. *Computers and Geosciences*, 49, pp.334–337.

Sun, S. -s. and McDonough, W.F., 1989. Chemical and isotopic systematics of oceanic basalts: implications for mantle composition and processes. *Geological Society, London, Special Publications*, 42, pp.313–345.

Thompson, T.B., 1988. Geology and uranium-thorium mineral deposits of the Bokan Mountain Granite Complex, southeastern Alaska. *Ore Geology Reviews*, 3, pp.193–210.

Timofeev, A. and Williams-Jones, A.E., 2014. Controls on the Distribution of Gallium in the Nechalacho REE Deposit, NWT, Canada. *Economic Geology*, 110, pp.173–185.

Timofeev, A. and Williams-Jones, A.E., The origin of niobium and tantalum mineralization in the Nechalacho REE deposit, NWT, Canada.

Watson, E.B., 1979. Zircon saturation in felsic liquids: Experimental results and applications to trace element geochemistry. *Contributions to Mineralogy and Petrology*, 70, pp.407–419.

Williams-Jones, A.E., Migdisov, A. a. and Samson, I.M., 2012. Hydrothermal mobilisation of the rare earth elements-a tale of "ceria" and "yttria." *Elements*, 8, pp.355–360.

Williams-Jones, A.E., Samson, I.M. and Olivo, G.R., 2000. The genesis of hydrothermal fluorite-REE deposits in the Gallinas Mountains, New Mexico. *Economic Geology and the Bulletin of the Society of Economic Geologists*, 95(2), pp.327–341.

Chapter 3: Conclusions and Contributions to Knowledge

Conclusions

The albitite overlying the Nechalacho REE deposit is a hydrothermal overprint caused by influx of external fluids into the NLAS also affecting the GLG. Formation waters held within the granitic units adjacent to the NLAS were responsible for albitisation. These fluids, in equilibrium with the GLG, were heated due to the emplacement of the NLAS. Heating of the fluids, initially in equilibrium with two alkali feldspars, expanded the field of stability of albite relative to k-feldspar with respect to the $a\mathrm{Na}^{+}/a\mathrm{K}^{+}$ ratio of the fluid, resulting in an albitisation. In addition, the increased temperature of the fluids resulted in the dissolution of quartz. The heated fluids albitised and desilicified the granite both pervasively and along vein conduits (type C veins) within the GLG to produce the TLS. The TLS, between the GLG and the silica-undersaturated NLAS, is an altered unit of the GLG that underwent episyenitisation and albitisation, altered by the albitising fluids. The T-zone, R-Zone, S-Zone and Fluorite-Zone satellite deposits located adjacent to the Nechalacho deposit were also affected by the same albitising fluids. Albitisation affected the NLAS pervasively, but had its greatest impact along the southern outer edge within the upper 300m, resulting in dissolution and replacement of the entire rock by secondary albite. As the fluids cooled, both due to adiabatic expansion caused by brecciation and further cooling of the NLAS, K-feldspar replaced albite and quartz was precipitated.

Fenitisation of the GLG and TLS is a late overprint cause by deuteric fluids exolved from the NLAS. Rocks in proximity to the NLAS exhibit characteristics common to other documented fenites adjacent to silica-undersaturated intrusions. Fenitisation is largely manifested as type B veins containing fluorite and carbonate minerals with albitised and aegirinised selvedges, and increase in intensity with proximity to the NLAS. Mass changes due to fenitisation in the GLG included additions of Ca, Mg, Fe^{3+}, Mn, Na and K, and large relative mass additions in REE.

Conditions of albitisation were determined considering phase stability relationships at 4kbar and 367°C obtained from regional studies by Mumford (2013) and studies on the adjacent T-zone by Feng (2014), respectively. The activities of Na^{+} and K^{+} were 2.80 and 0.14 respectively, calculated using fluid inclusion analyses from Feng (2014). The albitite contains ubiquitous hematite, notably the cause of the pink colouration in secondary albite, though adjacent rocks

units contain magnetite. The fO_2 conditions therefore surpassed the hematite-magnetite buffer, i.e. >-29.3 at a temperature of 367°C. The pH was constrained due to the stability of albite and hematite according to their reactions to paragonite and aegirine, respectively, to between 5.6 and 6.0. The $aSi0_2$ during albitisation was bound by the reactions of abite with muscovite and paragonite and the saturation of quartz. For conditions of pH=5.8 the minimum $log aSi0_2$ ranged between -2.4 and -2.0 for temperatures ranging from 250 to 400, respectively. As *a*Ca activity was negligible for magmatic conditions in the NLAS and fluorite and Ca-fluorocarbonates are relatively common in the albitite interstitial to secondary albite, it is believed that aCa^+ increased late- to post-albitisation and Ca was introduced by external fluids, further supporting the external source of albitising fluids.

The distribution of the albitite in the NLAS and textural evidence suggest that REE and HFSE mineralization was overprinted by albitisation. The REE-, Nb-, Y-, Zr-, Ti- and U-bearing solid micro-inclusions, and the presence of REE and HFSE minerals interstitial to secondary albite provides additional evidence that REE and HFSE were mobile in the albitising and post-albitising fluids. Although the chlorinity of the albitising fluids was likely adequate to transport the REE and other HFSE, relatively low pH conditions are required. As such, deuteric fluids are interpreted to have had an important role in transporting and redistributing the REE and HFSE within the albitite.

The albitite was porous, and provided an ideal environment for fluid mixing. In the NLAS, fluorite is commonly intergrown with acicular bastnäsite-(Ce) and monazite-(Ce), and minor sphalerite, suggesting that these minerals are genetically associated. The REE were transported as chloride complexes in the fluorite-rich magmatic hydrothermal fluid, and mixed with the albitising formation waters, thereby cooling them and increasing pH, leading to the precipitation of REE minerals.

Contributions to Knowledge

Hydrothermal alteration of rocks is an ubiquitous process often linked to the genesis of ore deposits, particularly those emplaced magmatically (e.g., porphyry deposits; White and Hedenquist 1990). There are few studies of alteration related to the emplacement of REE

deposits. Research on alteration related to agpaitic magmatism, which is often accompanied by enrichment in the REE, are limited to Ilímaussaq (Markl and Baumgartner 2002; Schönenberger et al. 2006; Graser and Markl 2008), Tamazeght (Salvi et al. 2000; Schilling et al. 2009) and Pilaneberg (Olivo and Williams-Jones 1999; Mitchell and Liferovich 2006). In addition, albitisation is an enigmatic alteration type that is under-reported in the scientific literature. It is present in a wide variety of geological settings such as halos around crustal scale fluid conduits (Boulvais et al. 2007; Engvik et al. 2008), as a type of fenitisation (Garson et al. 1984) and as the result of hydrothermal alteration in agpaitic rocks (Schilling et al. 2009). It is an alteration type associated with REE-bearing deposits, e.g., IOCG deposits (Hitzman et al. 1992). At the Nechalacho REE deposit, albitisation was a critical component in the mobilisation and redistribution of REE and HFSE.

This study has validated an hypothesis of fluid provenance and behavior resulting in alteration in relation to a REE-deposit within a layered agpaitic intrusion. The original research conducted was used to 1) identify albitisation mineral paragenesis within the albitite; 2) quantify the effects of alteration within the GLG as fenitisation (type B veins) by using the mass balance method; 3) identify fluid pathways as vein type 3 and the creation of isopach and cross section through the intrusion; 4) determine the likely source of alteration fluids as formation waters using stable isotopic data and by identifying the source of some chemical components (i.e. Ca); 5) constrain physicochemical conditions of alteration using phase relationships at fO_2 >-29.3, pH between 5.6 and 6.0, and log$a$Si0_2 from -2.4 and -1.4 for temperatures ranging from 250 to 400, respectively. In addition, this study builds on laboratory studies of REE and HFSE mobility in hydrothermal solutions (van Hinsberg et al. 2010; Migdisov et al. 2009; Williams-Jones et al. 2012; Loges et al. 2013) to evaluate the mobility of the REE and HFSE in alteration fluids. Albitisation of the NLAS and episyenitisation and fenitisation of the GLG is readily explained by formation waters heated and drawn towards the NLAS by the emplacement of the younger and hotter intrusion, and these both dissolved quartz in the GLG and TLS and promoted albitisation, brecciation and creation of porosity within the NLAS. Deuteric fluids exsolved from the NLAS altered the TLS, causing fenitisation. Mixing of the albitising fluids with exolved magmatic fluids resulted in precipitation of REE and HFSE within the albitised rocks. The results of this research as a case study of the Nechalacho deposit will guide further regional studies, and be applicable to all

research regarding albitisation, alteration of agpaitic intrusions and alteration related to REE deposits

References

Abdel-Rahman, M.A.-F. and El-kibbi, M.M., 2001. Anorogenic magmatism: chemical evolution of the Mount El-Sibai A-type complex (Egypt), and implications for the origin of within-plate felsic magmas. *Geological Magazine*, 138(1), pp.67–85.

Anderson, I.C., Frost, C.D. and Frost, B.R., 2003. Petrogenesis of the Red Mountain pluton, Laramie anorthosite complex, Wyoming: implications for the origin of A-type granite. *Precambrian Research*, 124, pp.243–267.

Appleyard, E.C. and Woolley, A.R., 1979. Fenitization: An example of the problems of characterizing mass transfer and volume changes. *Chemical Geology*, 26, pp.1–15.

Bailey, D.K., 1980. Volcanism, Earth degassing and replenished lithosphere mantle. *Philosophical Transactions of the Royal Society of London. Series A, Mathematical and Physical Sciences*, 297(1431), pp.309–322.

Bakker, F. et al., 2011. *Technical report on the nechalacho deposit, Thor Lake project, Northwest Territories, Canada*.

Banks, D.A.A. et al., 1994. REE composition of an aqueous magmatic fluid: A fluid inclusion study from the Capitan Pluton, New Mexico, U.S.A. *Chemical Geology*, 113, pp.259–272.

Bau, M. et al., 2003. Tracing element sources of hydrothermal mineral deposits: REE and Y distribution and Sr-Nd-Pb isotopes in fluorite from MVT deposits in the Pennine Orefield, England. *Mineralium Deposita*, 38, pp.992–1008.

Beitter, T., Wagner, T. and Markl, G., 2008. Formation of kyanite--quartz veins of the Alpe Sponda, Central Alps, Switzerland: implications for Al transport during regional metamorphism. *Contributions to Mineralogy and Petrology*, 156, pp.689–707.

Birkett, T., Richardson, D.G. and Sinclair, W.D., 1994. Gravity modelling of the Blatchford Lake Intrusive Suite , Northwest Territories. In *Studies of Rare-Metal Deposits in the Northwest Territories*. pp. 5–16.

Bleeker, W. and Hall, B., 2007. The Slave Craton: Geology and metallogenic evolution. In W. D. Goodfellow, ed. *Mineral Deposits of Canada : a Synthesis of Major Deposit-types, District Metallogeny, the Evolution of Geological Provinces, and Exploration Methods*. St. John's, NL: Geological Association of Canada, Mineral Deposits Division, pp. 849–879.

Boily, M. and Williams-Jones, A.E., 1994. The role of magmatic and hydrothermal processes in the chemical evolution of the Strange Lake plutonic complex, Québec-Labrador. *Contributions to Mineralogy and Petrology*, 118, pp.33–47.

Boone, G.M., 1969. Origin of Clouded Red Feldspars; Petrologic Contrasts in a Granitic Porphyry Intrusion. *American Journal of Science*, 267(6), pp.633–668.

Boulvais, P. et al., 2007. Cretaceous albitization and dequartzification of Hercynian peraluminous granite in the Salvezines Massif (French Pyrénées). *Lithos*, 93, pp.89–106.

Bowen, N.L., 1937. Recent high-temperature research on silicates and its significance in igneous geology. *American Journal of Science*, s5-33, pp.1–21.

Bowring, S.A., Van Schmus, W.R. and Hoffman, P.F., 1984. U-Pb Zircon ages from the Athupuscow Aulacogen, East Arm of Great Slave Lake, N.W.T., Canada. *Canadian Journal of Earth Sciences*, 21, pp.1315–1324.

Brögger, W.C., 1921. Die Eruptivgesteine des Kristianiagebeites, IV. Das Fengebeit in Telemark, Norwegen. *Vitensk. Skr., I Mat.-Naturvitensk. KI. 1920*, KL 1920(9), p.408 pp.

Černý, P. and Trueman, D.L., 1985. Polylithionite from the rare-metal deposits of the Blachford Lake alkaline complex, N.W.T., Canada. *American Mineralogist*, 70, pp.1127–1134.

Charbonneau, B.W. and Legault, M.I., 1994. Interpretation of airborne geophysical data for the Thor Lake Area, Northwest Territories. In D. G. R. W.D. Sinclair, ed. *Studies of Rare-Metal Deposits in the Northwest Territories*. St. John's N.L.: Geological Survey of Canada, pp. 17–31.

Ciuculescu, T. et al., 2013. *Technical report disclosing the results of the feasibility study on the Nechalacho Rare Earth Elements project*.

Collins, W.J. et al., 1982. Nature and origin of A-type granites with particular reference to southeastern Australia. *Contributions to Mineralogy and Petrology*, 80, pp.189–200.

Currie, K.L. and Ferguson, J., 1971. A Study of Fenitization Around the Alkaline Carbonatite Complex at Callander Bay, Ontario, Canada. *Canadian Journal of Earth Sciences*, 8, p.498.

Currie, K.L. and Ferguson, J., 1972. A Study of Fenitization in Mafic Rocks, with Special Reference to the Callander Bay Complex. *Canadian Journal of Earth Sciences*, 9, pp.1254–1261.

Currie, K.L., Knutson, J. and Temby, P.A., 1992. The Mud Tank carbonatite complex, central Australia ---an example of metasomatism at mid-crustal levels. *Contributions to Mineralogy and Petrology*, 109, pp.326–339.

Davidson, A., 1972. Granite Studies in the Slave Province (parts of 85 I). *Report of Activities, Part A, Geological Survey of Canada*, Paper 72-1, pp.109–112.

Davidson, A., 1982. Petrochemistry of the Blachford Lake complex near Yellowknife, Northwest Territories. In Y. T. Maurice, ed. *Uranium in Granites*. Ottawa, Ontario: Canadian Government Publishing Centre, pp. 71–79.

Davidson, A., 1981. Petrochemistry of the Blachford Lake Complex, District of MacKenzie. *Geological Survey of Canada Open File*, p.24.

Davidson, A., 1978. The Blachford Lake intrusive suite: an aphebian alkaline plutonic complex in the Slave Province, Northwest Territories. *Current Research, Part A, Geol. Surv, Can.*, Paper 78-1, pp.119–127.

Davies, G.R. and Macdonald, R., 1987. Crustal influences in the petrogenesis of the naivasha basalt - comendite complex: Combined trace element and Sr-Nd-Pb isotope constraints. *Journal of Petrology*, 28(6), pp.1009–1031.

Eby, G.N., 1992. Chemical subdivision of the A-type granitoids:Petrogenetic and tectonic implications. *Geology*, 20, pp.641–644.

Eby, G.N., 1985. Monteregian Hills II. Petrography, Major and Trace Element Geochemistry, and Strontium Isotopic Chemistry of the Eastern Intrusions: Mounts Shefford, Brome and Megantic. *Journal of Petrology*, 26(2), pp.418–448.

Engvik, A.K. et al., 2008. Albitization of granitic rocks: The mechanism of replacement of oligoclase by albite. *Canadian Mineralogist*, 46(6), pp.1401–1415.

Féménias, O. et al., 2005. Emplacement processes and cooling history of layered cyclic unit II-7 from the Lovozero alkaline massif (Kola Peninsula, Russia). *Lithos*, 83, pp.371–393.

Feng, Y., 2014. *Hydrothermal Geochemistry and Mineralizing Proessess in the T Zone, Thor Lake Rare-element Deposit, Northwest Territories*. University of Windsor.

Foland, K.A. et al., 1993. Formation of cogenetic quartz and nepheline syenites. *Geochimica et Cosmochimica Acta*, 57, p.7.

Garson, M.S. et al., 1984. Fenites, Breccia Dykes, Albitites, and Carbonatitic Veins Near the Great Glen Fault, Inverness, Scotland. *Journal of the Geological Society*, 141(4), pp.711–732.

Gerasimovsky, V.I. et al., 1966. *Geochemistry of the Lovozero Alkaline Massif (English Translation by Brown D.A. 1968. Austral. Nation. Univ. Press Camberra, 369 pp.)*, Nauka, Moscow.

Graser, G. et al., 2008. Isotope, major, minor and trace element geochemistry of late-magmatic fluids in the peralkaline IlÌmaussaq intrusion, South Greenland. *Lithos*, 106, pp.207–221.

Graser, G. and Markl, G., 2008. Ca-rich Ilvaite-Eepidote-hydrogarnet endoskarns: a record of late-magmatic fluid influx into the persodic Ilimaussaq Complex, South Greenland. *Journal of Petrology*, 49(2), pp.239–265.

Gysi, A.P. and Williams-Jones, A.E., 2013. Hydrothermal mobilization of pegmatite-hosted REE and Zr at Strange Lake, Canada: A reaction path model. *Geochimica et Cosmochimica Acta*, 122, pp.324–352.

Harris, C., 1995. Oxygen isotope geochemistry of the Mesozoic anorogenic complexes of Damaraland, northwest Namibia: evidence for crustal contamination and its effect on silica saturation. *Contributions to Mineralogy and Petrology*, 122, pp.308–321.

Helgeson, H.C., Kirkham, D.H. and Flowers, G.C., 1981. Theoretical prediction of the thermodynamic behavior of aqueous electrolytes by high pressure and temperatures; IV, Calculation of activity coefficients, osmotic coefficients, and apparent molal and standard and relative partial molal properties to 600 de. *American Journal of Science*, 281, pp.1249–1516.

Van Hinsberg, V.J., Migdisov, A.A. and Williams-Jones, A.E., 2010. Reading the mineral record of fluid composition from element partitioning. *Geology*, 38(9), pp.847–850.

Hitzman, M.W., Oreskes, N. and Einaudi, M.T., 1992. Geological characteristics and tectonic setting of Proterozoic iron oxide (Cu-U-Au-REE) deposits. *Precambrian Research*, 58, pp.241–287.

Hoefs, J. and Emmermann, R., 1983. The Oxygen Isotope Composition of Hercynian Granites and Pre-Hercynian Gneisses from the Schwarzwald, SW Germany. *Contributions to Mineralogy and Petrology*, 83, pp.320–329.

Holland, T. and Powell, R., 1998. An internally consistent thermodynamic data set for phases of petrological interest. *Journal of metamorphic Geology*, 16, pp.309–343.

Keppler, H., 1993. Influence of fluorine on the enrichment of high field strength trace elements in granitic rocks. *Contributions to Mineralogy and Petrology*, 114(4), pp.479–488.

Kogarko, L.N., Williams, C.T. and Woolley, A.R., 2002. Chemical evolution and petrogenetic implications of loparite in the layered, agpaitic Lovozero complex, Kola Peninsula, Russia. *Mineralogy and Petrology*, 74, pp.1–24.

Kogarko, L.N.N., 1990. Ore-forming potential of alkaline magmas A. R. Woolley and M. Ross, eds. *Lithos*, 26, pp.167–175.

Kramm, U. and Kogarko, L.N., 1994. Nd and Sr isotope signatures of the Khibina and Lovozero agpaitic centres, Kola Alkaline province, Russia. *Lithos*, 32, pp.225–242.

Kresten, P., 1988. The chemistry of fenitization: Examples from Fen, Norway. *Chemical Geology*, 68, pp.329–349.

Kresten, P. and Morogan, V., 1986. Fenitization at the Fen complex, southern Norway. *Lithos*, 19, pp.27–42.

Larsen, L.M., 1979. Distribution of REE and other trace elements between phynocrysts and peralkaline undersaturated magmas, explified by rocks from the Gardar igneous province, South Greenland. *Lithos*, 12, pp.303–315.

Linnen, R.L. and Keppler, H., 1997. Columbite solubility in granitic melts: consequences for the enrichment and fractionation of Nb and Ta in the Earth's crust. *Contributions to Mineralogy and Petrology*, 128, pp.213–227.

Loges, A. et al., 2013. An Experimental Study of the Aqueous Solubility and Speciation of Y(III) Fluoride at Temperatures up to 250°C. *Geochimica et Cosmochimica Acta*, 123, pp.403–415.

Markl, G. et al., 2001. Phase Equilibrium Constraints on Intensive Crystallization Parameters of the Ilimaussaq Complex, South Greenland. *Journal of Petrology*, 42(12), pp.2231–2257.

Markl, G. and Baumgartner, L., 2002. pH changes in peralkaline late-magmatic fluids. *Contributions to Mineralogy and Petrology*, 144, pp.331–346.

Marks, M. et al., 2004. Trace element variations in clinopyroxene and amphibole from alkaline to peralkaline syenites and granites: Implications for mineral-melt trace-element partitioning. *Chemical Geology*, 211, pp.185–215.

Marks, M. and Markl, G., 2001. Fractionation and assimilation processes in the alkaline augite syenite unit of the Ilimaussaq intrusion, South Greenland, as deduced from phase equilibria. *J. Petrology*, 42(10), pp.1947–1969.

Marks, M.A.W. et al., 2011. The Mineralogical Diversity of Alkaline Igneous Rocks: Critical Factors for the Transition from Miaskitic to Agpaitic Phase Assemblages. *Journal of Petrology*, 52(3), pp.439–455.

Martin, R.F., 2006. A-type granites of crustal origin ultimately result from open-system fenitization-type reactions in an extensional environment. *Lithos*, 91, pp.125–136.

Martin, R.F. and De Vito, C., 2005. The patterns of enrichment in felsic pegmatites ultimately depend on tectonic setting. *Canadian Mineralogist*, 43, pp.2027–2048.

Martin, R.F., Whitley, J.E. and Woolley, A.R., 1978. An Investigation of Rare-Earth Mobility: Fenitized Quartzites, Borralan Complex, N.W. Scotland. *Contributions to Mineralogy and Petrology*, 66, pp.69–73.

Mason, R.A., 1992. Models of order and iron-fluorine avoidance in biotite. *The Canadian Mineralogist*, 30, pp.343–354.

McLelland, J. et al., 2002. Hydrothermal alteration of late- to post-tectonic Lyon Mountain Granitic Gneiss, Adirondack Mountains, New York: Origin of quartz-sillimanite segregations, quartz-albite lithologies, and associated Kiruna-type low-Ti Fe-oxide deposits. *Journal of Metamorphic Geology*, 20, pp.175–190.

Migdisov, A. a. et al., 2014. A predictive model for the transport of copper by HCl-bearing water vapour in ore-forming magmatic-hydrothermal systems: Implications for copper porphyry ore formation. *Geochimica et Cosmochimica Acta*, 129, pp.33–53.

Migdisov, A.A. et al., 2011. An experimental study of the solubility of baddeleyite (ZrO2) in fluoride-bearing solutions at elevated temperature. *Geochimica et Cosmochimica Acta*, 75, pp.7426–7434.

Migdisov, A.A., Williams-Jones, A.E. and Wagner, T., 2009. An experimental study of the solubility and speciation of the Rare Earth Elements (III) in fluorite- and chloride-bearing aqueous solutions at temperatures up to 300˚C. *Geochimica et Cosmochimica Acta*, 73, pp.7087–7109.

Mitchell, R.H. and Chakhmouradian, A.R., 1996. Compositional variation of loparite from the Lovozero alkaline complex, Russia. *The Canadian Mineralogist*, 34, pp.977–990.

Mitchell, R.H. and Liferovich, R.P., 2006. Subsolidus deuteric/hydrothermal alteration of eudialyte in lujavrite from the Pilansberg alkaline complex, South Africa. *Lithos*, 91, pp.352–372.

Möller, V. and Williams-Jones, A.E., 2013. Magmatic Controls on the Formation of the Nechalacho Rare Metal Deposit (Thor Lake, NWT, Canada). In *Geoscience for Discovery (SEG 2013)*.

Monchoux, P. et al., 2006. IIgneous Albitite Dikes in Orogenic lherzolites, western Pyrénées, France: A Possible Source for Corundum and Alkali Feldspar Xenocrysts in Basaltic Terranes. I. Mineralogical Associations. *Canadian Mineralogist Mineral*, 44(4), pp.817–842.

Morogan, V., 1989. Mass transfer and REE mobility during fenitization at Alnö, Sweden. *Contributions to Mineralogy and Petrology*, 103, pp.25–34.

Morogan, V. and Martin, R.F., 1985. Mineralogy and partial melting of fenitized crustal xenoliths in the Oldoinyo Lengai carbonatitic volcano, Tanzania. *American Mineralogist*, 70, pp.1114–1126.

Morogan, V. and Woolley, A.R., 1988. Fenitization at the Alnö carbonatite complex, Sweden; distribution, mineralogy and genesis. *Contributions to Mineralogy and Petrology*, 100, pp.169–182.

Mumford, T.R., 2013. *Petrology of the Blatchford Lake Intrusive Suite, Northwest Territories, Canada*. Carleton University.

Mumford, T.R., Martins, T. and Falck, H., 2010. Geochemical Results from the Blachford Lake Intrusive Suite Mapping Project (2009 field season). *Northwest Territories Geoscience Office*, NWT Open R, p.25.

Olivo, G.R. and Williams-Jones, A.E., 1999. Hydrothermal REE-rich eudialyte from the Pilanesberg Complex, South Africa. *Canadian Mineralogist*, 37, pp.653–663.

Oreskes, N. and Einaudi, M.T., 1990. Origin of rare earth element-enriched hematite breccias at the Olympic Dam Cu-U-Au-Ag deposit, Roxby Downs, South Australia. *Economic Geology*, 85(1), pp.1–28.

Paul, J. and Stubens, T.C., 2009. *Thor Lake - Lake Zone mineral resource update* G. Arseneau, ed., Toronto: Wordrop.

Pearson, J.M., R., T.W. and Taylor, W.R., 1996. Mineralogy and geochemistry of fenitized alkaline ultrabasic sills of the Gifford Creek Complex, Gascoyne Province, Western Australia. *Can Mineral*, 34(2), pp.201–219.

Pederson, J.C. and Le Couteur, P.C., 1991. The Thor Lake beryllium-rare metal 103 deposits, Northwest Territories. In P. W.A. and A. D., eds. *Mineral deposits of the Slave Province, Northwest Territories (field trip 13)*. Open-File Report -- Geological Survey of Canada, pp. 128–136.

Pin, C. et al., 2006. Igneous Albitite Dikes in Orogenic lherzolites, western Pyrénées, France: A Possible Source for Corundum and Alkali Feldspar Xenocrysts in Basaltic Terranes. II. Geochemical and Petrogenetic Considerations. *Canadian Mineralogist*, 44, pp.843–856.

Pinkston, D.R. and Smith, D.G.W., 1995. Mineralogy of the Lake zone, Thor Lake rare-metals deposit, N.W.T., Canada. *Canadian Journal of Earth Sciences*, 32, pp.516–532.

Plümper, O. and Putnis, A., 2009. The complex hydrothermal history of granitic rocks: Multiple feldspar replacement reactions under subsolidus conditions. *Journal of Petrology*, 50(5), pp.967–987.

Porto da Silveira, C.L., Schorscher, H.D. and Miekeley, N., 1991. The geochemistry of albitization and related uranium mineralization, Espinharas, Paraiba (PB), Brazil. *Journal of Geochemical Exploration*, 40, pp.329–347.

Preston, R.F., Stevens, G. and McCarthy, T.S., 2003. Fluid compositions in equilibrium with silica-undersaturated magmas in the system Na2O–Al2O3–SiO2–H2O: clues to the composition of fenitizing fluids. *Contributions to Mineralogy and Petrology*, 144, pp.559–569.

Putnis, A. et al., 2007. Hematite in porous red-clouded feldspars: Evidence of large-scale crustal fluid-rock interaction. *Lithos*, 95, pp.10–18.

Putnis, C. V., Tsukamoto, K. and Nishimura, Y., 2005. Direct observations of pseudomorphism: Compositional and textural evolution at a fluid-solid interface. *American Mineralogist*, 90, pp.1909–1912.

Rataschabacher, B. et al., 2011. Mineral compositions indicate magma recharge processes in the Ilímaussaq Complex, Greenland. In *Goldschmidt conference proceedings*.

Robins, B., 1984. Petrography and petrogenesis of nephelinized metagabbros from Finnmark, Northern Norway. *Contributions to Mineralogy and Petrology*, 86, pp.170–177.

Rock, N.M.S., 1976. Fenitisation Around the Monchique Alkaline Complex, Portugal. *Lithos*, 9, pp.263–279.

Rubie, D.C., 1982. Mass transfer and volume change during alkali metasomatism at Kisingiri, Western Kenya. *Lithos*, 15, pp.99–109.

Salvi, S. et al., 2000. Hydrothermal Mobilization of High Field Strength Elements in Alkaline Igneous Systems: Evidence from the Tamazeght Complex (Morocco). *Economic Geology*, 95, pp.559–576.

Salvi, S. and Williams-Jones, A.E., 1996. The role of hydrothermal processes in concentrating high-field strength elements in the Strange Lake peralkaline complex, northeastern Canada. *Geochimica et Cosmochimica Acta*, 60(11), pp.1917–1932.

Salvi, S. and Williams-Jones, A.E., 1990. The role of hydrothermal processes in the granite-hosted Zr, Y, REE deposit at Strange Lake, Quebec/Labrador: Evidence from fluid inclusions. *Geochimica et Cosmochimica Acta*, 54, pp.2403–2418.

Schilling, J. et al., 2009. Reconstruction of magmatic to subsolidus processes in an agpaitic system using eudialyte textures and composition: a case study from tamazeght, morocco. *The Canadian Mineralogist*, 47, pp.351–365.

Schmitt, A.K. et al., 2000. Petrogenesis and 40Ar/39Ar Geochronology of the Brandberg Complex, Namibia: Evidence for a Major Mantle Contribution in Metaluminous and Peralkaline Granites. *Journal of Petrology*, 41(8), pp.1207–1239.

Schmitt, A.K. et al., 2002. Zr-Nb-REE Mineralization in Peralkaline Granites from the Amis Complex, Brandberg (Namibia): Evidence for Magmatic Pre-enrichment from Melt Inclusions. *Economic Geology*, 97, pp.399–413.

Schönenberger, J. et al., 2006. Fluid-rock interaction in autoliths of agpaitic nepheline syenites in the Ilímaussaq intrusion, South Greenland. *Lithos*, 91, pp.331–351.

Shand, S.J., 1947. *Eruptive rocks, their genesis, composition, classification, and their relation to ore-deposits, with a chapter on meteorites* 3rd ed., London: T. Murby.

Sheard, E.R. et al., 2012. Controls on the concentration of zirconium, niobium, and the rare earth elements in the Thor Lake rare metal deposit, Northwest Territories, Canada. *Economic Geology*, 107, pp.81–104.

Shock, E.L. and Helgeson, H.C., 1988. Calculation of the thermodynamic and transport properties of aqueous species at high pressures and temperatures: Correlation algorithms for ionic species and equation of state predictions to 5 kb and 1000°C. *Geochimica et Cosmochimica Acta*, 52, pp.2009–2036.

Siemiatkowska, K.M. and Martin, R.F., 1975. Fenitization of Mississagi Quartzite, Sudbury Area, Ontario. *Geological Society of America Bulletin*, 86, pp.1109–1122.

Sinclair, W.D., P.A., H. and Birkett, T.C., 1994. U-Pb zircon and monazite ages of the Grace Lake Granite, Blatchford Lake Intrusive Suite, Slave Province, Northwest Territories. In *Radiogenic Age and Isotopic Studies*. Current Research. Geological Survey of Canada, pp. 15–20.

Sörensen, H., 1969. Rhythmic igneous layering in peralkaline intrusions: An essay review on Ilímaussaq (Greenland) and Lovozero (Kola, USSR). *Lithos*, 2, pp.261–283.

Sörensen, H., 1997. The agpaitic rocks; an overview. *Mineral Mag*, 61, pp.485–498.

Sörensen, H., Bohse, H. and Bailey, J.C., 2006. The origin and mode of emplacement of lujavrites in the Ilímaussaq alkaline complex, South Greenland. *Lithos*, 91, pp.286–300.

Sörensen, H. and Laren, L.M., 2001. The hyper-agpaitic stage in the evolution of the Ilimaussaq alkaline complex, South Greenland. *Geology of Greenland survey bulletin*, 301, p.83.

Sørrensen, H., 1992. Agpaitic nepheline syenites: A potential source of rare elements. *Applied Geochemistry*, 7, pp.417–427.

De St. Jorre, L. and Smith, D.G.W., 1988. Cathodoluminescent gallium-enriched feldspars from the Thore Lake rare metal deposits, Northwest Territories. *Can Mineral*, 26, pp.301–308.

Steele-MacInnis, M., Lecumberri-Sanchez, P. and Bodnar, R.J., 2012. HokieFlincs_H2O-NaCl A Microsoft Excel spreadsheet for interpreting microthermometric data from fluid

inclusions based on the PVTX properties of H2O-NaCl. *Computers and Geosciences*, 49, pp.334–337.

Sun, S. -s. and McDonough, W.F., 1989. Chemical and isotopic systematics of oceanic basalts: implications for mantle composition and processes. *Geological Society, London, Special Publications*, 42, pp.313–345.

Taylor, R.P. and Pollard, P.J., 1996. Rare Earth Element Mineralization in Peralkaline Systems; the T-Zone-REE-Y-Be Deposit, Thor Lake, Northwest Territories. In *Rare earth minerals; chemistry, origin and ore deposits*. Mineralogical Society Series, pp. 167–192.

Thompson, T.B., 1988. Geology and uranium-thorium mineral deposits of the Bokan Mountain Granite Complex, southeastern Alaska. *Ore Geology Reviews*, 3, pp.193–210.

Thompson, T.B., Pierson, J.R. and Lyttle, T., 1982. Petrology and petrogenesis of the Bokan Granite Complex, southeastern Alaska. *Geological Society of America Bulletin*, 93(9), pp.898–908.

Timofeev, A. and Williams-Jones, A.E., 2014. Controls on the Distribution of Gallium in the Nechalacho REE Deposit, NWT, Canada. *Economic Geology*, 110, pp.173–185.

Timofeev, A. and Williams-Jones, A.E., The origin of niobium and tantalum mineralization in the Nechalacho REE deposit, NWT, Canada.

Trønnes, R. and Brandon, A., 1992. Mildly peraluminous high-silica granites in a continental rift: the Drammen and Finnemarka batholiths, Oslo Rift, Norway. *Contributions to Mineralogy and Petrology*, 109(3), pp.275–294.

Trueman, D.L. et al., 1988. The Thor Lake rare-metal deposits, Northwest Territories. In R. P. Talor and D. F. Strong, eds. *Recent Advances in the Geology of Granite-Related Mineral Deposits*. Canadian Institute of Mining and Metallurgy, pp. 280–290.

Turner, S.P., Foden, J.D. and Morrison, R.S., 1992. Derivation of some A-type magmas by fractionation of basaltic magma: An example from the Padthaway Ridge, South Australia. *Lithos*, 28, pp.151–179.

Ussing, N. V, 1912. Geology of the country around Julianehaab, Greenland. *Meddelelser om Grenland*, 38, p.426.

Veksler, I. V and Keppler, H., 2000. Partitioning of Mg , Ca , and Na between carbonatite melt and hydrous fluid at 0.1-0.2 GPa. *Contributions to Mineralogy and Petrology*, 138, pp.27–34.

Vermaak, C.F., 1976. The Merensky Reef; thoughts on its environment and genesis. *Economic Geology*, 71, pp.1270–1298.

Watson, E.B., 1979. Zircon saturation in felsic liquids: Experimental results and applications to trace element geochemistry. *Contributions to Mineralogy and Petrology*, 70, pp.407–419.

Whalen, J.B., Currie, K.L. and Chappell, B.W., 1987. A-type granites: geochemical characteristics, discrimination and petrogenesis. *Contributions to Mineralogy and Petrology*, 95, pp.407–419.

White, N.C. and Hedenquist, J.W., 1990. Epithermal environments and styles of mineralization: Variations and their causes, and guidelines for exploration. *Journal of Geochemical Exploration*, 36, pp.445–474.

Williams-Jones, A.E., Migdisov, A. a. and Samson, I.M., 2012. Hydrothermal mobilisation of the rare earth elements-a tale of "ceria" and "yttria." *Elements*, 8, pp.355–360.

Williams-Jones, A.E. and Palmer, D.A.S., 2002. The Evolution of Aqueous-Carbonic Fluids in the Amba Dongar Carbonatite, India: implications for Fenitisation. *Chemical Geology*, 185(3-4), pp.283–301.

Williams-Jones, A.E., Samson, I.M. and Olivo, G.R., 2000. The genesis of hydrothermal fluorite-REE deposits in the Gallinas Mountains, New Mexico. *Economic Geology and the Bulletin of the Society of Economic Geologists*, 95(2), pp.327–341.

Appendices

Appendix I: Microprobe analyses (wt%)

Analysis	Mineral	Sample	Na_2O	K_2O	SiO2	MgO	CaO	TiO_2	FeO	Al_2O_3	Cr_2O_3	MnO	Total
1	Aegirine	85L6-294.91	13.49	0.010	52.31	0.001	0.443	0.098	32.18	1.33	0.000	0.147	100.02
2	Aegirine	85L6-294.91	13.70	0.004	52.21	0.000	0.555	0.135	31.85	1.35	0.000	0.179	99.98
3	Aegirine	85L6-294.91	13.73	0.004	52.45	0.000	0.427	0.062	31.98	1.38	0.005	0.157	100.19
4	Aegirine	85L6-294.91	13.81	0.003	52.49	0.000	0.138	0.046	31.91	1.68	0.000	0.074	100.15
5	Aegirine	85L6-294.91	12.76	0.000	51.96	0.000	2.13	0.052	32.56	1.07	0.000	0.104	100.63
6	Aegirine	85L6-294.91	12.79	0.000	51.10	0.015	1.90	0.042	32.34	1.02	0.000	0.096	99.29
7	Aegirine	85L6-294.91	13.85	0.007	52.83	0.009	0.219	0.198	32.16	1.16	0.000	0.146	100.59
8	Aegirine	85L6-346.26	12.74	0.004	51.38	0.000	1.97	0.026	32.70	1.29	0.007	0.110	100.22
9	Aegirine	85L6-346.26	13.25	0.032	56.13	0.000	0.02	0.016	0.104	24.12	0.000	0.013	93.68
10	Aegirine	85L6-346.26	13.17	0.006	51.45	0.002	1.80	0.040	32.55	1.20	0.000	0.355	100.57
11	Aegirine	85L6-346.26	12.30	0.014	51.54	0.000	3.05	0.079	31.81	1.30	0.000	0.254	100.34

Analysis	Mineral	Sample	Na_2O	SiO_2	K2O	Al_2O_3	Ga_2O_3	MgO	Rb_2O
1	Albite (I)	85L6-294.91	11.69	68.70	0.069	18.72	NA	0.000	NA
2	Albite (I)	85L6-294.91	11.73	68.83	0.130	18.93	NA	0.009	NA
3	Albite (I)	L09-155-162.60	11.85	69.28	0.085	19.24	NA	0.009	NA
4	Albite (I)	L09-155-162.60	11.63	68.11	0.497	19.65	NA	0.216	NA
5	Albite (I)	L09-155-162.60	11.89	68.88	0.157	19.54	NA	0.000	NA
6	Albite (I)	L09-155-163.10	11.62	68.47	0.085	18.57	NA	0.021	NA
7	Albite (I)	L09-155-163.10	11.93	68.73	0.053	19.49	NA	0.019	NA
8	Albite (I)	L09-179-129.44	11.49	69.20	0.391	19.18	NA	0.010	NA
9	Albite (I)	L09-179-178.0	11.84	69.58	0.100	18.94	NA	0.005	NA
10	Albite (I)	L09-179-178.0	11.93	68.55	0.061	19.46	NA	0.009	NA
11	Albite (I)	L09-179-46.11	11.93	69.09	0.122	19.38	NA	0.019	NA
12	Albite (I)	L09-179-9.46	11.79	69.04	0.123	19.48	NA	0.005	NA
13	Albite (I)	L09-192-112.8	11.78	69.26	0.109	19.49	NA	0.000	NA
14	Albite (I)	L09-192-112.8	11.92	69.22	0.091	19.39	NA	0.010	NA
15	Albite (I)	L09-192-183.6	11.761	67.639	0.090	19.333	0.000	0.002	0.000
16	Albite (I)	L09-192-183.6	11.724	67.796	0.140	19.291	0.001	0.000	0.000
17	Albite (I)	L09-192-183.6	11.743	67.732	0.098	19.237	0.000	0.000	0.000
18	Albite (I)	L09-192-183.6	11.966	68.426	0.075	19.188	0.009	0.010	0.000
19	Albite (I)	L09-192-183.6	11.86	68.90	0.095	19.00	NA	0.000	NA

Analysis	Mineral	Sample	Na_2O	SiO_2	K2O	Al_2O_3	Ga_2O_3	MgO	Rb_2O
20	Albite (I)	L09-192-183.6	11.81	69.34	0.085	19.11	NA	0.014	NA
21	Albite (I)	L09-192-183.6	11.86	69.31	0.161	19.32	NA	0.000	NA
22	Albite (I)	L09-192-183.6	11.67	68.91	0.119	18.89	NA	0.000	NA
23	Albite (I)	L09-192-183.6	11.50	69.30	0.200	19.26	NA	0.000	NA
24	Albite (I)	L09-192-183.6	11.82	69.10	0.092	18.77	NA	0.082	NA
25	Albite (I)	L09-192-183.6	11.71	69.25	0.111	18.50	NA	0.000	NA
26	Albite (I)	L09-192-183.6	11.95	69.42	0.076	19.26	NA	0.010	NA
27	Albite (I)	L09-192-183.6	11.74	69.22	0.188	19.31	NA	0.002	NA
28	Albite (I)	L09-192-200.2	11.705	67.730	0.095	19.074	0.004	0.004	0.000
29	Albite (I)	L09-192-200.2	11.715	68.116	0.091	19.079	0.009	0.000	0.000
30	Albite (I)	L09-192-200.2	11.738	68.762	0.086	19.121	0.013	0.000	0.000
31	Albite (I)	L09-192-200.2	11.239	66.564	0.635	18.716	0.000	0.972	0.000
32	Albite (I)	L09-192-200.2	11.875	68.404	0.094	19.204	0.000	0.005	0.000
33	Albite (I)	L09-194-276.45	11.63	68.93	0.038	19.09	NA	0.029	NA
34	Albite (I)	L09-194-276.45	11.69	68.75	0.082	19.13	NA	0.028	NA
35	Albite (II)	KM10-002	11.608	67.842	0.158	18.798	0.142	0.001	0.000
36	Albite (II)	KM10-002	11.017	68.547	0.065	19.153	0.063	0.000	0.000
37	Albite (II)	KM10-002	11.453	68.320	0.158	19.098	0.144	0.000	0.000
38	Albite (II)	KM10-002	11.374	68.539	0.076	19.278	0.064	0.001	0.000
39	Albite (II)	L08-84-96.77	11.68	69.45	0.123	18.99	NA	0.027	NA
40	Albite (II)	L08-84-96.77	11.82	69.56	0.074	19.33	NA	0.000	NA
41	Albite (II)	L08-84-96.77	11.89	69.25	0.103	19.28	NA	0.000	NA
42	Albite (II)	L08-84-96.77	11.84	68.72	0.068	19.30	NA	0.019	NA
43	Albite (II)	L10-232A 100.75	11.888	68.816	0.022	19.449	0.006	0.000	0.000
44	Albite (II)	L10-232A 100.75	11.851	68.724	0.051	19.551	0.005	0.000	0.000
45	Albite (II)	L10-232A 100.75	11.69	68.616	0.099	19.522	0.009	0.000	0.000
46	Albite (II)	L10-232A 100.75	11.906	68.343	0.057	19.683	0.003	0.002	0.000
47	Albite (II)	L10-232A 100.75	11.791	68.542	0.033	19.522	0.009	0.000	0.000
48	Albite (II)	L10-232A 100.75	11.917	68.88	0.005	19.598	0.008	0.000	0.000
49	Albite (II)	L10-232A 100.75	11.851	68.714	0.027	19.527	0.000	0.000	0.000
50	Albite (II)	L10-232A 100.75	11.658	68.596	0.033	19.687	0.015	0.003	0.000
51	Albite (II)	L10-232A 100.75	11.975	68.683	0.033	19.642	0.009	0.000	0.000
52	Albite (II)	L10-232A 100.75	11.747	68.875	0.083	19.44	0.018	0.000	0.000
53	Albite (II)	L10-232A 100.75	11.724	68.712	0.115	19.526	0.013	0.000	0.000
54	Albite (II)	L10-232A 100.75	11.952	68.676	0.105	19.674	0.004	0.000	0.000

Analysis	Mineral	Sample	Na_2O	SiO_2	K2O	Al_2O_3	Ga_2O_3	MgO	Rb_2O
55	Albite (II)	L10-232A 100.75	11.795	68.575	0.054	19.639	0.016	0.000	0.000
56	Albite (II)	L10-232A 100.75	11.677	67.943	0.097	19.365	0.018	0.001	0.000
57	Albite (II)	L10-232A 100.75	11.783	68.729	0.081	19.569	0.014	0.003	0.000
58	Albite (II)	L10-232A 100.75	11.846	68.606	0.082	19.502	0.009	0.000	0.000
59	Albite (II)	L10-232A 44.2	11.847	69.202	0.11	19.363	0.000	0.000	0.000
60	Albite (II)	L10-232A 44.2	11.703	68.373	0.113	19.469	0.005	0.000	0.000
61	Albite (II)	L10-232A 44.2	11.834	68.596	0.082	19.453	0.000	0.000	0.000
62	Albite (II)	L10-232A 44.2	11.664	67.594	0.415	19.488	0.006	0.000	0.000
63	Albite (II)	L10-232A 44.2	11.871	67.907	0.112	19.317	0.000	0.000	0.000
64	Albite (II)	L10-232A 44.2	11.571	68.375	0.158	19.345	0.004	0.000	0.000
65	Albite (II)	L10-232A 51.25	11.833	67.307	0.114	19.659	0.02	0.003	0.000
66	Albite (II)	L10-232A 51.25	11.86	68.061	0.107	19.589	0.017	0.000	0.000
67	Albite (II)	L10-232A 51.25	11.651	68.226	0.188	19.459	0.009	0.000	0.000
68	Albite (II)	L10-232A 51.25	11.861	67.41	0.079	19.74	0.021	0.002	0.000
69	Albite (II)	L10-232A 51.25	11.851	67.807	0.091	19.51	0.016	0.000	0.000
70	Albite (II)	L10-232A 51.25	11.819	68.455	0.09	19.529	0.011	0.000	0.000
71	Albite (II)	L10-232A 51.25	11.821	67.882	0.091	19.639	0.012	0.014	0.000
72	Albite (II)	L10-232A 51.25	11.809	68.133	0.097	19.58	0.004	0.000	0.000
73	Albite (II)	L10-232A 51.25	11.851	68.507	0.062	19.664	0.005	0.005	0.000
74	Albite (II)	L10-232A 51.25	11.803	68.02	0.126	19.594	0.012	0.000	0.000
75	Albite (II)	L10-232A 51.25	11.788	68.015	0.134	19.629	0.018	0.011	0.000
76	Albite (II)	L10-232A 51.25	11.817	68.053	0.088	19.687	0.022	0.008	0.000
77	Albite (II)	L10-232A 54.35	11.703	68.801	0.103	19.468	0.003	0.000	0.000
78	Albite (II)	L10-232A 54.35	11.872	68.944	0.104	19.46	0.026	0.000	0.000
79	Albite (II)	L10-232A 54.35	11.603	68.5	0.26	19.299	0.025	0.001	0.000
80	Albite (II)	L10-232A 54.35	11.667	68.693	0.099	19.422	0.019	0.006	0.000
81	Albite (II)	L10-232A 54.35	11.818	68.667	0.09	19.586	0.007	0.000	0.000
82	Albite (II)	L10-232A 54.35	11.597	68.365	0.106	19.46	0.018	0.002	0.000
83	Albite (II)	L10-232A 54.35	11.668	68.599	0.087	19.471	0.008	0.000	0.000
84	Albite (II)	L10-232A 54.35	11.714	68.826	0.094	19.385	0.015	0.000	0.000
85	Albite (II)	L10-232A 54.35	11.64	68.634	0.148	19.515	0.004	0.000	0.000
86	Albite (II)	L10-232A 54.35	11.781	69.112	0.086	19.509	0.015	0.001	0.000
87	Albite (II)	L10-232A 54.35	11.731	68.847	0.078	19.398	0.022	0.000	0.000
88	Albite (II)	L10-232A 54.35	11.657	68.899	0.114	19.354	0.011	0.000	0.000
89	Albite (II)	L10-232A 54.35	11.678	68.777	0.08	19.466	0.008	0.003	0.000

Analysis	Mineral	Sample	Na_2O	SiO_2	K2O	Al_2O_3	Ga_2O_3	MgO	Rb_2O
90	Albite (II)	L10-232A 54.35	11.834	68.923	0.08	19.586	0.000	0.000	0.000
91	Albite (II)	L10-232A 54.35	11.783	68.238	0.116	19.546	0.000	0.000	0.000
92	Albite (II)	L10-232A 59.5	11.907	68.261	0.078	19.762	0.008	0.004	0.000
93	Albite (II)	L10-232A 59.5	11.659	67.708	0.216	19.69	0.000	0.000	0.000
94	Albite (II)	L10-232A 59.5	11.73	68.515	0.014	19.465	0.006	0.000	0.000
95	Albite (II)	L10-232A 59.5	11.899	68.188	0.153	19.866	0.004	0.005	0.000
96	Albite (II)	L10-232A 59.5	11.856	67.733	0.111	19.627	0.009	0.000	0.000
97	Albite (II)	L10-232A 59.5	11.943	67.833	0.103	19.731	0.023	0.000	0.000
98	Albite (II)	L10-232A 59.5	11.82	68.388	0.147	19.532	0.016	0.000	0.000
99	Albite (II)	L10-232A 59.5	11.787	69.073	0.127	19.538	0.017	0.000	0.000
100	Albite (II)	L10-232A 59.5	11.858	68.749	0.144	19.502	0.036	0.000	0.000
101	Albite (II)	L10-232A 59.5	11.817	68.246	0.034	19.691	0.005	0.000	0.000
102	Albite (II)	L10-232A 59.5	11.761	68.722	0.162	19.511	0.01	0.000	0.000
103	Albite (II)	L10-232A 59.5	11.807	68.6	0.111	19.694	0.011	0.003	0.000
104	Albite (II)	L10-232A 59.5	11.715	67.901	0.047	19.232	0.02	0.000	0.000
105	Albite (II)	L10-232A 59.5	11.656	67.631	0.105	19.11	0.014	0.012	0.000
106	Albite (II)	L10-232A 59.5	11.655	67.298	0.146	19.019	0.034	0.000	0.000
107	Albite (II)	L10-232A 59.5	11.735	68.344	0.182	19.649	0.02	0.000	0.000
108	Albite (II)	L10-232A 59.5	11.786	67.052	0.105	19.576	0.015	0.001	0.000
109	Albite (II)	L10-232A 59.5	11.802	67.291	0.097	19.693	0.015	0.000	0.000
110	Albite (II)	L10-232A 65.25	11.731	67.085	0.114	19.788	0.009	0.000	0.000
111	Albite (II)	L10-232A 65.25	11.814	67.196	0.102	19.752	0.012	0.000	0.000
112	Albite (II)	L10-232A 65.25	11.635	67.021	0.115	19.692	0.007	0.001	0.000
113	Albite (II)	L10-232A 65.25	11.78	68.113	0.083	19.675	0.006	0.004	0.000
114	Albite (II)	L10-232A 65.25	11.771	67.777	0.029	19.752	0.01	0.000	0.000
115	Albite (II)	L10-232A 65.25	11.654	68.088	0.081	19.803	0.014	0.000	0.000
116	Albite (II)	L10-232A 65.25	11.767	68.617	0.036	19.754	0.002	0.005	0.000
117	Albite (II)	L10-232A 65.25	11.616	68.101	0.127	19.651	0.015	0.008	0.000
118	Albite (II)	L10-232A 65.25	11.723	68.59	0.057	19.763	0.004	0.002	0.000
119	Albite (II)	L10-232A 65.25	11.856	68.666	0.041	19.751	0.011	0.008	0.000
120	Albite (II)	L10-232A 65.25	11.742	68.756	0.089	19.689	0.007	0.003	0.000
121	Albite (II)	L10-232A 65.25	11.854	68.438	0.043	19.631	0.001	0.000	0.000
122	Albite (II)	L10-232A 65.25	11.744	68.456	0.067	19.545	0.007	0.000	0.000
123	Albite (II)	L10-232A 65.25	11.805	68.702	0.041	19.484	0.000	0.000	0.000
124	Albite (II)	L10-232A 65.25	11.824	68.287	0.039	19.809	0.011	0.000	0.000
125	Albite (II)	L10-232A 75.2	11.836	68.519	0.007	19.658	0.014	0.000	0.000

Analysis	Mineral	Sample	Na_2O	SiO_2	K2O	Al_2O_3	Ga_2O_3	MgO	Rb_2O
126	Albite (II)	L10-232A 75.2	11.764	68.545	0.054	19.576	0.009	0.000	0.000
127	Albite (II)	L10-232A 75.2	11.655	68.738	0.027	19.578	0.011	0.000	0.000
128	Albite (II)	L10-232A 75.2	11.689	68.584	0.102	19.552	0.015	0.000	0.000
129	Albite (II)	L10-232A 78.25	11.84	68.187	0.035	19.744	0.005	0.000	0.000
130	Albite (II)	L10-232A 78.25	11.895	68.619	0.03	19.615	0.008	0.000	0.000
131	Albite (II)	L10-232A 78.25	11.563	68.477	0.198	19.512	0.007	0.000	0.000
132	Albite (II)	L10-232A 78.25	11.669	68.563	0.107	19.586	0.008	0.000	0.000
133	Albite (II)	L10-232A 78.25	11.596	68.553	0.179	19.484	0.005	0.000	0.000
134	Albite (II)	L10-232A 78.25	11.809	68.733	0.031	19.555	0.009	0.004	0.000
135	Albite (II)	L10-232A 78.25	11.617	68.365	0.066	19.549	0.025	0.002	0.000
136	Albite (II)	L10-232A 78.25	11.696	68.514	0.047	19.457	0.01	0.005	0.000
137	Albite (II)	L10-232A 78.25	11.608	68.652	0.182	19.684	0.009	0.000	0.000
138	Albite (II)	L10-232A 78.25	11.665	68.615	0.185	19.469	0.022	0.002	0.000
139	Albite (II)	L10-232A 78.25	11.762	68.638	0.065	19.468	0.000	0.000	0.000
140	Albite (II)	L10-232A 78.25	11.622	68.679	0.113	19.621	0.006	0.000	0.000
141	Albite (II)	L10-232A 78.25	11.158	68.549	0.818	19.47	0.008	0.000	0.000
142	Albite (II)	L10-232A 78.25	11.707	68.593	0.128	19.53	0.008	0.006	0.000
143	Albite (II)	L10-232A 78.25	11.702	68.559	0.307	19.48	0.000	0.009	0.000
144	Albite (II)	L10-232A 82.2	11.687	68.598	0.097	19.613	0.017	0.000	0.000
145	Albite (II)	L10-232A 82.2	11.827	68.688	0.111	19.542	0.012	0.000	0.000
146	Albite (II)	L10-232A 82.2	11.918	68.427	0.102	19.614	0.013	0.018	0.000
147	Albite (II)	L10-232A 82.2	11.737	68.731	0.11	19.689	0.01	0.006	0.000
148	Albite (II)	L10-232A 82.2	11.757	67.85	0.075	19.591	0.021	0.003	0.000
149	Albite (II)	L10-232A 82.2	11.778	68.303	0.089	19.825	0.019	0.000	0.000
150	Albite (II)	L10-232A 82.2	11.665	68.422	0.079	19.469	0.006	0.000	0.000
151	Albite (II)	L10-232A 82.2	11.86	68.434	0.081	19.675	0.000	0.000	0.000
152	Albite (II)	L10-232A 82.2	11.601	68.188	0.166	19.574	0.012	0.007	0.000
153	Albite (II)	L10-232A 82.2	11.774	68.628	0.104	19.459	0.023	0.000	0.000
154	Albite (II)	L10-232A 82.2	11.843	68.407	0.064	19.539	0.009	0.000	0.000
155	Albite (II)	L10-232A 87.1	11.729	68.694	0.047	19.651	0.007	0.000	0.000
156	Albite (II)	L10-232A 87.1	11.807	68.75	0.065	19.614	0.002	0.000	0.000
157	Albite (II)	L10-232A 87.1	11.844	68.68	0.076	19.729	0.002	0.001	0.000
158	Albite (II)	L10-232A 87.1	11.857	68.376	0.164	19.667	0.013	0.014	0.000
159	Albite (II)	L10-232A 87.1	11.81	68.267	0.124	19.818	0.01	0.001	0.000
160	Albite (II)	L10-232A 87.1	11.739	67.999	0.116	19.713	0.016	0.000	0.000

Analysis	Mineral	Sample	Na_2O	SiO_2	K2O	Al_2O_3	Ga_2O_3	MgO	Rb_2O
161	Albite (II)	L10-232A 87.1	11.717	68.489	0.097	19.651	0.008	0.000	0.000
162	Albite (II)	L10-232A 87.1	11.605	68.542	0.134	19.62	0.000	0.000	0.000
163	Albite (II)	L10-232A 87.1	11.651	67.597	0.08	19.578	0.014	0.001	0.000
164	Albite (II)	L10-232A 87.1	11.825	68.116	0.072	19.785	0.009	0.000	0.000
165	Albite (II)	L10-232A 87.1	11.456	68.292	0.572	19.668	0.004	0.000	0.000
166	Albite (II)	L10-232A 87.1	11.725	68.493	0.082	19.58	0.013	0.000	0.000
167	Albite (II)	L10-232A 87.1	11.671	68.603	0.078	19.631	0.011	0.000	0.000
168	Albite (II)	L10-232A 87.1	11.615	68.299	0.122	19.567	0.000	0.003	0.000
169	Albite (II)	L10-232A 87.1	11.433	68.099	0.361	19.648	0.000	0.000	0.000
170	Albite (II)	L10-232A 87.1	11.802	68.6	0.108	19.476	0.006	0.000	0.000
171	Albite (II)	L10-232A 87.1	11.655	68.319	0.139	19.533	0.000	0.000	0.000
172	Albite (II)	L10-232A 87.1	11.779	68.38	0.07	19.767	0.01	0.000	0.000
173	Albite (II)	L10-232A 94.75	11.857	68.91	0.06	19.527	0.001	0.000	0.000
174	Albite (II)	L10-232A 94.75	11.692	67.895	0.068	19.256	0.004	0.000	0.000
175	Albite (II)	L10-232A 94.75	11.82	68.641	0.062	19.64	0.011	0.000	0.000
176	Albite (II)	L10-232A 94.75	11.863	68.667	0.087	19.659	0.003	0.000	0.000
177	Albite (II)	L10-232A 94.75	11.766	68.478	0.073	19.677	0.022	0.000	0.000
178	Albite (II)	L10-232A 94.75	11.88	67.809	0.061	19.656	0.006	0.000	0.000
179	Albite (II)	L10-232A 94.75	11.894	68.319	0.041	19.751	0.001	0.001	0.000
180	Albite (II)	L10-232A 94.75	11.85	68.539	0.08	19.55	0.015	0.000	0.000
181	Albite (II)	L10-232A 94.75	11.991	68.833	0.044	19.712	0.004	0.000	0.000
182	Albite (II)	L10-232A 94.75	11.839	68.702	0.114	19.694	0.003	0.003	0.000
183	Albite (II)	L10-232A 94.75	11.937	68.517	0.101	19.586	0.011	0.000	0.000
184	Albite (II)	L10-232A 94.75	11.892	68.47	0.028	19.678	0.007	0.000	0.000
185	Albite (II)	L10-232A 94.75	11.918	69.16	0.041	19.641	0.009	0.000	0.000
186	Albite (II)	L10-232A 94.75	11.831	68.522	0.054	19.641	0.006	0.003	0.000
187	Albite (II)	L10-232A 94.75	11.693	68.111	0.166	19.697	0.008	0.000	0.000
188	Albite (II)	L10-232A 94.75	11.869	68.722	0.039	19.571	0.001	0.000	0.000
189	Albite (II)	L10-232A 94.75	11.738	68.59	0.041	19.607	0.000	0.002	0.000
190	Albite (II)	L10-232A 94.75	11.792	68.48	0.085	19.654	0.007	0.004	0.000
191	Albite (II)	L10-232A 94.75	11.683	68.482	0.101	19.655	0.006	0.000	0.000
192	Albite (II)	L10-232A 94.75	11.721	68.513	0.072	19.719	0.01	0.000	0.000
193	Albite (II)	L10-232A 94.75	11.766	68.733	0.105	19.66	0.005	0.001	0.000
194	Albite (II)	L10-232A 94.75	11.554	67.486	0.105	19.254	0.014	0.000	0.000
195	Albite (II)	L10-232A 94.75	11.785	68.531	0.098	19.608	0.014	0.000	0.000
196	Albite (II)	L10-232A 94.75	11.803	68.711	0.092	19.416	0.019	0.004	0.000

Analysis	Mineral	Sample	Na_2O	SiO_2	K2O	Al_2O_3	Ga_2O_3	MgO	Rb_2O
197	Albite (II)	L10-232A 94.75	11.789	69.003	0.106	19.587	0.013	0.001	0.000
198	Albite (II)	L10-232A-103.6	11.765	68.973	0.035	19.393	0.000	0.000	0.000
199	Albite (II)	L10-232A-103.6	11.753	68.896	0.056	19.434	0.02	0.000	0.000
200	Albite (II)	L10-232A-103.6	11.773	68.845	0.014	19.523	0.004	0.000	0.000
201	Albite (II)	L10-232A-103.6	11.787	69.075	0.017	19.423	0.022	0.000	0.000
202	Albite (II)	L10-232A-103.6	11.748	69.011	0.02	19.477	0.01	0.003	0.000
203	Albite (II)	L10-232A-54.35	11.757	67.677	0.115	19.210	0.017	0.006	0.000
204	Albite (II)	L10-232A-54.35	11.855	68.487	0.086	19.364	0.010	0.000	0.000
205	Albite (II)	L10-232A-54.35	11.824	67.455	0.096	19.184	0.008	0.000	0.000
206	Albite (II)	L10-232A-54.35	11.927	68.467	0.033	19.211	0.018	0.000	0.000
207	Albite (II)	L10-232A-54.35	11.764	68.265	0.087	19.369	0.008	0.000	0.000
208	Albite (II)	L10-232A-54.35	11.589	68.479	0.083	19.557	0.019	0.000	0.000
209	Albite (II)	L10-232A-57.55	11.733	68.465	0.047	19.548	0.004	0.002	0.000
210	Albite (II)	L10-232A-57.55	11.860	68.654	0.052	19.421	0.005	0.000	0.000
211	Albite (II)	L10-232A-57.55	11.753	68.443	0.091	19.519	0.013	0.000	0.000
212	Albite (II)	L10-232A-57.55	11.759	68.495	0.078	19.348	0.015	0.000	0.000
213	Albite (II)	L10-232A-57.55	11.816	68.585	0.036	19.414	0.015	0.000	0.000
214	Albite (II)	L10-232A-57.55	11.824	68.654	0.057	19.405	0.032	0.000	0.000
215	Albite (II)	L10-232A-57.55	11.752	68.385	0.101	19.397	0.005	0.000	0.000
216	Albite (II)	L10-232A-82.2	12.002	68.249	0.051	19.356	0.018	0.000	0.000
217	Albite (II)	L10-232A-82.2	11.757	68.431	0.093	19.248	0.016	0.000	0.000
218	Albite (II)	L10-232A-82.2	11.945	68.336	0.079	19.378	0.012	0.004	0.000
219	Albite (II)	L10-232A-82.2	11.867	68.136	0.112	19.331	0.016	0.000	0.000
220	Microcline (I)	85L6-294.91	0.536	64.70	16.98	17.69	NA	0.000	NA
221	Microcline (I)	85L6-294.91	0.512	64.38	17.25	17.70	NA	0.000	NA
222	Microcline (I)	L09-194-276.45	0.269	64.31	17.38	17.96	NA	0.006	NA
223	Microcline (I)	L09-194-276.45	0.759	63.52	16.92	18.16	NA	0.017	NA
224	Microcline (I)	L09-194-276.45	0.183	65.07	16.76	18.07	NA	0.000	NA
225	Microcline (II)	KM10-002	0.032	64.763	17.140	17.633	0.064	0.005	0.000
226	Microcline (II)	L09-155-163.10	0.441	64.74	17.09	18.35	NA	0.000	NA
227	Microcline (II)	L09-179-129.44	0.571	65.69	16.23	18.17	NA	0.000	NA
228	Microcline (II)	L09-179-129.44	0.509	65.57	16.16	18.15	NA	0.000	NA
229	Microcline (II)	L09-179-129.44	0.558	65.44	16.26	18.04	NA	0.014	NA

Analysis	Mineral	Sample	Na_2O	SiO_2	K2O	Al_2O_3	Ga_2O_3	MgO	Rb_2O
230	Microcline (II)	L09-179-178.0	0.586	65.46	16.19	18.35	NA	0.014	NA
231	Microcline (II)	L09-179-178.0	0.559	65.05	16.04	17.58	NA	0.000	NA
232	Microcline (II)	L09-179-46.11	0.538	65.39	16.28	18.35	NA	0.000	NA
233	Microcline (II)	L09-179-46.11	0.499	65.64	16.38	18.26	NA	0.000	NA
234	Microcline (II)	L09-179-9.46	0.417	65.35	16.45	18.37	NA	0.000	NA
235	Microcline (II)	L09-179-9.46	0.483	64.96	16.35	18.13	NA	0.010	NA
236	Microcline (II)	L09-179-9.46	0.476	64.99	16.18	18.36	NA	0.004	NA
237	Microcline (II)	L09-179-9.46	0.529	65.31	16.10	18.31	NA	0.000	NA
238	Microcline (II)	L09-192-112.8	0.592	63.89	16.02	18.22	NA	0.250	NA
239	Microcline (II)	L09-192-112.8	0.632	65.67	16.07	18.02	NA	0.000	NA
240	Microcline (II)	L09-192-112.8	0.603	65.78	16.14	18.25	NA	0.000	NA
241	Microcline (II)	L09-192-112.8	0.672	65.78	16.14	18.28	NA	0.000	NA
242	Microcline (II)	L09-192-112.8	0.410	64.76	16.43	18.29	NA	0.013	NA
243	Microcline (II)	L10-232A 51.25	0.576	64.865	16.724	18.615	0.008	0.000	0.141
244	Microcline (II)	L10-232A 51.25	0.469	64.662	17.06	18.61	0.004	0.005	0.024
245	Microcline (II)	L10-232A 51.25	0.477	63.747	16.739	18.324	0.01	0.000	0.11
246	Microcline (II)	L10-232A 51.25	0.573	63.677	16.855	18.653	0.007	0.000	0.003
247	Microcline (II)	L10-232A 65.25	0.418	61.671	15.876	20.387	0	0.000	0
248	Microcline (II)	L10-232A 75.2	0.533	63.966	16.952	18.56	0.004	0.000	0.068
249	Microcline (II)	L10-232A 75.2	0.679	64.583	16.636	18.624	0.007	0.000	0.123
250	Microcline (II)	L10-232A 75.2	0.72	64.44	16.613	18.658	0.027	0.003	0.1
251	Microcline (II)	L10-232A 75.2	0.631	65.009	16.784	18.443	0.016	0.000	0.099
252	Microcline (II)	L10-232A 75.2	0.649	64.998	16.796	18.581	0.014	0.000	0.089
253	Microcline (II)	L10-232A 75.2	0.305	64.962	17.142	18.44	0.024	0.003	0.098
254	Microcline (II)	L10-232A 78.25	0.582	65.075	16.955	18.648	0.001	0.001	0.041
255	Microcline (II)	L10-232A 78.25	0.446	65.056	17.071	18.566	0.011	0.002	0.146
256	Microcline (II)	L10-232A 78.25	0.424	65.095	17.108	18.528	0.023	0.001	0.146
257	Microcline (II)	L10-232A 78.25	0.476	65.169	17.036	18.675	0.005	0.000	0.138
258	Microcline (II)	L10-232A 78.25	0.702	64.651	16.703	18.554	0.014	0.000	0.12
259	Microcline (II)	L10-232A 78.25	0.444	64.953	17.074	18.66	0.013	0.000	0.115
260	Microcline (II)	L10-232A 78.25	0.449	64.76	17.002	18.553	0.004	0.000	0.115
261	Microcline (II)	L10-232A 78.25	0.398	64.969	17.137	18.598	0.003	0.000	0.136
262	Microcline (II)	L10-232A 78.25	0.495	65.213	17.039	18.649	0.000	0.000	0.045
263	Microcline (II)	L10-232A 82.2	0.344	64.692	17.121	18.486	0.023	0.002	0.114

Analysis	Mineral	Sample	Na_2O	SiO_2	K2O	Al_2O_3	Ga_2O_3	MgO	Rb_2O
264	Microcline (II)	L10-232A 82.2	0.592	64.99	16.709	18.567	0.026	0.000	0.142
265	Microcline (II)	L10-232A 82.2	0.568	64.783	16.784	18.479	0.016	0.000	0.149
266	Microcline (II)	L10-232A 82.2	0.594	64.933	16.844	18.509	0.021	0.004	0.156
267	Microcline (II)	L10-232A 82.2	0.501	64.887	16.955	18.635	0.016	0.000	0.136
268	Microcline (II)	L10-232A 87.1	0.492	64.798	17.095	18.308	0.018	0.000	0.113
269	Microcline (II)	L10-232A 87.1	0.481	65.134	17.053	18.354	0.008	0.003	0.115
270	Microcline (II)	L10-232A 87.1	0.502	63.868	16.969	18.019	0.016	0.000	0.158
271	Microcline (II)	L10-232A 87.1	0.59	63.928	16.847	18.208	0.022	0.000	0.119
272	Microcline (II)	L10-232A 87.1	1.659	64.732	15.396	18.862	0.000	0.005	0
273	Microcline (II)	L10-232A 94.75	0.633	64.671	16.785	18.507	0.013	0.000	0.127
274	Microcline (II)	L10-232A 94.75	0.274	64.892	17.169	18.52	0.01	0.003	0.049
275	Microcline (II)	L10-232A 94.75	0.531	65.275	16.847	18.6	0.018	0.000	0.142
276	Microcline (II)	L10-232A 94.75	0.63	65.447	16.756	18.515	0.023	0.000	0.115
277	Microcline (II)	L10-232A 94.75	0.626	64.663	16.783	18.644	0.01	0.002	0.123
278	Microcline (II)	L10-232A 94.75	0.541	64.996	16.939	18.68	0.012	0.000	0.139
279	Microcline (II)	L10-232A 94.75	0.438	65.37	17.11	18.614	0.023	0.000	0.107
280	Microcline (II)	L10-232A 94.75	0.388	65.301	17.157	18.51	0.009	0.000	0.124
281	Microcline (II)	L10-232A 94.75	0.676	64.832	16.723	18.676	0.011	0.011	0.098
282	Microcline (II)	L10-232A 94.75	0.231	64.343	17.35	18.628	0.011	0.000	0.007
283	Microcline (II)	L10-232A 94.75	0.288	64.645	17.237	18.564	0.023	0.000	0.06
284	Microcline (II)	L10-232A 94.75	0.198	64.624	17.516	18.602	0.008	0.000	0
285	Microcline (II)	L10-232A 94.75	0.338	64.586	17.102	18.529	0.013	0.000	0.083
286	Microcline (II)	L10-232A-103.6	0.454	64.759	16.96	18.066	0.015	0.000	0.107
287	Microcline (II)	L10-232A-103.6	0.46	64.616	16.833	18.134	0.001	0.000	0.122
288	Microcline (II)	L10-232A-103.6	0.517	64.491	16.792	18.202	0.012	0.000	0.129
289	Microcline (II)	L10-232A-103.6	0.6	65.529	16.742	18.525	0.009	0.000	0.139
290	Microcline (II)	L10-232A-103.6	0.501	65.103	16.819	18.448	0.011	0.002	0.112
291	Microcline (II)	L10-232A-57.55	0.097	64.662	17.609	18.282	0.007	0.000	0.000
292	Nepheline	85L6-294.91	15.95	44.66	5.87	32.16	NA	0.000	NA
293	Nepheline	L09-192-183.6	16.36	42.75	7.36	34.27	NA	0.000	NA
294	Sodalite	L09-192-183.6	25.80	38.06	0.000	31.62	NA	0.000	NA
295	Sodalite	L09-192-183.6	24.90	39.10	0.004	30.95	NA	0.000	NA
296	Sodalite	L09-192-183.6	25.63	37.92	0.000	31.75	NA	0.015	NA
297	Sodalite	L09-192-183.6	25.74	38.03	0.026	31.76	NA	0.000	NA
298	Sodalite	L09-192-183.6	25.73	38.25	0.007	31.83	NA	0.002	NA

Analysis	Mineral	Sample	Na_2O	SiO_2	K2O	Al_2O_3	Ga_2O_3	MgO	Rb_2O
299	Sodalite	L09-192-183.6	25.78	38.23	0.000	31.38	NA	0.000	NA
300	Sodalite	L09-192-183.6	25.49	38.40	0.019	31.25	NA	0.011	NA
301	Sodalite	L09-194-276.45	25.56	38.47	0.015	31.23	NA	0.000	NA

Analysis	Mineral	Sample	CaO	SrO	FeO	Nb_2O_5	BaO	Cl	Total
1	Albite (I)	85L6-294.91	0.107	NA	0.088	NA	0.000	0.053	99.41
2	Albite (I)	85L6-294.91	0.007	NA	0.284	NA	0.000	0.013	99.93
3	Albite (I)	L09-155-162.60	0.021	NA	0.224	NA	0.055	0.009	100.77
4	Albite (I)	L09-155-162.60	0.088	NA	0.387	NA	0.034	0.013	100.62
5	Albite (I)	L09-155-162.60	0.000	NA	0.084	NA	0.009	0.000	100.56
6	Albite (I)	L09-155-163.10	0.034	NA	0.017	NA	0.000	0.017	98.83
7	Albite (I)	L09-155-163.10	0.000	NA	0.001	NA	0.003	0.032	100.25
8	Albite (I)	L09-179-129.44	0.011	NA	0.146	NA	0.000	0.016	100.44
9	Albite (I)	L09-179-178.0	0.003	NA	0.193	NA	0.039	0.006	100.72
10	Albite (I)	L09-179-178.0	0.000	NA	0.381	NA	0.011	0.044	100.44
11	Albite (I)	L09-179-46.11	0.014	NA	0.189	NA	0.000	0.000	100.74
12	Albite (I)	L09-179-9.46	0.000	NA	0.006	NA	0.000	0.011	100.45
13	Albite (I)	L09-192-112.8	0.007	NA	0.035	NA	0.000	0.000	100.68
14	Albite (I)	L09-192-112.8	0.000	NA	0.043	NA	0.081	0.001	100.76
15	Albite (I)	L09-192-183.6	0.005	NA	0.056	0.000	NA	NA	98.886
16	Albite (I)	L09-192-183.6	0.011	NA	0.059	0.000	NA	NA	99.022
17	Albite (I)	L09-192-183.6	0.015	NA	0.069	0.000	NA	NA	98.894
18	Albite (I)	L09-192-183.6	0.004	NA	0.096	0.006	NA	NA	99.780
19	Albite (I)	L09-192-183.6	0.032	NA	0.268	NA	0.000	0.027	100.18
20	Albite (I)	L09-192-183.6	0.007	NA	0.268	NA	0.011	0.000	100.64
21	Albite (I)	L09-192-183.6	0.005	NA	0.249	NA	0.022	0.013	100.93
22	Albite (I)	L09-192-183.6	0.000	NA	0.190	NA	0.000	0.000	99.78
23	Albite (I)	L09-192-183.6	0.007	NA	0.113	NA	0.000	0.025	100.40
24	Albite (I)	L09-192-183.6	0.023	NA	0.330	NA	0.000	0.028	100.24
25	Albite (I)	L09-192-183.6	0.012	NA	0.251	NA	0.002	0.000	99.83
26	Albite (I)	L09-192-183.6	0.000	NA	0.125	NA	0.015	0.000	100.85
27	Albite (I)	L09-192-183.6	0.016	NA	0.126	NA	0.013	0.023	100.64
28	Albite (I)	L09-192-200.2	0.000	NA	0.104	0.000	NA	NA	98.716
29	Albite (I)	L09-192-200.2	0.000	NA	0.241	0.000	NA	NA	99.251
30	Albite (I)	L09-192-200.2	0.007	NA	0.306	0.000	NA	NA	100.033
31	Albite (I)	L09-192-200.2	0.020	NA	0.787	0.002	NA	NA	98.935
32	Albite (I)	L09-192-200.2	0.002	NA	0.273	0.000	NA	NA	99.857

Analysis	Mineral	Sample	CaO	SrO	FeO	Nb_2O_5	BaO	Cl	Total
33	Albite (I)	L09-194-276.45	0.096	NA	0.010	NA	0.000	0.012	99.83
34	Albite (I)	L09-194-276.45	0.069	NA	0.501	NA	0.000	0.010	100.26
35	Albite (II)	KM10-002	0.012	NA	0.128	0.000	NA	NA	98.689
36	Albite (II)	KM10-002	0.007	NA	0.069	0.007	NA	NA	98.928
37	Albite (II)	KM10-002	0.000	NA	0.131	0.003	NA	NA	99.307
38	Albite (II)	KM10-002	0.002	NA	0.074	0.014	NA	NA	99.422
39	Albite (II)	L08-84-96.77	0.049	NA	0.196	NA	0.015	0.009	100.54
40	Albite (II)	L08-84-96.77	0.023	NA	0.170	NA	0.030	0.003	101.01
41	Albite (II)	L08-84-96.77	0.020	NA	0.068	NA	0.041	0.000	100.65
42	Albite (II)	L08-84-96.77	0.009	NA	0.043	NA	0.054	0.069	100.11
43	Albite (II)	L10-232A 100.75	0.002	0.038	0.000	NA	NA	NA	100.221
44	Albite (II)	L10-232A 100.75	0.003	0.014	0.003	NA	NA	NA	100.202
45	Albite (II)	L10-232A 100.75	0.025	0.000	0.018	NA	NA	NA	99.979
46	Albite (II)	L10-232A 100.75	0.009	0.02	0.008	NA	NA	NA	100.031
47	Albite (II)	L10-232A 100.75	0.015	0.018	0.014	NA	NA	NA	99.944
48	Albite (II)	L10-232A 100.75	0.009	0.01	0.005	NA	NA	NA	100.432
49	Albite (II)	L10-232A 100.75	0.003	0.019	0.000	NA	NA	NA	100.141
50	Albite (II)	L10-232A 100.75	0.000	0.03	0.000	NA	NA	NA	100.022
51	Albite (II)	L10-232A 100.75	0.006	0.018	0.013	NA	NA	NA	100.379
52	Albite (II)	L10-232A 100.75	0.008	0.002	0.006	NA	NA	NA	100.179
53	Albite (II)	L10-232A 100.75	0.002	0.000	0.000	NA	NA	NA	100.092
54	Albite (II)	L10-232A 100.75	0.011	0.025	0.014	NA	NA	NA	100.461
55	Albite (II)	L10-232A 100.75	0.008	0.003	0.003	NA	NA	NA	100.093
56	Albite (II)	L10-232A 100.75	0.000	0.000	0.009	NA	NA	NA	99.11
57	Albite (II)	L10-232A 100.75	0.009	0.017	0.005	NA	NA	NA	100.21
58	Albite (II)	L10-232A 100.75	0.004	0.033	0.007	NA	NA	NA	100.089
59	Albite (II)	L10-232A 44.2	0.021	0.041	0.306	NA	NA	NA	100.89
60	Albite (II)	L10-232A 44.2	0.017	0.012	0.241	NA	NA	NA	99.933
61	Albite (II)	L10-232A 44.2	0.01	0.024	0.273	NA	NA	NA	100.272
62	Albite (II)	L10-232A 44.2	0.006	0.024	0.351	NA	NA	NA	99.548
63	Albite (II)	L10-232A 44.2	0.008	0.025	0.284	NA	NA	NA	99.524
64	Albite (II)	L10-232A 44.2	0.028	0.022	0.325	NA	NA	NA	99.828
65	Albite (II)	L10-232A 51.25	0.006	0.038	0.137	NA	NA	NA	99.117
66	Albite (II)	L10-232A 51.25	0.013	0.000	0.121	NA	NA	NA	99.768
67	Albite (II)	L10-232A 51.25	0.013	0.032	0.102	NA	NA	NA	99.68
68	Albite (II)	L10-232A 51.25	0.018	0.031	0.11	NA	NA	NA	99.272
69	Albite (II)	L10-232A 51.25	0.005	0.019	0.121	NA	NA	NA	99.42

Analysis	Mineral	Sample	CaO	SrO	FeO	Nb_2O_5	BaO	Cl	Total
70	Albite (II)	L10-232A 51.25	0.006	0.037	0.124	NA	NA	NA	100.071
71	Albite (II)	L10-232A 51.25	0.02	0.005	0.105	NA	NA	NA	99.589
72	Albite (II)	L10-232A 51.25	0.000	0.005	0.126	NA	NA	NA	99.754
73	Albite (II)	L10-232A 51.25	0.001	0.013	0.098	NA	NA	NA	100.206
74	Albite (II)	L10-232A 51.25	0.004	0.014	0.054	NA	NA	NA	99.627
75	Albite (II)	L10-232A 51.25	0.021	0.029	0.144	NA	NA	NA	99.789
76	Albite (II)	L10-232A 51.25	0.008	0.064	0.02	NA	NA	NA	99.767
77	Albite (II)	L10-232A 54.35	0.001	0.025	0.115	NA	NA	NA	100.219
78	Albite (II)	L10-232A 54.35	0.02	0.000	0.182	NA	NA	NA	100.608
79	Albite (II)	L10-232A 54.35	0.022	0.004	0.184	NA	NA	NA	99.898
80	Albite (II)	L10-232A 54.35	0.014	0.034	0.166	NA	NA	NA	100.12
81	Albite (II)	L10-232A 54.35	0.01	0.000	0.111	NA	NA	NA	100.289
82	Albite (II)	L10-232A 54.35	0.007	0.038	0.052	NA	NA	NA	99.645
83	Albite (II)	L10-232A 54.35	0.013	0.03	0.095	NA	NA	NA	99.971
84	Albite (II)	L10-232A 54.35	0.016	0.006	0.124	NA	NA	NA	100.18
85	Albite (II)	L10-232A 54.35	0.013	0.022	0.081	NA	NA	NA	100.057
86	Albite (II)	L10-232A 54.35	0.007	0.024	0.038	NA	NA	NA	100.573
87	Albite (II)	L10-232A 54.35	0.002	0.008	0.111	NA	NA	NA	100.197
88	Albite (II)	L10-232A 54.35	0.009	0.012	0.196	NA	NA	NA	100.252
89	Albite (II)	L10-232A 54.35	0.006	0.003	0.118	NA	NA	NA	100.139
90	Albite (II)	L10-232A 54.35	0.009	0.02	0.098	NA	NA	NA	100.55
91	Albite (II)	L10-232A 54.35	0.001	0.075	0.107	NA	NA	NA	99.866
92	Albite (II)	L10-232A 59.5	0.001	0.026	0.01	NA	NA	NA	100.057
93	Albite (II)	L10-232A 59.5	0.013	0.000	0.054	NA	NA	NA	99.34
94	Albite (II)	L10-232A 59.5	0.004	0.000	0.000	NA	NA	NA	99.734
95	Albite (II)	L10-232A 59.5	0.008	0.000	0.019	NA	NA	NA	100.142
96	Albite (II)	L10-232A 59.5	0.006	0.000	0.046	NA	NA	NA	99.388
97	Albite (II)	L10-232A 59.5	0.003	0.033	0.035	NA	NA	NA	99.704
98	Albite (II)	L10-232A 59.5	0.012	0.000	0.065	NA	NA	NA	99.98
99	Albite (II)	L10-232A 59.5	0.005	0.034	0.101	NA	NA	NA	100.682
100	Albite (II)	L10-232A 59.5	0.008	0.026	0.106	NA	NA	NA	100.429
101	Albite (II)	L10-232A 59.5	0.000	0.016	0.003	NA	NA	NA	99.812
102	Albite (II)	L10-232A 59.5	0.006	0.029	0.046	NA	NA	NA	100.247
103	Albite (II)	L10-232A 59.5	0.013	0.007	0.075	NA	NA	NA	100.321
104	Albite (II)	L10-232A 59.5	0.005	0.000	0.014	NA	NA	NA	98.934
105	Albite (II)	L10-232A 59.5	0.004	0.000	0.036	NA	NA	NA	98.568
106	Albite (II)	L10-232A 59.5	0.000	0.000	0.082	NA	NA	NA	98.234

Analysis	Mineral	Sample	CaO	SrO	FeO	Nb_2O_5	BaO	Cl	Total
107	Albite (II)	L10-232A 59.5	0.009	0.021	0.072	NA	NA	NA	100.032
108	Albite (II)	L10-232A 59.5	0.012	0.03	0.063	NA	NA	NA	98.64
109	Albite (II)	L10-232A 59.5	0.006	0.023	0.056	NA	NA	NA	98.983
110	Albite (II)	L10-232A 65.25	0.011	0.000	0.005	NA	NA	NA	98.743
111	Albite (II)	L10-232A 65.25	0.003	0.032	0.001	NA	NA	NA	98.912
112	Albite (II)	L10-232A 65.25	0.011	0.043	0.000	NA	NA	NA	98.525
113	Albite (II)	L10-232A 65.25	0.003	0.023	0.005	NA	NA	NA	99.692
114	Albite (II)	L10-232A 65.25	0.001	0.000	0.000	NA	NA	NA	99.34
115	Albite (II)	L10-232A 65.25	0.008	0.000	0.012	NA	NA	NA	99.66
116	Albite (II)	L10-232A 65.25	0.008	0.000	0.002	NA	NA	NA	100.191
117	Albite (II)	L10-232A 65.25	0.000	0.006	0.034	NA	NA	NA	99.558
118	Albite (II)	L10-232A 65.25	0.003	0.000	0.000	NA	NA	NA	100.142
119	Albite (II)	L10-232A 65.25	0.017	0.024	0.001	NA	NA	NA	100.375
120	Albite (II)	L10-232A 65.25	0.012	0.035	0.002	NA	NA	NA	100.335
121	Albite (II)	L10-232A 65.25	0.006	0.015	0.002	NA	NA	NA	99.99
122	Albite (II)	L10-232A 65.25	0.013	0.052	0.003	NA	NA	NA	99.887
123	Albite (II)	L10-232A 65.25	0.01	0.000	0.000	NA	NA	NA	100.042
124	Albite (II)	L10-232A 65.25	0.008	0.002	0.000	NA	NA	NA	99.98
125	Albite (II)	L10-232A 75.2	0.003	0.014	0.013	NA	NA	NA	100.064
126	Albite (II)	L10-232A 75.2	0.000	0.000	0.011	NA	NA	NA	99.959
127	Albite (II)	L10-232A 75.2	0.004	0.034	0.000	NA	NA	NA	100.047
128	Albite (II)	L10-232A 75.2	0.015	0.007	0.006	NA	NA	NA	99.97
129	Albite (II)	L10-232A 78.25	0.012	0.024	0.000	NA	NA	NA	99.847
130	Albite (II)	L10-232A 78.25	0.011	0.013	0.008	NA	NA	NA	100.199
131	Albite (II)	L10-232A 78.25	0.023	0.036	0.011	NA	NA	NA	99.827
132	Albite (II)	L10-232A 78.25	0.018	0.002	0.000	NA	NA	NA	99.953
133	Albite (II)	L10-232A 78.25	0.003	0.000	0.001	NA	NA	NA	99.821
134	Albite (II)	L10-232A 78.25	0.004	0.03	0.009	NA	NA	NA	100.184
135	Albite (II)	L10-232A 78.25	0.002	0.021	0.013	NA	NA	NA	99.66
136	Albite (II)	L10-232A 78.25	0.006	0.007	0.005	NA	NA	NA	99.747
137	Albite (II)	L10-232A 78.25	0.015	0.000	0.005	NA	NA	NA	100.155
138	Albite (II)	L10-232A 78.25	0.011	0.019	0.013	NA	NA	NA	100.001
139	Albite (II)	L10-232A 78.25	0.011	0.024	0.03	NA	NA	NA	99.998
140	Albite (II)	L10-232A 78.25	0.019	0.000	0.000	NA	NA	NA	100.06
141	Albite (II)	L10-232A 78.25	0.006	0.051	0.012	NA	NA	NA	100.072
142	Albite (II)	L10-232A 78.25	0.026	0	0.002	NA	NA	NA	100
143	Albite (II)	L10-232A 78.25	0.021	0.017	0.014	NA	NA	NA	100.109

Analysis	Mineral	Sample	CaO	SrO	FeO	Nb_2O_5	BaO	Cl	Total
144	Albite (II)	L10-232A 82.2	0.001	0.022	0.003	NA	NA	NA	100.038
145	Albite (II)	L10-232A 82.2	0.000	0.024	0.015	NA	NA	NA	100.219
146	Albite (II)	L10-232A 82.2	0.005	0.016	0.011	NA	NA	NA	100.124
147	Albite (II)	L10-232A 82.2	0.005	0.000	0.014	NA	NA	NA	100.302
148	Albite (II)	L10-232A 82.2	0.018	0.034	0.007	NA	NA	NA	99.356
149	Albite (II)	L10-232A 82.2	0.014	0.001	0.001	NA	NA	NA	100.03
150	Albite (II)	L10-232A 82.2	0.017	0.000	0.000	NA	NA	NA	99.658
151	Albite (II)	L10-232A 82.2	0.012	0.013	0.000	NA	NA	NA	100.075
152	Albite (II)	L10-232A 82.2	0.027	0.028	0.003	NA	NA	NA	99.606
153	Albite (II)	L10-232A 82.2	0.012	0.025	0.039	NA	NA	NA	100.064
154	Albite (II)	L10-232A 82.2	0.003	0.000	0.005	NA	NA	NA	99.87
155	Albite (II)	L10-232A 87.1	0.004	0.043	0.000	NA	NA	NA	100.175
156	Albite (II)	L10-232A 87.1	0.02	0.009	0.01	NA	NA	NA	100.277
157	Albite (II)	L10-232A 87.1	0.034	0.000	0.000	NA	NA	NA	100.366
158	Albite (II)	L10-232A 87.1	0.008	0.048	0.182	NA	NA	NA	100.329
159	Albite (II)	L10-232A 87.1	0.016	0.02	0.004	NA	NA	NA	100.07
160	Albite (II)	L10-232A 87.1	0.005	0.037	0.000	NA	NA	NA	99.625
161	Albite (II)	L10-232A 87.1	0.018	0.013	0.000	NA	NA	NA	99.993
162	Albite (II)	L10-232A 87.1	0.01	0.000	0.007	NA	NA	NA	99.918
163	Albite (II)	L10-232A 87.1	0.006	0.044	0.01	NA	NA	NA	98.981
164	Albite (II)	L10-232A 87.1	0.015	0.000	0.009	NA	NA	NA	99.831
165	Albite (II)	L10-232A 87.1	0.02	0.036	0.046	NA	NA	NA	100.094
166	Albite (II)	L10-232A 87.1	0.027	0.035	0.000	NA	NA	NA	99.955
167	Albite (II)	L10-232A 87.1	0.003	0.000	0.006	NA	NA	NA	100.003
168	Albite (II)	L10-232A 87.1	0.015	0.02	0.005	NA	NA	NA	99.646
169	Albite (II)	L10-232A 87.1	0.015	0.012	0.014	NA	NA	NA	99.582
170	Albite (II)	L10-232A 87.1	0.026	0.027	0.000	NA	NA	NA	100.045
171	Albite (II)	L10-232A 87.1	0.015	0.000	0.000	NA	NA	NA	99.661
172	Albite (II)	L10-232A 87.1	0.009	0.038	0.007	NA	NA	NA	100.06
173	Albite (II)	L10-232A 94.75	0.007	0.000	0.004	NA	NA	NA	100.366
174	Albite (II)	L10-232A 94.75	0.009	0.006	0.007	NA	NA	NA	98.937
175	Albite (II)	L10-232A 94.75	0.000	0.008	0.000	NA	NA	NA	100.182
176	Albite (II)	L10-232A 94.75	0.000	0.000	0.000	NA	NA	NA	100.279
177	Albite (II)	L10-232A 94.75	0.021	0.017	0.019	NA	NA	NA	100.073
178	Albite (II)	L10-232A 94.75	0.013	0.009	0.000	NA	NA	NA	99.434
179	Albite (II)	L10-232A 94.75	0.014	0.016	0.011	NA	NA	NA	100.048
180	Albite (II)	L10-232A 94.75	0.018	0.017	0.000	NA	NA	NA	100.069

Analysis	Mineral	Sample	CaO	SrO	FeO	Nb_2O_5	BaO	Cl	Total
181	Albite (II)	L10-232A 94.75	0.01	0.022	0.007	NA	NA	NA	100.623
182	Albite (II)	L10-232A 94.75	0.02	0.000	0.027	NA	NA	NA	100.402
183	Albite (II)	L10-232A 94.75	0.009	0.000	0.015	NA	NA	NA	100.176
184	Albite (II)	L10-232A 94.75	0.004	0.000	0.000	NA	NA	NA	100.079
185	Albite (II)	L10-232A 94.75	0.026	0.000	0.000	NA	NA	NA	100.795
186	Albite (II)	L10-232A 94.75	0.016	0.027	0.001	NA	NA	NA	100.101
187	Albite (II)	L10-232A 94.75	0.019	0.027	0.01	NA	NA	NA	99.731
188	Albite (II)	L10-232A 94.75	0.000	0.023	0.005	NA	NA	NA	100.23
189	Albite (II)	L10-232A 94.75	0.002	0.000	0.006	NA	NA	NA	99.986
190	Albite (II)	L10-232A 94.75	0.011	0.031	0.000	NA	NA	NA	100.064
191	Albite (II)	L10-232A 94.75	0.007	0.000	0.008	NA	NA	NA	99.942
192	Albite (II)	L10-232A 94.75	0.002	0.000	0.005	NA	NA	NA	100.042
193	Albite (II)	L10-232A 94.75	0.017	0.000	0.000	NA	NA	NA	100.287
194	Albite (II)	L10-232A 94.75	0.000	0.000	0.098	NA	NA	NA	98.511
195	Albite (II)	L10-232A 94.75	0.000	0.036	0.103	NA	NA	NA	100.175
196	Albite (II)	L10-232A 94.75	0.012	0.027	0.082	NA	NA	NA	100.166
197	Albite (II)	L10-232A 94.75	0.000	0.037	0.08	NA	NA	NA	100.616
198	Albite (II)	L10-232A-103.6	0.002	0.029	0.009	NA	NA	NA	100.206
199	Albite (II)	L10-232A-103.6	0.004	0.003	0.012	NA	NA	NA	100.178
200	Albite (II)	L10-232A-103.6	0.005	0.000	0.014	NA	NA	NA	100.178
201	Albite (II)	L10-232A-103.6	0.003	0.027	0.02	NA	NA	NA	100.374
202	Albite (II)	L10-232A-103.6	0.003	0.000	0.005	NA	NA	NA	100.277
203	Albite (II)	L10-232A-54.35	0.018	NA	0.008	0.000	NA	NA	98.808
204	Albite (II)	L10-232A-54.35	0.019	NA	0.007	0.000	NA	NA	99.828
205	Albite (II)	L10-232A-54.35	0.047	NA	0.073	0.001	NA	NA	98.688
206	Albite (II)	L10-232A-54.35	0.001	NA	0.000	0.001	NA	NA	99.658
207	Albite (II)	L10-232A-54.35	0.003	NA	0.030	0.006	NA	NA	99.532
208	Albite (II)	L10-232A-54.35	0.008	NA	0.089	0.008	NA	NA	99.832
209	Albite (II)	L10-232A-57.55	0.012	NA	0.015	0.010	NA	NA	99.836
210	Albite (II)	L10-232A-57.55	0.003	NA	0.000	0.000	NA	NA	99.995
211	Albite (II)	L10-232A-57.55	0.008	NA	0.004	0.000	NA	NA	99.831
212	Albite (II)	L10-232A-57.55	0.011	NA	0.000	0.002	NA	NA	99.708
213	Albite (II)	L10-232A-57.55	0.000	NA	0.000	0.002	NA	NA	99.868
214	Albite (II)	L10-232A-57.55	0.014	NA	0.002	0.000	NA	NA	99.988
215	Albite (II)	L10-232A-57.55	0.005	NA	0.000	0.000	NA	NA	99.645
216	Albite (II)	L10-232A-82.2	0.037	NA	0.022	0.001	NA	NA	99.736
217	Albite (II)	L10-232A-82.2	0.004	NA	0.011	0.000	NA	NA	99.560

Analysis	Mineral	Sample	CaO	SrO	FeO	Nb_2O_5	BaO	Cl	Total
218	Albite (II)	L10-232A-82.2	0.009	NA	0.011	0.003	NA	NA	99.777
219	Albite (II)	L10-232A-82.2	0.009	NA	0.008	0.000	NA	NA	99.479
220	Microcline (I)	85L6-294.91	0.000	NA	0.043	NA	0.000	0.024	99.96
221	Microcline (I)	85L6-294.91	0.000	NA	0.001	NA	0.000	0.000	99.85
222	Microcline (I)	L09-194-276.45	0.009	NA	0.304	NA	0.000	0.089	100.31
223	Microcline (I)	L09-194-276.45	0.033	NA	0.523	NA	0.000	0.166	100.06
224	Microcline (I)	L09-194-276.45	0.022	NA	0.740	NA	0.000	0.029	100.87
225	Microcline (II)	KM10-002	0.001	NA	0.084	0.000	NA	NA	99.722
226	Microcline (II)	L09-155-163.10	0.044	NA	0.025	NA	0.000	0.031	100.72
227	Microcline (II)	L09-179-129.44	0.000	NA	0.054	NA	0.012	0.010	100.73
228	Microcline (II)	L09-179-129.44	0.002	NA	0.043	NA	0.000	0.017	100.44
229	Microcline (II)	L09-179-129.44	0.005	NA	0.041	NA	0.028	0.006	100.39
230	Microcline (II)	L09-179-178.0	0.005	NA	0.046	NA	0.000	0.015	100.67
231	Microcline (II)	L09-179-178.0	0.000	NA	0.000	NA	0.000	0.003	99.23
232	Microcline (II)	L09-179-46.11	0.000	NA	0.024	NA	0.035	0.006	100.63
233	Microcline (II)	L09-179-46.11	0.000	NA	0.000	NA	0.000	0.020	100.79
234	Microcline (II)	L09-179-9.46	0.007	NA	0.005	NA	0.008	0.017	100.62
235	Microcline (II)	L09-179-9.46	0.005	NA	0.056	NA	0.000	0.003	100.00
236	Microcline (II)	L09-179-9.46	0.000	NA	0.010	NA	0.041	0.000	100.06
237	Microcline (II)	L09-179-9.46	0.009	NA	0.026	NA	0.038	0.005	100.32
238	Microcline (II)	L09-192-112.8	0.001	NA	0.542	NA	0.025	0.030	99.56
239	Microcline (II)	L09-192-112.8	0.000	NA	0.037	NA	0.000	0.012	100.43
240	Microcline (II)	L09-192-112.8	0.001	NA	0.016	NA	0.000	0.017	100.80
241	Microcline (II)	L09-192-112.8	0.007	NA	0.010	NA	0.043	0.003	100.94
242	Microcline (II)	L09-192-112.8	0.005	NA	0.019	NA	0.042	0.024	99.98
243	Microcline (II)	L10-232A 51.25	0.000	0.046	0.006	NA	NA	NA	100.981
244	Microcline (II)	L10-232A 51.25	0.000	0.066	0.029	NA	NA	NA	100.929
245	Microcline (II)	L10-232A 51.25	0.551	0.051	0.042	NA	NA	NA	100.051
246	Microcline (II)	L10-232A 51.25	0.007	0.071	0.048	NA	NA	NA	99.894
247	Microcline (II)	L10-232A 65.25	0.021	0.029	0.071	NA	NA	NA	98.473
248	Microcline (II)	L10-232A 75.2	0.000	0.077	0.014	NA	NA	NA	100.174
249	Microcline (II)	L10-232A 75.2	0.000	0.081	0.011	NA	NA	NA	100.744
250	Microcline (II)	L10-232A 75.2	0.000	0.085	0.013	NA	NA	NA	100.659
251	Microcline (II)	L10-232A 75.2	0.000	0.057	0.016	NA	NA	NA	101.055
252	Microcline (II)	L10-232A 75.2	0.000	0.038	0.035	NA	NA	NA	101.2
253	Microcline (II)	L10-232A 75.2	0.000	0.075	0.02	NA	NA	NA	101.069
254	Microcline (II)	L10-232A 78.25	0.000	0.051	0.008	NA	NA	NA	101.362

Analysis	Mineral	Sample	CaO	SrO	FeO	Nb_2O_5	BaO	Cl	Total
255	Microcline (II)	L10-232A 78.25	0.000	0.112	0.024	NA	NA	NA	101.434
256	Microcline (II)	L10-232A 78.25	0.000	0.062	0.052	NA	NA	NA	101.439
257	Microcline (II)	L10-232A 78.25	0.007	0.063	0.047	NA	NA	NA	101.616
258	Microcline (II)	L10-232A 78.25	0.000	0.069	0.039	NA	NA	NA	100.852
259	Microcline (II)	L10-232A 78.25	0.000	0.07	0.025	NA	NA	NA	101.354
260	Microcline (II)	L10-232A 78.25	0.000	0.07	0.026	NA	NA	NA	100.979
261	Microcline (II)	L10-232A 78.25	0.000	0.067	0.032	NA	NA	NA	101.34
262	Microcline (II)	L10-232A 78.25	0.000	0.088	0.012	NA	NA	NA	101.541
263	Microcline (II)	L10-232A 82.2	0.007	0.087	0.024	NA	NA	NA	100.9
264	Microcline (II)	L10-232A 82.2	0.005	0.051	0.03	NA	NA	NA	101.112
265	Microcline (II)	L10-232A 82.2	0.000	0.092	0.009	NA	NA	NA	100.88
266	Microcline (II)	L10-232A 82.2	0.000	0.084	0.025	NA	NA	NA	101.17
267	Microcline (II)	L10-232A 82.2	0.000	0.059	0.033	NA	NA	NA	101.222
268	Microcline (II)	L10-232A 87.1	0.000	0.083	0.052	NA	NA	NA	100.959
269	Microcline (II)	L10-232A 87.1	0.000	0.07	0.033	NA	NA	NA	101.251
270	Microcline (II)	L10-232A 87.1	0.000	0.105	0.018	NA	NA	NA	99.655
271	Microcline (II)	L10-232A 87.1	0.025	0.02	0.028	NA	NA	NA	99.787
272	Microcline (II)	L10-232A 87.1	0.018	0.069	0.186	NA	NA	NA	100.927
273	Microcline (II)	L10-232A 94.75	0.009	0.086	0.027	NA	NA	NA	100.858
274	Microcline (II)	L10-232A 94.75	0.000	0.103	0.068	NA	NA	NA	101.088
275	Microcline (II)	L10-232A 94.75	0.006	0.086	0.03	NA	NA	NA	101.535
276	Microcline (II)	L10-232A 94.75	0.005	0.101	0.025	NA	NA	NA	101.617
277	Microcline (II)	L10-232A 94.75	0.000	0.095	0.02	NA	NA	NA	100.966
278	Microcline (II)	L10-232A 94.75	0.000	0.059	0.018	NA	NA	NA	101.384
279	Microcline (II)	L10-232A 94.75	0.026	0.045	0.027	NA	NA	NA	101.76
280	Microcline (II)	L10-232A 94.75	0.000	0.093	0.03	NA	NA	NA	101.612
281	Microcline (II)	L10-232A 94.75	0.003	0.042	0.024	NA	NA	NA	101.096
282	Microcline (II)	L10-232A 94.75	0.000	0.078	0.027	NA	NA	NA	100.675
283	Microcline (II)	L10-232A 94.75	0.002	0.121	0.019	NA	NA	NA	100.959
284	Microcline (II)	L10-232A 94.75	0.000	0.089	0.105	NA	NA	NA	101.142
285	Microcline (II)	L10-232A 94.75	0.000	0.08	0.023	NA	NA	NA	100.754
286	Microcline (II)	L10-232A-103.6	0.000	0.055	0.022	NA	NA	NA	100.438
287	Microcline (II)	L10-232A-103.6	0.000	0.056	0.018	NA	NA	NA	100.24
288	Microcline (II)	L10-232A-103.6	0.000	0.063	0.022	NA	NA	NA	100.228
289	Microcline (II)	L10-232A-103.6	0.003	0.097	0.023	NA	NA	NA	101.667
290	Microcline (II)	L10-232A-103.6	0.011	0.083	0.027	NA	NA	NA	101.117
291	Microcline (II)	L10-232A-57.55	0.001	NA	0.005	0.000	NA	NA	100.663

Analysis	Mineral	Sample	CaO	SrO	FeO	Nb_2O_5	BaO	Cl	Total
292	Nepheline	85L6-294.91	0.025	NA	0.733	NA	0.042	0.032	99.47
293	Nepheline	L09-192-183.6	0.080	NA	0.144	NA	0.000	0.000	100.96
294	Sodalite	L09-192-183.6	0.005	NA	0.089	NA	0.023	6.83	100.88
295	Sodalite	L09-192-183.6	0.011	NA	0.011	NA	0.000	6.22	99.79
296	Sodalite	L09-192-183.6	0.000	NA	0.009	NA	0.025	6.70	100.54
297	Sodalite	L09-192-183.6	0.000	NA	0.057	NA	0.000	6.65	100.77
298	Sodalite	L09-192-183.6	0.000	NA	0.012	NA	0.000	6.59	100.93
299	Sodalite	L09-192-183.6	0.005	NA	0.067	NA	0.036	6.78	100.74
300	Sodalite	L09-192-183.6	0.010	NA	0.090	NA	0.000	6.68	100.44
301	Sodalite	L09-194-276.45	0.019	NA	0.040	NA	0.024	6.77	100.61

Analysis	Mineral	Sample	Rock Type	Na_2O	K_2O	Ga_2O_3	SiO_2	MgO	TiO_2	FeO
1*	Biotite	71B	aegirine syenite	0.071	9.116	0.036	42.029	18.587	0.727	12.455
2*	Biotite	71B	aegirine syenite	0.032	9.53	0.033	42.345	18.817	0.805	12.602
3*	Biotite	71B	aegirine syenite	0.061	9.506	0.042	41.703	19.142	0.666	12.541
4*	Biotite	71B	aegirine syenite	0.116	9.381	0.044	41.307	18.783	0.768	12.195
5*	Biotite	71B	aegirine syenite	0.07	8.932	0.043	42.274	18.906	0.825	12.295
6*	Biotite	71B	aegirine syenite	0.065	8.872	0.045	43.435	18.945	0.685	12.165
7*	Biotite	71B	aegirine syenite	0.04	8.878	0.066	42.594	19.036	0.61	12.634
8*	Biotite	71B	aegirine syenite	0.054	9.217	0.025	41.977	18.276	0.77	12.596
9*	Biotite	71B	aegirine syenite	0.069	8.751	0.047	43.034	18.901	0.445	12.278
10*	Biotite	81B	aegirine syenite	0.038	9.144	0.000	41.704	17.103	0.016	15.425
11*	Biotite	81B	aegirine syenite	0.074	9.622	0.011	41.1	17.465	0.018	15.451
12*	Biotite	81B	aegirine syenite	0.064	8.308	0.006	44.503	18.92	0.006	14.004
13*	Biotite	81B	aegirine syenite	0.059	9.625	0.013	39.905	16.315	0.000	16.443
14*	Biotite	81B	aegirine syenite	0.094	9.024	0.013	40.646	16.526	0.035	16.897
15*	Biotite	81B	aegirine syenite	0.205	7.37	0.002	43.602	19.001	0.003	13.798
16*	Biotite	81B	aegirine syenite	0.099	9.215	0.015	41.87	18.239	0.031	13.805
17*	Biotite	81B	aegirine syenite	0.05	8.802	0.017	42.961	18.672	0.141	13.469
18*	Biotite	81B	aegirine syenite	0.056	9.117	0.01	41.787	17.763	0.119	14.322
19*	Biotite	81B	aegirine syenite	0.129	9.207	0.018	39.949	16.29	0.334	16.239
20	Biotite	L07-53-40.3	aegirine syenite	0.027	9.354	0.016	38.702	10.809	0.508	23.737
21	Biotite	L07-53-40.3	aegirine syenite	0.053	7.535	0.024	35.45	10.342	0.267	27.081
22	Biotite	L07-53-40.3	aegirine syenite	0.03	9.146	0.01	37.353	10.742	0.469	25.025
23	Biotite	L07-53-40.3	aegirine syenite	0.028	9.746	0.021	38.91	11.172	0.522	22.536
24	Biotite	L07-53-40.3	aegirine syenite	0.041	8.19	0.021	36.673	10.624	0.471	24.728
25	Biotite	L07-53-40.3	aegirine syenite	0.074	9.914	0.014	37.698	11.826	0.328	22.396

Analysis	Mineral	Sample	Rock Type	Na_2O	K_2O	Ga_2O_3	SiO_2	MgO	TiO_2	FeO
26	Biotite	L07-53-40.3	aegirine syenite	0.036	9.948	0.012	38.502	11.358	0.389	23.016
27	Biotite	L07-53-40.3	aegirine syenite	0.037	10.273	0.007	40.302	16.279	0.225	15.783
28	Biotite	L07-53-40.3	aegirine syenite	0.056	10.359	0.015	39.926	15.803	0.283	15.741
29	Biotite	L07-53-40.3	aegirine syenite	0.093	10.196	0.003	40.449	16.431	0.229	15.513
30	Biotite	L07-53-40.3	aegirine syenite	0.048	10.32	0.015	39.007	15.357	0.259	16.802
31	Biotite	L07-55-100.1	aegirine syenite	0.102	9.941	0.014	39.322	15.92	0.26	15.716
32	Biotite	L07-55-100.1	aegirine syenite	0.075	9.536	0.002	38.525	15.308	0.284	17.663
33	Biotite	L07-55-100.1	aegirine syenite	0.055	9.961	0.016	38.729	14.963	0.3	17.776
34	Biotite	L07-55-100.1	aegirine syenite	0.105	10.172	0.03	39.188	15.107	0.241	17.737
35	Biotite	L07-55-100.1	aegirine syenite	0.022	10.453	0.033	39.343	15.722	0.128	16.808
36	Biotite	L07-55-100.1	aegirine syenite	0.012	9.996	0.025	41.185	17.202	0.104	15.612
37	Biotite	L07-55-100.1	aegirine syenite	0.025	10.294	0.032	39.45	15.269	0.172	17.794
38	Biotite	L07-55-100.1	aegirine syenite	0.035	9.232	0.04	40.455	15.844	0.23	18.61
39*	Biotite	L07-55-86-8	aegirine syenite	0.044	9.773	0.008	37.678	13.582	0.019	17.321
40*	Biotite	L07-55-86-8	aegirine syenite	0.052	10.006	0.003	37.516	13.431	0.001	17.035
41*	Biotite	L07-63-86-1	aegirine syenite	0.057	8.705	0.026	38.874	11.079	0.07	23.978
42*	Biotite	L07-63-86-1	aegirine syenite	0.041	8.802	0.016	35.963	9.658	0.085	25.402
43*	Biotite	L07-63-86-1	aegirine syenite	0.023	8.396	0.027	39.073	10.625	0.055	24.892
44*	Biotite	L07-63-86-1	aegirine syenite	0.018	8.984	0.017	37.807	10.067	0.382	24.967
45*	Biotite	L07-63-86-1	aegirine syenite	0.019	9.384	0.012	37.571	9.509	0.292	24.942
46*	Biotite	L07-63-86-1	aegirine syenite	0.039	8.471	0.016	39.251	10.764	0.143	24.433
47*	Biotite	L07-63-86-1	aegirine syenite	0.023	9.353	0.025	37.415	9.427	0.315	25.114
48*	Biotite	L07-63-86-1	aegirine syenite	0.032	8.919	0.032	38.493	9.926	0.352	25.344
49*	Biotite	L07-63-86-1	aegirine syenite	0.03	9.159	0.013	37.873	9.622	0.396	25.267
50*	Biotite	L07-63-86-1	aegirine syenite	0.037	9.101	0.012	37.312	10.145	0.143	25.194
51*	Biotite	L07-63-86-1	aegirine syenite	0.091	9.283	0.022	36.904	8.893	0.197	25.678
52*	Biotite	L08-118-85-6	aegirine syenite	0.022	9.315	0.029	38.357	12.804	0.136	21.046
53*	Biotite	L08-118-85-6	aegirine syenite	0.025	9.336	0.029	39.507	13.919	0.364	19.215
54*	Biotite	L08-118-85-6	aegirine syenite	0.094	9.047	0.012	39.655	14.428	0.19	18.238
55*	Biotite	L10-304-153.1	aegirine syenite	0.088	9.671	0.008	38.947	13.653	1.045	19.086
56*	Biotite	L10-304-153.1	aegirine syenite	0.034	9.781	0.006	37.959	10.438	0.768	24.306
57*	Biotite	L10-304-153.1	aegirine syenite	0.037	9.771	0.005	37.402	9.978	1.284	24.61
58*	Biotite	L10-304-153.1	aegirine syenite	0.081	9.687	0.013	37.012	9.449	1.002	25.155
59*	Biotite	L10-304-153.1	aegirine syenite	0.035	9.621	0.000	38.127	11.33	0.681	21.474
60*	Biotite	L10-304-153.1	aegirine syenite	0.08	9.796	0.008	38.687	13.348	0.743	20.059
61*	Biotite	L10-304-153.1	aegirine syenite	0.023	9.701	0.017	37.682	11.535	0.811	22.706
62*	Biotite	L10-304-153.1	aegirine syenite	0.117	9.745	0.002	37.713	11.097	0.995	22.833

Analysis	Mineral	Sample	Rock Type	Na_2O	K_2O	Ga_2O_3	SiO_2	MgO	TiO_2	FeO
63*	Biotite	L10-304-153.1	aegirine syenite	0.111	9.533	0.014	39.224	14.046	0.166	19.549
64*	Biotite	L10-304-153.1	aegirine syenite	0.043	9.858	0.009	37.862	12.586	0.734	20.256
65*	Biotite	L10-304-172.3	aegirine syenite	0.047	10.119	0.000	38.527	14.663	0.117	16.602
66*	Biotite	L10-304-172.3	aegirine syenite	0.098	9.52	0.01	37.823	15.108	0.065	16.362
67*	Biotite	L10-304-172.3	aegirine syenite	0.089	10.112	0.000	40.019	16.592	0.13	13.92
68*	Biotite	L10-304-172.3	aegirine syenite	0.088	10.139	0.000	39.616	17.005	0.055	13.659
69*	Biotite	L10-304-172.3	aegirine syenite	0.111	10.067	0.004	38.799	14.671	0.095	15.794
70*	Biotite	L10-304-172.3	aegirine syenite	0.052	9.752	0.005	37.587	12.949	0.047	18.275
71*	Biotite	L10-304-172.3	aegirine syenite	0.073	9.62	0.000	37.098	13.81	0.05	17.771
72*	Biotite	L10-304-172.3	aegirine syenite	0.086	9.981	0.000	40.505	16.043	0.036	14.105
73*	Biotite	L10-304-172.3	aegirine syenite	0.12	9.949	0.000	39.566	14.179	0.026	16.292
74*	Biotite	L10-304-180.6	aegirine syenite	0.04	9.491	0.000	38.141	11.359	0.232	23.268
75*	Biotite	L10-304-180.6	aegirine syenite	0.045	9.637	0.022	36.841	11.276	0.143	22.692
76*	Biotite	L10-304-180.6	aegirine syenite	0.018	9.107	0.005	39.949	13.268	0.261	20.349
77*	Biotite	L10-304-180.6	aegirine syenite	0.062	9.243	0.005	39.497	13.704	0.081	19.79
78*	Biotite	L10-304-180.6	aegirine syenite	0.034	9.143	0.000	37.869	11.647	0.331	23.101
79*	Biotite	L10-304-180.6	aegirine syenite	0.03	9.255	0.014	36.914	10.939	0.301	24.013
80*	Biotite	L10-304-180.6	aegirine syenite	0.029	9.458	0.011	37.494	10.825	0.275	24.027
81*	Biotite	L07.58.48	albitite	0.061	9.654	0.025	39.595	14.864	0.177	18.028
82*	Biotite	L07.58.48	albitite	0.057	9.094	0.031	39.413	15.286	0.108	18.02
83	Biotite	L10-232A 51.25	albitite	0.092	9.774	0.001	39.409	11.397	0.007	22.903
84	Biotite	L10-232A 51.25	albitite	0.074	8.103	0.007	37.783	11.34	0.004	24.424
85	Biotite	L10-232A 51.25	albitite	0.109	8.297	0.017	38.527	11.369	0.018	23.986
86	Biotite	L10-232A 51.25	albitite	0.06	8.456	0.009	35.97	9.476	0.012	27.063
87	Biotite	L10-232A 51.25	albitite	0.051	6.854	0.031	34.461	9.679	0.001	28.059
88	Biotite	L10-232A 51.25	albitite	0.077	9.596	0.007	39.646	11.094	0.005	23.703
89	Biotite	L10-232A-103.6	albitite	0.099	9.695	0.009	36.993	8.647	0.004	27.097
90	Biotite	L10-232A-103.6	albitite	0.251	9.173	0.016	36.562	8.739	0.037	26.766
91	Biotite	L10-232A-103.6	albitite	0.22	8.571	0.006	36.564	7.762	0.026	28.129
92	Biotite	L10-232A-103.6	albitite	0.192	9.006	0.01	37.552	8.523	0.017	26.985
93	Biotite	L10-232A-103.6	albitite	0.175	9.28	0.001	36.805	7.855	0.029	27.964
94	Biotite	L10-232A-103.6	albitite	0.163	9.573	0.01	37.9	8.779	0.018	26.785
95	Biotite	L10-232A-103.6	albitite	0.286	8.624	0.01	35.799	7.216	0.033	28.071
96	Biotite	L10-232A-103.6	albitite	0.158	8.402	0.004	36.508	8.528	0.019	27.25
97	Biotite	L10-232A-103.6	albitite	0.203	7.793	0.013	37.75	8.902	0.034	27.32
98	Biotite	L10-232A-103.6	albitite	0.157	8.937	0.017	36.871	8.463	0.002	27.653
99	Biotite	L10-232A-103.6	albitite	0.198	7.995	0.002	36.945	8.861	0.017	27.353

Analysis	Mineral	Sample	Rock Type	Na_2O	K_2O	Ga_2O_3	SiO_2	MgO	TiO_2	FeO
100	Biotite	L10-232A-103.6	albitite	0.09	9.678	0.007	36.696	8.788	0.081	27.513
101	Biotite	L10-232A-103.6	albitite	0.127	9.783	0.02	36.925	8.062	0.063	28.157
102	Biotite	L10-232A-103.6	albitite	0.049	8.92	0.014	35.316	8.386	0.052	28.631
103	Biotite	L10-232A-103.6	albitite	0.071	8.928	0.011	34.076	6.879	0.118	30.29
104	Biotite	L10-232A-103.6	albitite	0.17	8.689	0.013	37.041	8.916	0.024	26.907
105	Biotite	L10-232A-103.6	albitite	0.243	8.115	0.000	36.808	8.711	0.025	27.315
106	Biotite	L10-232A-103.6	albitite	0.079	8.617	0.014	35.225	8.314	0.146	28.691
107	Biotite	L10-232A-103.6	albitite	0.079	7.753	0.015	33.962	8.11	0.118	29.681
108	Biotite	L10-232A-103.6	albitite	0.513	6.849	0.007	37.044	8.296	0.017	28.512
109	Biotite	L10-232A-103.6	albitite	0.395	7.027	0.016	35.967	8.137	0.027	28.201
110	Biotite	L10-232A-103.6	albitite	0.188	8.599	0.014	36.453	8.135	0.062	29.067
111	Biotite	L10-232A-103.6	albitite	0.136	9.116	0.008	37.06	8.279	0.055	27.548
112	Biotite	L10-232A-103.6	albitite	0.053	10.017	0.01	37.299	8.387	0.006	27.469
113	Biotite	L10-232A-103.6	albitite	0.083	9.665	0.023	36.863	8.342	0.023	27.689
114	Biotite	L10-232A-103.6	albitite	0.108	9.789	0.000	37.677	8.508	0.064	27.355
115	Biotite	L10-232A-103.6	albitite	0.176	9.215	0.014	37.331	8.117	0.105	27.599
116	Biotite	L10-232A-103.6	albitite	0.143	8.95	0.008	36.801	7.904	0.101	27.959
117	Biotite	L10-232A-103.6	albitite	0.168	8.593	0.026	37.104	8.171	0.091	27.669
118	Biotite	L10-232A-103.6	albitite	0.092	10.049	0.000	36.785	7.792	0.174	28.423
119	Biotite	L10-232A-103.6	albitite	0.076	9.977	0.024	37.737	8.884	0.042	27.107
120*	Biotite	L10-304-74	albitite	0.065	9.714	0.035	36.938	9.58	0.394	25.21
121*	Biotite	L10-304-74	albitite	0.094	9.596	0.007	37.797	10.575	0.621	22.475
122*	Biotite	L10-304-74	albitite	0.108	9.407	0.025	36.053	9.292	0.454	24.843
123*	Biotite	L10-304-74	albitite	0.066	9.755	0.024	36.753	9.053	0.164	25.406
124*	Biotite	L10-304-74	albitite	0.095	9.722	0.027	36.514	8.648	0.38	25.671
125*	Biotite	L10-304-74	albitite	0.035	9.946	0.03	37.485	10.16	0.448	23.91
126*	Biotite	L10-304-74	albitite	0.064	9.622	0.028	36.093	8.972	0.372	26.122
127*	Biotite	L10-304-74	albitite	0.039	9.849	0.024	37.903	10.805	0.312	23.654
128*	Biotite	L10-304-74	albitite	0.04	9.561	0.025	36.592	9.05	0.148	25.6
129*	Biotite	L10-304-189.1	foyaite	0.078	9.521	0.004	38.426	10.86	0.103	23.699
130*	Biotite	L10-304-189.1	foyaite	0.089	9.57	0.002	36.785	9.148	0.094	26.516
131*	Biotite	L10-304-189.1	foyaite	0.076	8.737	0.000	35.854	9.081	0.143	27.058
132*	Biotite	L10-304-189.1	foyaite	0.099	8.341	0.013	36.474	9.137	0.09	26.965
133*	Biotite	L10-304-189.1	foyaite	0.063	7.648	0.002	36.057	9.913	0.188	27.203
134*	Biotite	L10-304-189.1	foyaite	0.023	7.79	0.013	35.229	9.478	0.203	27.889
135*	Biotite	L10-304-189.1	foyaite	0.043	8.885	0.009	37.013	9.387	0.465	26.903
136*	Biotite	L10-304-189.1	foyaite	0.083	9.578	0.009	37.206	9.979	0.051	25.372

Analysis	Mineral	Sample	Rock Type	Na_2O	K_2O	Ga_2O_3	SiO_2	MgO	TiO_2	FeO
137*	Biotite	L10-304-189.1	foyaite	0.047	7.27	0.013	35.479	9.992	0.236	27.91
138*	Biotite	L10-304-205.4	foyaite	0.054	9.353	0.004	38.897	12.949	0.454	20.885
139*	Biotite	L10-304-205.4	foyaite	0.114	9.441	0.008	38.82	12.629	1.272	21.007
140*	Biotite	L10-304-205.4	foyaite	0.059	9.165	0.023	38.457	12.881	0.343	21.388
141*	Biotite	L10-304-205.4	foyaite	0.173	9.539	0.000	39.188	12.652	1.4	20.528
142*	Biotite	L10-304-205.4	foyaite	0.029	9.608	0.014	39.01	12.412	0.274	21.812
143*	Biotite	L10-304-205.4	foyaite	0.1	9.354	0.011	37.77	12.184	0.272	22.345
144*	Biotite	L10-304-205.4	foyaite	0.161	8.6	0.012	37.746	13.517	0.32	21.371
145*	Biotite	L10-304-205.4	foyaite	0.066	9.687	0.007	38.952	12.626	1.122	20.962
146*	Biotite	21B	LOZ	0.088	9.095	0.015	41.961	20.176	0.274	10.065
147*	Biotite	21B	LOZ	0.05	9.246	0.000	43.049	20.525	0.143	9.171
148*	Biotite	21B	LOZ	0.077	8.977	0.005	43.846	20.783	0.254	9.449
149*	Biotite	21B	LOZ	0.059	9.171	0.006	43.563	20.709	0.216	9.273
150*	Biotite	21B	LOZ	0.07	9.379	0.000	42.522	20.262	0.187	9.411
151*	Biotite	L10-304-225.2	LOZ	0.026	9.901	0.007	40.032	17.59	0.27	14.08
152*	Biotite	L10-304-225.2	LOZ	0.085	9.895	0.003	39.995	16.845	0.000	14.904
153*	Biotite	L10-304-225.2	LOZ	0.125	9.898	0.006	40.599	17.599	0.023	14.087
154*	Biotite	L10-304-225.2	LOZ	0.112	9.721	0.000	40.494	16.608	0.033	15.129
155*	Biotite	L10-304-225.2	LOZ	0.055	10.135	0.021	40.449	18.166	0.387	13.119
156*	Biotite	L10-304-225.2	LOZ	0.057	9.966	0.001	40.733	18.491	0.284	12.672
157*	Biotite	L10-304-236.1	LOZ	0.089	10.135	0.01	39.504	17.457	0.134	13.945
158*	Biotite	L10-304-236.1	LOZ	0.137	9.997	0.008	39.456	17.055	0.024	13.818
159*	Biotite	L10-304-236.1	LOZ	0.049	10.206	0.004	40.31	18.998	0.121	11.849
160*	Biotite	L10-304-236.1	LOZ	0.086	10.108	0.006	39.061	17.327	0.03	13.539
161*	Biotite	L10-304-236.1	LOZ	0.182	9.655	0.001	39.288	15.041	0.012	16.098
162*	Biotite	L10-304-244.9	LOZ	0.042	10.072	0.000	41.916	20.866	0.026	9.216
163*	Biotite	L10-304-244.9	LOZ	0.071	10.089	0.007	42.032	21.105	0.033	9.056
164*	Biotite	L10-304-244.9	LOZ	0.067	10.042	0.000	41.173	20.431	0.015	9.843
165*	Biotite	L10-304-244.9	LOZ	0.065	10.321	0.000	40.685	20.179	0.037	10.134
166*	Biotite	L10-304-244.9	LOZ	0.076	9.952	0.000	39.518	19.673	0.02	10.997
167*	Biotite	L10-304-249.8-2	LOZ	0.027	8.804	0.000	46.443	23.832	0.000	6.25
168*	Biotite	L10-304-249.8-3	LOZ	0.057	9.221	0.003	45.284	23.136	0.015	5.798
169*	Biotite	L10-304-249.8-4	LOZ	0.036	8.848	0.000	46.917	23.884	0.021	5.182
170*	Biotite	L10-304-249.8-5	LOZ	0.05	9.753	0.008	43.668	23.031	0.044	6.472
171*	Biotite	L10-304-249.8-8	LOZ	0.054	8.711	0.000	47.055	23.489	0.036	5.59
172*	Biotite	L10-304-249.8-9	LOZ	0.032	9.181	0.002	45.675	23.793	0.006	5.592
173*	Biotite	L10-304-264-1	LOZ	0.052	10.045	0.024	38.996	14.515	0.031	17.139

Analysis	Mineral	Sample	Rock Type	Na_2O	K_2O	Ga_2O_3	SiO_2	MgO	TiO_2	FeO
174*	Biotite	L10-304-264-3	LOZ	0.046	10.104	0.018	37.982	12.456	0.026	18.509
175*	Biotite	L10-304-264-5	LOZ	0.094	10.173	0.016	39.43	14.571	0.02	16.076
176*	Biotite	L10-304-264-6	LOZ	0.07	9.953	0.021	40.24	15.013	0.034	14.783
177*	Biotite	L10-304-264-8	LOZ	0.063	10.255	0.016	39.37	14.891	0.046	15.992
178*	Biotite	L10-304-264-9	LOZ	0.152	10.428	0.019	41.61	7.009	0.035	12.059
179*	Biotite	L10-304-270.2	LOZ	0.04	9.147	0.012	38.879	14.881	0.138	18.462
180*	Biotite	L10-304-270.2	LOZ	0.018	9.007	0.004	38.777	14.746	0.134	18.859
181*	Biotite	L10-304-270.2	LOZ	0.031	8.486	0.006	39.14	15.592	0.077	19.361
182*	Biotite	L10-304-270.2	LOZ	0.023	8.782	0.002	39.831	15.754	0.094	17.988
183*	Biotite	L10-304-270.2	LOZ	0.062	9.581	0.021	39.431	15.012	0.139	18.677
184*	Biotite	L10-304-270.2	LOZ	0.07	9.058	0.008	39.859	15.623	0.091	18.441
185*	Biotite	L10-304-270.2	LOZ	0.058	9.528	0.012	39.41	15.558	0.08	17.381
186*	Biotite	L10-304-270.2	LOZ	0.09	9.247	0.006	40.38	16.617	0.053	16.411
187*	Biotite	L10-304-275.2	LOZ	0.074	9.749	0.012	39.424	15.777	0.185	17.213
188*	Biotite	L10-304-275.2	LOZ	0.102	9.764	0.014	41.031	16.9	0.104	15.851
189*	Biotite	L10-304-275.2	LOZ	0.095	9.592	0.004	40.95	17.814	0.037	13.715
190*	Biotite	L10-304-275.2	LOZ	0.092	9.714	0.004	41.021	17.347	0.017	14.654
191*	Biotite	L10-304-275.2	LOZ	0.047	9.586	0.012	38.735	14.969	0.381	18.412
192*	Biotite	L10-304-275.2	LOZ	0.052	9.923	0.002	41.275	17.251	0.301	15.355
193*	Biotite	L10-304-275.2	LOZ	0.124	9.357	0.000	40.974	17.342	0.104	14.55
194*	Biotite	L10-304-275.2	LOZ	0.068	9.535	0.007	41.06	16.747	0.374	16.421
195*	Biotite	L10-304:255.2	LOZ	0.085	9.216	0.033	44.681	23.962	0.033	5.365
196*	Biotite	L10-304:255.2	LOZ	0.049	8.918	0.013	45.697	23.94	0.036	5.149
197*	Biotite	L10-304:255.2	LOZ	0.104	9.351	0.002	44.005	23.573	0.055	5.659
198*	Biotite	L10-304:255.2	LOZ	0.041	9.464	0.006	45.127	23.717	0.016	5.997
199*	Biotite	L10-304:255.2	LOZ	0.065	8.903	0.000	45.588	23.414	0.05	5.658
200*	Biotite	L10-304:255.2	LOZ	0.047	9.391	0.01	44.768	23.869	0.039	5.867
201*	Biotite	L10-304:255.2	LOZ	0.039	8.881	0.000	45.695	23.639	0.000	5.776
202*	Biotite	L10-304:255.2	LOZ	0.083	9.759	0.004	43.251	22.962	0.000	6.269
203*	Biotite	L10-304:255.2	LOZ	0.091	9.569	0.004	43.403	23.245	0.008	6.13
204*	Biotite	L10-304:255.2	LOZ	0.096	9.845	0.000	43.213	23.273	0.000	6.118
205*	Biotite	L10-304:255.2	LOZ	0.124	9.228	0.000	44.546	23.572	0.000	5.556
206*	Biotite	L10-304:255.2	LOZ	0.099	8.962	0.012	44.881	23.568	0.019	5.838
207*	Biotite	L10-304:255.2	LOZ	0.035	9.116	0.006	44.868	23.789	0.001	5.299
208*	Biotite	L10-304:257.9	LOZ	0.073	10.026	0.012	43.148	23.705	0.059	5.838
209*	Biotite	L10-304:257.9	LOZ	0.069	10.302	0.014	42.407	23.237	0.033	6.117
210*	Biotite	L10-304:257.9	LOZ	0.06	9.252	0.000	45.866	23.986	0.011	4.725

Analysis	Mineral	Sample	Rock Type	Na_2O	K_2O	Ga_2O_3	SiO_2	MgO	TiO_2	FeO
211*	Biotite	L10-304:257.9	LOZ	0.062	8.839	0.000	47.977	24.602	0.000	4.048
212*	Biotite	L10-304:257.9	LOZ	0.082	9.23	0.008	45.16	23.912	0.09	4.8
213*	Biotite	L10-304:257.9	LOZ	0.072	8.866	0.01	47.862	24.855	0.058	4.277
214*	Biotite	L10-304:257.9	LOZ	0.087	9.556	0.008	44.608	23.863	0.000	5.335
215*	Biotite	L10-304:257.9	LOZ	0.075	9.53	0.007	44.752	24.477	0.018	4.687
216*	Biotite	L10-304:257.9	LOZ	0.138	10.012	0.011	42.877	22.678	0.011	6.203
217*	Biotite	L10-304:257.9	LOZ	0.093	10.237	0.011	41.552	22.446	0.014	6.663
218*	Biotite	L10-304:257.9	LOZ	0.065	9.536	0.000	45.543	24.422	0.008	5.009
219*	Biotite	L10-304:257.9	LOZ	0.076	9.815	0.009	44.478	23.7	0.056	5.67
220*	Biotite	L10-304:257.9	LOZ	0.077	10.32	0.014	41.74	22.255	0.000	6.447
221*	Biotite	L10-304:257.9	LOZ	0.103	9.742	0.022	44.462	23.566	0.02	5.049
222*	Biotite	L10-304:257.9	LOZ	0.077	9.596	0.012	44.897	24.367	0.124	5.242
223*	Biotite	41B	UOZ	0.017	9.458	0.043	40.278	12.978	0.591	20.3
224*	Biotite	41B	UOZ	0.062	8.814	0.038	41.676	14.478	0.508	18.114
225*	Biotite	41B	UOZ	0.019	7.245	0.019	41.908	13.466	0.366	22.526
226*	Biotite	41B	UOZ	0.107	8.947	0.04	41.412	15.495	0.285	17.999
227*	Biotite	41B	UOZ	0.043	9.425	0.047	39.902	13.419	0.484	19.907
228*	Biotite	41B	UOZ	0.075	9.241	0.047	40.495	14.131	0.319	19.936
229*	Biotite	41B	UOZ	0.104	9.437	0.042	38.586	12.058	0.881	21.188
230*	Biotite	41B	UOZ	0.041	9.395	0.042	39.116	12.751	0.386	20.522
231*	Biotite	41B	UOZ	0.032	8.757	0.037	38.834	13.132	0.428	21.808
232*	Biotite	41B	UOZ	0.056	8.635	0.04	39.97	11.825	0.832	23.076
233*	Biotite	41B	UOZ	0.049	9.395	0.045	39.953	12.774	0.721	20.278
234*	Biotite	61B	UOZ	0.061	9.671	0.049	41.149	18.209	0.664	13.451
235*	Biotite	61B	UOZ	0.042	9.77	0.034	41.178	18.436	0.632	13.137
236*	Biotite	61B	UOZ	0.076	9.497	0.049	41.156	17.421	0.651	14.628
237*	Biotite	61B	UOZ	0.093	9.522	0.034	41.315	17.97	0.78	13.909
238*	Biotite	61B	UOZ	0.057	9.744	0.03	41.251	18.124	0.347	13.723
239*	Biotite	61B	UOZ	0.073	9.816	0.04	40.793	18.267	0.499	13.476
240*	Biotite	61B	UOZ	0.069	9.654	0.053	41.023	17.931	0.494	14.229
241*	Biotite	61B	UOZ	0.069	9.634	0.058	41.623	18.242	0.724	13.412
242*	Biotite	61B	UOZ	0.09	9.684	0.024	41.089	18.138	0.707	13.317
243*	Biotite	61B	UOZ	0.046	9.763	0.047	40.585	17.433	1.049	14.137
244*	Biotite	61B	UOZ	0.061	9.598	0.046	40.847	18.479	0.831	12.725
245*	Biotite	61B	UOZ	0.063	9.645	0.031	40.821	17.867	0.611	13.949
246*	Biotite	61B	UOZ	0.073	9.663	0.042	40.886	18.159	0.431	13.268
247*	Biotite	L10-304-111.9	UOZ	0.073	9.83	0.01	37.514	11.062	0.034	23.323

Analysis	Mineral	Sample	Rock Type	Na_2O	K_2O	Ga_2O_3	SiO_2	MgO	TiO_2	FeO
248*	Biotite	L10-304-111.9	UOZ	0.05	9.905	0.002	38.431	12.741	0.141	20.261
249*	Biotite	L10-304-111.9	UOZ	0.055	9.845	0.007	36.497	10.295	0.053	23.549
250*	Biotite	L10-304-111.9	UOZ	0.051	9.768	0.005	37.465	11.425	0.027	22.062
251*	Biotite	L10-304-111.9	UOZ	0.078	9.543	0.009	37.965	11.527	0.014	22.481
252*	Biotite	L10-304-111.9	UOZ	0.149	9.623	0.014	37.093	10.734	0.009	23.487
253*	Biotite	L10-304-111.9	UOZ	0.091	9.767	0.006	37.226	10.964	0.057	23.717
254*	Biotite	L10-304-111.9	UOZ	0.068	9.194	0.017	37.571	12.199	0.268	22.351
255*	Biotite	L10-304-111.9	UOZ	0.055	9.469	0.000	36.775	10.784	0.172	23.801
256*	Biotite	L10-304-111.9	UOZ	0.048	7.479	0.014	36.708	12.092	0.21	24.469
257*	Biotite	L10-304-123	UOZ	0.062	10.069	0.018	38.445	13.953	0.032	19.479
258*	Biotite	L10-304-123	UOZ	0.103	10.002	0.004	38.409	14.213	0.015	19.345
259*	Biotite	L10-304-123	UOZ	0.084	9.906	0.000	38.057	14.002	0.033	18.903
260*	Biotite	L10-304-123	UOZ	0.046	10.046	0.006	38.691	13.427	0.058	20.23
261*	Biotite	L10-304-123	UOZ	0.055	9.975	0.014	38.308	12.053	0.051	21.869
262*	Biotite	L10-304-123	UOZ	0.071	9.868	0.017	37.901	13.714	0.019	19.685
263*	Biotite	L10-304-123	UOZ	0.064	10.114	0.009	38.593	14.357	0.016	18.513
264*	Biotite	L10-304-123	UOZ	0.077	9.979	0.015	38.374	13.503	0.049	20.273
265*	Biotite	L10-304-123	UOZ	0.094	10.006	0.004	38.098	13.37	0.029	20.093
266*	Biotite	L10-304-123	UOZ	0.096	9.96	0.01	37.736	13.082	0.032	20.758
267*	Biotite	L10-304-130	UOZ	0.103	10.081	0.02	37.431	12.834	0.029	20.863
268*	Biotite	L10-304-130	UOZ	0.061	9.827	0.016	38.57	13.272	0.08	20.734
269*	Biotite	L10-304-130	UOZ	0.058	9.13	0.018	37.23	12.194	0.073	22.804
270*	Biotite	L10-304-130	UOZ	0.163	9.89	0.021	37.726	13.301	0.003	19.46
271*	Biotite	L10-304-130	UOZ	0.024	9.648	0.02	38.912	12.27	0.104	22.534
272*	Biotite	L10-304-130	UOZ	0.048	9.459	0.013	38.474	11.852	0.036	22.885
273*	Biotite	L10-304-130	UOZ	0.06	9.953	0.021	37.777	12.819	0.005	20.201
274*	Biotite	L10-304-130	UOZ	0.081	9.84	0.015	37.904	13.292	0.022	19.47
275*	Biotite	L10-304-130	UOZ	0.06	9.756	0.013	38.889	14.591	0.163	18.756
276*	Biotite	L10-304-130	UOZ	0.108	9.952	0.009	38.147	13.979	0.003	18.734
277*	Biotite	L10-304-139.4	UOZ	0.11	8.926	0.014	43.571	18.373	0.000	13.599
278*	Biotite	L10-304-139.4	UOZ	0.053	9.895	0.003	38.463	12.947	0.236	21.179
279*	Biotite	L10-304-139.4	UOZ	0.075	9.711	0.021	39.338	14.999	0.312	18.314
280*	Biotite	L10-304-139.4	UOZ	0.069	9.723	0.013	40.371	15.095	0.256	17.519
281*	Biotite	L10-304-139.4	UOZ	0.021	8.894	0.017	41.132	14.427	0.08	20.061
282*	Biotite	L10-304-139.4	UOZ	0.08	9.569	0.016	40.906	15.624	0.037	17.37
283*	Biotite	L10-304-139.4	UOZ	0.041	9.587	0.005	40.928	15.237	0.109	17.524
284*	Biotite	L10-304-144.7	UOZ	0.049	9.929	0.009	36.901	10.652	0.006	23.381

Analysis	Mineral	Sample	Rock Type	Na_2O	K_2O	Ga_2O_3	SiO_2	MgO	TiO_2	FeO
285*	Biotite	L10-304-144.7	UOZ	0.095	8.335	0.01	35.852	11.013	0.053	25.335
286*	Biotite	L10-304-144.7	UOZ	0.099	9.913	0.012	37.479	12.715	0.037	20.265
287*	Biotite	L10-304-144.7	UOZ	0.097	9.876	0.000	38.807	13.743	0.05	19.179
288*	Biotite	L10-304-144.7	UOZ	0.069	9.929	0.001	36.675	12.211	0.004	20.491
289*	Biotite	L10-304-144.7	UOZ	0.089	9.912	0.000	39.388	13.501	0.004	17.458
290*	Biotite	L10-304-144.7	UOZ	0.05	10.032	0.013	37.948	11.134	0.024	20.156
291*	Biotite	L10-304-144.7	UOZ	0.046	8.906	0.000	37.405	11.985	0.000	23.36
292*	Biotite	L10-304-144.7	UOZ	0.065	9.864	0.023	36.83	11.801	0.047	20.497
293*	Biotite	L10-304-69.3	UOZ	0.07	9.758	0.013	37.023	9.411	0.012	25.85
294*	Biotite	L10-304-69.3	UOZ	0.101	9.736	0.024	37.656	10.081	0.01	24.632
295*	Biotite	L10-304-69.3	UOZ	0.032	9.558	0.015	38.253	10.99	0.079	23.231
296*	Biotite	L10-304-69.3	UOZ	0.025	9.404	0.017	38.797	11.57	0.225	22.865
297*	Biotite	L10-304-69.3	UOZ	0.066	9.53	0.02	36.002	8.938	0.048	25.753
298*	Biotite	L10-304-69.3	UOZ	0.01	9.515	0.02	39.303	11.657	0.23	22.691
299*	Biotite	L10-304-69.3	UOZ	0.151	9.336	0.008	37.495	9.691	0.006	25.109
300*	Biotite	L10-304-69.3	UOZ	0.043	9.694	0.012	38.927	11.906	0.189	22.334
301*	Biotite	L10-304-90.4	UOZ	0.025	8.624	0.026	36.667	10.476	0.442	25.712
302*	Biotite	L10-304-90.4	UOZ	0.029	8.447	0.021	37.338	11.794	0.497	23.876
303*	Biotite	L10-304-90.4	UOZ	0.105	9.863	0.01	38.528	13.182	0.479	20.103
304*	Biotite	L10-304-90.4	UOZ	0.053	10.039	0.019	37.118	11.669	0.22	21.979
305*	Biotite	L10-304-90.4	UOZ	0.092	9.844	0.018	38.124	12.565	0.001	21.153
306*	Biotite	L10-304-90.4	UOZ	0.09	9.894	0.023	38.056	12.681	0.005	20.873
307*	Biotite	L10-304-90.4	UOZ	0.118	8.991	0.019	36.591	12.513	0.027	22.15
308*	Biotite	L10-304-98	UOZ	0.115	9.849	0.017	36.839	10.948	0.04	22.152
309*	Biotite	L10-304-98	UOZ	0.047	9.89	0.022	36.84	11.038	0.024	21.45
310*	Biotite	L10-304-98	UOZ	0.073	9.907	0.018	37.636	12.663	0.058	20.236
311*	Biotite	L10-304-98	UOZ	0.102	9.922	0.017	36.299	10.887	0.072	22.524
312*	Biotite	L10-304-98	UOZ	0.055	9.494	0.007	36.021	9.721	0.096	24.223
313*	Biotite	L10-304-98	UOZ	0.115	9.473	0.03	36.757	10.865	0.136	23.591
314*	Biotite	L10-304-98	UOZ	0.083	9.828	0.007	38.181	12.736	0.081	19.896

Analysis	Mineral	Sample	Rock Type	Al_2O_3	CaO	MnO	Cl	F	$H_2O^{\dagger}$	Total‡
1*	Biotite	71B	aegirine syenite	10.795	0.014	0.375	0.129	0.28	3.89	98.49
2*	Biotite	71B	aegirine syenite	11.282	0.028	0.346	0.101	1.171	3.53	100.60
3*	Biotite	71B	aegirine syenite	11.415	0.038	0.363	0.048	1.002	3.61	100.11
4*	Biotite	71B	aegirine syenite	11.359	0.036	0.338	0.098	0.642	3.72	98.77
5*	Biotite	71B	aegirine syenite	10.469	0.026	0.337	0.108	0.749	3.68	98.69

Analysis	Mineral	Sample	Rock Type	Al_2O_3	CaO	MnO	Cl	F	$H_2O^{\dagger}$	Total‡
6*	Biotite	71B	aegirine syenite	10.625	0.032	0.344	0.111	0.851	3.69	99.85
7*	Biotite	71B	aegirine syenite	10.13	0.033	0.368	0.26	0.257	3.88	98.78
8*	Biotite	71B	aegirine syenite	11.079	0.044	0.369	0.128	0.867	3.61	99.00
9*	Biotite	71B	aegirine syenite	10.238	0.035	0.337	0.334	0.562	3.72	98.74
10*	Biotite	81B	aegirine syenite	11.577	0.026	0.215	0.236	1.027	3.50	99.99
11*	Biotite	81B	aegirine syenite	11.647	0.043	0.258	0.258	1.267	3.38	100.56
12*	Biotite	81B	aegirine syenite	9.603	0.04	0.237	0.249	0.94	3.62	100.48
13*	Biotite	81B	aegirine syenite	11.707	0.057	0.304	0.519	0.889	3.40	99.22
14*	Biotite	81B	aegirine syenite	11.089	0.04	0.268	0.398	0.957	3.42	99.39
15*	Biotite	81B	aegirine syenite	9.647	0.363	0.239	0.211	0.607	3.74	98.77
16*	Biotite	81B	aegirine syenite	11.375	0.062	0.205	0.18	1.157	3.46	99.69
17*	Biotite	81B	aegirine syenite	10.504	0.017	0.184	0.079	0.928	3.62	99.42
18*	Biotite	81B	aegirine syenite	11.452	0.042	0.254	0.078	0.791	3.66	99.43
19*	Biotite	81B	aegirine syenite	11.608	0.072	0.259	0.325	1.14	3.33	98.88
20	Biotite	L07-53-40.3	aegirine syenite	11.621	0.023	0.038	0.097	1.794	2.96	99.65
21	Biotite	L07-53-40.3	aegirine syenite	12.689	0.008	0.128	0.052	1.356	3.07	98.03
22	Biotite	L07-53-40.3	aegirine syenite	11.738	0.012	0.078	0.173	0.699	3.41	98.87
23	Biotite	L07-53-40.3	aegirine syenite	11.451	0.012	0.029	0.092	2.069	2.83	99.37
24	Biotite	L07-53-40.3	aegirine syenite	12.594	0.035	0.056	0.087	1.758	2.91	98.15
25	Biotite	L07-53-40.3	aegirine syenite	11.674	0.024	0.208	0.076	2.02	2.83	99.03
26	Biotite	L07-53-40.3	aegirine syenite	11.603	0.011	0.115	0.164	2.064	2.82	99.99
27	Biotite	L07-53-40.3	aegirine syenite	12.278	0.009	0.073	0.121	2.404	2.83	100.57
28	Biotite	L07-53-40.3	aegirine syenite	12.396	0.007	0.027	0.125	2.294	2.85	99.83
29	Biotite	L07-53-40.3	aegirine syenite	12.157	0.054	0.031	0.114	2.511	2.78	100.51
30	Biotite	L07-53-40.3	aegirine syenite	12.641	0.024	0.031	0.218	2.256	2.81	99.74
31	Biotite	L07-55-100.1	aegirine syenite	12.158	0.021	0.13	0.223	1.174	3.31	98.27
32	Biotite	L07-55-100.1	aegirine syenite	12.714	0.015	0.085	0.273	1.461	3.16	99.06
33	Biotite	L07-55-100.1	aegirine syenite	12.773	0.008	0.018	0.182	1.572	3.14	99.45
34	Biotite	L07-55-100.1	aegirine syenite	12.09	0.006	0.067	0.15	1.712	3.08	99.65
35	Biotite	L07-55-100.1	aegirine syenite	12.495	0.000	0.135	0.201	1.256	3.31	99.88
36	Biotite	L07-55-100.1	aegirine syenite	11.201	0.000	0.115	0.181	0.917	3.54	100.07
37	Biotite	L07-55-100.1	aegirine syenite	12.375	0.011	0.085	0.203	1.376	3.26	100.31
38	Biotite	L07-55-100.1	aegirine syenite	10.677	0.000	0.093	0.208	1.471	3.21	100.07
39*	Biotite	L07-55-86-8	aegirine syenite	16.53	0.004	0.143	0.094	2.131	2.94	100.22
40*	Biotite	L07-55-86-8	aegirine syenite	16.44	0.021	0.12	0.107	2.174	2.89	99.75
41*	Biotite	L07-63-86-1	aegirine syenite	11.626	0.001	0.13	0.325	0.588	3.48	98.92
42*	Biotite	L07-63-86-1	aegirine syenite	13.981	0.022	0.045	0.094	0.61	3.45	98.16

Analysis	Mineral	Sample	Rock Type	Al_2O_3	CaO	MnO	Cl	F	$H_2O^{\dagger}$	Total‡
43*	Biotite	L07-63-86-1	aegirine syenite	11.389	0.000	0.084	0.291	0.665	3.44	98.94
44*	Biotite	L07-63-86-1	aegirine syenite	12.27	0.012	0.057	0.282	0.687	3.41	98.94
45*	Biotite	L07-63-86-1	aegirine syenite	12.542	0.008	0.029	0.248	0.875	3.31	98.72
46*	Biotite	L07-63-86-1	aegirine syenite	11.51	0.011	0.055	0.239	0.73	3.44	99.08
47*	Biotite	L07-63-86-1	aegirine syenite	12.753	0.034	0.04	0.26	0.761	3.36	98.86
48*	Biotite	L07-63-86-1	aegirine syenite	12.245	0.02	0.051	0.378	0.746	3.39	99.91
49*	Biotite	L07-63-86-1	aegirine syenite	12.943	0.009	0.047	0.211	0.734	3.43	99.72
50*	Biotite	L07-63-86-1	aegirine syenite	13.469	0.004	0.117	0.158	0.542	3.54	99.76
51*	Biotite	L07-63-86-1	aegirine syenite	13.479	0.006	0.145	0.571	0.385	3.46	99.10
52*	Biotite	L08-118-85-6	aegirine syenite	13.418	0.013	0.064	0.18	1.777	3.02	100.14
53*	Biotite	L08-118-85-6	aegirine syenite	12.479	0.003	0.086	0.074	1.988	2.98	99.96
54*	Biotite	L08-118-85-6	aegirine syenite	12.083	0.058	0.119	0.062	2.24	2.84	99.02
55*	Biotite	L10-304-153.1	aegirine syenite	12.237	0.000	0.268	0.34	2.85	2.49	100.61
56*	Biotite	L10-304-153.1	aegirine syenite	12.191	0.000	0.103	0.296	1.866	2.88	100.59
57*	Biotite	L10-304-153.1	aegirine syenite	12.453	0.000	0.094	0.255	1.837	2.90	100.58
58*	Biotite	L10-304-153.1	aegirine syenite	13.299	0.000	0.117	0.199	1.639	3.00	100.62
59*	Biotite	L10-304-153.1	aegirine syenite	12.613	0.000	0.156	0.146	2.198	2.76	99.09
60*	Biotite	L10-304-153.1	aegirine syenite	12.463	0.000	0.255	0.108	2.839	2.55	100.87
61*	Biotite	L10-304-153.1	aegirine syenite	12.079	0.000	0.099	0.039	2.093	2.83	99.56
62*	Biotite	L10-304-153.1	aegirine syenite	12.52	0.000	0.106	0.197	2.166	2.77	100.21
63*	Biotite	L10-304-153.1	aegirine syenite	12.115	0.000	0.242	0.405	2.866	2.46	100.66
64*	Biotite	L10-304-153.1	aegirine syenite	12.984	0.000	0.22	0.254	2.265	2.73	99.75
65*	Biotite	L10-304-172.3	aegirine syenite	15.195	0.000	0.28	0.14	2.835	2.62	101.08
66*	Biotite	L10-304-172.3	aegirine syenite	14.406	0.000	0.351	0.173	3.495	2.22	99.56
67*	Biotite	L10-304-172.3	aegirine syenite	13.553	0.000	0.34	0.148	3.76	2.20	100.78
68*	Biotite	L10-304-172.3	aegirine syenite	13.271	0.000	0.353	0.172	3.854	2.12	100.25
69*	Biotite	L10-304-172.3	aegirine syenite	14.17	0.000	0.354	0.193	3.193	2.38	99.76
70*	Biotite	L10-304-172.3	aegirine syenite	15.397	0.000	0.282	0.154	2.23	2.82	99.50
71*	Biotite	L10-304-172.3	aegirine syenite	15.074	0.000	0.317	0.214	2.728	2.55	99.24
72*	Biotite	L10-304-172.3	aegirine syenite	13.37	0.000	0.282	0.115	3.89	2.14	100.46
73*	Biotite	L10-304-172.3	aegirine syenite	14.213	0.000	0.322	0.159	3.442	2.30	100.49
74*	Biotite	L10-304-180.6	aegirine syenite	13.091	0.000	0.078	0.228	1.086	3.31	100.30
75*	Biotite	L10-304-180.6	aegirine syenite	14.546	0.000	0.14	0.195	0.89	3.39	99.80
76*	Biotite	L10-304-180.6	aegirine syenite	11.484	0.000	0.056	0.056	1.381	3.24	99.14
77*	Biotite	L10-304-180.6	aegirine syenite	12.644	0.000	0.16	0.323	1.241	3.27	99.99
78*	Biotite	L10-304-180.6	aegirine syenite	12.969	0.000	0.05	0.184	1.199	3.25	99.75
79*	Biotite	L10-304-180.6	aegirine syenite	13.66	0.000	0.067	0.156	0.908	3.37	99.60

Analysis	Mineral	Sample	Rock Type	Al_2O_3	CaO	MnO	Cl	F	$H_2O^{\dagger}$	Total‡
80*	Biotite	L10-304-180.6	aegirine syenite	13.819	0.000	0.054	0.173	0.917	3.40	100.46
81*	Biotite	L07.58.48	albitite	12.348	0.018	0.148	0.165	1.554	3.17	99.77
82*	Biotite	L07.58.48	albitite	12.014	0.019	0.138	0.167	1.744	3.06	99.11
83	Biotite	L10-232A 51.25	albitite	11.537	0.025	0.236	0.234	3.104	2.34	100.99
84	Biotite	L10-232A 51.25	albitite	12.728	0.035	0.226	0.222	2.795	2.46	100.14
85	Biotite	L10-232A 51.25	albitite	12.1	0.058	0.217	0.215	2.778	2.48	100.10
86	Biotite	L10-232A 51.25	albitite	14.128	0.006	0.202	0.217	2.091	2.75	100.39
87	Biotite	L10-232A 51.25	albitite	14.52	0.025	0.12	0.134	1.562	2.96	98.42
88	Biotite	L10-232A 51.25	albitite	12.157	0.016	0.227	0.198	2.907	2.48	102.05
89	Biotite	L10-232A-103.6	albitite	12.237	0.034	0.371	0.284	1.687	2.88	100.00
90	Biotite	L10-232A-103.6	albitite	11.958	0.061	0.29	0.267	1.589	2.89	98.56
91	Biotite	L10-232A-103.6	albitite	13.411	0.201	0.329	0.414	1.416	2.99	100.00
92	Biotite	L10-232A-103.6	albitite	12.631	0.172	0.317	0.326	1.807	2.85	100.35
93	Biotite	L10-232A-103.6	albitite	13.139	0.167	0.306	0.416	1.459	2.98	100.54
94	Biotite	L10-232A-103.6	albitite	12.528	0.123	0.347	0.273	1.956	2.82	101.23
95	Biotite	L10-232A-103.6	albitite	13.203	0.185	0.312	0.5	1.297	2.95	98.45
96	Biotite	L10-232A-103.6	albitite	12.117	0.355	0.348	0.311	1.724	2.81	98.50
97	Biotite	L10-232A-103.6	albitite	12.783	0.387	0.35	0.306	1.632	2.97	100.40
98	Biotite	L10-232A-103.6	albitite	12.558	0.257	0.354	0.338	1.499	2.97	100.04
99	Biotite	L10-232A-103.6	albitite	12.494	0.311	0.344	0.337	1.737	2.85	99.41
100	Biotite	L10-232A-103.6	albitite	12.883	0.027	0.313	0.088	1.674	2.97	100.77
101	Biotite	L10-232A-103.6	albitite	12.558	0.024	0.388	0.363	1.72	2.87	101.02
102	Biotite	L10-232A-103.6	albitite	12.82	0.02	0.309	0.298	1.444	2.94	99.17
103	Biotite	L10-232A-103.6	albitite	14.375	0.023	0.278	0.368	0.854	3.19	99.44
104	Biotite	L10-232A-103.6	albitite	11.835	0.312	0.351	0.236	1.789	2.83	99.07
105	Biotite	L10-232A-103.6	albitite	12.257	0.21	0.319	0.329	1.696	2.85	98.84
106	Biotite	L10-232A-103.6	albitite	13.463	0.091	0.235	0.337	1.233	3.06	99.47
107	Biotite	L10-232A-103.6	albitite	13.978	0.061	0.232	0.288	1.064	3.10	98.42
108	Biotite	L10-232A-103.6	albitite	12.733	0.275	0.336	0.319	1.277	3.08	99.23
109	Biotite	L10-232A-103.6	albitite	12.867	0.473	0.316	0.495	1.433	2.90	98.22
110	Biotite	L10-232A-103.6	albitite	13.399	0.202	0.254	0.389	1.169	3.14	101.04
111	Biotite	L10-232A-103.6	albitite	12.55	0.161	0.369	0.369	1.67	2.88	100.16
112	Biotite	L10-232A-103.6	albitite	12.641	0.013	0.333	0.266	1.672	2.93	101.06
113	Biotite	L10-232A-103.6	albitite	12.495	0.049	0.358	0.307	1.687	2.89	100.43
114	Biotite	L10-232A-103.6	albitite	12.38	0.03	0.376	0.362	1.935	2.80	101.33
115	Biotite	L10-232A-103.6	albitite	12.882	0.133	0.379	0.173	1.644	2.97	100.70
116	Biotite	L10-232A-103.6	albitite	13.355	0.289	0.369	0.101	1.571	3.02	100.53

Analysis	Mineral	Sample	Rock Type	Al_2O_3	CaO	MnO	Cl	F	$H_2O^{\dagger}$	Total‡
117	Biotite	L10-232A-103.6	albitite	13.57	0.423	0.365	0.116	1.494	3.08	100.84
118	Biotite	L10-232A-103.6	albitite	13.322	0.007	0.391	0.205	1.461	3.06	101.73
119	Biotite	L10-232A-103.6	albitite	12.096	0.018	0.388	0.326	2.008	2.77	101.41
120*	Biotite	L10-304-74	albitite	13.37	0.000	0.191	0.327	1.721	2.92	100.42
121*	Biotite	L10-304-74	albitite	12.965	0.000	0.251	0.141	2.328	2.69	99.49
122*	Biotite	L10-304-74	albitite	14.349	0.000	0.16	0.363	1.552	2.96	99.53
123*	Biotite	L10-304-74	albitite	14.317	0.000	0.252	0.316	1.563	3.01	100.64
124*	Biotite	L10-304-74	albitite	14.522	0.000	0.255	0.414	1.558	2.98	100.75
125*	Biotite	L10-304-74	albitite	13.232	0.000	0.086	0.25	1.798	2.92	100.26
126*	Biotite	L10-304-74	albitite	14.146	0.000	0.102	0.315	1.343	3.08	100.23
127*	Biotite	L10-304-74	albitite	12.901	0.000	0.101	0.21	2.026	2.84	100.62
128*	Biotite	L10-304-74	albitite	14.34	0.000	0.178	0.307	1.317	3.11	100.24
129*	Biotite	L10-304-189.1	foyaite	12.327	0.000	0.194	0.054	2.075	2.85	100.14
130*	Biotite	L10-304-189.1	foyaite	12.997	0.000	0.096	0.208	1.715	2.92	100.10
131*	Biotite	L10-304-189.1	foyaite	13.429	0.000	0.088	0.265	1.424	3.01	99.13
132*	Biotite	L10-304-189.1	foyaite	12.709	0.000	0.079	0.296	1.528	2.94	98.64
133*	Biotite	L10-304-189.1	foyaite	12.811	0.000	0.038	0.155	1.576	2.96	98.58
134*	Biotite	L10-304-189.1	foyaite	13.474	0.000	0.041	0.212	1.299	3.07	98.69
135*	Biotite	L10-304-189.1	foyaite	12.354	0.000	0.058	0.209	1.611	2.97	99.87
136*	Biotite	L10-304-189.1	foyaite	12.732	0.000	0.143	0.418	1.732	2.87	100.14
137*	Biotite	L10-304-189.1	foyaite	12.815	0.000	0.044	0.125	1.515	2.98	98.39
138*	Biotite	L10-304-205.4	foyaite	12.326	0.000	0.094	0.065	1.757	3.05	99.85
139*	Biotite	L10-304-205.4	foyaite	12.091	0.000	0.043	0.156	1.852	2.99	100.38
140*	Biotite	L10-304-205.4	foyaite	12.61	0.000	0.13	0.278	1.574	3.08	99.95
141*	Biotite	L10-304-205.4	foyaite	11.908	0.000	0.049	0.141	2.009	2.93	100.47
142*	Biotite	L10-304-205.4	foyaite	11.943	0.000	0.055	0.258	1.942	2.90	100.21
143*	Biotite	L10-304-205.4	foyaite	12.807	0.000	0.054	0.199	1.786	2.96	99.80
144*	Biotite	L10-304-205.4	foyaite	12.325	0.000	0.041	0.092	1.904	2.93	98.98
145*	Biotite	L10-304-205.4	foyaite	11.747	0.000	0.058	0.214	1.866	2.96	100.22
146*	Biotite	21B	LOZ	11.73	0.024	0.333	0.016	2.004	3.13	98.87
147*	Biotite	21B	LOZ	11.245	0.021	0.319	0.019	2.299	3.01	99.05
148*	Biotite	21B	LOZ	10.946	0.021	0.313	0.016	2.1	3.16	99.90
149*	Biotite	21B	LOZ	11.073	0.031	0.304	0.017	2.139	3.12	99.64
150*	Biotite	21B	LOZ	11.279	0.03	0.299	0.015	1.776	3.24	98.43
151*	Biotite	L10-304-225.2	LOZ	12.03	0.000	0.328	0.214	3.447	2.30	100.15
152*	Biotite	L10-304-225.2	LOZ	11.824	0.000	0.4	0.494	3.175	2.33	99.88
153*	Biotite	L10-304-225.2	LOZ	12.184	0.000	0.401	0.367	3.382	2.33	100.92

Analysis	Mineral	Sample	Rock Type	Al_2O_3	CaO	MnO	Cl	F	$H_2O^{\dagger}$	Total‡
154*	Biotite	L10-304-225.2	LOZ	12.459	0.000	0.427	0.346	2.946	2.53	100.74
155*	Biotite	L10-304-225.2	LOZ	11.972	0.000	0.299	0.15	3.551	2.30	100.52
156*	Biotite	L10-304-225.2	LOZ	11.676	0.000	0.322	0.123	3.496	2.33	100.07
157*	Biotite	L10-304-236.1	LOZ	12.19	0.000	0.621	0.458	3.531	2.18	100.17
158*	Biotite	L10-304-236.1	LOZ	12.506	0.000	0.648	0.398	3.532	2.18	99.68
159*	Biotite	L10-304-236.1	LOZ	11.578	0.000	0.521	0.185	4.054	2.03	99.81
160*	Biotite	L10-304-236.1	LOZ	11.848	0.000	0.629	0.384	3.39	2.21	98.54
161*	Biotite	L10-304-236.1	LOZ	12.304	0.000	0.704	0.521	2.967	2.37	99.07
162*	Biotite	L10-304-244.9	LOZ	11.344	0.000	0.69	0.037	3.977	2.19	100.29
163*	Biotite	L10-304-244.9	LOZ	11.227	0.000	0.693	0.032	3.904	2.24	100.40
164*	Biotite	L10-304-244.9	LOZ	11.23	0.000	0.599	0.035	3.586	2.33	99.27
165*	Biotite	L10-304-244.9	LOZ	11.859	0.000	0.783	0.083	3.674	2.28	100.02
166*	Biotite	L10-304-244.9	LOZ	12.132	0.000	0.768	0.064	3.44	2.34	98.90
167*	Biotite	L10-304-249.8-2	LOZ	8.671	0.000	0.802	0.016	2.658	2.97	100.42
168*	Biotite	L10-304-249.8-3	LOZ	9.719	0.000	1.065	0.018	2.348	3.09	99.70
169*	Biotite	L10-304-249.8-4	LOZ	8.69	0.000	0.978	0.011	2.699	2.97	100.17
170*	Biotite	L10-304-249.8-5	LOZ	10.353	0.000	0.497	0.019	1.902	3.24	99.00
171*	Biotite	L10-304-249.8-8	LOZ	8.739	0.000	0.684	0.018	2.623	2.99	99.94
172*	Biotite	L10-304-249.8-9	LOZ	9.308	0.000	0.98	0.01	2.713	2.93	100.17
173*	Biotite	L10-304-264-1	LOZ	14.47	0.000	0.225	0.1	2.712	2.68	100.93
174*	Biotite	L10-304-264-3	LOZ	15.647	0.000	0.255	0.138	1.88	3.01	100.03
175*	Biotite	L10-304-264-5	LOZ	14.448	0.000	0.326	0.122	3.145	2.47	100.82
176*	Biotite	L10-304-264-6	LOZ	14.207	0.000	0.206	0.063	3.12	2.51	100.15
177*	Biotite	L10-304-264-8	LOZ	14.306	0.000	0.251	0.088	2.935	2.58	100.73
178*	Biotite	L10-304-264-9	LOZ	24.758	0.000	0.115	0.038	1.265	3.60	101.06
179*	Biotite	L10-304-270.2	LOZ	12.068	0.000	0.037	0.076	1.989	2.93	98.62
180*	Biotite	L10-304-270.2	LOZ	11.825	0.000	0.032	0.17	1.667	3.04	98.24
181*	Biotite	L10-304-270.2	LOZ	12.143	0.000	0.074	0.13	1.704	3.11	99.81
182*	Biotite	L10-304-270.2	LOZ	11.646	0.000	0.094	0.103	1.681	3.12	99.08
183*	Biotite	L10-304-270.2	LOZ	12.42	0.000	0.074	0.109	1.882	3.04	100.41
184*	Biotite	L10-304-270.2	LOZ	11.864	0.000	0.083	0.165	1.766	3.09	100.07
185*	Biotite	L10-304-270.2	LOZ	11.765	0.000	0.115	0.159	1.987	2.94	98.94
186*	Biotite	L10-304-270.2	LOZ	11.98	0.000	0.144	0.172	2.013	3.00	100.07
187*	Biotite	L10-304-275.2	LOZ	11.864	0.000	0.099	0.179	2.816	2.56	99.88
188*	Biotite	L10-304-275.2	LOZ	11.344	0.000	0.119	0.176	2.875	2.60	100.82
189*	Biotite	L10-304-275.2	LOZ	11.584	0.000	0.248	0.194	2.816	2.62	99.61
190*	Biotite	L10-304-275.2	LOZ	11.592	0.000	0.212	0.195	3.019	2.53	100.33

Analysis	Mineral	Sample	Rock Type	Al_2O_3	CaO	MnO	Cl	F	$H_2O^{\dagger}$	Total‡
191*	Biotite	L10-304-275.2	LOZ	12.078	0.000	0.073	0.07	2.677	2.62	99.60
192*	Biotite	L10-304-275.2	LOZ	11.121	0.000	0.039	0.149	3.26	2.44	101.10
193*	Biotite	L10-304-275.2	LOZ	11.01	0.000	0.276	0.178	2.545	2.73	99.13
194*	Biotite	L10-304-275.2	LOZ	10.899	0.000	0.055	0.136	2.929	2.58	100.75
195*	Biotite	L10-304:255.2	LOZ	9.55	0.000	0.95	0.012	2.476	3.01	99.32
196*	Biotite	L10-304:255.2	LOZ	8.791	0.000	0.966	0.018	2.852	2.83	99.20
197*	Biotite	L10-304:255.2	LOZ	9.66	0.000	0.956	0.028	2.819	2.80	98.95
198*	Biotite	L10-304:255.2	LOZ	9.706	0.000	0.732	0.016	2.725	2.92	100.41
199*	Biotite	L10-304:255.2	LOZ	8.45	0.000	0.956	0.023	2.656	2.89	98.60
200*	Biotite	L10-304:255.2	LOZ	9.638	0.000	0.962	0.027	2.817	2.86	100.23
201*	Biotite	L10-304:255.2	LOZ	8.837	0.000	0.83	0.016	3.011	2.76	99.41
202*	Biotite	L10-304:255.2	LOZ	10.211	0.000	1.118	0.02	2.424	2.98	99.02
203*	Biotite	L10-304:255.2	LOZ	10.052	0.000	1.035	0.012	2.671	2.86	99.03
204*	Biotite	L10-304:255.2	LOZ	10.474	0.000	1.18	0.022	2.864	2.79	99.81
205*	Biotite	L10-304:255.2	LOZ	9.429	0.000	0.951	0.056	2.84	2.80	99.04
206*	Biotite	L10-304:255.2	LOZ	9.124	0.000	0.711	0.02	2.627	2.91	98.71
207*	Biotite	L10-304:255.2	LOZ	9.094	0.000	0.957	0.012	2.471	2.98	98.58
208*	Biotite	L10-304:257.9	LOZ	10.352	0.000	0.635	0.065	3.594	2.42	99.85
209*	Biotite	L10-304:257.9	LOZ	11.271	0.000	0.797	0.135	3.599	2.40	100.30
210*	Biotite	L10-304:257.9	LOZ	8.457	0.000	0.448	0.018	3.883	2.32	98.94
211*	Biotite	L10-304:257.9	LOZ	7.858	0.000	0.46	0.013	4.381	2.17	100.32
212*	Biotite	L10-304:257.9	LOZ	9.1	0.000	0.665	0.018	3.606	2.45	99.04
213*	Biotite	L10-304:257.9	LOZ	8.172	0.000	0.532	0.016	3.865	2.45	100.95
214*	Biotite	L10-304:257.9	LOZ	9.628	0.000	0.699	0.017	3.601	2.46	99.79
215*	Biotite	L10-304:257.9	LOZ	9.343	0.000	0.665	0.018	3.902	2.32	99.71
216*	Biotite	L10-304:257.9	LOZ	10.99	0.000	0.806	0.05	3.364	2.52	99.59
217*	Biotite	L10-304:257.9	LOZ	11.531	0.000	0.83	0.112	3.205	2.54	99.16
218*	Biotite	L10-304:257.9	LOZ	9.491	0.000	0.596	0.022	3.956	2.35	100.91
219*	Biotite	L10-304:257.9	LOZ	9.988	0.000	0.563	0.049	3.731	2.41	100.46
220*	Biotite	L10-304:257.9	LOZ	11.76	0.000	0.816	0.081	3.106	2.61	99.15
221*	Biotite	L10-304:257.9	LOZ	10.089	0.000	0.662	0.039	3.975	2.28	99.92
222*	Biotite	L10-304:257.9	LOZ	9.451	0.000	0.664	0.021	3.743	2.43	100.54
223*	Biotite	41B	UOZ	12.056	0.003	0.025	0.029	1.371	3.30	100.42
224*	Biotite	41B	UOZ	10.232	0.025	0.007	0.038	1.595	3.18	98.73
225*	Biotite	41B	UOZ	9.077	0.049	0.031	0.038	1.213	3.34	99.27
226*	Biotite	41B	UOZ	10.985	0.074	0.117	0.279	1.444	3.25	100.40
227*	Biotite	41B	UOZ	11.644	0.016	0.027	0.076	1.505	3.19	99.65

Analysis	Mineral	Sample	Rock Type	Al_2O_3	CaO	MnO	Cl	F	$H_2O^{\dagger}$	Total‡
228*	Biotite	41B	UOZ	11.487	0.029	0.126	0.221	0.541	3.66	100.29
229*	Biotite	41B	UOZ	12.452	0.07	0.015	0.026	1.152	3.33	99.32
230*	Biotite	41B	UOZ	12.356	0.03	0.025	0.029	1.348	3.25	99.26
231*	Biotite	41B	UOZ	12.163	0	0.028	0.229	1.191	3.28	99.89
232*	Biotite	41B	UOZ	11.412	0.015	0.02	0.135	0.873	3.47	100.34
233*	Biotite	41B	UOZ	11.503	0.019	0.014	0.161	1.196	3.30	99.38
234*	Biotite	61B	UOZ	11.07	0.025	0.232	0.05	1.155	3.47	99.23
235*	Biotite	61B	UOZ	11.278	0.027	0.276	0.047	1.038	3.54	99.41
236*	Biotite	61B	UOZ	11.284	0.031	0.228	0.076	1.1	3.49	99.66
237*	Biotite	61B	UOZ	11.131	0.034	0.2	0.033	1.277	3.43	99.70
238*	Biotite	61B	UOZ	11.427	0.034	0.271	0.099	1.249	3.43	99.75
239*	Biotite	61B	UOZ	11.37	0.026	0.244	0.051	1.307	3.39	99.32
240*	Biotite	61B	UOZ	11.279	0.013	0.206	0.113	1.377	3.35	99.76
241*	Biotite	61B	UOZ	11.507	0.03	0.264	0.043	1.233	3.48	100.30
242*	Biotite	61B	UOZ	11.172	0.033	0.244	0.059	1.173	3.46	99.16
243*	Biotite	61B	UOZ	11.287	0.041	0.238	0.061	1.192	3.43	99.28
244*	Biotite	61B	UOZ	11.009	0.028	0.222	0.043	1.296	3.38	98.54
245*	Biotite	61B	UOZ	11.218	0.028	0.233	0.069	1.117	3.47	99.09
246*	Biotite	61B	UOZ	11.12	0.021	0.252	0.059	1.269	3.38	98.60
247*	Biotite	L10-304-111.9	UOZ	13.388	0.000	0.287	0.55	1.464	3.02	100.52
248*	Biotite	L10-304-111.9	UOZ	12.724	0.000	0.235	0.176	2.331	2.72	99.67
249*	Biotite	L10-304-111.9	UOZ	13.67	0.000	0.287	0.497	1.508	2.95	99.17
250*	Biotite	L10-304-111.9	UOZ	13.406	0.000	0.257	0.41	1.965	2.80	99.59
251*	Biotite	L10-304-111.9	UOZ	13.244	0.000	0.273	0.473	2.165	2.72	100.44
252*	Biotite	L10-304-111.9	UOZ	13.561	0.000	0.31	0.478	1.886	2.81	100.11
253*	Biotite	L10-304-111.9	UOZ	13.705	0.000	0.275	0.394	1.615	2.99	100.77
254*	Biotite	L10-304-111.9	UOZ	12.529	0.000	0.224	0.202	2.102	2.79	99.47
255*	Biotite	L10-304-111.9	UOZ	14.137	0.000	0.269	0.325	1.65	2.98	100.38
256*	Biotite	L10-304-111.9	UOZ	13.597	0.000	0.273	0.059	1.952	2.91	99.77
257*	Biotite	L10-304-123	UOZ	12.826	0.000	0.247	0.509	2.647	2.53	100.75
258*	Biotite	L10-304-123	UOZ	13.442	0.000	0.282	0.285	2.259	2.80	101.11
259*	Biotite	L10-304-123	UOZ	12.743	0.000	0.261	0.489	2.407	2.61	99.44
260*	Biotite	L10-304-123	UOZ	12.827	0.000	0.146	0.211	2.612	2.62	100.87
261*	Biotite	L10-304-123	UOZ	12.804	0.000	0.167	0.485	2.133	2.74	100.60
262*	Biotite	L10-304-123	UOZ	13.426	0.000	0.252	0.387	2.354	2.69	100.33
263*	Biotite	L10-304-123	UOZ	13.304	0.000	0.255	0.288	2.745	2.56	100.76
264*	Biotite	L10-304-123	UOZ	12.806	0.000	0.204	0.5	2.421	2.63	100.77

Analysis	Mineral	Sample	Rock Type	Al_2O_3	CaO	MnO	Cl	F	$H_2O^{\dagger}$	Total‡
265*	Biotite	L10-304-123	UOZ	12.978	0.000	0.214	0.425	2.225	2.72	100.21
266*	Biotite	L10-304-123	UOZ	13.609	0.000	0.265	0.594	2.07	2.77	100.93
267*	Biotite	L10-304-130	UOZ	13.729	0.000	0.276	0.516	2.491	2.57	100.89
268*	Biotite	L10-304-130	UOZ	12.414	0.000	0.209	0.373	2.617	2.56	100.67
269*	Biotite	L10-304-130	UOZ	12.955	0.000	0.187	0.37	2.059	2.77	99.80
270*	Biotite	L10-304-130	UOZ	13.697	0.000	0.293	0.262	2.885	2.45	100.09
271*	Biotite	L10-304-130	UOZ	11.829	0.000	0.147	0.017	2.28	2.80	100.53
272*	Biotite	L10-304-130	UOZ	11.921	0.000	0.191	0.015	2.207	2.80	99.85
273*	Biotite	L10-304-130	UOZ	13.927	0.000	0.272	0.536	2.703	2.48	100.69
274*	Biotite	L10-304-130	UOZ	13.318	0.000	0.29	0.443	2.928	2.37	99.91
275*	Biotite	L10-304-130	UOZ	12.44	0.000	0.214	0.074	3.414	2.29	100.58
276*	Biotite	L10-304-130	UOZ	13.254	0.000	0.302	0.275	3.078	2.37	100.14
277*	Biotite	L10-304-139.4	UOZ	9.318	0.000	0.207	0.081	4.352	1.96	100.42
278*	Biotite	L10-304-139.4	UOZ	12.413	0.000	0.16	0.111	2.829	2.52	100.75
279*	Biotite	L10-304-139.4	UOZ	11.663	0.000	0.209	0.083	3.035	2.46	100.16
280*	Biotite	L10-304-139.4	UOZ	11.632	0.000	0.219	0.159	3.539	2.24	100.76
281*	Biotite	L10-304-139.4	UOZ	10.312	0.000	0.106	0.041	3.121	2.45	100.60
282*	Biotite	L10-304-139.4	UOZ	10.621	0.000	0.177	0.163	3.161	2.41	100.06
283*	Biotite	L10-304-139.4	UOZ	10.767	0.000	0.176	0.124	3.472	2.27	100.16
284*	Biotite	L10-304-144.7	UOZ	14.947	0.000	0.186	0.232	2.015	2.86	101.12
285*	Biotite	L10-304-144.7	UOZ	13.983	0.000	0.141	0.215	1.923	2.84	99.75
286*	Biotite	L10-304-144.7	UOZ	14.262	0.000	0.27	0.204	2.474	2.67	100.34
287*	Biotite	L10-304-144.7	UOZ	12.988	0.000	0.227	0.216	3.176	2.36	100.65
288*	Biotite	L10-304-144.7	UOZ	15.456	0.000	0.273	0.247	2.394	2.69	100.39
289*	Biotite	L10-304-144.7	UOZ	14.209	0.000	0.228	0.147	3.34	2.34	100.54
290*	Biotite	L10-304-144.7	UOZ	15.833	0.000	0.226	0.169	2.077	2.90	100.51
291*	Biotite	L10-304-144.7	UOZ	12.981	0.000	0.085	0.027	2.301	2.74	99.79
292*	Biotite	L10-304-144.7	UOZ	15.606	0.000	0.291	0.196	2.278	2.76	100.21
293*	Biotite	L10-304-69.3	UOZ	13.326	0.000	0.273	0.506	1.549	2.95	100.70
294*	Biotite	L10-304-69.3	UOZ	12.881	0.000	0.266	0.375	2.047	2.76	100.52
295*	Biotite	L10-304-69.3	UOZ	12.383	0.000	0.245	0.232	2.26	2.71	99.93
296*	Biotite	L10-304-69.3	UOZ	12.189	0.000	0.074	0.187	2.499	2.64	100.43
297*	Biotite	L10-304-69.3	UOZ	13.882	0.000	0.25	0.383	1.545	2.93	99.31
298*	Biotite	L10-304-69.3	UOZ	11.936	0.000	0.155	0.159	2.444	2.69	100.75
299*	Biotite	L10-304-69.3	UOZ	13.087	0.000	0.279	0.431	1.915	2.80	100.26
300*	Biotite	L10-304-69.3	UOZ	11.517	0.000	0.06	0.125	2.633	2.57	99.95
301*	Biotite	L10-304-90.4	UOZ	12.57	0.000	0.092	0.194	1.448	3.05	99.30

Analysis	Mineral	Sample	Rock Type	Al_2O_3	CaO	MnO	Cl	F	$H_2O^{\dagger}$	Total‡
302*	Biotite	L10-304-90.4	UOZ	12.392	0.000	0.094	0.097	1.905	2.90	99.35
303*	Biotite	L10-304-90.4	UOZ	13.088	0.000	0.228	0.183	2.309	2.78	100.81
304*	Biotite	L10-304-90.4	UOZ	14.306	0.000	0.279	0.346	1.609	3.03	100.63
305*	Biotite	L10-304-90.4	UOZ	13.531	0.000	0.281	0.363	2.326	2.71	100.95
306*	Biotite	L10-304-90.4	UOZ	13.358	0.000	0.279	0.326	2.662	2.55	100.73
307*	Biotite	L10-304-90.4	UOZ	13.432	0.000	0.263	0.305	2.081	2.76	99.20
308*	Biotite	L10-304-98	UOZ	14.841	0.000	0.274	0.405	1.615	2.99	100.05
309*	Biotite	L10-304-98	UOZ	14.917	0.000	0.27	0.37	1.71	2.94	99.48
310*	Biotite	L10-304-98	UOZ	13.851	0.000	0.254	0.163	2.02	2.88	99.71
311*	Biotite	L10-304-98	UOZ	14.803	0.000	0.295	0.348	1.627	2.98	99.83
312*	Biotite	L10-304-98	UOZ	14.594	0.000	0.223	0.484	1.14	3.13	99.16
313*	Biotite	L10-304-98	UOZ	13.627	0.000	0.214	0.336	1.809	2.88	99.79
314*	Biotite	L10-304-98	UOZ	13.109	0.000	0.259	0.253	2.529	2.60	99.51

*data acquired by Alex Timofeev

†calculated by oxygen normalisation

‡totals include calculated H_2O

Appendix II: Trace element data (ppm)

Analysis	Sample	Mineral	Rock Type	Li^{7}	Be^{9}	B^{10}	Na^{23}	P^{31}	K^{39}	Ca^{42}
1	L10-252 349.1p	Aegirine	aegirine syenite	18.05	1.05	3.84	N/A	0.98	N/A	9515.34
2	L10-252 349.1p	Aegirine	aegirine syenite	15.03	0.502	1.76	N/A	0.29	N/A	8704.54
3	85-L6 294.91p	Aegirine	aegirine-nepheline syenite	6.41	0.379	0.52	N/A	0.92	N/A	16311.53
4	85-L6 294.91p	Aegirine	aegirine-nepheline syenite	12.11	0.5	2.07	N/A	0.94	N/A	6336.89
5	L09-162 203.45p	Aegirine	aegirine-nepheline syenite	15.57	0.179	0.287	N/A	1	N/A	7311.26
6	L09-162 203.45p	Aegirine	aegirine-nepheline syenite	19.71	0.166	0.176	N/A	0.65	N/A	7358.04
7	L09-162 203.45p	Aegirine	aegirine-nepheline syenite	13.83	0.099	0.136	N/A	0.56	N/A	7649.58
8	L09-162 203.45p	Aegirine	aegirine-nepheline syenite	12.78	0.114	0.151	N/A	1.3	N/A	9575.02
9	L09-162 210p	Aegirine	aegirine-nepheline syenite	11.15	0.72	0.48	N/A	0.98	N/A	2493.12
10	L09-192 183.6p	Albite (I)	aegirine nepheline syenite	0.0203	0.573	1.43	N/A	0.69	N/A	2.82
11	L09-192 183.6p	Albite (I)	aegirine nepheline syenite	0.0013	0.294	0.74	N/A	1.23	N/A	40.34
12	L09-192 183.6p	Albite (I)	aegirine nepheline syenite	0.007	0.406	0.57	N/A	1.13	N/A	203.03
13	L09-162 210p	Albite (I)	aegirine-nepheline syenite	0.205	0.65	0.38	N/A	1.33	N/A	13.61
14	L09-162 210p	Albite (I)	aegirine-nepheline syenite	0.0138	0.318	0.18	N/A	1.01	N/A	16.01
15	L09-162 210p	Albite (I)	aegirine-nepheline syenite	0.0059	0.456	0.91	N/A	1.53	N/A	16.12
16	L09-162 210p	Albite (I)	aegirine-nepheline syenite	0	0.347	0.67	N/A	1.33	N/A	20.22
17	L09-162 210p	Albite (I)	aegirine-nepheline syenite	0.0208	0.312	1.84	N/A	1.58	N/A	18.45
18	L09-162 210p	Albite (I)	aegirine-nepheline syenite	0.0069	0.513	0.37	N/A	2.05	N/A	27.39
19	L09-162 210p	Albite (I)	aegirine-nepheline syenite	0.0103	0.41	1.79	N/A	2.18	N/A	19.35
20	L09-162 210p	Albite (I)	aegirine-nepheline syenite	0.065	0.571	0.79	N/A	3.23	N/A	18.98
21	L09-192 154.25p	Albite (I)	lujavrite (altered)	0.0763	0.393	0.41	N/A	1.56	N/A	10.94
22	L09-192 154.25p	Albite (I)	lujavrite (altered)	0.0228	0.481	0.75	N/A	2.47	N/A	9.82
23	L09-192 154.25p	Albite (I)	lujavrite (altered)	0.0298	0.331	0.35	N/A	2.19	N/A	10.7
24	L09-192 154.25p	Albite (I)	lujavrite (altered)	0.0111	0.541	0.44	N/A	0.89	N/A	14.13
25	L09-192 154.25p	Albite (I)	lujavrite (altered)	0.0069	0.415	0	N/A	0.84	N/A	12.77
26	L09-192 154.25p	Albite (I)	lujavrite (altered)	0.0264	0.551	0.57	N/A	1.33	N/A	10.34
27	L09-192 154.25p	Albite (I)	lujavrite (altered)	0.0127	0.44	0.37	N/A	1.12	N/A	4.51
28	L09-192 154.25p	Albite (I)	lujavrite (altered)	0.0061	0.395	0.31	N/A	0.6	N/A	9.15
29	L09-192 154.25p	Albite (I)	lujavrite (altered)	0.0268	0.528	0.55	N/A	1.69	N/A	16.17
30	L09-192 154.25p	Albite (I)	lujavrite (altered)	0.0204	0.515	0.41	N/A	1.2	N/A	12.9
31	L09-192 154.25p	Albite (I)	lujavrite (altered)	0.0215	0.404	0.17	N/A	1.27	N/A	12.74
32	L09-192 154.25p	Albite (I)	lujavrite (altered)	0.0071	0.484	0.38	N/A	0.83	N/A	7.55
33	L09-192 154.25p	Albite (I)	lujavrite (altered)	0.0269	0.681	0.36	N/A	0.99	N/A	14.4
34	L09-192 154.25p	Albite (I)	lujavrite (altered)	0.003	0.54	0.54	N/A	0.96	N/A	16.72

Analysis	Sample	Mineral	Rock Type	Li^{7}	Be^{9}	B^{10}	Na^{23}	P^{31}	K^{39}	Ca^{42}
35	L09-192 154.25p	Albite (I)	lujavrite (altered)	0.0561	0.58	0.45	N/A	1.21	N/A	11.57
36	L09-155 163.1p	Albite (II)	aegirine syenite	0.081	0.562	1.22	N/A	1.6	N/A	24.11
37	L09-155 163.1p	Albite (II)	aegirine syenite	0.0322	0.721	0.54	N/A	1.31	N/A	533.38
38	L09-155 163.1p	Albite (II)	aegirine syenite	0.026	0.8	0.9	N/A	2.39	N/A	13.61
39	L09-155 163.1p	Albite (II)	aegirine syenite	0.518	0.773	0.77	N/A	1.32	N/A	2.37
40	L09-155 163.1p	Albite (II)	aegirine syenite	0.11	0.609	0.48	N/A	1.69	N/A	11.68
41	L09-155 163.1p	Albite (II)	aegirine syenite	255.88	0.61	1.22	N/A	1.44	N/A	89.3
42	L09-155 163.1p	Albite (II)	aegirine syenite	0.0446	0.441	0.05	N/A	0.64	N/A	5.97
43	L09-155 163.1p	Albite (II)	aegirine syenite	0.0436	0.518	0.34	N/A	1.11	N/A	13.9
44	L09-155 163.1p	Albite (II)	aegirine syenite	0.015	0.537	0.22	N/A	1.29	N/A	0
45	L09-155 163.1p	Albite (II)	aegirine syenite	0.0561	0.642	0.26	N/A	0.91	N/A	13.17
46	L09-155 163.1p	Albite (II)	aegirine syenite	0.096	0.442	0.48	N/A	0.96	N/A	12.69
47	L09-192 112.8p	Albite (II)	aegirine syenite	0.0385	0.798	0.5	N/A	1.32	N/A	14.71
48	L09-192 112.8p	Albite (II)	aegirine syenite	0.076	0.417	0.49	N/A	1.38	N/A	4.23
49	L09-192 112.8p	Albite (II)	aegirine syenite	0.031	2.04	1.16	N/A	2.3	N/A	212.28
50	L09-192 112.8p	Albite (II)	aegirine syenite	0.121	1.11	0.67	N/A	0.66	N/A	8.95
51	L09-192 112.8p	Albite (II)	aegirine syenite	0.0233	1.19	1.02	N/A	1.4	N/A	10.18
52	L09-192 112.8p	Albite (II)	aegirine syenite	0.043	1.34	0.48	N/A	1.34	N/A	15.6
53	L09-192 112.8p	Albite (II)	aegirine syenite	0.125	0.431	0.84	N/A	1.36	N/A	7.1
54	L09-192 112.8p	Albite (II)	aegirine syenite	0.263	3.4	1.02	N/A	2.64	N/A	46.44
55	85-L6 294.91p	Albite (II)	aegirine-nepheline syenite	0.0128	0.25	0.42	N/A	0.46	N/A	15.18
56	85-L6 294.91p	Albite (II)	aegirine-nepheline syenite	0.0013	0.36	0.46	N/A	1.28	N/A	86.16
57	85-L6 294.91p	Albite (II)	aegirine-nepheline syenite	0.0017	0.286	0.88	N/A	0.68	N/A	17.24
58	85-L6 294.91p	Albite (II)	aegirine-nepheline syenite	0.009	0.48	1.33	N/A	1.04	N/A	1817.36
59	L09-162 203.45p	Albite (II)	aegirine-nepheline syenite	64.45	0.95	2.27	N/A	2.01	N/A	138.42
60	L09-162 203.45p	Albite (II)	aegirine-nepheline syenite	6.5	1.13	1.01	N/A	2.57	N/A	145.59
61	L08-84 96.77p	Albite (II)	albitite	0.025	0.75	0.73	N/A	3	N/A	1.96
62	L08-84 96.77p	Albite (II)	albitite	0.39	0.443	0.9	N/A	1.79	N/A	22.81
63	L08-84 96.77p	Albite (II)	albitite	0.156	0.251	0.49	N/A	2.07	N/A	33.28
64	L08-84 96.77p	Albite (II)	albitite	0.211	0.411	0.43	N/A	0.9	N/A	31.19
65	L08-84 96.77p	Albite (II)	albitite	0.161	0.165	0.5	N/A	0.6	N/A	15.36
66	L08-84 96.77p	Albite (II)	albitite	0.035	0.065	0.06	N/A	1.43	N/A	6.54
67	L08-84 96.77p	Albite (II)	albitite	0.0317	0.124	0.34	N/A	1.01	N/A	55.59
68	L08-84 96.77p	Albite (II)	albitite	0.0602	0.684	0.65	N/A	1.14	N/A	11.44
69	L08-84 96.77p	Albite (II)	albitite	0.474	0.98	3.14	N/A	3.91	N/A	13.07
70	L08-84 96.77p	Albite (II)	albitite	0.0063	0.816	0.51	N/A	2.09	N/A	1.64
71	L08-84 96.77p	Albite (II)	albitite	0.082	0.28	0.76	N/A	1.63	N/A	22.41

Analysis	Sample	Mineral	Rock Type	Li^{7}	Be^{9}	B^{10}	Na^{23}	P^{31}	K^{39}	Ca^{42}
72	L08-84 96.77p	Albite (II)	albitite	0.0631	0.389	0.17	N/A	1.21	N/A	8.28
73	L08-84 96.77p	Albite (II)	albitite	0.0337	0.086	0.4	N/A	1.56	N/A	23.3
74	L10-232A 65.25	Albite (II)	albitite	0.172	0.99	2.14	N/A	0.9	N/A	99.99
75	L10-232A 65.26	Albite (II)	albitite	0.17	0.242	1.7	N/A	2.77	N/A	114.14
76	L10-232A 65.27	Albite (II)	albitite	0.095	0.241	2.14	N/A	1.59	N/A	114.72
77	L10-232A 65.28	Albite (II)	albitite	0.307	0.446	2.14	N/A	0	N/A	87.9
78	L10-232A 65.29	Albite (II)	albitite	0.7	0.272	1.35	N/A	0.52	N/A	101.03
79	L10-232A 65.30	Albite (II)	albitite	0.471	0.283	1.25	N/A	1.18	N/A	126.2
80	L10-232A 65.31	Albite (II)	albitite	0.6	0.244	1.61	N/A	2.41	N/A	83.71
81	L10-232A 65.32	Albite (II)	albitite	0.196	0.28	1.62	N/A	0.74	N/A	122.32
82	L10-232A 65.33	Albite (II)	albitite	0.361	0.294	1.54	N/A	0.79	N/A	98.59
83	L10-232A 65.34	Albite (II)	albitite	0.203	0.267	1.3	N/A	1.83	N/A	51.7
84	L10-232A 65.35	Albite (II)	albitite	0.16	0.125	0.88	N/A	0.89	N/A	78.66
85	L10-232A 65.36	Albite (II)	albitite	0.103	0.394	1.63	N/A	0.45	N/A	56.7
86	L10-232A 65.37	Albite (II)	albitite	0.098	0.286	1.04	N/A	0.79	N/A	68.8
87	L10-232A 65.38	Albite (II)	albitite	0.426	0.95	1.93	N/A	0.69	N/A	49.75
88	L10-232A 78.25ts	Albite (II)	albitite	0.164	1.59	1.39	N/A	0.01	N/A	67.24
89	L10-232A 78.25ts	Albite (II)	albitite	0.062	0.205	0.5	N/A	0.5	N/A	28.34
90	L10-232A 78.25ts	Albite (II)	albitite	0.0443	0.511	0.75	N/A	0.76	N/A	27.31
91	L10-232A 78.25ts	Albite (II)	albitite	0.207	0.199	1.08	N/A	0.93	N/A	80.89
92	L10-232A 78.25ts	Albite (II)	albitite	0.2	0.302	0.73	N/A	0	N/A	58.29
93	L10-232A 78.25ts	Albite (II)	albitite	0.129	0.259	1.48	N/A	1.42	N/A	80.72
94	L10-232A 78.25ts	Albite (II)	albitite	0.131	0.446	0.69	N/A	1.76	N/A	70.2
95	L10-232A 78.25ts	Albite (II)	albitite	0.0458	0.114	0.64	N/A	1.16	N/A	39.57
96	L10-232A 87.10	Albite (II)	albitite	0.09	0.515	0.7	N/A	0.91	N/A	24.53
97	L10-232A 87.11	Albite (II)	albitite	0.135	0.486	0.89	N/A	0.64	N/A	34.48
98	L10-232A 87.12	Albite (II)	albitite	0.117	0.26	1.47	N/A	0.88	N/A	65.04
99	L10-232A 87.13	Albite (II)	albitite	0.412	0.39	2.4	N/A	0.76	N/A	123.89
100	L10-232A 87.14	Albite (II)	albitite	0.192	0.27	1.36	N/A	0.53	N/A	72.44
101	L10-232A 87.15	Albite (II)	albitite	0.0215	0.101	0.5	N/A	7.97	N/A	20.58
102	L10-232A 87.16	Albite (II)	albitite	0.0637	0	0.62	N/A	0.96	N/A	30.36
103	L10-232A 87.17	Albite (II)	albitite	0.486	0.126	2.33	N/A	1.61	N/A	96.16
104	L10-232A 87.18	Albite (II)	albitite	0.91	0.179	1.86	N/A	2.06	N/A	102.68
105	L10-232A 87.19	Albite (II)	albitite	0.134	0.253	1.41	N/A	1.47	N/A	101.46
106	L10-232A 94.10	Albite (II)	albitite	0.189	0.44	1.63	N/A	0.52	N/A	89.76
107	L10-232A 94.5	Albite (II)	albitite	0.052	0.228	0.52	N/A	0.04	N/A	27.92
108	L10-232A 94.6	Albite (II)	albitite	0.0312	0.244	0.3	N/A	0.51	N/A	16.78

Analysis	Sample	Mineral	Rock Type	Li^{7}	Be^{9}	B^{10}	Na^{23}	P^{31}	K^{39}	Ca^{42}
109	L10-232A 94.7	Albite (II)	albitite	0.049	0.176	0.52	N/A	0.69	N/A	35.58
110	L10-232A 94.8	Albite (II)	albitite	0.231	0.312	1.22	N/A	1.22	N/A	74.61
111	L10-232A 94.9	Albite (II)	albitite	0.154	0.93	1.27	N/A	0.15	N/A	84.62
112	L09-192 112.8p	Fluorite	aegirine syenite	0	0	0.97	N/A	2.72	N/A	513298.34
113	L09-192 112.8p	Fluorite	aegirine syenite	0.077	0	1	148.02	3.64	8.55	513298.22
114	L09-192 112.8p	Fluorite	aegirine syenite	0.039	0	0	57.67	1.57	7.09	513298.22
115	L09-192 112.8p	Fluorite	aegirine syenite	0.049	0.4	1.85	204.59	16.4	17.64	513298.28
116	L09-192 112.8p	Fluorite	aegirine syenite	0.514	0.018	0.84	N/A	2.58	N/A	513298.31
117	L09-192 112.8p	Fluorite	aegirine syenite	0.07	0	0	59.1	5.83	1.27	513155.31
118	L09-192 112.8p	Fluorite	aegirine syenite	0.001	0.104	1.08	N/A	6.02	N/A	513298.31
119	L09-192 112.8p	Fluorite	aegirine syenite	0	0	0.99	45.91	0.7	5.18	513298.25
120	L09-192 112.8p	Fluorite	aegirine syenite	0	0	0.03	37.73	5.89	11.55	513298.31
121	L09-192 112.8p	Fluorite	aegirine syenite	0.051	0	0.32	133.85	1.67	22.67	513298.25
122	L09-192 112.8p	Fluorite	aegirine syenite	0.107	0	0.18	473.56	0.38	54.43	513298.28
123	L09-192 112.8p	Fluorite	aegirine syenite	0.125	0.057	0	143.63	4.45	15.52	513298.25
124	L09-192 112.8p	Fluorite	aegirine syenite	0.012	0.44	0.75	167.51	44.12	11.65	513298.25
125	L10-232A 78.25ts	Fluorite	albitite	0.86	0.15	0	N/A	1.75	N/A	357350.5
126	L10-232A 78.25ts	Fluorite	albitite	0.191	0.022	0	N/A	6.29	N/A	357350.53
127	L10-232A 78.25ts	Fluorite	albitite	0.284	0.13	0	N/A	2.19	N/A	357350.5
128	L10-232A 78.25ts	Fluorite	albitite	0.138	0	0	N/A	0	N/A	357350.5
129	L10-232A 78.25ts	Fluorite	albitite	0.74	0	1.19	N/A	9.67	N/A	357350.53
130	L10-252 349.1p	Microcline (I)	aegirine syenite	0.0287	0.072	0.83	N/A	0.81	N/A	2.29
131	L10-252 349.1p	Microcline (I)	aegirine syenite	0.0096	0.138	1.17	N/A	0.98	N/A	1.57
132	L10-252 349.1p	Microcline (I)	aegirine syenite	0.0174	0.146	0.64	N/A	0.75	N/A	1.98
133	L10-252 349.1p	Microcline (I)	aegirine syenite	0.0094	0.173	3.42	N/A	1.24	N/A	4.5
134	L10-252 349.1p	Microcline (I)	aegirine syenite	0.0253	0.046	0.94	N/A	0.36	N/A	2.09
135	L10-252 349.1p	Microcline (I)	aegirine syenite	0.0262	0.17	0.64	N/A	5.96	N/A	5.82
136	L10-252 349.1p	Microcline (I)	aegirine syenite	0.053	0.086	1.07	N/A	1.73	N/A	9.36
137	L10-252 349.1p	Microcline (I)	aegirine syenite	0.025	0.12	1.08	N/A	1.31	N/A	7.67
138	L10-252 349.1p	Microcline (I)	aegirine syenite	0.0295	0.175	1.22	N/A	1.84	N/A	1.16
139	L10-252 349.1p	Microcline (I)	aegirine syenite	0.0099	0.17	0.97	N/A	0	N/A	0.35
140	85-L6 294.91p	Microcline (I)	aegirine-nepheline syenite	0.0121	0.103	0.98	N/A	1.09	N/A	14.67
141	85-L6 294.91p	Microcline (I)	aegirine-nepheline syenite	0.0106	0.205	1.03	N/A	1.69	N/A	46.78
142	85-L6 294.91p	Microcline (I)	aegirine-nepheline syenite	0.0134	0.107	1.11	N/A	0	N/A	8.31
143	85-L6 294.91p	Microcline (I)	aegirine-nepheline syenite	0.48	1.65	4.73	N/A	0.09	N/A	275.35
144	85-L6 294.91p	Microcline (I)	aegirine-nepheline syenite	0.81	1.49	8.13	N/A	1.3	N/A	12291.4
145	85-L6 294.91p	Microcline (I)	aegirine-nepheline syenite	0.113	0.61	3.43	N/A	1.4	N/A	242.31

Analysis	Sample	Mineral	Rock Type	Li^{7}	Be^{9}	B^{10}	Na^{23}	P^{31}	K^{39}	Ca^{42}
146	L09-162 203.45p	Microcline (I)	aegirine-nepheline syenite	0.064	2.23	3.36	N/A	3.84	N/A	8.2
147	L09-162 203.45p	Microcline (I)	aegirine-nepheline syenite	0.0058	1.4	3.12	N/A	4.07	N/A	2.42
148	L09-162 203.45p	Microcline (I)	aegirine-nepheline syenite	0.0074	0.337	0.4	N/A	1.34	N/A	2.3
149	L09-162 203.45p	Microcline (I)	aegirine-nepheline syenite	0.0101	0.484	4.8	N/A	1.54	N/A	29.27
150	L09-162 203.45p	Microcline (I)	aegirine-nepheline syenite	0.0713	0.261	1.27	N/A	1.01	N/A	6.26
151	L09-162 203.45p	Microcline (I)	aegirine-nepheline syenite	0.588	0.875	2.14	N/A	1.75	N/A	10.24
152	L09-162 203.45p	Microcline (I)	aegirine-nepheline syenite	3.89	1.5	2.19	N/A	3.32	N/A	5.84
153	L09-155 163.1p	Microcline (II)	aegirine syenite	0.102	0.134	0.6	N/A	2.53	N/A	1.61
154	L09-155 163.1p	Microcline (II)	aegirine syenite	0.0421	0.179	0.85	N/A	2.01	N/A	16.3
155	L09-155 163.1p	Microcline (II)	aegirine syenite	0.0777	0.064	0.26	N/A	1.11	N/A	21.18
156	L09-155 163.1p	Microcline (II)	aegirine syenite	0.0406	0.06	0.51	N/A	1.44	N/A	8.63
157	L09-155 163.1p	Microcline (II)	aegirine syenite	0.0503	0.122	0.89	N/A	1.67	N/A	14.01
158	L09-155 163.1p	Microcline (II)	aegirine syenite	0.141	0.095	0.68	N/A	0.71	N/A	14.62
159	L09-155 163.1p	Microcline (II)	aegirine syenite	0.0434	0.117	0.32	N/A	1.06	N/A	4.66
160	L09-155 163.1p	Microcline (II)	aegirine syenite	0.0648	0.179	1.06	N/A	0.5	N/A	11
161	L09-155 163.1p	Microcline (II)	aegirine syenite	0.0188	0.161	0.73	N/A	2.17	N/A	8.03
162	L09-155 163.1p	Microcline (II)	aegirine syenite	0.0213	0.155	0.49	N/A	1.38	N/A	50.68
163	L09-155 163.1p	Microcline (II)	aegirine syenite	3.45	0.205	0.99	N/A	3.33	N/A	5.6
164	L09-192 112.8p	Microcline (II)	aegirine syenite	0.0449	0.653	1.67	N/A	3.48	N/A	4.66
165	L09-192 112.8p	Microcline (II)	aegirine syenite	0.059	0.92	0.99	N/A	1.21	N/A	2.14
166	L09-192 112.8p	Microcline (II)	aegirine syenite	0.087	0.554	1.58	N/A	3.22	N/A	8.78
167	L10-232A 87.1	Microcline (II)	albitite	0.142	1.62	12.08	N/A	5.97	N/A	7.96
168	L10-232A 87.1	Microcline (II)	albitite	0.141	1.05	5.09	N/A	4.12	N/A	0.28
169	L10-232A 87.1	Microcline (II)	albitite	0.071	0.96	9.23	N/A	3.76	N/A	1.16
170	L10-232A 87.1	Microcline (II)	albitite	0.046	0.169	1.35	N/A	4.02	N/A	3.75
171	L10-232A 87.1	Microcline (II)	albitite	0.03	0.213	2.36	N/A	5.34	N/A	13.57
172	L10-232A 87.1	Microcline (II)	albitite	0.128	0.75	11.38	N/A	6.59	N/A	4.21
173	L10-232A 87.1	Microcline (II)	albitite	0.177	1.13	15.11	N/A	1.87	N/A	9.5
174	L10-232A 87.1	Microcline (II)	albitite	0.033	0.406	1.97	N/A	2.11	N/A	20.22
175	L10-232A 87.1	Microcline (II)	albitite	0.166	0.458	3.29	N/A	4.51	N/A	22.06
176	L10-232A 94.11	Microcline (II)	albitite	0.0503	0.211	1.34	N/A	7.51	N/A	13.54
177	L10-232A 94.12	Microcline (II)	albitite	0.063	0.157	1.87	N/A	3.39	N/A	7.45
178	L10-232A 94.13	Microcline (II)	albitite	0.0414	0.132	1.15	N/A	2.29	N/A	15.29
179	L10-232A 94.14	Microcline (II)	albitite	0.147	0.087	5.04	N/A	5.97	N/A	26.99
180	L10-232A 94.15	Microcline (II)	albitite	0.183	0.15	0.67	N/A	2.28	N/A	25.11
181	L10-232A 94.16	Microcline (II)	albitite	0.224	0.117	1.33	N/A	3.23	N/A	52.1
182	L09-192 183.6p	Sodalite	aegirine nepheline syenite	70.41	5.3	0.99	N/A	0.29	N/A	431.12

Analysis	Sample	Mineral	Rock Type	Li^{7}	Be^{9}	B^{10}	Na^{23}	P^{31}	K^{39}	Ca^{42}
183	L09-192 183.6p	Sodalite	aegirine nepheline syenite	75.57	5.66	0.97	N/A	1.22	N/A	218.4
184	L09-192 183.6p	Sodalite	aegirine nepheline syenite	32.9	6.01	0.76	N/A	0.94	N/A	306.39
185	L09-192 183.6p	Sodalite	aegirine nepheline syenite	33.51	6.75	0.35	N/A	0.91	N/A	117.72
186	L09-192 183.6p	Sodalite	aegirine nepheline syenite	30.97	6.55	0.9	N/A	0.98	N/A	266.05
187	L09-192 183.6p	Sodalite	aegirine nepheline syenite	36.75	6.31	0.93	N/A	0.72	N/A	347.75
188	L09-192 183.6p	Sodalite	aegirine nepheline syenite	39.76	6.37	2.54	N/A	1.34	N/A	322.46
189	L09-192 183.6p	Sodalite	aegirine nepheline syenite	40.55	6.36	0.48	N/A	0.75	N/A	92.11

Analysis	Ca^{44}	Sc^{45}	Ti^{49}	Ga^{71}	Ge^{72}	Ge^{73}	Rb^{85}	Sr^{88}	Y^{89}	Zr^{90}	Nb^{93}	Sn^{118}	Cs^{133}
1	9584.27	2.14	263.11	35.53	4.17	3.85	0.1555	0.326	2.83	2687.09	3.99	103.28	0.00355
2	8786.08	1.9	303.72	36.94	4.09	3.82	0.0624	0.207	2.21	2317.52	1.92	91.36	0.00203
3	16320.02	2.8	359.74	31.18	5.17	5.15	0.057	0.355	4.66	3598.96	15.37	108.4	0.00018
4	6400.95	1.17	418.17	46.66	5.04	4.53	0.205	3.9	2.01	916.71	187.75	95.11	0.82
5	7397.46	2.47	339.17	39.73	4.31	4.03	0.0533	0.1423	1.875	2966.81	0.793	91.27	0.00215
6	7357.89	3.05	522.6	51.52	4.55	4.38	0.00827	0.1704	2.101	3780.02	0.656	183.62	0.00059
7	7648.63	2.306	313.95	41.89	4.1	3.9	0.0192	0.1359	2.48	2420.58	1.549	110.12	0.00069
8	9562.41	3.22	329.01	40.31	4.16	4.03	0.00568	0.1285	2.46	3983.57	0.2006	138.43	0.00056
9	2566.12	1.59	457.76	41.99	5.24	4.8	1.65	0.0739	2.21	1674.58	3.44	94.57	0.0284
10	25.94	0.6	0.032	72.05	0.775	0.797	0.731	0.124	0.00162	0.00193	0.00345	0.0143	0
11	140.56	0.702	0.293	85.27	0.788	0.77	1.343	0.381	0.0036	0.0295	0.0516	0.0028	0.0206
12	314.08	0.691	0.192	84.46	0.879	0.882	1.446	1.332	0.0239	0.0242	0.0497	0.0101	0.00095
13	32.38	0.81	0.66	100	0.607	0.623	1.41	0.81	0.065	0.254	0.155	0.0123	0.0028
14	26.71	0.82	0.607	97.31	0.76	0.713	1.1	0.505	0.0292	0.128	0.0397	0.0089	0.00126
15	41.58	0.81	0.65	86.57	0.69	0.697	1.14	0.86	0.107	0.57	0.197	0.0131	0.00084
16	33.03	0.81	0.408	85.34	0.688	0.687	1.58	0.552	0.262	0.116	0.076	0.0111	0.00271
17	49.96	0.84	1.09	98.24	0.85	0.884	1.29	0.406	0.2	0.82	0.111	0.022	0.00065
18	49	0.84	0.37	102.57	0.654	0.673	1.34	1.149	0.102	0.434	0.98	0.0084	0.00053
19	40.73	0.83	0.668	84.3	0.767	0.757	1.03	0.764	0.263	0.316	0.125	0.0091	0.00178
20	118.73	0.829	2.5	101.48	0.598	0.63	1.98	0.467	0.372	3.6	1.4	0.159	0.0075
21	79.38	0.744	0.336	92.82	0.559	0.627	4.75	0.438	0.0177	0.0193	0.0416	0.0251	0.00783
22	41.27	0.648	0.261	117.35	0.572	0.529	3.05	0.305	0.0371	0.183	0.0854	0.04	0.00565
23	86.08	0.698	0.342	91.42	0.484	0.604	1.611	0.436	0.0615	0.1232	0.1171	0.0609	0.00434
24	68.85	0.722	0.33	105.3	0.578	0.543	3.04	0.369	0.0336	0.0425	0.0178	0.0232	0.00075
25	105.92	0.746	0.344	91.74	0.537	0.592	1.76	0.388	0.0427	0.0308	0.0508	0.0152	0.00277
26	83.61	0.723	1.887	128.16	0.538	0.516	1.323	0.373	0.1075	1.001	0.82	0.388	0.00525
27	52	0.683	0.05	175.79	0.499	0.426	0.786	0.0656	0.0029	0.0335	0.0547	0.0203	0.00035
28	60.67	0.676	0.258	115.85	0.557	0.54	1.879	0.335	0.00552	0.0303	0.0316	0.0158	0.00031

Analysis	Ca^{44}	Sc^{45}	Ti^{49}	Ga^{71}	Ge^{72}	Ge^{73}	Rb^{85}	Sr^{88}	Y^{89}	Zr^{90}	Nb^{93}	Sn^{118}	Cs^{133}
29	59.11	0.663	0.344	105.75	0.617	0.607	2.094	0.464	0.013	0.0494	0.0261	0.0213	0.00605
30	49.99	0.685	0.356	102.79	0.553	0.598	1.719	0.385	0.0178	0.1316	0.0836	0.0499	0.00291
31	52.71	0.653	0.287	118.47	0.57	0.529	2.152	0.318	0.00849	0.1111	0.1066	0.0389	0.00427
32	54.39	0.687	0.227	117.39	0.569	0.564	2.15	0.1895	0.0148	0.1574	0.0231	0.0283	0.00321
33	51.2	0.659	0.274	97.75	0.588	0.524	2.153	0.422	0.055	0.169	0.037	0.0328	0.0037
34	23.43	0.642	0.361	93.16	0.618	0.615	2.561	0.56	0.0082	0.028	0.0084	0.0339	0.0008
35	44.16	0.663	0.261	126.44	0.561	0.543	2.8	0.3	0.0124	0.1367	0.0506	0.0294	0.00523
36	112.73	0.842	0.142	169.49	0.567	0.585	2.023	1.072	0.0385	0.0572	0.051	0.0491	0.0075
37	606.48	0.805	0.165	184.73	0.597	0.569	2.081	0.427	0.0332	0.0219	0.0543	0.017	0.00321
38	27.9	0.722	0.161	221.09	0.65	0.587	1.338	0.66	0.0148	0.0205	0.0248	0.0233	0.0035
39	65.69	0.801	0.067	204.19	0.585	0.536	1.293	0.076	0.0157	0.0329	0.021	0.0162	0.00147
40	63.42	0.775	0.221	148.82	0.634	0.614	3.27	0.406	0.0253	0.1099	0.1574	0.0279	0.00824
41	115.19	0.7	0.257	225.14	0.744	0.573	2.164	0.974	0.1097	0.701	0.824	0.055	0.0733
42	52.98	0.736	0	142.31	0.502	0.545	0.349	0.224	0.00555	0.00627	0.048	0.0305	0.00196
43	51.86	0.72	0	161.64	0.476	0.516	0.2064	0.265	0.0156	0.045	0.1226	0.0219	0.00413
44	39.78	0.712	0.04	168.88	0.446	0.475	0.1726	0.0156	0.00397	0.00361	0.00083	0.0083	0.00046
45	54.49	0.697	0.128	194.81	0.593	0.584	2.017	0.347	0.0296	0.053	0.1661	0.0781	0.00604
46	44.71	0.688	0.036	177.21	0.554	0.586	0.2358	0.343	0.00021	0.00835	0.0742	0.0102	0.00316
47	23.74	1.118	7.45	357.47	0.568	0.668	0.214	0.383	0.00751	0.0515	152.7	0.309	0.0024
48	11.18	1.159	0.02	417.31	0.488	0.481	0.1437	0.1075	0.00127	0.00456	0.00817	0.0223	0.00322
49	228.24	1.167	0.567	345.37	0.601	0.684	0.276	0.0541	4.28	0.391	9.65	0.025	0.0022
50	20.35	1.12	0.034	400.73	0.453	0.429	0.339	0.519	0.0012	0.0086	0.00262	0.0132	0.00692
51	21.73	1.068	0.019	412.27	0.578	0.559	0.311	0.718	0.0118	0.0163	0.0129	0.0187	0.00327
52	25.49	1.073	0.169	448.47	0.422	0.486	0.292	0.836	1.59	38.44	9.98	0.0944	0.0091
53	22.36	1.062	0.046	405.74	0.421	0.454	0.216	0.376	0.0683	0.599	0.167	0.0428	0.00222
54	68.75	1.084	3.39	117.81	0.04	0.066	0.368	3.53	0.39	1.93	67.03	0.344	0.014
55	54.36	0.79	0.494	74.14	0.73	0.75	0.82	0.82	0.037	0.186	1.87	0.052	0.00002
56	126.92	0.76	0.45	83.56	0.67	0.66	0.67	0.412	0.104	0.29	3.42	0.0223	0.00004
57	50.54	0.77	0.7	72.47	0.79	0.78	0.74	0.53	0.2	1.09	22.41	0.031	0
58	1534.4	0.76	1.03	74.13	0.83	0.94	0.76	1.95	2.59	5.37	3.99	0.126	0.00033
59	155.84	1.286	19.2	120.91	0.718	0.714	113.59	6.3	2.084	15.22	1.469	0.356	1.184
60	120.43	1.194	0.469	70.42	0.388	0.407	25.33	3.48	0.104	0.514	0.1345	0.0477	0.2065
61	24.58	0.624	0.127	147.7	0.565	0.548	1.737	0.2	0.0287	0.0781	0.0849	0.0249	0.031
62	55.55	0.688	0.121	121.87	0.611	0.497	0.458	0.817	0.0674	0.1069	0.329	0.0798	0.0117
63	72.81	0.627	0.115	112.91	0.242	0.236	0.351	2.21	0.1318	0.286	0.374	0.1349	0.0258
64	80.04	0.662	0.171	119.48	0.576	0.557	1.9	0.675	0.0855	0.254	0.2009	0.1022	0.0208
65	99.21	0.758	0.097	102.36	0.214	0.217	0.1418	0.526	0.0612	0.1329	0.215	0.197	0.0121

Analysis	Ca^{44}	Sc^{45}	Ti^{49}	Ga^{71}	Ge^{72}	Ge^{73}	Rb^{85}	Sr^{88}	Y^{89}	Zr^{90}	Nb^{93}	Sn^{118}	Cs^{133}
66	39.9	0.65	0	79.2	0.246	0.231	0.0185	0.1208	0.00242	0.00644	0.0182	0.0106	0.00086
67	112.54	0.646	0	83.08	0.442	0.488	0.1185	1.742	0.0176	0.0513	0.0583	0.113	0.0181
68	60.95	0.669	0.084	120.46	0.477	0.465	0.58	0.335	0.1281	0.095	0.1035	0.0356	0.00701
69	55.81	0.651	0.226	111.59	0.772	0.783	3.21	0.591	0.19	0.581	0.901	0.434	0.0372
70	30.03	0.634	0.025	99.88	0.812	0.845	0.33	0.0205	0.23	0.0139	0.0178	0.0166	0.0353
71	42.83	0.649	0.135	128.97	0.099	0.12	0.1741	0.963	0.0106	0.0533	0.043	0.0548	0.013
72	73.6	0.675	0.242	152.29	0.548	0.525	1.3	0.1511	0.0495	0.173	0.31	0.0691	0.0132
73	55.89	0.651	0	96.61	0.307	0.376	0.197	1.266	0	0.00172	0.0147	0.023	0.0149
74	133.77	1.09	0.429	103.09	0.168	N/A	3.59	4.7	0.233	5.25	0.9	1.88	0.13
75	137.48	1.05	0.9	90.18	0.475	N/A	2.19	4.38	0.087	2.44	1.39	1.83	0.0507
76	137.29	1.03	0.77	90.64	0.498	N/A	1.51	4.35	0.031	0.75	1.27	3.35	0.0479
77	118.8	1.1	0.074	60.54	0.194	N/A	1.76	4.1	0.09	0.142	0.102	0.49	0.0398
78	134.01	1.08	0.84	70.69	0.371	N/A	1.96	3.35	0.079	0.028	0.317	11.27	0.0285
79	163.24	1.11	1.6	75.49	0.419	N/A	1.67	4.25	0.00481	0.011	0.79	0.63	0.0545
80	115.24	1.09	0.177	67.38	0.399	N/A	1.3	4.52	0.81	9.49	0.433	0.101	0.0571
81	172.77	1.11	0.7	71.17	0.301	N/A	1.81	4.04	0.93	26.36	1.28	4.37	0.065
82	138.19	1.15	0.055	68.82	0.317	N/A	1.58	4.74	0.11	0.15	0.0606	0.067	0.0537
83	80.4	1.08	0.041	60.62	0.252	N/A	0.587	2.41	0.0233	0.217	0.162	0.086	0.0407
84	84.89	1.05	0.087	67.69	0.499	N/A	1.07	3.99	0.00125	0.0051	0.108	0.217	0.0358
85	93.7	1.09	0.211	100.04	0.159	N/A	2.23	3.07	0.0077	0.227	0.31	0.473	0.0309
86	104.62	1.08	0.052	74	0.247	N/A	27.63	3.61	0.00546	0.0133	0.0559	0.0426	0.0575
87	82.1	1.07	0.106	97.26	0.125	N/A	0.78	2.57	0.106	0.532	0.231	0.055	0.035
88	90.18	1.39	0.828	104.12	0.068	N/A	1.1	4.08	0.0186	0.303	0.198	0.463	0.0605
89	39.88	1.37	0.024	86.72	0.315	N/A	0.345	0.91	0.08	0.114	0.0345	0.0498	0.0105
90	58.95	1.39	0.215	76.16	0.13	N/A	0.91	2.35	0.00222	0.0429	0.19	0.157	0.0119
91	105.48	1.35	0.877	202.67	0.297	N/A	1.7	2.14	0.00326	0.0138	0.915	0.418	0.0261
92	96.03	1.35	0.153	66.73	0.131	N/A	0.676	2.03	0.00481	0.0226	0.0801	0.152	0.0142
93	106.46	1.36	0.182	140.04	0.355	N/A	4.71	2.93	0.0304	0.0593	0.194	0.199	0.0243
94	92.7	1.34	0.284	90.47	0.218	N/A	1.44	3.72	0.0085	0.139	0.46	0.719	0.0273
95	62.67	1.32	0.017	92.56	0.637	N/A	0.579	1.65	0.0022	0.0202	0.0149	0.31	0.0141
96	51.52	1.74	0.411	121.38	0.085	N/A	0.223	1.32	0.0131	0.0602	0.125	0.209	0.0175
97	71.61	1.73	0.126	124.82	0.079	N/A	0.414	1.77	0.00525	0.0649	0.0939	0.093	0.0228
98	116.39	1.73	0.104	79.83	0.183	N/A	1.42	3.56	0.116	0.513	0.132	0.618	0.0382
99	166.95	1.65	0.068	74.51	0.316	N/A	1.61	4.3	0.0284	0.0352	0.093	0.197	0.0632
100	114.42	1.66	0.003	98.86	0.416	N/A	1.02	3.74	0.0401	0.0613	0.0364	0.248	0.0317
101	75.02	1.65	0.292	201.08	0.419	N/A	0.823	0.269	0.0086	0.158	0.152	0.564	0.00302
102	90.4	1.67	0.068	170.61	0.523	N/A	0.624	0.781	0.0309	0.0927	0.0967	0.517	0.0111

Analysis	Ca^{44}	Sc^{45}	Ti^{49}	Ga^{71}	Ge^{72}	Ge^{73}	Rb^{85}	Sr^{88}	Y^{89}	Zr^{90}	Nb^{93}	Sn^{118}	Cs^{133}
103	181.74	1.64	1.39	58.87	0.299	N/A	2.62	4.05	0.382	1.78	0.978	0.158	0.0987
104	167.49	1.63	2.05	76.53	0.366	N/A	5.55	2.47	0.0342	0.486	0.733	2.4	0.056
105	167.97	1.63	0.478	80.04	0.367	N/A	1.98	3.14	0.0212	0.165	0.305	0.458	0.038
106	106.83	1.2	0.89	107.31	0.326	N/A	1	3.81	0.0382	0.0323	0.434	0.292	0.077
107	51.5	1.23	0.271	113.47	0.72	N/A	0.485	1.12	0.0296	0.073	0.1	0.132	0.0108
108	28.53	1.22	0.028	85.98	0.599	N/A	0.262	0.91	0.0051	0.0082	0.0097	0.0329	0.0081
109	59.82	1.23	0.027	108.54	0.422	N/A	0.92	0.9	0.0538	0.151	0.0658	0.085	0.0127
110	86.89	1.22	0.145	115.46	1.14	N/A	1.66	2.28	0.217	0.0592	0.0308	0.086	0.0213
111	112.57	1.23	0.421	100.94	0.122	N/A	1.17	3.52	0.081	0.232	0.111	0.109	0.0396
112	411416.94	0.019	0.036	0.0155	0.018	0	0.155	13.18	95.96	0.0117	0	0.01	0.0136
113	526102.69	0.021	0.013	0.0072	0.024	0.044	0.0914	13.17	187.63	0.0634	0.755	0.0266	0.0062
114	525945	0	0	0.0595	0.011	0.144	0.0452	51.23	138.4	0.0049	0.0217	0.0153	0.0149
115	461536.5	0.01	0.2	0.001	0	0	0.103	370.51	260.04	0.0104	0.0188	0.019	0.0082
116	475054.44	0.0235	0.039	0.0055	0.058	0.02	0.613	462	17.23	0.021	0.0015	0.0349	0.1274
117	471771.66	0	0	0.023	0	0.085	0	16.02	355.86	0.0215	0	0	0.0073
118	496351.84	0.023	0	0.0002	0	0.024	0.018	25.72	125.84	0.0292	0.337	0.0298	0.0027
119	522128.88	0	0.07	0	0	0.065	0.073	47.53	103.42	0.0084	0.0388	0.026	0.0223
120	531157.19	0.019	0	0.0419	0.018	0.095	0.0899	46.75	46.13	0.0046	0.0867	0.013	0.0133
121	539232.69	0.008	0.187	0.0259	0	0.055	0.177	21.52	131.31	0.0099	3.12	0.05	0.0269
122	542482.19	0.009	0.132	0.0494	0.024	0.137	0.478	17.53	102.77	0.00084	0.00039	0.0198	0.0899
123	499915.19	0	0.049	0.0316	0.041	0.159	0.1044	17.14	114.85	0.0159	0.0863	0.0146	0.0096
124	531414.44	0.027	0.158	0.157	0.079	0.408	0.0982	14.11	304.9	0.0094	0.00186	0.0251	0.0163
125	370843.03	0.008	0	0.0134	0	N/A	1.011	21.97	174.8	0.0241	0.0031	0.003	0.177
126	348081.91	0.05	0	0	0.01	N/A	0.0597	18.21	311.05	0.144	0.1135	0.051	0.0168
127	311936.13	0	0.16	0.022	0.134	N/A	0.415	15.52	38.15	0.375	0.0478	0.067	0.0583
128	327493.25	0.059	0	0.073	0.18	N/A	0.013	14.32	141.01	0.0147	0.0399	0.026	0
129	393307.13	0.085	0.23	0.0072	0.134	N/A	0.917	21.59	109.87	0.133	0.1112	4.38	0.1035
130	110.44	0.73	0.021	63.39	0.68	0.636	1179.46	0.0371	0.0804	0.26	0.0648	0.038	0.92
131	72.66	0.664	0	60.63	0.552	0.564	1141.95	0.0589	0.0496	0.0444	0.1251	0.0108	0.784
132	69.84	0.628	0	59.87	0.529	0.49	1088.54	0.097	0.0817	0.306	0.0926	0.0206	0.436
133	93.49	0.664	0.046	64.23	0.414	0.401	1226.49	0.34	0.0375	0.0632	0.1	0.0113	0.297
134	73.42	0.648	0	62.54	0.432	0.413	1119.47	1.278	0.00108	0.00503	0.0218	0.0044	0.278
135	164.14	0.82	0.029	66.72	0.771	0.821	1062.18	0.215	0.00416	0.1017	0.00999	0.01	0.222
136	126.12	0.706	0	69.58	0.372	0.395	1169.63	1.016	0.00163	0.0846	0.00632	0.0075	0.273
137	94.69	0.653	0.001	60.18	0.604	0.612	1133.19	0.967	0.0458	0.64	0.113	0.0133	0.344
138	132.45	0.734	0	57.79	0.502	0.518	1122.09	0.1248	0.0655	0.305	0.0709	0.0237	0.506
139	94.14	0.663	0.038	54.47	0.562	0.573	1092.98	0.0929	0.013	0.0235	0.041	0.0114	0.699

Analysis	Ca^{44}	Sc^{45}	Ti^{49}	Ga^{71}	Ge^{72}	Ge^{73}	Rb^{85}	Sr^{88}	Y^{89}	Zr^{90}	Nb^{93}	Sn^{118}	Cs^{133}
140	51.91	0.78	0.086	56.4	0.59	0.611	918.15	0.552	0.0164	0.198	0.146	0.045	0.235
141	87	0.8	0.02	58.46	0.61	0.557	968.28	0.345	0.05	0.229	0.082	0.07	0.24
142	26.71	0.75	0.039	56.72	0.62	0.582	910.53	0.112	0.015	0.264	0.068	0.0124	0.236
143	305.56	0.76	0.283	59.26	0.155	0.163	3.91	25.79	0.43	3.24	25.58	0.335	43.62
144	12526.1	0.73	0.47	64.45	0.22	0.252	4.78	27.07	4.04	4.99	3.03	1.59	45.4
145	263	0.74	0	65.44	0.107	0.127	3.01	19.34	0.106	2.65	1.01	0.0281	34.72
146	80.77	0.943	5.79	63.92	0.822	0.736	1125.76	0.0577	0.192	4.26	0.1478	0.295	0.726
147	80.09	0.993	0.017	60.03	0.658	0.671	1057.77	0.1719	0.0507	0.529	0.0775	0.0217	0.583
148	63.7	1.017	0.861	75.64	0.805	0.777	1181.17	0.331	0.015	0.0356	0.0233	0.0141	2.191
149	202.23	1.177	0.077	65.43	0.424	0.41	1399.39	2.86	0.0778	1.674	0.277	0.0188	0.566
150	124.37	1.141	0.866	67.81	0.78	0.686	1201.97	1.258	0.0219	0.229	0.0802	0.0174	2.138
151	84.46	1.259	0.323	56.78	0.62	0.61	1037.11	0.731	0.0588	0.421	0.811	0.032	0.479
152	30.17	1.106	0.741	58.61	0.68	0.676	1072.18	0.804	0.0463	0.573	0.0999	0.0515	0.527
153	129.98	0.939	0.069	101.9	0.509	0.504	1803.43	0.0329	0.01014	0.03	0.0956	0.0218	0.583
154	135.75	0.875	0.018	93.59	0.487	0.469	1649.32	1.245	0.0178	0.0622	0.15	0.0185	0.516
155	155.84	0.889	0.018	122.9	0.584	0.598	1647.18	0.896	0.01098	0.0542	0.0288	0.0322	0.544
156	118.34	0.874	0.07	103.66	0.505	0.497	1697.43	0.583	0.0305	0.0318	0.428	0.0201	0.523
157	83.32	0.773	0.035	107.28	0.528	0.556	1817.36	0.1725	0.00304	0.0179	0.0522	0.0136	0.554
158	116.81	0.822	0.08	104.5	0.462	0.471	1833.74	0.604	0.00961	0.0253	0.057	0.0143	0.499
159	61.53	0.765	0.052	111.27	0.532	0.495	1850.65	0.1061	0.00709	0.0433	0.0719	0.0186	0.554
160	67.52	0.724	0.096	109.31	0.571	0.538	1850.86	1.006	0.0407	0.0509	0.1972	0.0235	0.602
161	55.76	0.71	0.042	119.83	0.532	0.584	1851.48	0.244	0.0857	0.269	0.1023	0.0255	0.567
162	108.78	0.739	0.089	106.08	0.542	0.562	1839.07	0.399	0.0526	0.051	0.1012	0.0204	0.583
163	102.19	0.72	0.127	117.31	0.512	0.504	1888.39	0.2182	0.488	0.277	4.05	0.021	0.524
164	29.4	1.023	2.65	114.61	0.598	0.671	1993.27	0.0678	0.087	0.281	1.349	0.0862	0.726
165	32.11	0.987	5.1	121.05	0.629	0.599	2062.25	0.0327	0.034	0.171	1.031	0.117	0.869
166	32.94	0.999	1.82	162.31	0.513	0.557	2059.49	1.095	0.151	2.09	29.36	1.89	0.542
167	27.43	2.04	1.01	117.1	0.599	N/A	2234.4	0.198	0.232	0.391	12.35	0.084	0.854
168	75.79	1.95	0.355	118.05	0.561	N/A	2017.73	3.95	0.268	1.44	12.26	0.146	0.758
169	39.4	1.97	0.407	119.1	0.544	N/A	2125.89	3.47	0.163	0.232	7.26	0.113	0.834
170	36.83	1.9	0.111	132.47	0.523	N/A	2134.87	0.639	0.055	0.095	0.822	0.0563	0.88
171	50.71	1.85	0.336	138.36	0.563	N/A	2213.96	2.31	0.0404	0.305	3	0.165	0.729
172	37.72	1.81	0.597	128.14	0.646	N/A	2313.35	0.0695	0.149	0.114	9.25	0.085	0.878
173	32.22	1.73	29.42	162.05	0.5	N/A	2342.33	2.15	0.0395	0.541	25.7	0.63	0.521
174	67.4	1.7	0.161	152.15	0.695	N/A	2331.21	2.96	0.012	0.0419	2.76	0.081	0.688
175	56.49	1.71	0.305	143.43	0.563	N/A	2081.32	3.07	0.0263	0.343	3.96	0.0354	0.715
176	69.72	1.21	0.032	143.35	0.456	N/A	2300.68	0.486	0.083	1.22	0.246	0.0305	0.518

Analysis	Ca^{44}	Sc^{45}	Ti^{49}	Ga^{71}	Ge^{72}	Ge^{73}	Rb^{85}	Sr^{88}	Y^{89}	Zr^{90}	Nb^{93}	Sn^{118}	Cs^{133}
177	91.14	1.27	0.055	143.57	0.45	N/A	2305.18	0.334	0.0715	0.482	0.16	0.0229	0.537
178	75.59	1.23	0.115	156.54	0.422	N/A	2190.59	1.57	0.0342	0.106	0.353	0.0567	0.506
179	82.51	1.22	0.037	133.99	0.508	N/A	2256.64	2.53	0.0329	0.086	0.368	0.074	0.529
180	52.38	1.16	2.53	117.86	0.505	N/A	1770.16	3.97	0.072	1.21	0.769	0.357	0.565
181	95.89	1.16	0.16	113.5	0.486	N/A	1853.23	2.88	0.0215	0.106	0.384	0.158	0.534
182	464.66	0.321	0.466	75.18	0.332	0.325	157.86	30.82	0.00484	0.0745	0.01305	0.0801	0.95
183	240.53	0.326	0.477	75.76	0.336	0.361	145.03	22.74	0.00304	0.0201	0.0229	0.0693	0.259
184	351.57	0.341	0.48	72.18	0.367	0.35	112.04	20.7	0.00226	0.0185	0.00783	0.0797	0.486
185	153.89	0.34	0.377	69.87	0.339	0.345	102.96	7.13	0.00099	0.0179	0.0073	0.0835	0.484
186	302.49	0.332	18.13	69.41	0.32	0.285	102.27	16.81	0.00397	0.0425	0.0261	0.0776	0.444
187	397.22	0.338	0.431	68.57	0.31	0.314	116.64	23.24	0.00153	0.0165	0.0157	0.0726	0.672
188	372.76	0.345	32.25	72.13	0.332	0.265	112.99	22.12	0.035	0.0334	0.0208	0.0907	1.95
189	127.81	0.35	1.183	67.37	0.317	0.313	106.79	2.71	0.001	0.0209	0.00705	0.0799	0.237

Analysis	Ba^{137}	La^{139}	Ce^{140}	Pr^{141}	Nd^{146}	Sm^{147}	Eu^{151}	Gd^{157}	Tb^{159}	Dy^{163}	Ho^{165}	Er^{167}	Tm^{169}
1	0.148	2.53	8.16	1.397	7.28	1.813	0.203	1.14	0.1454	0.805	0.1551	0.652	0.186
2	0.0716	2.03	6.58	1.197	6.14	1.442	0.1598	0.891	0.1131	0.666	0.1306	0.584	0.173
3	0.055	3.32	14.18	2.64	13.46	3.16	0.35	1.98	0.26	1.42	0.26	0.97	0.25
4	1.88	3.65	6.94	0.89	4.02	0.87	0.104	0.6	0.075	0.44	0.081	0.26	0.061
5	0.0032	0.886	4.36	0.867	4.63	1.141	0.1295	0.732	0.098	0.545	0.1127	0.515	0.1582
6	0.007	0.766	3.98	0.819	4.46	1.062	0.1071	0.59	0.0697	0.398	0.0929	0.488	0.1614
7	0.00152	1.012	4.98	0.978	5.2	1.224	0.1407	0.788	0.1049	0.635	0.1421	0.698	0.2078
8	0.0004	1.15	5.95	1.224	6.74	1.745	0.1942	1.045	0.1398	0.761	0.1571	0.733	0.233
9	0.0183	0.263	0.91	0.14	0.69	0.19	0.0285	0.181	0.037	0.292	0.076	0.31	0.085
10	0.019	0.00062	0.0016	0.00035	0	0.0017	0.00063	0	0.00004	0.0002	0.00037	0.00067	0.00041
11	0.0377	0.00061	0.00168	0.00031	0.003	0	0.00121	0	0.00019	0.00084	0	0.0005	0.00012
12	0.0087	0.00651	0.0153	0.00184	0.006	0.0037	0.00146	0.0007	0.0005	0.00205	0.00067	0.0034	0
13	0.072	0.0063	0.0247	0.00152	0.0109	0.0041	0.00094	0.0133	0.0021	0.0138	0.0034	0.0134	0.00038
14	0.0323	0.0038	0.0182	0.00072	0.0057	0	0.0038	0.0034	0.00183	0.0087	0.00064	0.0048	0.00071
15	0.0378	0.0108	0.0477	0.0059	0.0328	0.0139	0.0042	0.0157	0.0039	0.025	0.0046	0.0071	0.00109
16	0.0317	0.315	0.75	0.084	0.32	0.062	0.0094	0.056	0.0076	0.045	0.009	0.0291	0.0035
17	0.0184	0.48	1.16	0.136	0.57	0.12	0.0134	0.092	0.0118	0.046	0.0069	0.0214	0.00189
18	0.0354	0.0284	0.078	0.0101	0.0517	0.0152	0.00233	0.0134	0.00269	0.0181	0.0043	0.0106	0.00003
19	0.0488	0.0161	0.088	0.0136	0.055	0.0266	0.0088	0.0358	0.0058	0.0427	0.0054	0.0112	0.00155
20	0.0411	0.387	0.89	0.093	0.3	0.067	0.0105	0.062	0.0061	0.072	0.0141	0.0342	0.0038
21	0.244	0.00149	0.00361	0.00034	0.0022	0.0045	0.00248	0.0028	0.0005	0.00336	0.00063	0.0012	0
22	0.0821	0.0062	0.02	0.00248	0.0137	0.0006	0.00141	0.0073	0.00166	0.0086	0.00167	0.0018	0.00053

Analysis	Ba^{137}	La^{139}	Ce^{140}	Pr^{141}	Nd^{146}	Sm^{147}	Eu^{151}	Gd^{157}	Tb^{159}	Dy^{163}	Ho^{165}	Er^{167}	Tm^{169}
23	0.161	0.0015	0.00616	0.00094	0.0007	0.0071	0.00259	0.0087	0.00269	0.0127	0.00211	0.0039	0.00051
24	0.0453	0.00185	0.00522	0.00047	0.0069	0.0035	0.00135	0.0028	0.00073	0.006	0.00167	0.00437	0.00047
25	0.0419	0.00405	0.0209	0.00221	0.016	0.008	0.00221	0.0071	0.00163	0.0093	0.00075	0.0057	0.00127
26	0.176	0.00252	0.00796	0.00106	0.0075	0.0046	0.00353	0.0114	0.00406	0.0267	0.00519	0.0148	0.00061
27	0.0218	0.00076	0.00218	0	0	0.00138	0.00017	0	0.00052	0.00051	0.00039	0.0026	0
28	0.0329	0.00454	0.0145	0.00117	0.0035	0.0024	0.00212	0	0.00009	0.00133	0.00002	0.00081	0.00039
29	0.197	0.00777	0.0201	0.00202	0.0068	0.0037	0.00322	0.0035	0.00039	0	0.00065	0.00111	0.00062
30	0.251	0.01023	0.039	0.00474	0.0158	0.0042	0.00232	0.0081	0.0005	0.0016	0.00069	0.0006	0.0001
31	0.406	0.0223	0.064	0.00635	0.0268	0.0059	0.00206	0.0053	0.00013	0.00006	0.00011	0.0021	0.00003
32	0.0441	0.00496	0.0215	0.00286	0.0115	0.005	0.00105	0.0065	0.00076	0.00506	0.00084	0.00215	0.00007
33	0.0553	0.00377	0.016	0.00186	0.0075	0.0009	0.00508	0.0084	0.00227	0.0121	0.00088	0.0073	0.0006
34	0.059	0.0037	0.0097	0.00042	0.0096	0.0002	0.0038	0	0.00118	0.0006	0.00172	0	0
35	0.1002	0.00391	0.01166	0.00135	0.0096	0.0008	0.00193	0.0057	0.0005	0.0053	0.00064	0	0
36	1.237	0.00091	0.00535	0.00056	0.0017	0.0024	0.0014	0.0009	0.0009	0.0081	0.00145	0.0055	0.0017
37	0.232	0.00595	0.018	0.00175	0.0088	0.0057	0.00126	0.002	0.00054	0.0013	0.00101	0.0029	0
38	0.332	0.00157	0.00348	0.00069	0.0024	0.0039	0.00375	0.0027	0.00083	0.0004	0.00045	0.0016	0.00131
39	0.0347	0.00162	0.00601	0.00056	0.0057	0.0042	0	0.0052	0.0006	0.00207	0.00059	0.00074	0.00025
40	0.301	0.00223	0.0117	0.00067	0.0033	0.0052	0.00203	0.0032	0.0009	0.0037	0.00176	0.0028	0.00063
41	3.05	0.0063	0.0249	0.00141	0.0081	0	0.0023	0.0174	0.0059	0.033	0.0029	0.0135	0
42	0.173	0.0154	0.00622	0.00062	0.0047	0	0.00108	0.0001	0	0	0.00007	0.0022	0.0002
43	0.1092	0.002	0.00373	0.00045	0.0026	0	0.00246	0.0001	0.00023	0.0031	0.00094	0.0009	0.00015
44	0.0271	0	0.00009	0.00016	0	0	0	0	0	0.0003	0.0001	0	0
45	0.339	0.00133	0.00454	0.00068	0	0.0016	0.0029	0.0026	0.00149	0.0075	0.00043	0.0063	0
46	0.1267	0.00046	0.00162	0.00014	0.00146	0.00092	0.00032	0.0022	0.00018	0	0	0.0003	0
47	0.276	11.43	25.5	2.15	5.92	0.403	0.0224	0.15	0.00388	0.0079	0.00019	0.0011	0.00065
48	0.0256	0.0007	0.00111	0.00047	0.0012	0.00116	0.00043	0.0009	0.00035	0.00039	0	0	0.0007
49	0.0365	0.953	3.16	0.428	2.46	1.13	0.152	1.16	0.16	0.926	0.139	0.299	0.0307
50	0.323	0.00121	0.0021	0.00042	0.0018	0.0017	0.0003	0	0.00064	0	0	0.0006	0.0004
51	0.148	0.00127	0.00462	0	0.0073	0	0.0005	0	0.00055	0.0021	0.00088	0.0013	0.00007
52	0.415	0.859	2.35	0.27	1.29	0.399	0.0439	0.438	0.052	0.272	0.0562	0.187	0.044
53	0.296	0.0815	0.16	0.0152	0.0585	0.0112	0.0025	0.0156	0.00116	0.0146	0.00229	0.0064	0.00125
54	2.59	0.244	0.969	0.159	0.63	0.156	0.0237	0.143	0.0302	0.105	0.0138	0.031	0.00355
55	0.126	0.05	0.174	0.0237	0.11	0.024	0.0053	0.0147	0.0022	0.0102	0.00124	0.0013	0.00043
56	0.068	0.115	0.39	0.052	0.211	0.048	0.0075	0.03	0.0041	0.02	0.0022	0.0079	0.00057
57	0.15	0.53	2.16	0.3	1.46	0.39	0.052	0.28	0.028	0.105	0.0113	0.0141	0.0019
58	0.15	7.95	18.06	1.88	6.93	1.42	0.166	0.95	0.123	0.71	0.096	0.18	0.022
59	0.157	0.1885	0.808	0.0848	0.45	0.177	0.0281	0.216	0.0401	0.29	0.0562	0.182	0.0268

Analysis	Ba^{137}	La^{139}	Ce^{140}	Pr^{141}	Nd^{146}	Sm^{147}	Eu^{151}	Gd^{157}	Tb^{159}	Dy^{163}	Ho^{165}	Er^{167}	Tm^{169}
60	0.0198	0.0127	0.0395	0.00343	0.0308	0.0119	0.00095	0.0093	0.00071	0.0104	0.00206	0.0066	0
61	0.114	0.0009	0.00332	0	0	0.0103	0.00034	0.0054	0.00114	0.0137	0.00068	0.0019	0.00098
62	0.968	0.00119	0.00524	0.00107	0.01	0.0078	0.0031	0.019	0.00421	0.0177	0.00246	0.0037	0.00077
63	2.34	0.00332	0.00758	0.0007	0.0034	0.0052	0.00468	0.0267	0.00532	0.0296	0.00381	0.0091	0.00134
64	0.498	0.00265	0.00592	0.00085	0.0037	0.0038	0.00256	0.0153	0.00264	0.0151	0.00252	0.0058	0.0014
65	0.833	0.00052	0.00298	0.00072	0.0058	0.0031	0.00157	0.0124	0.00175	0.0128	0.00175	0.0015	0.00045
66	0.0473	0.00029	0.00008	0.00008	0	0	0	0.0011	0.00018	0	0.00024	0	0.0004
67	0.764	0.00139	0.00337	0.00023	0.0036	0.0022	0.00044	0.0019	0.00071	0.00112	0.00053	0.0007	0.00006
68	0.912	0.00391	0.0134	0.0017	0.0066	0.0071	0.0022	0.0127	0.00389	0.0256	0.00466	0.0151	0.00292
69	6.4	0.0179	0.0475	0.00467	0.0192	0.0135	0.00264	0.0256	0.00569	0.0305	0.00608	0.0119	0.00199
70	0.0389	0.07	0.386	0.0342	0.1209	0.0455	0.00548	0.0459	0.00992	0.0569	0.0104	0.02	0.00241
71	3.82	0.00002	0.00163	0.00027	0.0018	0.0008	0.00112	0	0	0.0015	0.00091	0.0007	0
72	0.0719	0.00194	0.00619	0.00063	0.0029	0.002	0.00165	0.0114	0.00208	0.0063	0.00168	0.0042	0.00088
73	0.271	0.00003	0	0.00007	0.0007	0	0.00043	0.0019	0	0	0	0	0.00055
74	32.68	0.0097	0.066	0.0155	0.099	0.0313	0.0047	0.0275	0.006	0.0485	0.0094	0.0251	0.00311
75	17.75	0.0163	0.0552	0.0105	0.057	0.0142	0.00164	0.0103	0.00181	0.0167	0.0025	0.0058	0.00001
76	12.85	0.0095	0.0245	0.00415	0.0207	0.0036	0.00166	0.0034	0.00006	0.0062	0.002	0.0025	0.0004
77	26.61	0	0.00087	0.00018	0.00223	0.00092	0.0007	0.002	0.0013	0.0181	0.00494	0.017	0.00237
78	36	0.0025	0.00483	0.00075	0.0034	0.0023	0.00124	0.0015	0.00104	0.0169	0.00359	0.0182	0.00167
79	27.67	0.00084	0.00106	0.00008	0.00124	0.00075	0.00073	0.00129	0.0002	0.00099	0.00029	0.00152	0
80	39.63	0.0174	0.134	0.0313	0.193	0.0598	0.0078	0.061	0.0182	0.181	0.0395	0.117	0.0142
81	53.67	0.0316	0.333	0.084	0.548	0.167	0.0186	0.128	0.0239	0.178	0.0326	0.085	0.0081
82	48.94	0.00151	0.00367	0.00059	0.00223	0.00124	0.0023	0.0026	0.00238	0.0231	0.0055	0.0172	0.00279
83	7.14	0.0019	0.0062	0.00077	0.0009	0.0005	0.0005	0.0023	0.00077	0.0024	0.00128	0.0042	0.00005
84	16.86	0.00029	0.00128	0.00012	0.00035	0.0015	0.00075	0	0	0.00136	0	0.003	0.00012
85	15.8	0.00153	0.00456	0.00092	0.0033	0.0019	0.0011	0.00149	0.0003	0.00101	0.00029	0.00162	0.00031
86	47.22	0.00052	0.00079	0.00001	0	0.00035	0.00208	0.00022	0.0001	0.00227	0.00006	0.00124	0.00001
87	24.37	0.00046	0.00296	0.00068	0.0057	0.0016	0.00005	0.0067	0.00241	0.0258	0.0056	0.0198	0.00183
88	30.22	0.00109	0.00371	0.00087	0.00421	0.00341	0.00202	0.0028	0.00059	0.00126	0.00038	0.00098	0.00013
89	3.14	0.00021	0.00152	0.00029	0.00086	0	0.00061	0.00288	0.00104	0.0088	0.00264	0.0093	0.00289
90	6.91	0.00263	0.00811	0.00066	0.0039	0.00296	0.00085	0.00114	0	0.00059	0.0002	0.00041	0.00004
91	20.9	0.00062	0.00258	0.00049	0.00002	0.00103	0.00065	0.0025	0.00019	0.00124	0.00016	0.00156	0
92	4.94	0.00144	0.00203	0.00057	0.0023	0	0.0006	0.0019	0	0.00018	0	0.0021	0
93	38.71	0.00136	0.00227	0.00017	0.0037	0.0022	0.0022	0.002	0.00009	0.0032	0.00046	0.0039	0.00052
94	24.59	0.00129	0.00352	0.00045	0.0025	0.0035	0.00256	0	0.00046	0.0011	0	0.0004	0
95	10.73	0.00028	0.00084	0.00021	0.00036	0.00163	0.00064	0	0	0.00032	0.00024	0.00012	0
96	4.23	0.00028	0.00052	0.00004	0	0	0	0	0.00024	0.00266	0.00069	0.00236	0.00026

Analysis	Ba^{137}	La^{139}	Ce^{140}	Pr^{141}	Nd^{146}	Sm^{147}	Eu^{151}	Gd^{157}	Tb^{159}	Dy^{163}	Ho^{165}	Er^{167}	Tm^{169}
97	4.91	0.00025	0.00058	0.00041	0.00033	0.0011	0.00016	0.00039	0	0.00158	0.00037	0.00196	0.0003
98	12.23	0.001	0.00375	0.00064	0.0049	0.004	0.0004	0.006	0.00177	0.0196	0.006	0.0182	0.00356
99	19.7	0.00008	0.00081	0.00021	0.00095	0.0003	0.00037	0	0.00096	0.0068	0.00183	0.007	0.00074
100	44.21	0.00044	0.00049	0.00017	0.0005	0	0.00166	0.0028	0.00155	0.013	0.00303	0.0056	0.00062
101	1.83	0.0098	0.0231	0.00336	0.0143	0.0039	0.0012	0.005	0	0.0013	0.00111	0.0015	0.00047
102	2.2	0.00091	0.00662	0.00075	0.0054	0.0026	0.00047	0.0044	0.0014	0.0085	0.00147	0.007	0.00054
103	27.3	0.0101	0.0552	0.00656	0.0549	0.0325	0.0066	0.0398	0.0108	0.095	0.0212	0.0509	0.0079
104	12.8	0.00651	0.0183	0.00235	0.0126	0.0051	0.00489	0.0059	0.00077	0.0093	0.00208	0.00387	0.00085
105	16.18	0.00421	0.0126	0.00141	0.0043	0.0029	0.00235	0.0004	0.00066	0.003	0.00083	0.00129	0.00006
106	9.91	0.00054	0.00048	0.0001	0.00091	0.0022	0.00047	0.0027	0.0015	0.0136	0.00214	0.0075	0.00086
107	9.03	0.00046	0.00067	0.00021	0.00302	0	0.00012	0.00079	0.00103	0.0047	0.00114	0.007	0.00098
108	3.03	0.00018	0.00102	0.00028	0.00006	0	0.00013	0.0011	0.00012	0.00147	0.00023	0	0.00005
109	6.04	0.0009	0.00339	0.00029	0.0054	0.0046	0.00152	0.0103	0.00172	0.0124	0.00252	0.0041	0.00085
110	10.17	0.0065	0.0199	0.00358	0.0085	0.0111	0.0015	0.0312	0.0061	0.0477	0.0101	0.0283	0.00371
111	7.76	0	0.00135	0.00003	0.00057	0.00013	0.00127	0.0024	0.00143	0.0128	0.00284	0.0119	0.00188
112	0.258	0.274	1.205	0.355	2.2	1.957	0.442	5.47	0.878	3.42	0.36	0.579	0.0299
113	0.0601	0.1458	0.673	0.229	1.99	4.45	1.472	22.89	4.11	16.32	1.379	1.57	0.0779
114	0.322	1.066	5.06	1.125	7.57	6.26	1.361	16.1	2.63	9.03	0.955	1.132	0.0581
115	0.288	1.153	3.89	0.743	3.33	1.69	0.401	5.53	1.06	5.66	0.948	1.7	0.125
116	1.304	0.127	0.335	0.0796	0.873	0.708	0.098	0.947	0.0629	0.273	0.0486	0.0938	0.00518
117	0.091	0.792	2.19	0.273	1.5	0.932	0.319	6.02	1.453	10.89	2.01	4.1	0.35
118	0.181	0.0821	0.2316	0.0385	0.229	0.286	0.0913	1.776	0.269	1.622	0.236	0.363	0.022
119	0.121	0.0687	0.1418	0.0202	0.12	0.144	0.0532	0.974	0.164	1.047	0.154	0.22	0.0177
120	0.251	1.362	4.5	0.723	3.36	1.273	0.207	1.61	0.256	1.057	0.1327	0.222	0.0174
121	0.516	0.533	2.6	0.519	3.47	2.82	0.792	9.73	1.6	5.7	0.647	0.855	0.05
122	1.107	1.235	5.73	1.212	7.88	4.27	0.79	7.46	1.09	3.88	0.391	0.556	0.0388
123	0.08	0.774	3.84	0.811	4.76	3.43	0.793	8.16	1.205	4.76	0.534	0.741	0.0456
124	0.187	4.52	18.96	3.52	19.42	13.6	3.08	31.69	5.12	21.15	2.56	4.35	0.31
125	1.129	0.371	1.403	0.308	2.37	1.82	0.475	5.32	0.959	4.47	0.619	0.877	0.0427
126	0.414	0.38	1.687	0.328	2.17	1.84	0.437	6.42	1.43	8.95	1.44	2.59	0.172
127	0.976	0.956	3.69	0.509	3.36	1.46	0.206	2.08	0.338	1.28	0.139	0.241	0.0119
128	0.049	0.545	2.43	0.507	2.9	2.27	0.403	4.54	0.812	3.07	0.513	0.689	0.0421
129	1.256	0.489	1.423	0.217	1.33	1.015	0.222	2.59	0.488	2.64	0.379	0.564	0.03
130	6.57	0.011	0.0434	0.00642	0.0253	0.0224	0.0036	0.0405	0.00347	0.0227	0.00129	0.0043	0.00011
131	4.82	0.00976	0.0447	0.00778	0.0462	0.0369	0.00396	0.0305	0.00244	0.014	0.00162	0.00303	0.0004
132	4.1	0.00522	0.0234	0.00419	0.0203	0.0194	0.00434	0.0167	0.00329	0.0177	0.00228	0.0007	0.0008
133	4.75	0.00356	0.0152	0.00253	0.0155	0.0062	0.00121	0.0109	0.00115	0.007	0.00145	0.0017	0.00014

Analysis	Ba^{137}	La^{139}	Ce^{140}	Pr^{141}	Nd^{146}	Sm^{147}	Eu^{151}	Gd^{157}	Tb^{159}	Dy^{163}	Ho^{165}	Er^{167}	Tm^{169}
134	5.51	0.00163	0.01242	0.00182	0.008	0.0033	0.0005	0.0045	0.00027	0.00096	0.00009	0.00041	0.00012
135	2.43	0.00265	0.0113	0.00124	0.0084	0.0015	0.00023	0.0014	0.00002	0.0021	0.00026	0.00108	0
136	3.23	0.00204	0.00769	0.00062	0.0041	0.0013	0.00038	0.0009	0.00011	0.00094	0.00027	0	0.00017
137	5.37	0.00702	0.0353	0.00334	0.0265	0.0186	0.0059	0.0189	0.00279	0.0094	0.002	0	0.00001
138	4.27	0.0085	0.0411	0.0059	0.0361	0.0427	0.0075	0.0392	0.00254	0.0119	0.00285	0.0002	0.00091
139	4.2	0.00324	0.0148	0.00181	0.0176	0.0084	0.00093	0.0039	0.00111	0.0037	0.00051	0	0.00034
140	4.49	0.0195	0.038	0.0058	0.0279	0.0046	0.00061	0.008	0.00044	0.0019	0.00114	0.00047	0
141	2.57	0.102	0.244	0.0324	0.135	0.027	0.004	0.0222	0.0023	0.0076	0.00121	0.0026	0.00008
142	1.6	0.007	0.0306	0.0035	0.017	0.0101	0.0002	0.0024	0.00085	0.0037	0.00099	0.0022	0.00033
143	1.24	0.222	1.44	0.095	0.51	0.151	0.0176	0.109	0.0154	0.086	0.016	0.038	0.0027
144	0.92	0.66	1.49	0.169	0.67	0.158	0.0265	0.18	0.045	0.42	0.101	0.37	0.072
145	0.45	0.121	0.212	0.0207	0.081	0.0148	0.002	0.0163	0.0034	0.022	0.0037	0.0108	0.0008
146	0.648	0.0133	0.0843	0.0111	0.0613	0.0296	0.0044	0.0248	0.00299	0.0218	0.0012	0.0065	0
147	0.59	0.0121	0.0431	0.00434	0.0377	0.0075	0	0.0168	0.00144	0.0083	0	0	0
148	2.26	0.00536	0.0214	0.00275	0.0104	0.0049	0.00163	0.0033	0	0.00258	0	0.0005	0.00022
149	0.85	0.0531	0.149	0.0161	0.0647	0.0202	0.0021	0.0153	0.00176	0.0081	0.00164	0.0035	0.00062
150	1.772	0.0497	0.1228	0.01053	0.0563	0.0024	0.0003	0.0007	0.00005	0.0038	0	0.00089	0.00043
151	0.882	0.0449	0.1783	0.0229	0.1078	0.0303	0.00248	0.017	0.00133	0.0103	0.00194	0.0029	0.00056
152	1.396	0.0189	0.0735	0.00705	0.0311	0.0069	0.0006	0.0116	0.00154	0.004	0.00062	0.0005	0.00089
153	2.086	0.00619	0.0291	0.00289	0.0158	0.0054	0.00036	0.0069	0.00051	0	0.00032	0.0014	0.00057
154	30	0.00703	0.03	0.00273	0.0126	0.0013	0.00184	0.0056	0.00033	0.0032	0.00067	0.0043	0.00083
155	9.34	0.00156	0.0048	0.00014	0.0056	0.0018	0.00159	0.0024	0.00048	0.00315	0.00041	0.0016	0.00013
156	6.79	0.00745	0.0329	0.00519	0.0228	0.0083	0.00488	0.0133	0.00258	0.0164	0.00151	0.00149	0.00005
157	4.32	0.00465	0.0205	0.00205	0.0095	0.0045	0.0006	0.0044	0	0.0021	0	0.00077	0.00024
158	9.7	0.00481	0.0167	0.00172	0.0079	0.0055	0.00076	0.0011	0.00021	0.00394	0.00043	0	0.00079
159	3.65	0.01146	0.0343	0.0042	0.0191	0.0043	0.00101	0.0006	0.00058	0.00002	0	0.00149	0
160	18	0.00777	0.0349	0.00398	0.014	0.0083	0.00302	0.0077	0.0011	0.0058	0.00066	0.00378	0.00022
161	5.04	0.0178	0.0487	0.00561	0.0251	0.0081	0.00179	0.0103	0.00251	0.0156	0.00374	0.0122	0.00038
162	4.45	0.00984	0.0382	0.00581	0.0272	0.0086	0.00246	0.0115	0.00125	0.0129	0.00166	0.0059	0.00091
163	1.826	0.0355	0.1908	0.0253	0.1072	0.0653	0.0136	0.114	0.0329	0.253	0.0374	0.0825	0.00942
164	3.17	0.0285	0.13	0.0209	0.109	0.0732	0.0084	0.0633	0.0083	0.0317	0.00329	0.0036	0.00065
165	2.67	0.016	0.0646	0.0098	0.0433	0.0202	0.00261	0.0195	0.00175	0.0066	0.00082	0.0002	0
166	14.2	0.195	0.523	0.0619	0.253	0.072	0.0093	0.08	0.0088	0.0414	0.0068	0.0063	0.00019
167	3.96	0.0398	0.24	0.0469	0.317	0.17	0.0151	0.082	0.0073	0.0382	0.0009	0.0103	0
168	30.27	0.0441	0.249	0.0469	0.311	0.119	0.0085	0.057	0.0106	0.0416	0.0028	0.0124	0.00011
169	30.62	0.0833	0.442	0.0702	0.406	0.095	0.0103	0.0577	0.00472	0.0233	0.00328	0.0073	0.00061
170	10.59	0.0282	0.128	0.0212	0.0854	0.0273	0.00395	0.0173	0.00253	0.0141	0.00202	0	0.00021

Analysis	Ba^{137}	La^{139}	Ce^{140}	Pr^{141}	Nd^{146}	Sm^{147}	Eu^{151}	Gd^{157}	Tb^{159}	Dy^{163}	Ho^{165}	Er^{167}	Tm^{169}
171	25.63	0.0265	0.1062	0.0169	0.0842	0.0248	0.0062	0.0117	0.00236	0.0038	0.00114	0.00248	0.00069
172	3.38	0.193	0.911	0.151	0.717	0.103	0.0089	0.0586	0.00321	0.0265	0.00369	0.0014	0.00127
173	23.95	0.222	0.791	0.124	0.606	0.112	0.01	0.0296	0.00335	0.0143	0.00109	0.0015	0
174	49.74	0.107	0.414	0.0584	0.345	0.068	0.0089	0.0223	0.00063	0.0039	0	0.0017	0.00065
175	54.36	0.14	0.507	0.0742	0.366	0.0682	0.0041	0.025	0.00138	0.0055	0.00092	0.0019	0.00004
176	8.61	0.0311	0.118	0.0092	0.0482	0.0219	0.00375	0.025	0.00462	0.0218	0.00246	0.0039	0.00038
177	7.22	0.0197	0.0554	0.0075	0.0398	0.0161	0.00221	0.0172	0.00253	0.0125	0.00248	0.0057	0.00042
178	20.78	0.0157	0.0381	0.00378	0.0207	0.0084	0.00247	0.0077	0.00088	0.0063	0.00091	0.00024	0.00036
179	38.48	0.023	0.0612	0.0083	0.0345	0.0146	0.00225	0.0154	0.00127	0.0049	0.00069	0.0016	0
180	90.56	0.0145	0.0475	0.0075	0.0431	0.0288	0.0092	0.022	0.00255	0.0177	0.00183	0.0022	0.00063
181	48.64	0.0093	0.0274	0.00319	0.0158	0.0077	0.00307	0.0067	0.00126	0.00082	0.00034	0	0.00019
182	0.157	0.0224	0.0503	0.00334	0.0108	0.0019	0	0	0	0.00062	0	0.00039	0
183	0.0669	0.0334	0.0853	0.00683	0.0254	0.0062	0.00059	0.0016	0.00017	0	0.00001	0	0.00036
184	0.0508	0.0185	0.0434	0.00493	0.014	0.00037	0.00042	0.0002	0.00009	0.00113	0	0.00251	0.00003
185	0.0278	0.0407	0.0731	0.00572	0.0143	0.00171	0.00091	0.00249	0.00009	0	0	0	0.00019
186	0.0646	0.0226	0.0504	0.0046	0.0146	0	0.00078	0.0031	0.00012	0	0	0	0
187	0.1204	0.0231	0.0476	0.00317	0.0117	0.0034	0.00112	0.00108	0.00001	0.00088	0.00015	0.00014	0
188	0.152	0.1056	0.1163	0.0098	0.0304	0.0094	0.00072	0.0034	0.00093	0.0034	0.00037	0.002	0.00031
189	0.0079	0.00426	0.01276	0.00101	0.0009	0	0.00015	0.00042	0	0.00102	0.00007	0.00065	0.00018

Analysis	Yb^{173}	Lu^{175}	Hf^{177}	Ta^{181}	Pb^{206}	Pb^{207}	Pb^{208}	Th^{232}	U^{238}	Co^{59}	Si^{29}	Mg^{25}	Fe^{57}
1	2.4	0.613	96.08	0.258	1.273	1.276	1.272	0.247	0.051	0.0563	243068.5	381.75	154841.09
2	2.29	0.585	77.08	0.1466	0.739	0.761	0.763	0.0661	0.0214	0.0543	243068.47	75.07	157299.48
3	3.08	0.78	133.9	0.52	0.81	0.66	0.65	0.061	0.097	0.065	243070.33	114.29	146766.03
4	0.75	0.19	37.65	78.27	12.56	9.51	9.68	0.19	22.91	0.084	243071.03	147.24	134227.84
5	2.13	0.566	117.5	0.1035	0.1685	0.1317	0.1579	0.0436	0.00262	0.0511	243068.45	12.39	136180.48
6	2.19	0.573	123.5	0.0569	0.22	0.069	0.0748	0.00386	0.00626	0.1006	243068.47	21.95	140181.66
7	2.63	0.66	97.34	0.072	0.0918	0.076	0.0913	0.00712	0.00598	0.0495	243068.47	8.23	136756.25
8	3.28	0.908	155.63	0.0803	0.0572	0.0558	0.0555	0.00846	0.001	0.0693	243068.47	11.06	143702.89
9	1.15	0.33	89.53	0.199	0.228	0.191	0.213	0.131	0.0245	0.0401	243068.84	262.7	148923.59
10	0.0025	0.00078	0	0.0005	0.0325	0.0144	0.0312	0.00474	0.00208	0.0058	317858.81	1.27	529.48
11	0.0008	0	0	0.00058	0.08	0.0677	0.0864	0.0266	0.00548	0.0084	317858.81	0.052	1323.44
12	0.00029	0	0.0004	0.00053	0.0527	0.0417	0.0708	0.0841	0.00913	0.00593	317858.81	7.02	1147.84
13	0.0054	0.00152	0.0066	0.0075	0.265	0.227	0.256	0.061	0.0029	0.0049	317859.69	62.39	806.66
14	0.007	0.00125	0.0129	0.00225	0.118	0.084	0.102	0.047	0.0021	0.0055	317859.56	1.01	1131.84
15	0.0111	0.00077	0.0163	0.0148	0.372	0.241	0.275	0.092	0.0046	0.0074	317859.41	1.91	1029.35
16	0.0213	0.0034	0.0062	0.0064	0.154	0.138	0.173	0.107	0.0043	0.0057	317859.13	0.463	1124.9

Analysis	Yb^{173}	Lu^{175}	Hf^{177}	Ta^{181}	Pb^{206}	Pb^{207}	Pb^{208}	Th^{232}	U^{238}	Co^{59}	Si^{29}	Mg^{25}	Fe^{57}
17	0.0107	0.00106	0.0183	0.0078	0.69	0.54	0.61	0.104	0.00291	0.0055	317858.88	8.61	682.54
18	0.0043	0.00102	0.013	0.073	0.168	0.116	0.126	0.0394	0.0062	0.0057	317858.41	2.42	1028.73
19	0.0058	0.00082	0.0126	0.008	0.188	0.147	0.165	0.083	0.00295	0.0059	317858.53	0.521	972.54
20	0.051	0.0092	0.077	0.13	0.404	0.26	0.351	0.372	0.109	0.013	317858.31	16.1	1239.2
21	0.0038	0.00042	0.0019	0.00481	0.0732	0.0509	0.0619	0.0356	0.01045	0.00601	317858.78	2.12	953.18
22	0.002	0.00048	0.004	0.00476	0.0645	0.0448	0.059	0.0832	0.0121	0.0085	317858.78	1.046	980.82
23	0	0.00067	0.0063	0.00493	0.0729	0.0571	0.0619	0.0575	0.0143	0.0078	317858.78	0.647	852.75
24	0.0012	0.00035	0.0019	0.00131	0.0636	0.0504	0.0673	0.0642	0.0134	0.00813	317858.78	0.469	911.87
25	0.0041	0.00032	0.0028	0.0014	0.0655	0.0532	0.0682	0.0907	0.0162	0.0069	317858.78	0.294	940.23
26	0.0074	0.00042	0.0642	0.00735	0.064	0.0529	0.0537	0.0338	0.0093	0.00962	317858.78	3.16	869.36
27	0.0016	0	0.0045	0.00198	0.0286	0.0276	0.0241	0.00867	0.00139	0.00567	317858.78	0.711	508.62
28	0	0	0.004	0.00227	0.044	0.0382	0.0387	0.0367	0.00782	0.00774	317858.78	0.243	913.09
29	0.0008	0.00077	0.0034	0.00178	0.1056	0.102	0.1058	0.037	0.00653	0.00569	317858.78	1.537	981.52
30	0.0049	0.00031	0.0029	0.0043	0.1194	0.0918	0.1083	0.1095	0.0236	0.00795	317858.78	1.497	1031.98
31	0	0.00072	0.007	0.01187	0.0953	0.0759	0.094	0.0762	0.0163	0.0077	317858.78	1.024	1035.82
32	0	0	0.0307	0.00311	0.0476	0.0301	0.03	0.0511	0.0106	0.00748	317858.78	1.76	1051.25
33	0.0036	0.00086	0.006	0.00106	0.0856	0.0549	0.0695	0.0657	0.0148	0.0054	317858.78	1.56	965.88
34	0	0	0	0	0.0462	0.0509	0.0415	0.0181	0.0038	0.0068	317858.78	0.072	1017.53
35	0.0035	0	0.0091	0.00389	0.0615	0.0582	0.0444	0.0302	0.00408	0.0085	317858.78	2.97	917.45
36	0.0032	0.00076	0.0045	0.00086	0.0536	0.0496	0.0661	0.0128	0.00574	0.0116	317858.78	13.77	761.89
37	0	0.00028	0.0035	0.00015	0.0446	0.076	0.0473	0.0158	0.00688	0.0052	317858.78	8.64	770.9
38	0.0007	0.00018	0	0.00059	0.0602	0.0672	0.0664	0.0124	0.00239	0.0007	317858.78	0.692	596.04
39	0.0009	0	0.0034	0.00055	0.0226	0.0101	0.0122	0.0179	0.0047	0.00709	317858.78	53.52	566.7
40	0.0049	0.00022	0.0103	0.00113	0.0429	0.0352	0.0433	0.0338	0.00634	0.00606	317858.78	15.34	1012.95
41	0.0269	0	0.0211	0.0103	0.139	0.066	0.0838	0.031	0.0281	0.0136	317858.78	132.57	1266.08
42	0.0016	0.00027	0.0001	0.00085	0.0277	0.0246	0.0408	0.00433	0.00097	0.0068	317858.78	3.57	123.78
43	0.0033	0.00037	0.0001	0.00087	0.0571	0.0401	0.0323	0.0342	0.00486	0.00633	317858.78	3.01	133.42
44	0.0013	0.0001	0.00308	0	0.0031	0.0077	0.001	0.00073	0.00049	0.0077	317858.78	0.234	123.62
45	0.0041	0.00066	0.002	0.00572	0.0737	0.0177	0.0338	0.0378	0.0113	0.0082	317858.78	6.56	618.2
46	0.0033	0	0	0.00076	0.0751	0.0638	0.0646	0.00143	0.00315	0.0073	303835.59	7.69	169.65
47	0.0014	0.00034	0.0055	0.866	10.18	1.57	0.108	0.0863	8.54	0.0074	303833.91	0.628	126.03
48	0.0026	0	0.00051	0.00127	0.0166	0.0102	0.0129	0.00046	0.00008	0.00545	317857.06	3.21	96.58
49	0.156	0.0172	0.0024	0.089	0.582	0.091	0.0126	0.0208	0.548	0.0088	317857.13	0.373	180.43
50	0.0006	0.00022	0	0.00151	0.072	0.0686	0.0769	0.00043	0.00114	0.005	317857.19	5.35	159.95
51	0	0	0.0023	0.00252	0.0391	0.0471	0.0461	0.00359	0.00133	0.0059	317857.28	1.88	144.78
52	0.462	0.083	0.82	0.517	0.351	0.126	0.111	0.0317	0.635	0.004	317857.31	0.147	160.64
53	0.0072	0.00049	0.0118	0.0173	0.044	0.0381	0.0442	0.00197	0.0039	0.0049	317857.41	11.5	185.56

Analysis	Yb^{173}	Lu^{175}	Hf^{177}	Ta^{181}	Pb^{206}	Pb^{207}	Pb^{208}	Th^{232}	U^{238}	Co^{59}	Si^{29}	Mg^{25}	Fe^{57}
54	0.0118	0.00151	0.061	12.17	3.01	1.36	1.09	0.044	1.86	0.0054	317857.47	16.65	154.41
55	0.0029	0.00045	0.0045	0.043	1.25	1.02	1.1	0.071	0.018	0.0034	317862.31	0.522	1123.23
56	0.0086	0.00106	0.0118	0.102	0.59	0.43	0.46	0.056	0.026	0.0079	317862.47	0.85	879.12
57	0.0036	0.00052	0.035	0.82	2.12	1.68	1.84	0.067	0.03	0.0084	317862.72	0.573	979.52
58	0.133	0.0082	0.18	0.37	3.16	3.16	3.16	0.127	0.101	0.0058	317862.91	0.6	1110.68
59	0.187	0.024	0.44	0.1387	3.86	2.21	2.44	0.42	0.0562	0.0296	317858.78	6931.94	1945.98
60	0.0017	0.00077	0.0256	0.0144	0.512	0.451	0.492	0.0478	0.0403	0.0045	303835.59	769.42	194.33
61	0.0036	0.00031	0.0094	0.0104	0.0752	0.055	0.0678	0.0086	0.00331	0.0045	317858.81	4.09	808.2
62	0.0014	0.00125	0.0057	0.0686	0.114	0.091	0.0879	0.0047	0.0081	0.0079	317858.81	116.19	506.03
63	0.0114	0.00051	0.0134	0.282	0.172	0.132	0.1345	0.00432	0.0094	0.006	317858.81	54.07	515.74
64	0.0049	0.00048	0.0111	0.0582	0.141	0.1052	0.1075	0.0153	0.00649	0.0074	317858.81	50.71	1016.32
65	0.0031	0.00053	0.0042	0.0563	0.0612	0.0353	0.0424	0.00522	0.00435	0.0054	317858.81	42.87	366.2
66	0.0013	0	0.0002	0.00078	0.0084	0.0041	0.0082	0.0005	0.00065	0.0059	317858.81	9.48	19.3
67	0.003	0	0.0005	0.00592	0.1016	0.0952	0.082	0.00082	0.00036	0.0042	317858.78	8.77	107.54
68	0.0196	0.00182	0.0057	0.00722	0.0656	0.052	0.0583	0.0327	0.0029	0.0068	317858.81	6.95	295.34
69	0.0103	0.00071	0.0195	0.25	0.2	0.162	0.1501	0.0156	0.019	0.0076	317858.78	208.91	1276.24
70	0.0087	0.00157	0	0.001	0.0302	0.0273	0.0304	0.0429	0.00152	0.0075	317858.81	2	259.24
71	0.0007	0.00018	0.0007	0.0115	0.138	0.0872	0.1272	0.00295	0.00107	0.0088	317858.81	3	70.15
72	0.0008	0.00062	0.0062	0.061	0.0552	0.0523	0.0579	0.013	0.00262	0.00581	317858.78	13.62	881.96
73	0.003	0.0006	0	0.00107	0.0467	0.0354	0.0379	0.00105	0.00057	0.0059	317858.84	8.44	19.87
74	0.0167	0.00137	0.102	0.077	1.13	0.71	0.68	0.0134	0.21	N/A	317858.75	7.99	224.84
75	0.0054	0.00056	0.045	0.13	0.62	0.423	0.39	0.00308	0.085	N/A	317858.78	18.98	166.88
76	0	0	0.012	0.14	0.63	0.434	0.444	0.0064	0.0483	N/A	317858.75	7.38	142.65
77	0.0139	0.00179	0.0075	0.0147	0.235	0.103	0.098	0.0169	0.00281	N/A	317858.72	30.91	122.43
78	0.0119	0.00145	0.001	0.0448	0.557	0.219	0.187	0.0072	0.01	N/A	317858.72	95.29	310.38
79	0.0008	0	0.00002	0.093	0.526	0.332	0.339	0.00125	0.00058	N/A	317858.72	74.93	233.56
80	0.068	0.009	0.128	0.0241	1.42	0.8	0.77	0.0399	0.301	N/A	317858.75	25.34	47.08
81	0.0428	0.00355	0.338	0.096	0.91	0.64	0.59	0.0225	0.88	N/A	317858.75	14.15	65.95
82	0.0136	0.00077	0.0043	0.011	0.7	0.67	0.63	0.0088	0.067	N/A	317858.75	20.02	52.33
83	0.0046	0	0.0071	0.0153	0.269	0.292	0.254	0.00394	0.0077	N/A	317858.75	8.04	13.77
84	0.0021	0.00021	0.00157	0.0071	0.416	0.303	0.316	0.0001	0	N/A	317858.75	49.44	190.04
85	0.00038	0.00012	0.0063	0.0401	0.6	0.367	0.356	0.00034	0.0159	N/A	317858.75	11.89	112.02
86	0.0057	0.00005	0.0041	0.0247	0.239	0.182	0.202	0.00082	0.00347	N/A	317858.75	6.8	45.16
87	0.0112	0.00129	0.0263	0.0192	0.164	0.141	0.144	0.0118	0.00347	N/A	317858.72	8.08	37.16
88	0.00194	0.00035	0.0275	0.0374	0.202	0.126	0.122	0.00355	0.0176	N/A	317858.78	15.38	39.33
89	0.0196	0.00247	0.0071	0.00506	0.12	0.084	0.082	0.0092	0.00345	N/A	317858.78	1.88	8.41
90	0.00187	0.00015	0	0.0149	0.186	0.0723	0.0802	0.00411	0.0091	N/A	317858.78	3.82	33.78

Analysis	Yb^{173}	Lu^{175}	Hf^{177}	Ta^{181}	Pb^{206}	Pb^{207}	Pb^{208}	Th^{232}	U^{238}	Co^{59}	Si^{29}	Mg^{25}	Fe^{57}
91	0.00075	0.00001	0.00022	0.0232	0.204	0.152	0.138	0.00327	0.00596	N/A	317858.78	45	129.6
92	0	0	0.0001	0.00374	0.271	0.226	0.195	0.00174	0.0073	N/A	317858.78	31.58	41.65
93	0.0065	0.0013	0.0033	0.0179	0.461	0.239	0.244	0.00384	0.0267	N/A	317858.78	18.01	134.79
94	0.0028	0.00041	0.0052	0.0216	0.241	0.115	0.119	0.00369	0.0118	N/A	317858.78	10.93	70.82
95	0	0.00018	0.00092	0.00331	0.126	0.087	0.082	0.00099	0.00003	N/A	317858.78	3.65	35.66
96	0.00069	0.00039	0.0078	0.01	0.0557	0.0484	0.0499	0.00281	0.0163	N/A	317858.81	6.15	15.22
97	0	0.00022	0.0045	0.00628	0.0745	0.0518	0.0622	0.00082	0.00028	N/A	317858.81	6.73	20.67
98	0.0291	0.00313	0.0195	0.0184	3.57	1.11	1.04	0.0227	0.0238	N/A	317858.81	9.39	24.67
99	0.0046	0.00005	0.0008	0.00698	0.388	0.298	0.286	0.00631	0.00157	N/A	317858.81	54.53	92.36
100	0.0064	0.00047	0.0014	0.00753	0.142	0.096	0.08	0.00516	0.00254	N/A	317858.81	15.5	28.49
101	0.0028	0	0.0019	0.0077	0.202	0.081	0.0827	0.00146	0.0205	N/A	317858.81	2.5	28.64
102	0.0047	0.0003	0.0038	0.00733	0.119	0.0645	0.07	0.0137	0.0187	N/A	317858.81	8.05	25.73
103	0.0379	0.00308	0.0356	0.119	0.584	0.386	0.366	0.0476	2.06	N/A	317858.81	20.93	80.18
104	0.004	0.00048	0.0121	0.0589	0.643	0.249	0.215	0.00515	0.127	N/A	317858.81	131.28	326.49
105	0	0	0.0032	0.0195	0.448	0.347	0.359	0.00375	0.0598	N/A	317858.81	21.88	55.15
106	0.0048	0	0.0022	0.0323	0.235	0.193	0.196	0.0089	0.00519	N/A	317858.75	27.13	30.18
107	0.0052	0.00051	0.0035	0.00535	0.114	0.079	0.0679	0.0058	0.0013	N/A	317858.78	2.91	23.32
108	0	0	0.0003	0.00004	0.042	0.0333	0.0329	0.00195	0.00046	N/A	317858.75	2.98	18.42
109	0.0059	0.00025	0.0066	0.0077	0.16	0.0408	0.0501	0.0089	0.0171	N/A	317858.72	6.34	26.74
110	0.0385	0.00345	0.0002	0.00277	0.369	0.255	0.288	0.122	0.0101	N/A	317858.75	21.04	35.28
111	0.0061	0.00043	0.0105	0.0122	0.217	0.221	0.216	0.0061	0.00242	N/A	317858.75	13.45	31.04
112	0.138	0.0106	0.0001	0	0.004	0.012	0.0057	0.0036	0.0013	9.27	21.27	2.76	131.73
113	0.192	0.0132	0.005	0.0533	0.0389	0.0374	0.0154	0.0136	0.0173	28.24	23.78	3.36	137.4
114	0.177	0.0164	0.0045	0.0097	0.032	0.0056	0.0072	0.006	0.0031	18.92	31.79	0.85	149.21
115	0.536	0.0504	0	0.0039	0.022	0	0	0.0809	0.0186	3.05	70.7	6.78	166.06
116	0.0221	0.00199	0.0034	0.00067	0.118	0.121	0.138	0.00396	0	73.25	7.35	3.12	135.85
117	1.97	0.222	0	0.0022	0	0.019	0	0.0572	0.0015	0.355	63.09	0.57	161.02
118	0.0762	0.0084	0.0011	0.00238	0.0458	0.0193	0.0243	0.0054	0.0438	64.17	29.68	0.601	141.64
119	0.096	0.0088	0.0084	0	0.018	0.016	0	0.0035	0.015	23.12	68.72	0.76	177.54
120	0.0513	0.005	0.0025	0.0093	0.0351	0	0.0129	0.019	0.0031	53.11	55.54	1.51	164.77
121	0.14	0.0113	0.006	0.198	0.054	0.065	0.0528	0.0102	0.0345	0.645	55.41	1.29	152.19
122	0.165	0.0116	0	0.00164	0.0458	0.0134	0.0253	0.0109	0.00017	39.28	26.1	1.59	158.76
123	0.154	0.0152	0	0.0019	0	0.0232	0	0.008	0.0067	14.13	34.67	1.08	146.12
124	1.255	0.1066	0.0006	0	0.0316	0.006	0.0425	0.162	0.0008	50.91	32.98	47.36	149.51
125	0.159	0.0072	0.0172	0	0	0	0.031	0.0204	0	N/A	17.46	3.14	103.51
126	0.58	0.0423	0.0073	0.0042	0.128	0	0.019	0.143	0.144	N/A	28.53	6.1	102.88
127	0.049	0.0013	0.0125	0.0004	0.126	0.042	0.034	0.0547	0.328	N/A	18.99	0.66	112.93

Analysis	Yb^{173}	Lu^{175}	Hf^{177}	Ta^{181}	Pb^{206}	Pb^{207}	Pb^{208}	Th^{232}	U^{238}	Co^{59}	Si^{29}	Mg^{25}	Fe^{57}
128	0.138	0.017	0	0.0023	0.054	0	0	0.0373	0.0322	N/A	62.41	1.63	112.53
129	0.179	0.0123	0.0016	0.007	0.111	0.035	0.0076	0.178	0.205	N/A	8893.68	3.3	90.48
130	0.0014	0.00048	0.006	0.00197	0.472	0.239	0.291	0.168	0.0678	0.00016	303835.63	0.332	137.11
131	0.0016	0.00048	0.0008	0.00149	0.479	0.34	0.368	0.207	0.0547	0.00026	303835.63	0.096	119.16
132	0.0004	0.00131	0.006	0.00471	0.436	0.345	0.426	0.21	0.0819	0	303835.63	0	114.02
133	0.0006	0	0.0017	0.00247	0.929	0.935	0.905	0.164	0.0389	0.00068	303835.63	0.05	104.2
134	0.0003	0	0	0.00097	1.359	1.431	1.395	0.0322	0.00119	0.00052	303835.63	0.02	105.49
135	0	0.00024	0.0067	0.00135	0.123	0.127	0.1358	0.0202	0.00116	0.00211	303835.63	0.051	92.96
136	0.0005	0	0.0023	0.00125	0.868	0.936	0.941	0.00477	0.0003	0.00128	303835.63	0.086	95.41
137	0.0018	0.0003	0.0235	0.00302	0.655	0.577	0.573	0.195	0.1143	0.00087	303835.63	0.195	93.69
138	0.0144	0.00039	0.0126	0.0038	0.427	0.278	0.274	0.172	0.179	0	303835.63	0.197	118.2
139	0.0028	0	0.0017	0.00119	0.433	0.41	0.439	0.0904	0.0189	0	303835.63	0.046	133.69
140	0.0033	0	0.0093	0.00124	0.72	0.76	0.8	0.146	0.0048	0.00162	303837.31	0.691	132.72
141	0	0.00058	0.0095	0.0013	1.85	1.82	1.77	0.165	0.099	0.00224	303837.47	0.89	136.01
142	0.001	0.00002	0.0075	0.0007	1.23	1.31	1.31	0.071	0.0052	0.00097	303837.63	0.216	132.16
143	0.034	0.0044	0.21	4.49	8.1	6.98	7.18	0.43	1.36	0.0084	303838.28	9.64	1154.24
144	0.54	0.063	0.22	0.088	20.73	15.83	17.48	0.32	1.87	0.0129	303838.47	26.38	652.71
145	0.0113	0.00125	0.074	0.046	34.14	27.05	29.46	0.58	0.9	0.0088	303838.59	1.19	20.27
146	0.0028	0.00067	0.0961	0.0047	1.017	0.776	1.929	0.465	0.1096	0.004	303835.59	0.174	667.12
147	0	0.00043	0.0171	0.00186	1.575	1.422	1.491	0.226	0.052	0.0013	303835.59	0.654	363.57
148	0.0019	0.00019	0	0.0008	0.372	0.383	0.413	0.1166	0.0188	0.00228	317858.78	0.092	678.39
149	0.0046	0.00092	0.025	0.0164	10.34	10.3	10.41	0.214	0.0553	0.00149	303835.59	0.059	244.85
150	0.0033	0.00033	0.002	0.00236	2.24	2.48	2.53	0.0629	0.0125	0.00153	303835.59	4.92	691.35
151	0	0	0.0113	0.00334	12.51	10.67	12.3	0.328	1.439	0.00075	303835.59	104.11	363.27
152	0.0041	0.00026	0.0115	0.00465	1.504	1.35	1.385	0.373	0.1166	0.0007	303835.59	491.18	414.28
153	0	0	0.0008	0.00172	0.0179	0.0143	0.035	0.0724	0.0876	0.00049	303835.59	0.604	127.91
154	0.0064	0.00135	0.0009	0.0108	0.1397	0.148	0.1537	0.0497	0.0236	0.00155	303835.59	2.54	131.76
155	0.004	0.00024	0.0026	0.00241	0.1347	0.127	0.1225	0.01168	0.1209	0.00064	303835.59	12.59	166.37
156	0.0015	0.00023	0.0023	0.01069	0.1315	0.1126	0.1147	0.1001	0.1203	0.00115	303835.59	9.73	149.05
157	0.0007	0	0.0001	0.00174	1.605	1.846	1.763	0.0492	0.0141	0	303835.59	2.24	130.98
158	0.0046	0.00015	0.0007	0.00195	0.538	0.61	0.58	0.0357	0.0199	0.00129	303835.59	32.83	148.18
159	0	0	0.0018	0.00173	0.017	0.0119	0.0317	0.0713	0.00348	0.00022	303835.59	2.69	121.74
160	0.0025	0	0.0027	0.0157	0.206	0.192	0.1956	0.0861	0.0213	0.00039	303835.59	4.81	139.3
161	0.013	0.00087	0.002	0.00576	0.332	0.1468	0.1857	0.1071	0.323	0.00099	303835.59	1.95	144.3
162	0.0021	0.00067	0.0031	0.00191	0.0867	0.0551	0.0825	0.1081	0.0145	0.00116	303835.59	34.39	138.16
163	0.037	0.00258	0.004	0.0197	1.546	0.212	0.1263	0.1642	5.25	0.00771	303835.59	301.27	169.27
164	0.0022	0.00031	0.0066	0.00494	0.458	0.249	0.299	0.472	5.52	0	303834.44	2.07	247.22

Analysis	Yb^{173}	Lu^{175}	Hf^{177}	Ta^{181}	Pb^{206}	Pb^{207}	Pb^{208}	Th^{232}	U^{238}	Co^{59}	Si^{29}	Mg^{25}	Fe^{57}
165	0.0059	0.0002	0	0.0066	0.0309	0.0183	0.0715	0.29	0.0067	0.00276	303834.5	1.121	389.57
166	0.0125	0.00026	0.052	0.502	0.47	0.134	0.202	0.28	0.122	0.00239	303834.56	39.2	2507.32
167	0.0211	0.00012	0	0.0284	0.178	0.072	0.332	1.2	0.056	N/A	303835.63	0.48	87.5
168	0.0127	0.00111	0.0153	0.0845	0.817	0.745	0.815	1.14	0.159	N/A	303835.63	1.27	70.2
169	0.0033	0.00038	0.0062	0.0297	0.573	0.479	0.615	0.696	0.0943	N/A	303835.63	0.689	87.53
170	0.0013	0.0003	0.0088	0.0092	0.123	0.0707	0.103	0.16	0.0674	N/A	303835.63	1.31	110
171	0.0005	0	0.0235	0.182	0.538	0.234	0.277	0.204	1.254	N/A	303835.63	2.14	102.17
172	0	0.00106	0.003	0.0197	0.102	0.0217	0.18	0.811	0.0757	N/A	303835.63	0.262	86.48
173	0.0004	0.00049	0.0142	0.538	0.397	0.216	0.35	0.773	1.52	N/A	303835.63	4.78	535.26
174	0.0063	0.0006	0.0033	0.0175	0.491	0.443	0.566	0.569	0.079	N/A	303835.63	1.36	124.05
175	0.0034	0.00061	0.0062	0.015	0.509	0.45	0.57	0.502	0.0302	N/A	303835.63	33.05	170.51
176	0.0015	0.00041	0.151	0.36	0.315	0.139	0.151	0.154	0.14	N/A	303835.56	3.98	121.9
177	0.00242	0.00013	0.0235	0.0248	0.117	0.0506	0.07	0.071	0.0298	N/A	303835.56	2.52	117.95
178	0.0029	0	0.0035	0.0121	0.654	0.451	0.429	0.075	0.107	N/A	303835.56	1.75	143.17
179	0.0011	0	0.0084	0.009	0.72	0.531	0.567	0.134	0.0434	N/A	303835.56	5.2	126.5
180	0.0007	0.00002	0.0329	0.0509	0.79	0.552	0.557	0.157	0.079	N/A	303835.53	71.14	355.66
181	0.0006	0.00041	0.006	0.0197	0.506	0.339	0.339	0.114	0.156	N/A	303835.56	29.48	153.26
182	0	0.00001	0.0001	0.00067	0.314	0.316	0.319	0.0113	0.00618	0.00757	172952.58	0.169	3785.96
183	0.0027	0	0	0.00021	0.258	0.265	0.278	0.00428	0.00055	0.0547	172952.58	0.139	4310.46
184	0	0	0.00032	0.00007	0.416	0.45	0.445	0.00109	0.00049	0.00618	172952.58	0.121	4025.18
185	0.00213	0	0.0008	0.00016	0.288	0.296	0.293	0.00031	0.00226	0.00669	172952.58	0.825	4280.21
186	0.00314	0.00017	0.00067	0.00129	0.332	0.322	0.337	0.00103	0.00043	0.00744	172952.58	0.119	3947.8
187	0.00082	0.00015	0.00029	0.00038	0.563	0.575	0.588	0.0025	0.00027	0.00761	172952.58	0.186	3796.81
188	0.0026	0.0006	0	0.0006	2.34	2.34	2.44	0.0058	0.0316	0.0082	172952.58	1.27	4185.38
189	0.00073	0	0.00101	0.00007	0.216	0.236	0.23	0.00071	0	0.00769	172952.58	0.149	3952.61

Appendix III: Fluid inclusion data from Feng 2014

FI ID	Sample	Rock Unit	Type	Character	Eutectic melt (°C)	Ice melt (°C)	Salinity (wt%)	ThV-L (°C)	P (bar)	Tt† (°C)
NTZ-6_B3-1_1	NTZ-6	quartz-bastnäsite	1a	LV	n.d.	-23	24	375	4000	722
NTZ-6_B3-1_2	NTZ-6	quartz-bastnäsite	1a	LVS	n.d.	-23	24	245	4000	479
NTZ-6_B3-1_3	NTZ-6	quartz-bastnäsite	1a	LVS	n.d.	-17	21	400	4000	816
NTZ-6_B3-1_4	NTZ-6	quartz-bastnäsite	1a	LVS	n.d.	-22	23	342	4000	661
NTZ-6_B3-1_5	NTZ-6	quartz-bastnäsite	1a	LV	n.d.	-8	12	158	4000	356
NTZ-6_B3-1_7	NTZ-6	quartz-bastnäsite	1a	LV	n.d.	-18	21	n.d.	4000	-
NTZ-6_B3-1_8	NTZ-6	quartz-bastnäsite	1a	LV	n.d.	-16	19	249	4000	497
NTZ-6_B3-1_9	NTZ-6	quartz-bastnäsite	1a	LV	n.d.	-16	19	100	4000	250
NTZ-6_B3-1_11	NTZ-6	quartz-bastnäsite	1a	LV	n.d.	-12	16	280	4000	571
NTZ-6_B3-2_1	NTZ-6	quartz-bastnäsite	1a	LV	n.d.	-8	12	340	4000	734
NTZ-6_B3-2_2	NTZ-6	quartz-bastnäsite	1a	LV	n.d.	-23	24	146	4000	319
NTZ-6_B3-2_3	NTZ-6	quartz-bastnäsite	1a	LV	n.d.	-23	24	220	4000	436
NTZ-6_B3-2_4	NTZ-6	quartz-bastnäsite	1a	LV	n.d.	-16	19	105	4000	258
NTZ-6_B3-2_5	NTZ-6	quartz-bastnäsite	1a	LV	n.d.	-20	23	198	4000	402
NTZ-6_B3-2_6	NTZ-6	quartz-bastnäsite	1a	LV	n.d.	-9	13	280	4000	584
NTZ-6_B3-2_7	NTZ-6	quartz-bastnäsite	1a	LV	n.d.	-20	22	105	4000	257
NTZ-6_B3-2_8	NTZ-6	quartz-bastnäsite	1a	LV	n.d.	-21	23	149	4000	323
NTZ-6_B2_3_10	NTZ-6	quartz-bastnäsite	1b	LV	n.d.	-22	24	92	4000	239
NTZ-6_B2_3_11	NTZ-6	quartz-bastnäsite	1b	LVS	n.d.	-14	17	84	4000	228
NTZ-6_B2_3_20	NTZ-6	quartz-bastnäsite	1b	LV	n.d.	-19	22	112	4000	267
NTZ-6_B2_3_35	NTZ-6	quartz-bastnäsite	1b	LV	n.d.	-17	21	97	4000	246
X21_P4	X21	phenakite	1c	LV	n.d.	-18	21	n.d.	4000	-
X21_P5	X21	phenakite	1c	LV	n.d.	-21	23	121	4000	281
X21_P7	X21	phenakite	1c	LV	n.d.	-22	24	150	4000	325
X21_P8	X21	phenakite	1c	LV	n.d.	-22	24	140	4000	310
X21_P9	X21	phenakite	1c	LVS	n.d.	-24	25	n.d.	4000	-
X21_P11	X21	phenakite	1c	LV	n.d.	-22	23	n.d.	4000	-
X21_P16	X21	phenakite	1c	LV	n.d.	-23	24	n.d.	4000	-
X21_P17	X21	phenakite	1c	LV	n.d.	-22	24	n.d.	4000	-
X21_P18	X21	phenakite	1c	LV	n.d.	-14	18	n.d.	4000	-
X21_P19	X21	phenakite	1c	LV	n.d.	-24	25	n.d.	4000	-
X21_P20	X21	phenakite	1c	LV	n.d.	-24	25	n.d.	4000	-
82-6_P-1	84-82-6	QP	2a	LVS	n.d.	-9	13	299	4000	627

FI ID	Sample	Rock Unit	Type	Character	Eutectic melt (°C)	Ice melt (°C)	Salinity (wt%)	ThV-L (°C)	P (bar)	Tt† (°C)
82-6_P-3	84-82-6	QP	2a	LVS	n.d.	-10	13	286	4000	593
82-6_P-4	84-82-6	QP	2a	LVS	n.d.	-4	7	286	4000	628
82-6_P-5	84-82-6	QP	2a	LVS	n.d.	-3	5	285	4000	633
82-6_P-6	84-82-6	QP	2a	LVS	n.d.	-5	8	274	4000	593
82-6_P-7	84-82-6	QP	2a	LVS	n.d.	-22	24	107	4000	261
82-6_P-8	84-82-6	QP	2a	LVS	n.d.	-12	16	175	4000	373
82-6_P-11	84-82-6	QP	2a	LVS	n.d.	-12	15	n.d.	4000	-
82-6_P-12	84-82-6	QP	2a	LVS	n.d.	-4	6	298	4000	659
82-6_P-14	84-82-6	QP	2a	LVS	n.d.	-14	17	306	4000	618
82-6_P-16	84-82-6	QP	2a	LVS	n.d.	-9	13	283	4000	591
82-6_P-18	84-82-6	QP	2a	LVS	n.d.	-8	12	342	4000	739
82-6_P-20	84-82-6	QP	2a	LVS	n.d.	-9	12	n.d.	4000	-
82-6_P-22	84-82-6	QP	2a	LVS	-25	-11	15	n.d.	4000	-
82-6_P-145	84-82-6	QP	2a	LVS	n.d.	-6	9	278	4000	596
82-6_P-146	84-82-6	QP	2a	LVS	n.d.	-13	17	305	4000	620
82-6_P-147	84-82-6	QP	2a	LV	n.d.	-13	17	292	4000	592
82-6_P-79	84-82-6	QP	2a	LVS?	n.d.	-1	2	285	4000	646
82-6_P-81	84-82-6	QP	2a	LV	-24	-15	19	291	4000	583
82-6_P-82	84-82-6	QP	2a	LVS?	n.d.	-1	2	291	4000	665
82-6_P-83	84-82-6	QP	2a	LV	n.d.	-1	2	306	4000	717
82-6_P-84	84-82-6	QP	2a	LV	-25	-15	19	153	4000	332
82-6_P-85	84-82-6	QP	2a	LVS	n.d.	-6	10	314	4000	684
82-6_P-86	84-82-6	QP	2a	LV	n.d.	-7	11	248	4000	527
82-6_P-88	84-82-6	QP	2a	LV	-24	-12	16	223	4000	458
82-6_P-89	84-82-6	QP	2a	LV	n.d.	-8	11	291	4000	614
82-6_P-90	84-82-6	QP	2a	LV	-22	-14	18	268	4000	539
82-6_P-91	84-82-6	QP	2a	LV	n.d.	-7	10	289	4000	616
82-6_P-93	84-82-6	QP	2a	LVS	n.d.	-9	13	253	4000	527
82-6_P-94	84-82-6	QP	2a	LV	n.d.	-12	16	212	4000	438
82-6_P-96	84-82-6	QP	2a	LVS	n.d.	-7	10	301	4000	644
82-6_P-97	84-82-6	QP	2a	LV	n.d.	-1	2	293	4000	671
82-6_P-98	84-82-6	QP	2a	LVS	n.d.	-4	6	323	4000	730
82-6_P-149	84-82-6	QP	2a	LVS	n.d.	-4	7	249	4000	544
82-6_P-150	84-82-6	QP	2a	LVS	n.d.	-6	9	294	4000	634
82-6_P-151	84-82-6	QP	2a	LV	n.d.	-5	8	306	4000	671
82-6_P-131	84-82-6	QP	2a	LVS	n.d.	-10	14	307	4000	640
82-6_P-132	84-82-6	QP	2a	LVS	n.d.	-1	1	292	4000	668

FI ID	Sample	Rock Unit	Type	Character	Eutectic melt (°C)	Ice melt (°C)	Salinity (wt%)	ThV-L (°C)	P (bar)	Tt† (°C)
82-6_P-133	84-82-6	QP	2a	LVS	n.d.	-7	11	292	4000	623
82-6_P-139	84-82-6	QP	2a	LVS	n.d.	-3	5	289	4000	643
82-6_P-140	84-82-6	QP	2a	LVS	n.d.	-3	5	313	4000	712
82-6_P-141	84-82-6	QP	2a	LV	n.d.	-3	4	265	4000	584
82-6_P-143	84-82-6	QP	2a	LV	n.d.	-10	13	317	4000	663
82-21_P-8	84-82-21	QP	2b	LV	n.d.	-15	19	270	4000	540
82-21_P-9	84-82-21	QP	2b	LV	-23	-22	23	133	4000	299
82-21_P-45	84-82-21	QP	2b	LV	n.d.	-22	24	262	4000	510
82-21_P-46	84-82-21	QP	2b	LV	n.d.	-22	24	180	4000	372
82-21_P-47	84-82-21	QP	2b	LV	n.d.	-15	19	128	4000	293
82-21_P-53	84-82-21	QP	2b	LV	-24	-18	21	99	4000	248
82-21_P-48	84-82-21	QP	2b	LV	n.d.	-23	24	110	4000	266
82-21_P-49	84-82-21	QP	2b	LV	-25	-22	24	161	4000	342
82-21_P-50	84-82-21	QP	2b	LV	-24	-22	24	106	4000	260
82-21_P-51	84-82-21	QP	2b	LV	n.d.	-21	23	112	4000	268
82-21_P-52	84-82-21	QP	2b	LV	n.d.	-24	25	180	4000	371
83-2_P-1	83-2-11.2	QP	2b	LVS	n.d.	-22	24	109	4000	264
83-2_P-2	83-2-11.2	QP	2b	LV	n.d.	-22	24	91	4000	238
83-2_P-3	83-2-11.2	QP	2b	LV	n.d.	-20	23	n.d.	4000	-
83-2_P-5	83-2-11.2	QP	2b	LV	n.d.	-15	18	161	4000	345
83-2_P-6	83-2-11.2	QP	2b	LV	n.d.	-18	21	141	4000	311
83-2_P-21	83-2-11.2	QP	2b	LV	n.d.	-23	24	129	4000	294
83-2_P-22	83-2-11.2	QP	2b	LV	n.d.	-9	13	141	4000	325
83-2_P-24	83-2-11.2	QP	2b	LV	n.d.	-20	22	114	4000	271
83-2_P-25	83-2-11.2	QP	2b	LV	n.d.	-19	22	180	4000	373
83-2_P-27	83-2-11.2	QP	2b	LV	n.d.	-19	22	142	4000	313
NTZ-7_4_1	NTZ-7	quartz-bastnäsite	3a	LVS	n.d.	-22	24	241	4000	473
NTZ-7_4_3	NTZ-7	quartz-bastnäsite	3a	LVS	n.d.	-22	24	252	4000	492
NTZ-7_4_4	NTZ-7	quartz-bastnäsite	3a	LVS	n.d.	-23	24	266	4000	516
NTZ-7_4_5	NTZ-7	quartz-bastnäsite	3a	LVS	n.d.	-23	24	240	4000	470
NTZ-7_4_6	NTZ-7	quartz-bastnäsite	3a	LV	n.d.	-22	24	147	4000	320
NTZ-7_4_7	NTZ-7	quartz-bastnäsite	3a	LVS	n.d.	-23	24	235	4000	462
NTZ-7_4_8	NTZ-7	quartz-bastnäsite	3a	LVS	n.d.	-23	24	152	4000	328
NTZ-7_4_9	NTZ-7	quartz-bastnäsite	3a	LV	n.d.	-22	24	202	4000	407
NTZ-7_4_10	NTZ-7	quartz-bastnäsite	3a	LV	n.d.	-21	23	113	4000	269
NTZ-7_4_11	NTZ-7	quartz-bastnäsite	3a	LV	n.d.	-22	24	109	4000	264
NTZ-7_4_12	NTZ-7	quartz-bastnäsite	3a	LV	n.d.	-21	23	124	4000	286

FI ID	Sample	Rock Unit	Type	Character	Eutectic melt (°C)	Ice melt (°C)	Salinity (wt%)	ThV-L (°C)	P (bar)	Tt† (°C)
NTZ-7_4_15	NTZ-7	quartz-bastnäsite	3a	LVS	n.d.	-22	24	150	4000	325
NTZ-7_4_16	NTZ-7	quartz-bastnäsite	3a	LV	n.d.	-22	24	185	4000	380
NTZ-7_4_17	NTZ-7	quartz-bastnäsite	3a	LV	n.d.	-22	23	141	4000	311
NTZ-7_4_18	NTZ-7	quartz-bastnäsite	3a	LV	n.d.	-23	24	190	4000	387
NTZ-7_4_19	NTZ-7	quartz-bastnäsite	3a	LV	n.d.	-23	24	136	4000	304
NTZ-7_4_20	NTZ-7	quartz-bastnäsite	3a	LV	n.d.	-21	23	190	4000	388
NTZ-7_6_1	NTZ-7	quartz-bastnäsite	3a	LV	n.d.	-23	24	117	4000	276
NTZ-7_6_2	NTZ-7	quartz-bastnäsite	3a	LV	n.d.	-22	24	128	4000	292
NTZ-7_6_3	NTZ-7	quartz-bastnäsite	3a	LV	n.d.	-24	25	126	4000	290
NTZ-7_6_4	NTZ-7	quartz-bastnäsite	3a	LV	n.d.	-24	25	115	4000	274
NTZ-7_6_6	NTZ-7	quartz-bastnäsite	3a	LV	n.d.	-24	25	115	4000	274
NTZ-7_6_7	NTZ-7	quartz-bastnäsite	3a	LV	n.d.	-7	10	319	4000	688
NTZ-7_6_8	NTZ-7	quartz-bastnäsite	3a	LVS	n.d.	-25	25	240	4000	468
NTZ-7_6_9	NTZ-7	quartz-bastnäsite	3a	LVS	n.d.	-24	25	112	4000	269
NTZ-7_6_10	NTZ-7	quartz-bastnäsite	3a	LV	n.d.	-24	25	173	4000	361
NTZ-7_6_12	NTZ-7	quartz-bastnäsite	3a	LV	n.d.	-23	24	131	4000	297
NTZ-7_6_13	NTZ-7	quartz-bastnäsite	3a	LV	n.d.	-22	24	267	4000	519
82-23_B7_1	84-82-23	quartz-xenotimethorite	3c	LV	n.d.	-25	25	191	4000	389
82-23_B7_2	84-82-23	quartz-xenotimethorite	3c	LV	n.d.	-24	25	138	4000	307
82-23_B7_3	84-82-23	quartz-xenotimethorite	3c	LV	n.d.	-23	24	154	4000	331
82-23_B7_4	84-82-23	quartz-xenotimethorite	3c	LV	n.d.	-24	25	155	4000	333
82-23_B7_5	84-82-23	quartz-xenotimethorite	3c	LVS	n.d.	-24	25	133	4000	300
82-23_B7_6	84-82-23	quartz-xenotimethorite	3c	LV	n.d.	-23	24	110	4000	266
82-23_B7_7	84-82-23	quartz-xenotimethorite	3c	LV	n.d.	-22	24	185	4000	380
82-23_B7_9	84-82-23	quartz-xenotimethorite	3c	LV	n.d.	-17	20	148	4000	323
82-23_B7_11	84-82-23	quartz-xenotimethorite	3c	LVS	n.d.	-25	26	172	4000	359
82-23_B7_12	84-82-23	quartz-xenotimethorite	3c	LV	n.d.	-23	24	164	4000	347
82-23_B7_13	84-82-23	quartz-xenotimethorite	3c	LV	n.d.	-23	24	150	4000	325
TH-34_1_11	TH-34	quartz-bastnäsite	6	LV	n.d.	-24	25	227	4000	447
TH-34_1_12	TH-34	quartz-bastnäsite	6	LV	n.d.	-22	23	241	4000	473
TH-34_1_14	TH-34	quartz-bastnäsite	6	LVS	n.d.	-27	27	219	4000	433
TH-34_1_19	TH-34	quartz-bastnäsite	6	LVS	n.d.	-28	27	276	4000	525
82-13_B16_3	84-82-13	quartz-bastnäsite	6	LV	-21	-5	8	223	4000	486
82-13_B16_4	84-82-13	quartz-bastnäsite	6	LV	-20	-6	9	275	4000	590
82-13_B16_5	84-82-13	quartz-bastnäsite	6	LV	-24	-5	8	268	4000	580
82-13_B16_6	84-82-13	quartz-bastnäsite	6	LV	n.d.	-3	5	252	4000	554
82-13_B16_7	84-82-13	quartz-bastnäsite	6	LV	n.d.	-3	5	242	4000	533

FI ID	Sample	Rock Unit	Type	Character	Eutectic melt (°C)	Ice melt (°C)	Salinity (wt%)	ThV-L (°C)	P (bar)	Tt† (°C)
82-13_B16_8	84-82-13	quartz-bastnäsite	6	LV	-22	-5	8	230	4000	500
82-13_B16_11	84-82-13	quartz-bastnäsite	6	LV	-22	-11	15	237	4000	488
82-13_B16_17	84-82-13	quartz-bastnäsite	6	LV	-22	-4	7	282	4000	618
82-13_B4_1	84-82-13	quartz-bastnäsite	6	LV	-21	-12	16	315	4000	647
82-13_B4_3	84-82-13	quartz-bastnäsite	6	LV	n.d.	-13	17	315	4000	642
82-13_B4_4	84-82-13	quartz-bastnäsite	6	LV	-19	-6	9	319	4000	697
82-13_B4_5	84-82-13	quartz-bastnäsite	6	LV	-20	-2	4	294	4000	665
82-13_B4_6	84-82-13	quartz-bastnäsite	6	LV	-20	-8	12	308	4000	654
82-13_B4_7	84-82-13	quartz-bastnäsite	6	LV	-21	-7	10	256	4000	543
82-13_B4_8	84-82-13	quartz-bastnäsite	6	LV	-24	-22	24	184	4000	378
82-13_B18_1	84-82-13	quartz-bastnäsite	6	LV	-23	-5	7	267	4000	578
82-13_B18_3	84-82-13	quartz-bastnäsite	6	LV	-22	-5	7	325	4000	723
82-13_B18_4	84-82-13	quartz-bastnäsite	6	LV	-22	-6	9	332	4000	732
82-13_B18_5	84-82-13	quartz-bastnäsite	6	LV	-19	-4	7	283	4000	621
82-13_B18_7	84-82-13	quartz-bastnäsite	6	LVS	n.d.	-6	10	293	4000	631
82-13_B18_9	84-82-13	quartz-bastnäsite	6	LV	-23	-6	9	300	4000	648
82-13_B18_11	84-82-13	quartz-bastnäsite	6	LV	n.d.	-5	8	299	4000	653
82-13_B18_12	84-82-13	quartz-bastnäsite	6	LV	-21	-6	9	317	4000	691
82-13_B18_13	84-82-13	quartz-bastnäsite	6	LV	-23	-6	9	263	4000	563
82-13_B18_15	84-82-13	quartz-bastnäsite	6	LV	-22	-10	14	307	4000	640
82-13_B18_19	84-82-13	quartz-bastnäsite	6	LVS	n.d.	-10	14	278	4000	575
82-13_B17_1	84-82-13	quartz-bastnäsite	6	LV	-21	-9	13	298	4000	625
82-13_B17_2	84-82-13	quartz-bastnäsite	6	LVS	n.d.	-8	11	287	4000	605

†entrapment temperature calculated using method provided in Steele-MacInnis et al. 2012

Appendix IV: Granite sample whole rock analyses

Sample number	Sample	Easting	Northing	From	To	Dens.	Distance	Ba (ppm)	Ce (ppm)
G0692373	K01	415510	6886626	-	-	-	50	546	280
G0692374	L10-251 10.75	415271	6886532	10.75	11.15	2.67	306.82	496	260
G0692375	K02	415027	6886287	-	-	-	640.09	107	294
G0692376	K03	415034	6886349	-	-	-	600.73	156	189
G0692377	K04	415012	6886158	-	-	-	733.39	92.2	326
G0692378	K05	414894	6886042	-	-	-	898.83	131	246
G0692379	K06	414829	6885826	-	-	-	1100.60	70.5	545
G0692380	K07	414516	6885463	-	-	-	1579.90	392	897
G0692381	G1	414408	6884379	-	-	-	2552.68	117	277
G0692382	G2	414098	6882353	-	-	-	4550.25	161	266
G0692383	L11-373	416287	6885698	14	14.4	2.68	190.15	124.5	153.5
G0692384	L11-373	416287	6885698	69.15	69.65	2.67	135	151	141.5
G0692385	L11-373	416287	6885698	131.37	132.05	2.67	72.78	262	240
G0692386	L11-373	416287	6885698	169.4	170.2	2.69	34.75	282	361
G0692387	L11-373	416287	6885698	187.7	188.4	2.68	16.45	282	406
G0692388	L11-373	416287	6885698	198.3	199	2.69	5.85	306	196
G0692389	L11-373	416287	6885698	203.1	203.5	2.72	1.05	92.1	261
G0692390	L11-373	416287	6885698	203.65	204.05	2.72	0.4	123.5	144.5
G0692391	L11-377	416287	6885698	2.6	3.05	2.71	289.55	253	257
G0692392	L11-377	416287	6885698	93.2	93.65	2.70	198.95	149	188.5
G0692393	L11-377	416287	6885698	171	171.5	2.65	121.15	234	197
G0692394	L11-377	416287	6885698	219.15	219.55	2.64	73	182	181.5
G0692395	L11-377	416287	6885698	251.85	252.3	2.67	40.3	363	172
G0692396	L11-377	416287	6885698	274.35	274.75	2.68	17.8	177.5	192
G0692397	L11-377	416287	6885698	282.05	282.55	2.61	10.1	132	605
G0692398	L11-377	416287	6885698	291.65	292	2.77	1.15	180	232
G0692399	L11-377	416287	6885698	186.2	186.65	2.65	105.95	91.6	199.5
VeinB*						1.03	45.75	-0.28	2.07
VeinC**						1.00	44.95	-0.50	0.10

Sample number	Co (ppm)	Cr (ppm)	Cs (ppm)	Cu (ppm)	Dy (ppm)	Er (ppm)	Eu (ppm)	Ga (ppm)	Gd (ppm)	Hf (ppm)	Ho (ppm)
G0692373	0.9	10	1.8	<5	17.3	8.13	5.87	55.8	22	23.3	3.22
G0692374	3	10	1.95	143	15.1	7.05	5.74	53	19.35	23.8	2.8
G0692375	0.8	30	2.71	<5	17.4	8.12	3.46	57.6	23.4	20.3	3.32
G0692376	0.7	20	3	9	12.35	5.5	2.59	55.6	15.9	17.7	2.31
G0692377	<0.5	20	1.76	<5	17.8	7.99	3.51	56.3	22.9	30.3	3.27
G0692378	0.5	20	0.95	<5	18.1	9.17	3.16	54.6	22.3	44.9	3.5
G0692379	0.6	20	1.33	<5	21.4	9.01	5.68	53.8	36.6	64.5	3.81
G0692380	0.7	10	1.27	7	48.6	21.4	8.45	53	64.5	65.3	8.87
G0692381	0.7	20	1.61	<5	18.35	8.68	3.11	54.3	21.6	26.8	3.49
G0692382	0.8	20	0.89	20	10.1	4.27	1.64	49.5	13.4	14.2	1.83
G0692383	<0.5	20	0.58	<5	10.6	5.23	2.62	54.9	13.55	11.3	2.07
G0692384	<0.5	20	0.86	<5	9.34	4.68	2.45	56.6	12	14.4	1.84
G0692385	0.7	20	0.98	7	14.85	6.86	4.43	60.2	18.7	25.7	2.76
G0692386	1	10	0.8	<5	25.5	10.9	6.69	61.8	31.5	26.2	4.53
G0692387	0.7	10	0.9	<5	21.7	8.66	6.15	67.2	29.4	15.6	3.76

Sample number	Co (ppm)	Cr (ppm)	Cs (ppm)	Cu (ppm)	Dy (ppm)	Er (ppm)	Eu (ppm)	Ga (ppm)	Gd (ppm)	Hf (ppm)	Ho (ppm)
G0692388	0.9	10	0.91	6	14.3	6.52	4.2	61.1	18.15	19	2.66
G0692389	0.5	10	0.51	<5	19.4	7.88	4.5	64.7	25.5	10.2	3.39
G0692390	1.8	10	0.29	26	9.8	4.17	2.59	66.1	12.95	11.6	1.78
G0692391	2	10	0.9	6	19.9	9.45	4.64	60.1	24.2	26.8	3.78
G0692392	1.5	10	0.94	11	13.05	6.12	3.01	55.5	16.5	16.6	2.4
G0692393	0.7	20	0.85	<5	13.35	6.09	3.91	59.3	17	17.3	2.47
G0692394	0.5	20	0.71	<5	12	5.5	2.89	53.4	14.95	16	2.26
G0692395	0.7	20	0.73	<5	13.05	5.85	3.89	52.9	15.5	18.5	2.37
G0692396	0.7	20	0.71	5	10.7	4.82	2.86	57.1	14.05	11.1	1.95
G0692397	0.7	10	1.01	<5	34.6	14.35	8.07	55.4	48.6	12.2	6.06
G0692398	1	10	0.41	15	14.3	6.19	3.3	69.6	17.8	18.1	2.52
G0692399	1.1	10	0.16	<5	16.5	7.42	2.99	57.5	17.85	12.2	3.05
VeinB*	-0.03	-0.51	0.39	-	2.15	1.90	1.75	-0.05	2.37	0.07	2.03
VeinC**	1.20	-0.50	-0.77	-	0.38	0.35	0.04	0.08	0.20	-0.24	0.35

Sample number	La (ppm)	Lu (ppm)	Mo (ppm)	Nb (ppm)	Nd (ppm)	Ni (ppm)	Pb (ppm)	Pr (ppm)	Rb (ppm)	Sm (ppm)	Sn (ppm)
G0692373	131.5	1.07	8	146.5	147.5	<5	7	37	173	26.5	8
G0692374	127	0.82	7	136	131.5	<5	19	32.9	154.5	23.6	6
G0692375	145.5	0.87	4	108	148	<5	5	37.9	180	27.4	7
G0692376	87.9	0.53	7	110	97	<5	12	24.3	163.5	18.25	7
G0692377	160.5	0.95	2	164.5	155.5	<5	8	41.2	185.5	27.7	10
G0692378	107	1.33	4	185.5	139.5	<5	<5	33.9	150.5	26.3	9
G0692379	259	1.05	4	522	268	<5	<5	70.4	197	48.2	17
G0692380	409	2.36	11	255	442	<5	14	115	235	80.5	20
G0692381	134	1.03	11	122	134.5	<5	5	35	214	25.7	7
G0692382	126.5	0.43	2	146.5	117.5	<5	<5	32.6	158	19.1	7
G0692383	73	0.62	11	67.5	83.7	<5	6	20.5	175	15.8	4
G0692384	68.9	0.48	10	71.7	72.2	<5	8	18.2	149	13.7	5
G0692385	114	0.78	8	136	124.5	<5	8	31.1	175.5	22.9	5
G0692386	199	1.05	8	176	196	<5	8	50.2	160	39.7	11
G0692387	213	0.89	5	109.5	211	<5	8	55.3	204	39.3	5
G0692388	94.4	0.79	5	90.4	108.5	<5	8	26.5	178.5	22.5	4
G0692389	144	0.69	4	124	148	<5	<5	36.7	153	31.4	11
G0692390	71.7	0.52	4	72.4	76.7	<5	14	18.95	94	15.95	1
G0692391	138	1.1	9	132.5	146.5	<5	9	37	132.5	29.6	7
G0692392	93.3	0.78	11	116	99.9	<5	7	25.2	151.5	20.5	5
G0692393	97.5	0.69	6	83.8	104.5	<5	<5	26	169.5	21.5	2
G0692394	95.3	0.56	8	88.2	88.9	<5	5	22.8	135	17.75	3
G0692395	81.9	0.75	7	94.6	97.3	<5	7	23.6	145.5	20.2	6
G0692396	102	0.56	10	78.1	94.8	<5	6	24.4	148	18.2	4
G0692397	304	1.91	33	127	318	<5	<5	82.7	202	63.9	10
G0692398	133.5	0.56	14	134	123	<5	<5	31.9	132	24	20
G0692399	108.5	0.87	5	106.5	112	<5	<5	28.5	13.1	21.7	3
VeinB*	1.90	2.32	2.21	0.58	2.27	-	-	2.30	0.33	2.42	1.44
VeinC**	0.14	0.56	-0.37	0.21	0.26	-	-	0.25	-0.90	0.22	0.00

Sample number	Sr (ppm)	Ta (ppm)	Tb (ppm)	Th (ppm)	Tl (ppm)	Tm (ppm)	U (ppm)	V (ppm)	W (ppm)	Y (ppm)	Yb (ppm)
G0692373	72	9	3.02	17.8	<0.5	1.09	3.67	<5	3	75.9	6.98

Sample number	Sr (ppm)	Ta (ppm)	Tb (ppm)	Th (ppm)	Tl (ppm)	Tm (ppm)	U (ppm)	V (ppm)	W (ppm)	Y (ppm)	Yb (ppm)
G0692374	95.9	8.5	2.63	22.2	<0.5	0.94	4.06	<5	15	72.8	5.77
G0692375	16	6.7	3.11	25.7	<0.5	1.05	2.76	<5	5	93.6	6.23
G0692376	24.8	6.9	2.2	17.9	<0.5	0.69	2.6	<5	6	65.2	3.92
G0692377	38.3	9.7	3.16	34.1	<0.5	1.02	4.11	<5	6	91.1	6.38
G0692378	16	12.4	3.12	19.7	<0.5	1.31	5.4	<5	3	89.4	8.58
G0692379	15.3	22.1	4.33	29.9	<0.5	1.15	11.25	<5	5	101.5	7.19
G0692380	105.5	12.8	8.77	87.3	<0.5	2.72	14.85	<5	4	206	16.6
G0692381	18.4	8.3	3.16	27.1	<0.5	1.16	3.94	<5	3	90.3	6.98
G0692382	14.5	8.8	1.85	18.85	<0.5	0.54	2.76	<5	5	50.3	3.2
G0692383	34.1	4.1	1.85	10.45	<0.5	0.68	1.78	<5	2	58.6	4.17
G0692384	38.6	4.4	1.64	11.6	<0.5	0.59	2.07	<5	2	54.7	3.52
G0692385	56.9	9.4	2.58	19.3	<0.5	0.88	3.85	<5	2	77.8	5.4
G0692386	61	10.7	4.8	22.1	<0.5	1.38	4.93	<5	4	119	7.63
G0692387	65.9	6.2	4.23	21.4	<0.5	1.07	2.95	<5	5	97.8	6.25
G0692388	61.2	5.5	2.73	9.77	<0.5	0.86	2.49	<5	4	69.5	5.19
G0692389	27.7	4.7	3.82	33.5	<0.5	0.94	2.33	<5	7	90.8	5.29
G0692390	42.4	4	1.91	12	<0.5	0.54	1.46	<5	6	50.4	3.32
G0692391	46.9	8.3	3.66	18.55	<0.5	1.26	5.09	<5	4	98.5	7.41
G0692392	37.2	6.4	2.45	9.99	<0.5	0.77	2.53	<5	4	69	4.94
G0692393	57.3	4.6	2.53	10.75	<0.5	0.78	2.17	<5	4	64.9	4.5
G0692394	41.1	6.2	2.23	10.8	<0.5	0.69	2.69	<5	4	59.8	4.04
G0692395	79.5	7.6	2.38	12.4	<0.5	0.77	2.98	<5	3	55.2	5.02
G0692396	47	4.5	2.01	8.87	<0.5	0.62	1.84	<5	6	53.8	3.69
G0692397	33.6	5.3	6.94	63.7	<0.5	1.84	1.21	<5	5	167	11.85
G0692398	30.8	7.7	2.71	14.5	<0.5	0.75	3.13	<5	5	68	4.03
G0692399	34.7	4.5	2.95	12.95	<0.5	0.95	1.69	<5	17	81.8	5.74
VeinB*	-0.30	0.15	2.36	6.00	-	1.89	-0.36	-	-0.19	2.02	2.13
VeinC**	-0.15	-0.27	0.33	0.20	-	0.38	-0.37	-	3.26	0.37	0.42

Sample number	Zn (ppm)	Zr (ppm)	REE (wt%)	SiO_2 (wt%)	Al_2O_3 (wt%)	Fe_2O_3 (wt%)	Fe_2O_3 (wt%)†	FeO (wt%)†	CaO (wt%)
G0692373	34	793	0.065418	64.5	14.85	6.99	1.53	4.92	0.46
G0692374	80	968	0.06023	66.6	14.7	4.47	1.16	2.98	0.64
G0692375	35	763	0.068186	70.7	11.25	5	1.10	3.51	1.03
G0692376	37	602	0.043814	69.6	12.1	4.96	1.06	3.51	1.11
G0692377	34	1040	0.073668	70.5	11.25	5.63	2.90	2.46	1.21
G0692378	25	1680	0.058937	71.3	11.1	4.69	1.96	2.46	0.95
G0692379	34	2400	0.121042	71.8	10.55	5.29	1.84	3.11	0.96
G0692380	133	3150	0.201077	65.9	13.55	5.95	2.43	3.17	0.97
G0692381	60	974	0.063876	70.1	11.65	5.28	2.75	2.28	0.81
G0692382	16	330	0.056636	69.8	12.2	3.71	0.81	2.61	0.52
G0692383	52	425	0.036739	70.2	12.35	6.24	3.71	2.28	1.12
G0692384	32	618	0.033284	69.7	13	5.73	2.42	2.98	1.07
G0692385	30	974	0.055864	64.8	14.6	7.09	3.34	3.38	1.21
G0692386	70	843	0.088968	65	13.85	7.08	3.03	3.65	1.17
G0692387	89	584	0.095141	64.9	14.4	5.99	3.10	2.6	1.47
G0692388	46	664	0.04768	65.9	14	6.46	2.92	3.19	1.12
G0692389	65	386	0.065581	63.8	14.75	6.11	4.25	1.68	1.9
G0692390	581	431	0.034643	60.8	16.3	2.62	0.68	1.75	3.38
G0692391	51	1040	0.06465	65.5	12.8	6.37	1.19	4.66	1.43
G0692392	49	619	0.045222	65.1	11.25	8.27	2.20	5.47	1.51

Sample number	Zn (ppm)	Zr (ppm)	REE (wt%)	SiO_2 (wt%)	Al_2O_3 (wt%)	Fe_2O_3 (wt%)	Fe_2O_3 (wt%)†	FeO (wt%)†	CaO (wt%)
G0692393	37	710	0.047182	69.7	12.5	5.46	2.15	2.98	1.09
G0692394	27	566	0.042857	69.5	12.3	5.26	2.23	2.73	0.99
G0692395	41	539	0.042098	67.5	13.35	6.35	3.10	2.93	0.83
G0692396	81	396	0.044826	67.9	12.4	6.27	2.82	3.11	1.11
G0692397	106	428	0.142512	59.9	11.35	9.48	6.53	2.66	2.64
G0692398	43	559	0.056466	61.8	14.95	8.69	5.96	2.46	1.2
G0692399	20	512	0.050002	49.7	13.4	3.53	0.64	2.6	7.97
VeinB*	0.27	0.05	2.10	-0.14	-0.11	0.47	1.26	-0.17	1.32
VeinC**	-0.26	-0.09	0.17	-0.28	0.09	-0.33	-0.71	-0.05	7.06

Sample number	MgO (wt%)	Na_2O (wt%)	K_2O (wt%)	Cr_2O_3 (wt%)	TiO_2 (wt%)	MnO (wt%)	P_2O_5 (wt%)	SrO (wt%)	BaO (wt%)	LOI (wt%)	Total (wt%)
G0692373	1.35	4.89	5.42	<0.01	0.51	0.14	0.07	0.01	0.06	1.19	100.5
G0692374	0.5	4.69	5.59	<0.01	0.52	0.1	0.05	0.01	0.05	2.3	100
G0692375	0.97	3.54	4.56	<0.01	0.64	0.08	0.01	<0.01	0.01	2.29	100
G0692376	0.91	3.76	5.01	<0.01	0.83	0.07	<0.01	<0.01	0.02	1.89	100.5
G0692377	0.2	3.55	4.77	<0.01	0.46	0.07	0.02	<0.01	0.01	1.79	99.5
G0692378	0.59	3.41	4.43	<0.01	0.5	0.07	<0.01	<0.01	0.01	1.49	98.5
G0692379	0.54	3.14	4.61	<0.01	0.43	0.06	<0.01	<0.01	0.01	0.9	98.3
G0692380	0.4	4.81	5.68	<0.01	0.33	0.1	0.05	0.01	0.04	1.3	99.1
G0692381	0.68	3.79	4.7	<0.01	0.4	0.06	0.01	<0.01	0.01	0.8	98.3
G0692382	0.31	3.97	4.9	<0.01	0.21	0.07	<0.01	<0.01	0.02	2.47	98.2
G0692383	0.38	3.78	5.33	<0.01	0.55	0.05	0.02	<0.01	0.01	1.69	101.5
G0692384	0.28	4.13	5.23	<0.01	0.47	0.07	0.01	<0.01	0.02	1.69	101.5
G0692385	0.45	4.88	5.46	<0.01	0.46	0.07	0.06	0.01	0.03	1.3	100.5
G0692386	0.57	5.28	5.18	<0.01	0.48	0.11	0.07	0.01	0.03	1.6	100.5
G0692387	0.47	5.92	5.58	<0.01	0.5	0.11	0.06	0.01	0.03	1.79	101
G0692388	0.46	5.15	5.33	<0.01	0.41	0.09	0.06	0.01	0.03	1.89	101
G0692389	0.72	5.99	5.09	<0.01	0.48	0.11	0.05	<0.01	0.01	1.69	100.5
G0692390	1.1	7.54	4.22	<0.01	0.47	0.22	0.05	<0.01	0.01	4.49	101
G0692391	1.41	3.73	4.46	<0.01	0.58	0.06	0.07	<0.01	0.03	2.98	99.4
G0692392	1.16	3.68	4.69	<0.01	0.94	0.2	0.05	<0.01	0.02	2.89	99.8
G0692393	0.51	4.4	4.91	<0.01	0.47	0.09	0.04	0.01	0.03	1.49	100.5
G0692394	0.39	4.49	4.68	<0.01	0.53	0.06	0.02	<0.01	0.02	2.68	101
G0692395	0.38	4.93	5.21	<0.01	0.47	0.07	0.04	0.01	0.04	2.1	101.5
G0692396	0.41	4.75	5.24	<0.01	0.38	0.09	0.05	<0.01	0.02	2.7	101.5
G0692397	1.52	5.32	5.54	<0.01	0.69	0.12	0.04	<0.01	0.01	3.27	99.9
G0692398	0.43	7.14	4.89	<0.01	0.71	0.11	0.02	<0.01	0.02	0.99	101
G0692399	3.62	7.07	2.16	<0.01	0.46	0.22	0.06	<0.01	0.01	11.4	99.6
VeinB*	2.61	0.09	0.03	-	0.77	0.30	-0.22	-	-0.51	0.18	-0.04
VeinC**	8.30	0.58	-0.54	-	-0.13	2.67	2.01	-	-0.50	3.26	-0.01

*Mass change conserving volume for Vein type B (G0692397/G0692396)

** Mass change conserving volume for Vein type C (G0692399/G0692394)

†Recalculated value

Appendix V: Activities calculated

FIA	1, 2b, 3, 4, 5	2a and 6
T (˚C)	367	592
P (bar)	4000	4000
mNa+	4.24	2.14
mK+	0.27	0.04
mCa2+	0.01	0.00
Ionic Strength	4.53	2.18
Molality	9.04	4.35
A	0.82	1.16
B	0.37	0.40
bgamma	0.07	0.02
logγNa+	-0.18	-0.51
γNa+	0.66	0.31
aNa+	2.80	0.66
log(aNa+)	0.45	-0.18
logγK+	-0.28	-0.62
γK+	0.53	0.24
aK+	0.14	0.01
log(aK+)	-0.85	-2.04
logγCa2+	-0.97	-1.52
γCa+	0.11	0.03
aCa+	0.00	0.00
aNa+/aK+	19.84	72.65

constant	a-halo	z
Na+	4.0	1
K+	3.0	1
Ca2+	6.0	2

Appendix VI: Isotope analyses

Sample	Batch	Mineral	Type	Yield	$\delta^{18}O_{VSMOW}$	Amt%H2O	δD_{VSMOW}	R_{samp}/R_{stand}	367	592	δD_{VSMOW}
L10-253-164	1	Quartz	GLG	14.8	9.0	-	-	1.00897	4.10	7.36	-
L10-232a 78.25	2	Quartz	Albitite	18.4	13.7	0.23	-61	1.01370	8.81	12.08	-61
L11-380 28	2	Quartz	Albitite	16.1	16.4	0.39	-35	1.01636	11.45	14.74	-35
L10-232A 65.25	1	Albite	Albitite	12.8	12.6	0.19	-78	1.01256	8.83	12.08	-78
L10-232A 75.2	1	Albite	Albitite	11.3	13.6	0.19	-123	1.01360	9.86	13.11	-123
L11-380 28	2	Albite	Albitite	10.2	19.9	0.19	-96	1.01990	16.14	19.41	-96
L10-232a 94.7	2	Albite	Albitite	10.1	15.8	0.14	-106	1.01580	12.06	15.31	-106
L09-203 6.5	2	Albite	Albitite	14.2	12.5	0.12	-113	1.01250	8.77	12.02	-113
L09-192 154.2	2	Albite	White	9.1	14.4	0.07	-109	1.01440	10.66	13.92	-109
L10-232A 75.2	1	Microcline	Albitite	10.8	10.6	0.11	-125	1.01060	6.87	10.11	-125
L10-232A 75.2 B	1	Microcline	Albitite	11.4	13.8	0.09	-104	1.01379	10.06	13.31	-104
L09-203 6.5	2	Microcline	Albitite	9.9	16.4	0.11	-115	1.01640	12.66	15.91	-115
L10-232a 94.7	2	Microcline	Albitite	12.3	14.4	0.09	-153	1.01440	10.66	13.92	-153
L10-253 349.1	1	Microcline	Deep	13.5	11.6	0.11	-112	1.01161	7.88	11.13	-112
L10-253 349.1	2	Microcline	Deep	10.4	15.0	0.11	-115	1.01500	11.26	14.52	-115
TZ-23		Quartz	T-Zone	-	11.5	0.14	-64	1.01150	6.62	9.88	-64
TZ-119		Quartz	T-Zone	-	9.2	0.13	-73	1.00920	4.33	7.59	-73
TZ-122		Quartz	T-Zone	-	11.0	0.16	-57	1.01100	6.12	9.38	-57
TZ-132/2A		Quartz	T-Zone	-	8.5	0.13	-76	1.00850	3.63	6.89	-76
TZ-132/2B		Quartz	T-Zone	-	n.d.	0.13	-49				-49

Appendix VII: Reactions and thermodynamic constants

Reaction	Equation
aegirine -> hematite	2NaFeSi2O6+2H+->Fe2O3+4SiO2(aq)+2Na++H2O
aegirine -> magnetite	6NaFeSi2O6+6H+->2Fe3O4+12SiO2(aq)+6Na++3H2O+0.5O2
aegirine + albite -> daphnite	H2O+14H++10NaFeSi2O6+4NaAlSi3O8->2Fe5Al2Si3O10(OH)8+14Na++26SiO2(aq)+5/2O2
aegirine + microcline -> daphnite	H2O+14H++10NaFeSi2O6+4KAlSi3O8->2Fe5Al2Si3O10(OH)8+10Na++4K++26SiO2(aq)+5/2O2
aegirine + muscovite -> daphnite	3H2O+34H++30NaFeSi2O6+4KAl3Si3O10(OH)2->6Fe5Al2Si3O10(OH)8+30Na++4K++54SiO2+15/2O2
aegirine + paragonite -> annite	14H++6K++18NaFeSi2O6+2NaAl3Si3O10(OH)2->6KFe3AlSi3O10(OH)2+20Na++3H2O+24SiO2(0)+9/2O2
aegirine + paragonite -> daphnite	3H2O+34H++30NaFeSi2O6+4KAl3Si3O10(OH)2->6Fe5Al2Si3O10(OH)8+34Na++54SiO2+15/2O2
albite -> muscovite	2H++K++3NaAlSi3O8->KAl3Si3O10(OH)2+3Na++6SiO2(aq)
albite + aegirine -> annite	6H++K++2NaAlSi3O8+6NaFeSi2O6->12SiO2+2KFe3AlSi3O10(OH)2+8Na++H2O+3/2O2
albite->microcline	NaAlSi3O8+K+->KAlSi3O8+Na+
albite+hematite->daphnite	6H2O+4H++5Fe2O3+4NaAlSi3O8->2Fe5Al2Si3O10(OH)8+6SiO2(aq)+4Na++5/2O2
analcime -> muscovite	K++2H++3NaAlSi2O6(H2O)->KAl3Si3O10(OH)2+3SiO2(aq)+3Na++3H2O
analcime->albite	SiO2(aq)+NaAlSi2O6(H2O)->NaAlSi3O8+H2O
annite -> albite + hematite	3O2+4Na++4KFe3AlSi3O10(OH)2->4NaAlSi3O8+6Fe2O3+4K++4H2O
annite -> albite + magnetite	1/2O2+Na++KFeAlSi3O10(OH)2->NaAlSi3O8+Fe3O4+K++H2O
annite -> analcime + aegirine	10SiO2+3H2O+8Na++2KFe3AlSi3O10(OH)2->2NaAlSi2O6(H2O)+6NaFeSi2O6+2K+
annite -> analcime + hematite	3/2O2+2Na++2KFe3AlSi3O10(OH)2->2NaAlSi2O6(H2O)_3Fe2O3+2SiO2+2K+
annite -> daphnite + aegirine	3H2O+2H++2Na++4KFe3AlSi3O10(OH)2->2Fe5Al2Si3O10(OH)8+2NaFeSi2O6+2SiO2(aq)+4K+
annite -> daphnite + hematite	1/2O2+2H2O+4H++4KFe3AlSi3O10(OH)2->Fe2O3+4K++6SiO2(aq)+2Fe5Al2Si3O10(OH)8
annite -> daphnite + magnetite	1/2O2+6H++6KF3AlSi3O10(OH)2+3H2O->3Fe4l4Si2O10(OH)8+1Fe3O4+6K++90SiO2(aq)
annite -> muscovite + magnetite	(3/2)O2+2H++3KFe3AlSi3O10(OH)2->KAl3Si3O10(OH)2+3Fe3O4+6SiO2(aq)+2K++3H2O
annite -> nepheline + aegirine	H2O+3/2O2+8Na++8SiO2+2KFe3AlSi3O10->2NaAlSiO4+6NaFeSi2O6+2K++6H+
annite -> nepheline + hematite	3/2O2+2Na++2KFe3AlSi3O10(OH)2->2NaAlSiO4+3Fe2O3+4SiO2+2K++2H2O
annite-> muscovite +hematite	9O2+8H++12KFe3AlSi3O10(OH)2->4KAl3Si3O10(OH)2+18Fe2O3+8K++12H2O+24SiO2(aq)
daphnite -> analcime + aegirine	22SiO2+3H2O+14Na++2Fe5Al2Si3O10(OH)8->4NaAlSi2O6(H2O)+10NaFeSi2O6+14H+
daphnite -> analcime + hematite	5/2O2+2SiO2+4Na++2KFe3AlSi3O10(OH)2->4NaAlSi2O6(H2O)+5Fe2O3+4H++2H2O
daphnite -> nepheline + aegirine	5/2O2+14Na++18SiO2+2Fe5Al2Si3O10(OH)8->4NaAlSiO4+10NaFeSi2O6+14H++H2O

Reaction	Equation
daphnite -> nepheline + hematite	5/2O2+4Na++2Fe5Al2Si3O10(OH)8->4NaAlSiO4+5Fe2O3+2SiO2+4H++6H2O
hematite + muscovite -> daphnite	6SiO2(aq)+4H++15Fe2O3+4KAl3Si3O10(OH)2+18H2O->6Fe5Al2Si3O10(OH)8+4K++15/2O2
hematite + paragonite -> annite	12SiO2+6K++9Fe2O3+2NaAl3Si3O10(OH)2+6H2O->6KFe3AlSi3O10(OH)2+2Na++4H++9/2O2
hematite + paragonite -> daphnite	6SiO2(aq)+4H++15Fe2O3+4NaAl3Si3O10(OH)2+18H2O->6Fe5Al2Si3O10(OH)8+4Na++15/2O2
magnetite -> hematite	2Fe3O4+0.5O2->3Fe2O3
microcline -> analcime	H2O+Na++KAlSi3O8->NaAlSi2O6(H2O)+SiO2(aq)+K+
microcline -> nepheline	Na++KAlSi3O8->NaAlSiO4+2SiO2(aq)+K+
microcline + aegirine -> annite	6H++2KAlSi2O8+6NaFeSi2O6->2KFe3AlSi3O10(OH)2+6Na++12SiO2+H2O+3/2O2
microcline + hematite -> daphnite	6H2O+4H++5Fe2O3+4KAlSi3O8->Fe5Al2Si3O10(OH)8+6SiO2+4K++5/2O2
microcline + magnetite-> annite	H2O+KALSi3O8+Fe3O4->KFe3AlSi3O10(OH)2+1/2O2
microcline->muscovite	2H++3KAlSi3O8->KAl3Si3O10(OH)2+6SiO2(aq)+2K+
microcline+hematite -> annite	4H2O+4KAlSi3O8+6Fe2O3->4KFe3AlSi3O10(OH)2+3O2
muscovite -> analcime	3SiO2+3H2O+3Na++KAl3Si3O10(OH)2->3NaAlSi2O6(H2O)+K++2H+
muscovite + aegirine -> annite	14H++4K++18NaFeSi2O6+2KAL3Si3O10(OH)2->6KFE3AlSi3O10(OH)2+24SiO2+18Na++3H2O+9/2O2
muscovite-> nepheline	3Na++KAl3Si3O10(OH)2->3NaAlSiO4+K++2H+
nepheline -> albite	NaAlSiO4+2SiO2(aq)->NaAlSi3O8
nepheline->analcime	SiO2(aq)+H2O+NaAlSiO4->NaAlSi2O6(H2O)
paragonite -> albite	NaAl3Si3O10(OH)2+6SiO2(aq)+2Na+->3NaAlSi3O8+2H+
paragonite -> analcime	3H2O+2Na++3SiO2+NaAl3Si3O10(OH)2->3NaAlSi2O6(H2O)+2H+
paragonite -> muscovite	NaAl3Si3O10(OH)2+K+->KAl3Si3O10(OH)2+Na+
paragonite -> nepheline	2Na++NaAl3Si3O10(OH)2->3NaAlSiO4+2H+
sodalite-> albite	12SiO2(aq)+Na8Al6Si6O24Cl2->6NaAlSi3O8+2NaCl(aq)

Species (4kbar)	ΔG_f(kJ) 367 °C	ΔG_f(kJ) 100 °C	ΔG_f(kJ) 200 °C	ΔG_f(kJ) 300 °C	ΔG_f(kJ) 400 °C	ΔG_f(kJ) 500 °C
aegirine	-2480.367	-2407.825	-2431.387	-2459.394	-2491.298	-2526.666
albite	-3779.273	-3689.559	-3718.616	-3753.26	-3792.852	-3836.886
analcime	-3166.04	-3071.312	-3102.371	-3138.844	-3180.198	-3226.005
annite (biotite)	-4942.865	-4769.796	-4826.774	-4893.417	-4968.522	-5051.138
daphnite (chlorite)	-6731.523	-6496.142	-6572.067	-6663.022	-6767.331	-6883.614
H+	0	0	0	0	0	0
H2O	-263.525	-236.043	-245.167	-255.751	-267.535	-280.348
hematite	-779.085	-739.132	-751.885	-767.365	-785.225	-805.23
K+	-315.106	-285.09	-295.924	-307.275	-319.02	-331.067
magnetite	-1070.129	-1006.853	-1027.315	-1051.753	-1079.74	-1111.067
microcline	-3815.213	-3724.702	-3754.181	-3789.102	-3828.813	-3872.792
muscovite	-5702.985	-5572.257	-5614.047	-5664.653	-5723.072	-5788.475
Na+	-289.096	-265.201	-273.027	-282.274	-292.614	-303.83
nepheline	-2021.313	-1969.072	-1986.077	-2006.286	-2029.12	-2054.302
O2	-34.55	18.709	1.697	-18.99	-42.669	-68.983
paragonite	-5662.243	-5535.93	-5576.101	-5625.044	-5681.768	-5745.457
quartz*	-869.384	-850.913	-856.826	-863.971	-872.224	-881.498
silica* (aquious)	-849.937	-827.068	-834.659	-843.25	-853.507	-865.384

* Data from Shock and Helgeson (1988); Holland and Powell (1998)